Sensing of Inorganic Ions and Organic Molecules Using Fluorescence and Plasmonic Nanomaterials

A thesis

submitted in fulfilment of the requirements for the degree of

Doctor of Philosophy

In

Chemistry

By

Shagun Kainth

(Regn. No: 901609010)

Under the supervision of

Dr. Soumen Basu

(Associate Professor)

School of Chemistry and Biochemistry

Thapar Institute of Engineering & Technology

(Deemed to be University)

Patiala, Punjab

India

August, 2020

CERTIFICATE

This is to certify that thesis entitled "**Sensing of Inorganic Ions and Organic Molecules Using Fluorescence and Plasmonic Nanomaterials**", being submitted by Ms Shagun Kainth in fulfilment of the requirement for the award of the Degree of Doctor of Philosophy in the School of Chemistry and Biochemistry, Thapar Institute of Engineering and Technology, Patiala, is a record of candidate's own independent and original research work carried out by her under my supervision and guidance. The matter presented in the thesis has not been submitted in part or full for the award of any degree in any other University or Institute.

(**Supervisor**)
Dr. Soumen Basu
Associate Professor
School of Chemistry and Biochemistry
Thapar Institute of Engineering and Technology
Patiala- 147004, Punjab (India)

(**Head**) 18/06/2020
Dr. Amjad Ali
Professor
School of Chemistry and Biochemistry
Thapar Institute of Engineering and Technology
Patiala- 147004, Punjab (India)

CANDIDATE'S DECLARATION

I, hereby declare that the work presented in the thesis entitled "**Sensing of Inorganic Ions and Organic Molecules Using Fluorescence and Plasmonic Nanomaterials**", in fulfillment of the requirement for the award of the Degree of **Doctor of Philosophy**, School of Chemistry and Biochemistry, Thapar Institute of Engineering and Technology, Patiala, is an authentic record of my own work carried out under the supervision of Dr. Soumen Basu, Associate Professor, School of Chemistry and Biochemistry, Thapar Institute of Engineering and Technology, Patiala, India. The matter embodied in this thesis has not been submitted in part or full to any other university or institute for the award of any degree in India or Abroad.

Shagun Kainth

.....

Shagun Kainth

Acknowledgment

Through this section of the thesis, I would like to express my heartiest thankfulness to all those who encouraged and supported me in many ways for the accomplishment of this study and made it an unforgettable journey for me.

This work was carried out in the Advanced Nanomaterials Laboratory (Thapar Institute of Engineering and Technology) between 2016-2020. I would like to express my sincere thanks to my supervisor Dr. Soumen Basu, for giving me the opportunity to work on such a fascinating project with all necessary supports and continuous guidance throughout my study.

Many thanks to Dr. Amjad Ali, Head of School of Chemistry and Biochemistry Thapar Institute of Engineering and Technology, Patiala for his ever-helping attitude and good wishes. I would also like to express my special regards to the members of my doctoral committee, Dr. Satnam Singh, Dr. Vijay Luxmi, Dr. Banibarata Maity and Dr. Shekhar Agnihotri for their perceptive comments, advices and scientific discussions. Special thanks to all the ***Teaching Faculty*** *of the department for their cooperation and guidance. Also, special thanks to Mr. Chander Thakur and office staff Mr. Mayank Sharma for their cooperation and timely support. I sincerely acknowledge Dr. Rafat Siddique Dean R & SP for finical support. The help from different laborites like SAI labs, CeNS Bengaluru and Sprint Testing Solutions is highly acknowledged.*

I warmly thank all my friends and lab mates Ms Surbhi Sharma, Ms. Neeraj Sohal, Ms. Aanchal Ms. Divya Monga, Ms. Aayushi kundu and Ms. Aashna for great time and moral support. I will forever cherish the warmth shown by them, whose smiling faces always inspired me. Special thanks to Raveena, Ruhi, Santosh, Ashok, Adil and Piyush for guidance, support and precious friendship.

The words are insufficient to convey my heartfelt gratitude to my father Mr. Manoj Kumar Kainth and my mother Mrs. Rita Kainth for their encouragement and inspiration throughout my research work. I owe everything to them. My special thanks to my elder brother, Dr. Ram Wargantiwar and Yatin Verma, my grandma and the whole Kainth family for unconditional love and support from childhood.

Besides this, I am thankful to the persons who knowingly and unknowingly helped me during the successful completion of this work.

Shagun Kainth

.....

Shagun Kainth

TABLE OF CONTENT

Chapter-3

Selective Detection of Fluoride Ions by Using Nitrogen and Oxygen Rich C-dots and its Logic Gate Implementation

Chapter-4

Effect of Acids and Solvents on the Photoluminescence Properties of C-dots and Its Sensing Efficacy Towards Metal Ions

Chapter-5
Impact of Different Nitrogen Surface Passivation in C-dots and Its Sensing Efficacy Towards Picric Acid and Creatinine

ABSTRACT

The thesis entitled "**Sensing of Inorganic Ions and Organic Molecules Using Fluorescence and Plasmonic Nanomaterials"** is divided into five chapters.

CHAPTER-1: It describes the informative details related to sensor, nanomaterials and sensing methods and its mechanism, literature survey and scope of work. The section contains elaborate discussion about metal-based SPR active (AuNPs) as well as the carbon-based fluorescent nanomaterials (C-dots). Another section focuses on various methods to developed C-dots with tunable emission and different size AuNPs. Moreover, a description of research gaps, objectives and characterization techniques also integrated.

CHAPTER-2: It involves the description of the synthesis of different size AuNPs which attained through varying the citrate salt concentration. The SPR signals were studied with the help of UV-visible spectroscopy and size was evaluated from TEM analysis which showed absorption in the range of 518-535 nm with size range from 8-30 nm. AuNPs showed extensive stability in the pH range of 3-9 and high ionic strength of NaCl (0.1 M). The interaction of purines was studied with various size AuNPs which indicated that amino and thiol rich purines disturb the interparticle distance through surface charge neutralization and Au-S (HSAB rule) interaction. These interactions cause place exchange reaction between purines and AuNPs which leads to their aggregation with the increment in its size. These variations were observed by naked eyes through color change from red to blue. The UV-visible spectra showed bathochromic shift~10nm was observed in SPR signal of AuNPs. Various other studies related to time, pH of a colloidal sol, the concentration of purines, and peak displacement vs particle size was also done for purine detection. The larger size excellent selectivity and high limit of detection (10^{-7} M) due to less negative surface charge which induces fast aggregation at the lower concentration of the analyte. These different sizes of AuNPs found an efficient analytical tool that has huge potential for practical application in clinical chemistry and medicinal diagnosis.

CHAPTER-3: Green methodology and cheap precursors (citric acid, urea, and mosambi peel) were used to obtain oxygen and nitrogen-rich C-dots. It involves detailed information related to turn-on/off ability of C-dots as a nanoprobe. Both the OC-dots and NC-dots were found partially monodispersed and spherical with an average diameter of 2-4 nm. These prepared two C-dots exhibited good interaction with Fe^{3+} ions. These systems were explored further with F^-

ions which were confirmed through PL and zeta potential studies. The mixture of OC-dots and Fe^{3+} ions showed sensitivity than NC-dots towards F^- ions with a LOD of 0.01 μM. Moreover, different molecular logic gate such as NOT, IMP, AND and OR were developed based on experimental results by using metal ions and anions as the chemical input for the practical application. The validation was investigated in real samples (lake and tap water) and compared with the ICP-AES results. The discovered studies with carbon-based fluorescent nano-probes were found ecological and portable probe for remote sensing of F^- ions.

CHAPTER-4: In this new approach was followed to synthesis C-dots using heteroatoms as dopants, solvent medium to tune its emission properties. Sucrose was a carbon source and variant combination of acids (H_2SO_4 + H_3PO_4, H_2SO_4 + HNO_3) were used to attained C-dots. Primarily, H_2SO_4+H_3PO_4 (1:2) mixture induces dual emissive characteristics in C-dots. The dual characteristics were observed through HRTEM with the particle size of 4-7 nm. These C-dots showed high PLQY (0.50, 078, 0.86 and 0.56) in water, CCl_4, $CHCl_3$ and CH_2Cl_2, respectively. These dual emissive C-dots exhibit bathochromic emission in both the shorter and longer wavelengths, as well as both the emission maxima, appear as prominent peaks in the halogenated medium. This behavior was observed due to the formation of donor-π-acceptor interaction between sp^2 domain, electron-rich hetero-atoms on the surface of C-dots and increases its ICT character in the excited state. Afterwards, the probe was explored with various metal ions that exhibited utmost selectivity for Fe^{3+} ions in both the organic and aqueous medium with maximum and minimum detecting limit of 1 μM and 0.4 μM respectively. The quenching efficacy was evaluated by recording the PLQY of C-dots in presence of water, CCl_4, $CHCl_3$ and CH_2Cl_2 i.e. decline as 0.27, 0.34, 0.31 and 0.14, respectively. This sensing ability obeyed photoinduced electron transfer mechanism (PET). These experimental results were also validated through real samples (Ferric citrate tablets 200 mg) and it showed excellent metal ion sensing accuracy which justified its sensing efficiency. Overall, these studies explained the importance of acids mixture to attain dual emissive behavior that increases its probability as a versatile label-free sensing probe.

CHAPTER-5: In the field of biochemistry and biosensors, nitrogen-doped carbon dots (NC-dots) have attracted an efficient strategy to improve the high photoluminescence (PL) behaviour especially the quantum yield. However, the impact of chemical composition, optoelectronic properties of different multifunctional nitrogen precursors of NC-dots is still hardly explored. Herein, we have synthesized different NC-dots via green and straightforward

microwave-assisted pyrolysis technique using a mixture of ascorbic acid as carbon source and different nitrogen-rich precursors such as urea, thiourea, cysteine and glycine. The PL analysis revealed that surface doping is dependent on the type of nitrogen precursors, which causes a bathochromic emission shift and generates excitation dependent emission properties in them. These variant nitrogen precursors also bring significant change in its surface states through development of -NH_2 pyridinic and pyrrolic nitrogen species i.e. evident from X-ray photoelectron spectroscopy which increases its PL quantum yields (PLQY~58%) and average lifetime values. Moreover, these NC-dots were used as fluorescent off-on sensing applications towards toxic nitroaromatic compounds such as 2,4,6 trinitrophenol (picric acid) and creatinine. In the presence of picric acid (PA), NC-dots exhibited maximum fluorescence quenching up to ~80% and decline in the maximum lifetime value (τ_{av}) from 1.08 to 0.59 ns, which is explained based on acid-base interaction and energy transfer mechanism. Consequently, PA-infested NC-dots solution was used for creatinine detection and exhibited maximum (50%) PL turn-on response. Fundamentally, this turn-on response was achieved due to the formation of Jaffe chromogen between creatinine and PA. Also, this PL turn off-on methodology for creatinine determination has shown satisfactory good linearity range between 0-0.65 μM with a detection limit of 36 nM. The three inputs based molecular logic gates were also designed based on the turn-off-on response of NC-dots@PA towards creatinine. Moreover, for analytical method validation real sample analysis was also done for creatinine which showed good recoveries (84-90%), and demonstrates that the nitrogen doping tailored the physio-chemical properties and enhance its sensing ability.

LIST OF FIGURES

Chapter-3

Chapter-4

LIST OF TABLES

Chapter-4

Chapter-5

LIST OF ABBREVIATIONS

SPR	Surface Plasmon resonance
UV-vis	Ultraviolet-visible
AuNPs	Gold nanoparticles
PET	Photoinduced electron transfer
FRET	Fourier resonance electron transfer
IFE	Inner filter effect
C-dots	carbon quantum dots
PL	Photoluminescence
PLQY	Photoluminescence quantum yield
EDX	Energy-dispersive X-ray spectroscopy
AgNPs	Silver nanoparticles
HBA	Hydrogen bond accepting ability
HBD	Hydrogen bond donating ability
HRTEM	High resolution transmission electron microscopy
XPS	X-ray photoelectron spectroscopy
DLS	Microtrac's dynamic light scattering
6-TG	6-thioguanine
6-MP	6- mercaptopurine
NPs	Nanoparticles
NMs	Nanomaterials
HPLC	High-Performance Liquid Chromatography
SEM	Surface electrochemical method
DPV	differential pulse voltammetry
GC	Gas chromatographic
EPA	Environmental Protection Agency
NIOSH	National Institute for Occupational Safety and Health
SQDs	Semiconductor quantum dots
ICP-AES	Inductively coupled plasma atomic emission spectroscopy

LIST OF SYMBOLS

mM	Milli-molar
µM	Micro-molar
nM	Nano-molar
µM/l	Micro-molar per litre
mg/ml	Milligram per millilitre
ng/ml	Nanogram per millilitre
nm	Nanometer
µl	Microlitre
ml	Mllitre
ns	Nanoseconds
mV	Millivolts
g	Gram
λ	Wavelength
°	Degree
%	Percentage
π^*	Polarizability
α	Hydrogen bond donating ability
β	Hydrogen bond accepting ability
Δf	Orientation polarizability
φ_f	Photoluminescence quantum yield
τ_{av}	Average lifetime
k_r	Radiative constant
k_{nr}	Non-radiative constant
k_{ET}	Rate of electron transfer

CHAPTER-1

Introduction and Literature

1.1 Background

1.1.1 Sensor

Sensors are the sophisticated devices whose purpose is to detect events or changes in its environment and send the information to other electronics, frequently a computer processor. The real-time example of a sensor is the autopilot system in aircraft. Where several sensors (speed, height, temperature and position) give signals to computer controls which directly control the different parts to run the plane at auto mode. These sensors are classified into many categories, i.e. mentioned in follow diagram (Fig. 1.1)

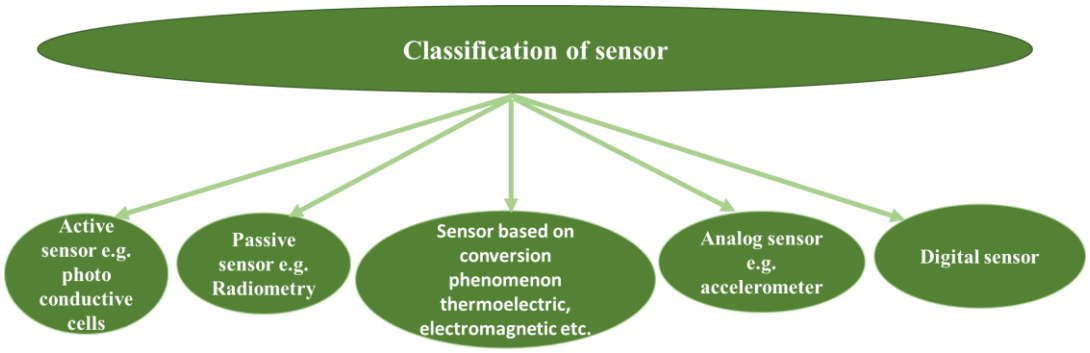

Fig. 1.1: Flow-chart presentation to the categorized type of sensors.

These various sensors need to be implemented for the appropriate determination of biomolecules, anions and cations because disturbance may cause imbalance in the ecological system. So, quantification of biomolecules/anions in body fluid and water sources is very crucial these days.

Several traditional methods were available for the quantification of toxins and biological important moieties such as voltammetry[1], fluorimetry[2], luminescence analysis[3], HPLC[4–7] and electrochemical strategy[8], Field-effect transistors (FETs)[9]. Still a few points of confinement in these strategies. One critical point of confinement of HPLC and spectrometric techniques is that they lack sufficient UV absorption and also need a suitable mobile phase.

Even voltammetry technique is not helpful for selective detection due to instability in the electrode material[8]. Overall, all these techniques are not suitable due to the requirement of sophisticated instrumentation, expensive reagents, cumbersome sample preparation, higher cost and analytical complexity. Thus, to overcome the greatest challenges for clean and purified environment researcher interest is shifting towards the nanotechnology for sustainability.

1.1.2 Bio-affinity nanoprobes

Nano-technology leads to the upliftment in the field of sensors due to the existence of comparable sizes with biomolecules which is a useful factor for the selective and sensitive ultrasensitive detection. The nanomaterials are classified into four types, i.e. mentioned below:

1. **Carbon-based nanomaterials:** These nanomaterials contain carbon with different morphologies such as hollow tubes, ellipsoids or spheres. It includes fullerenes (C-60), carbon nanotubes (CNTs), carbon nanofibers, carbon black, graphene (Gr) carbon dots (C-dots), and carbon onions. The production methods for carbon materials involves laser ablation, arc discharge, and chemical vapor deposition (CVD) methods.

2. **Inorganic-based nanomaterials:** Metal and metal oxide were used as a precursor to obtain different nanoparticles. These materials include metals such as gold and silver nanoparticles (Au or AgNPs), metal oxides such as TiO_2 and ZnONPs, and semiconductors such as silicon and ceramics.

3. **Organic-based nanomaterials:** These materials produced from organic matter which leads to self-assembly and design of molecules to transform the organic nanomaterials into desired structures such as dendrimers, micelles, liposomes and polymer nanoparticles.

4. **Composite-based nanomaterials:** These materials have multiphase, one phase on the nanoscale dimension that can either combined with larger or with bulk-type materials (e.g., hybrid nanofibers) or more complicated structures, such as metal-organic frameworks. The composites may be any combinations of carbon-based, metal-based, or organic-based NMs with any form of metal, ceramic, or polymer bulk materials.

These reported developments were occurred because of ever-increasing understanding of nanoscale phenomenon and growth of innovative nanofabrication techniques.

Aforementioned categories of materials were known for various applications such as water purification, clean energy, good health and greenhouse management. Still, before the removal of various toxins, there is a huge requirement to quantify them accurately. So, various optical probes based on colorimetry and fluorescence were chosen as sensing tool to detect metal ions and biological molecules in living cells, food and aquatic system due to low cost, rugged and easy utility.

1.1.3 Colorimetric sensor

Colorimetry is a well-known principle in sensing that relates with color change during the interaction between the analyte and the probe. There are some metal-based (gold and silver) nanoparticles that have smaller size that helps them to confine their electron for production quantum effects. Mainly, the existence of specific functional groups (-OH, -NH_2, -COOH groups) on its surface [9] brings variation in their interparticle distance between intermolecular ions in the presence of foreign moieties. Further, originate the different level of aggregation, i.e. driven by the London/van der Waals attractive forces[10] which is a key factor for naked-eye colorimetric biomolecule sensing[11,12] among these metal nanoparticles. These estimation for the change in the interparticle distance of metal nanoparticles was obtained through its surface plasmon resonance (SPR) profiles[13–16] which can be used for the determinations of toxins.

Among plasmonic nanoparticles, gold nanoparticles (AuNPs) have attracted much concern for usage as an optical nanoprobe in chemical and biochemical sensing, medical diagnostics and therapeutics and biological imaging. AuNPs exhibited a wide variety of color ranging from red to purple (and blue) or almost black which is attributed to the variation in their shape and sizes.[17–19] The different shape and size of AuNPs can be achieved by using Turkevich Brust and Schiffrin method, i.e. controlled by varying the ratio of reducing and capping agents. Kundu *et al.* used different molar ratio of 2,7- dihydroxy naphthalene (2,7 DHN) and cetyltrimethylammonium bromide respectively to obtain the different shapes of AuNPs.[20,21] Wangoo *et al*. prepared different sizes of AuNPs using octadecylamine as reducing agent. Subsequently to improves the hydrophilicity capping was also done with anionic surfactant sodium bis(2-ethylhexyl)-sulfosuccinate and used to determine the binding ability with protein[22].

Due to its unique properties and versatility its being used as label-free colorimetric sensor for sensitive, selective, simple detection of toxins through ultraviolet-visible (UV-vis)

absorption spectroscopy. Many reported experiments specify that citrate-capped AuNPs when interact with highly charged nucleotides or uncharged nucleosides the weakly bound citrate ions gets displaced through metal-ligand interactions. This leads to gain or loss of surface charges which can increase AuNPs stabilization or trigger their aggregation, respectively.[10] Additionally, experimental details based on its interparticle cross-linking sensing applications is mentioned in Table-1.1.

Table 1.1: Detection of metal ions and bio-molecules using AuNPs.

Nanoparticle	Analyte	Sample/interferent	Functionalization	Analytical performance	Ref
AuNPs	tetracycline	Environmental water samples	Label free probe	LOD: 0.071 μM	[23]
AuNPs	Mercury Hg^{+2}	Tap and river water	Citrate-AuNPs + 2, 2'-bipyridyl (Bipy)	LOD: 38 nM	[24]
AuNPs	Uranium (VI)	Ground water	12F6 antibody	LOD: 36.38 nM	[25]
AuNPs	Iodide	----------	Citrate-AuNPs	LOD: 0.30 μM	[26]
AuNPs (12 nm)	H_2O_2	Interferent solutions at different concentration	Citrate-AuNPs	LOD: 1.3 mM	[27]
AuNPs (20 nm)	Mercury Hg^{+2}	Target-doped blood serum	AuNPs and conjugated polyelectrolyte	LOD: 50 mM	[28]
AuNPs (13 nm)	Pb^{+2}	RNA-cleaving DNA enzyme	Aptamer–AuNPs	LODs: 10 mM	[29]

AuNPs (40 - 50 nm)	Concanavalin A	Lectin (jack beans)	Thioglucose-AuNPs	LOD: 9 nM	[30]
AuNPs (15, 20, and 2.5nm) Monodisperse	Cysteine, glutathione and glutathione disulfide	Blood/serum	Citrate-AuNPs: 15 nm CTAB-AuNPs: 20 nm $NaBH_4$-coated AuNPs: 2.5nm	LOD: cysteine <0.5 LOD: glutathione 10 mM LOD: glutathione disulfide 10 mM	[31]
AuNPs (13 nm) Monodisperse	Ascorbic acid	Fruit juices	Alkyne–azide click reaction	LOD: 3.0 nM	[32]

1.1.4 Fluorescent sensor

Another sensing principle is based on the fluorescence behavior of the chemical compound which response to the specific stimulus by energy transfer efficiency that affects its emission properties in the excited state that leads to either fluorescence quenching and enhancement. Quenching mechanism of fluorophore includes static, dynamic quenching, energy transfer Photoinduced Electron Transfer (PET), Fourier Resonance Electron Transfer (FRET) and Inner Filter Effect (IFE). The details of these mechanisms are discussed in details in Table 1.2.

Table 1.2: Difference between various quenching mechanism followed by fluorophores.

Parameters	Static quenching	Dynamic quenching	FRET	PET	IFE
Distance	Temperature-dependent	Viscosity dependent	1-10 nm, Lifetime of the donor reduced	Not critical	>20 nm
Mechanism	Complex formation in the ground state	Particle diffuse and colloid to cause excited-state deactivation	Dipole interaction	Electron transfer between fluorophore and quencher	Radiative re-absorption
Orientation	Not critical	Not critical	Requires good orientation of (excited state) dipoles	Not critical	Not critical
Redox potential	Not critical	Not critical	Not important	Redox potential must be high enough to allow for electron transfer	Not critical
Spectral overlap needed	Not required	Not required	Mandatory	Not required	Required

On the basis of these energy transfer behavior of fluorophore, several materials such as semiconductor quantum dots[33–36], polymer dots[37,38], molecular nanomaterial[18,39], and organic dyes[40,41] were synthesized for the detection of toxins. Still there is requirement of developing green material and methods to enhance the selectivity and sensing efficacy. Thus, carbon quantum dots (C-dots) can be a cost-effective and environmentally friendly way for the quantification of biomolecules/metal ions [42,43]. This material has excellent optical properties, good biocompatibility and low toxicity. The fluorescence characteristics in C-dots arose from the combination of large conjugated π-domain, several functional groups (hydroxyl, carboxyl, amine, and so on) and surface defects. These carbon core state and chemical surroundings which can be controlled by using different precursor and techniques that brings variation in its color emitting, photoluminescence quantum yield (PLQY) and decay lifetime that modulates its selectivity and sensitivity towards toxins. Due to these unique properties' researchers were giving them incredible attention as fluorescent sensors.

Numerous top-down, bottom-up approaches such as chemical oxidation, electrochemical, solvothermal synthesis, microwave, ultrasonic, hydrothermal, laser ablation, etc.[44–47] were known to synthesized C-dots. Moreover, these huge emphasis were given on precursors such as chitosan[48], amino acids[49], human hairs[50] vegetables[51] , orange juice[52] and few synthetic organic moities[53,54] to enhance its emission range and PLQY. There are several reports mentioned by different research groups that used the different molar ratio of the precursor such as Yuan *et al.* synthesized multi-color C-dots by controlling the molar ratio of citric acid (CA) and guanidine hydrochloride which showed excitation dependent emission with low nitrogen content. But it undergoes excitation independent emission with high NH_2 group surface density. These tunable fluorescent C-dots were used for semi-quantitative monitoring of intracellular Hg^{+2} [55]. Hola *et al.* synthesized different surface charged C-dots by the solvothermal process using urea and CA in formamide. The C-dots have graphitic like nitrogen structure which reduces the energy gap and results into red-shift in emission wavelength [56]. Hill *et al.* prepared C-dots using different carbohydrates such as sucrose, fructose and glucose at low temperature 70 °C which showed orange-red emission under UV-lamp [57,58]. Hung *et al.* also prepared N, S, B doped red-emitting C-dots using 3-aminobenzeneboronic acid and 2,5-diaminobenzenesulfonic acid as precursors for the detections of Ag^+ and L-cysteine with detection limits as low as 0.350 and 0.045 mM, respectively [59]. This work indicates that molar ratio of different precursor plays vital role in the

synthesis of multi-color C-dots. These properties increase its applicability for sensing and bio-imaging applications, i.e. mentioned in Table 1.3.

Table 1.3: Different precursor for C-dots and its detection limit for various biological moieties and metal ions.

Precursor/method	Applications	Limit of detection (LOD)	Ref
chopped kelp, nitrogen dopant ethylenediamine	Detection of Co^{+2} ions	3.9 µM/l	[60]
Chemical oxidative polymerization of o-phenylenediamine (*o*-PD) and ammonium persulphate (APS)	Detection of eight metal ions, including Cr^{3+}, Cu^{2+}, Fe^{3+}, Hg^{2+}, Cd2+, Pb^{2+}, Co^{2+}, and Ni^{2+}.	0.5 µM	[61]
C-dots synthesis using chitosan and in vitro formation AuNPs to obtain C-dots@AuNPs	Detection of iodine by colorimetric method	2.3 µM	[62]
Sucrose, ascorbic acid to prepare C-dots and 4-Azidoailine (for carbodiimide coupling)	Detection of pesticide flumioxazin via alkyne azide click reaction	0.027 µg/l	[63]
Citric acid, thiourea and 3-amino phenyl boronic acid by hydrothermal method	Detection of glucosamine	2.5 µM	[64]

PVP, hydrothermal method	Detection of choline and acetylcholine (ACh) based on the detection of H_2O_2	Choline-0.1 µM (ACh)-0.5 µM	[65]
Garlic carbon source Hydrothermal method	Selective detection of Fe^{+3}	0.2-500 µM	[66]
Pawn shell containing chitosan	Selective detection of Cu^{+2}	5 nM	[67]
Rice carbon source/ microwave heating	Detection of Fe^{+3}, S_2O_3 off-on and Zn^{+2}, PO_4^{-3} fluorescence sensing	Fe^{+3}-2.5×10^{-4} M S_2O_3-2×10^{-4} M-3×10^{-3} M Zn^{+2} -2.5×10^{-4} M PO_4^{-3}-2×10^{-4} M-3.5×10^{-3} M	[68]
Starch Tapioca –carbon source	Detection of fluoride anions	75% PL recovery using 4.14 mg/ml	[69]
Mixture of 18 vegetables	Detection of periodate	19 µM	[70]
Ionic liquids carbon source nitrogen-doped carbon dots, microwave method used	Selective detection of Cu^{+2}/Fe^{+3}	Fe^{+3}-20 nM Cu^{+2}- 5 nM	[71]
L-Glutamic acid/thermal carbonization	Detection of cardiac marker myoglobin	1-10^5 ng/ml	[72]

Nitrogen doped carbon dots using L-ascorbic acid and ethylene diamine	Detection of Cr (VI)	2.6 nM	[73]

1.1.5 Effect of solvent on sensing ability of C-dots

The dispersed phase plays a vital role in modulating the PL properties of the fluorophores. These studies were named as solvatochromism which was firstly introduced by Hantzsch (1992) and described through Onsager Reaction field (1936). This phenomenon was explained based on solvent-solute interaction because it disturbed the geometry, charge distribution of fluorophore which affects the stability of the excited/ground states and their band-gap energy. This causes a bathochromic or hypsochromic shift in their emission and absorption spectra among polar molecules with a change in the polarity of the solvent. This phenomenon is of two types, positive solvatochromism, i.e. attained when moiety undergoes red band shift and blue band shift in case of negative solvatochromism with the increase in solvent polarity. The occurrence of these shifts in emission spectra due to the existence of permanent dipole moment in the excited state, i.e. positive solvatochromism and vice-versa for negative solvatochromism. The explanation for the specific interaction between solute and solvent several models such as Lippert Mataga (LM) model, Kamlet-Taft model which relates with the polarity of medium polarizability (π^*), hydrogen bond accepting ability (HBA, β) and hydrogen bond donating ability (HBD, α) of solvents. These models stated the general trend that the enhanced polarity of medium directly caused a red-shift in their emission wavelength among various fluorophore.

Similar photoluminescence (PL) behavior in C-dots was examined by many researcher groups. This observed inflection in the solvent system leads to the formation of new functional groups, different surface states and new energy levels into their electronic structure which contributes to different emission properties in C-dots. Few reports by some groups such as Pan *et al*. synthesized solvent-dependent C-dots by a one-step pyrolytic route using ethylenediamine-tetraacetic acid salts as the resource. Their optical properties were investigated in an organic polar solvent (water, ethanol, methanol, glycol and acetone). In methanol, glycol and ethanol they showed similar PL behavior as water but in the acetone medium, the emission wavelength gets broader and undergoes redshift from 400 nm to 430 nm due to lewis acid and base properties of acetone and C-dots respectively.[74] Ding *et al.*

synthesized C-dots using L-glutamic acid and o-phenylenediamine *via* solvothermal method. They exhibited tunable emissive features in the range of 443-745 nm by using four different solvent media. They showed high quantum yield in the range of 43-54% which used for bioimaging fluorescent sensor.[75] Zhan *et al.* used 1,3,6-trinitropyrene as a carbon and nitrogen source to fabricate the C-dots and its emission properties were tuned by changing the solvent composition.[76] Yuan *et al.* followed solvothermal process to prepare C-dots using 1,2,4-diaminobenzene and polyethylene glycol (PEG200) as a passivating agent. The C-dots were dissolved in different solvents such as ethyl acetate, ethanediamine, oleyamine and DMSO. These solvents have variant electron-donating ability due to different surface functional groups S=O>-NH_2>-OCO which leads to multi-color emission helps to construct the warm WLEDs.[77] Still, more solvent-dependent studies with multi-color or dual emissive C-dots need to be discovered its photophysical and physio-chemical properties. Therefore, too apt environmental sustenance SPR and quantum confinement effect-based nano-materials such as AuNPs, C-dots can be effectively used as an analytical tool in future development.

1.2 Research gaps as listed below

Based on the literature review following gaps has been found, i.e. mentioned below:

1. Limited studies were done with different sizes of AuNPs to detect biomolecules.
2. Till now the impact of pH on the synthesis of C-dots were not discussed in details.
3. Simple, cost-effective methods were not known much for dual emissive C-dots.
4. Solvatochromic studies of dual emissive C-dots yet to be explored.
5. Little work was reported with diverse surface passivated C-dots and its sensing efficacy towards biomolecules and metal ions.

1.3 Objectives

1. Synthesis of gold nanoparticles (AuNPs) and fluorescent carbon quantum dots (C-dots) with variable size.
2. Detection of biomolecules/metal ions by studying the variation in optical properties of different size and shape AuNPs.
3. Multi-color C-dots will be used for detecting different biomolecules/metal ions, based on turn on/off photoluminescence methodology.

1.4 Methodology

1.4.1 Synthesis of AuNPs of different sizes and shapes

a) Schematic diagram of Fern's method to prepare different sizes of AuNPs.

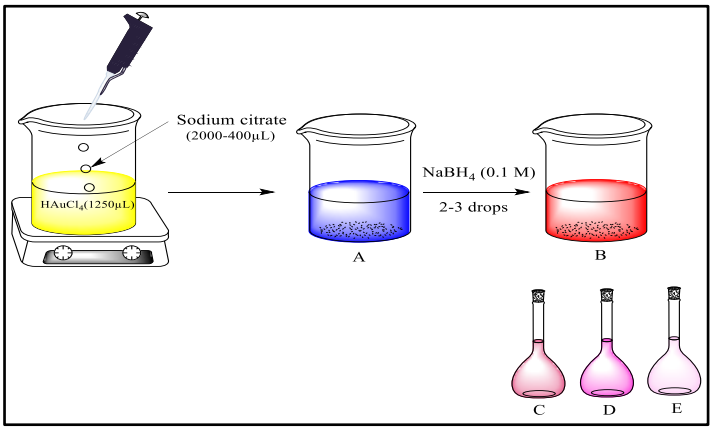

1.4.2 Synthesis of multi-color C-dots

The Multiwave-300 microwave synthesis reactor (Anton Paar, USA) was utilized to obtain C-dots. Different precursor and reaction conditions was followed to obtain long range emissive C-dots, i.e. listed as follows:

a) Single emissive C-dots using various precursor

The details of the following protocol for the synthesis of single emissive C-dots

Carbon source	Nitrogen source	Reaction conditions
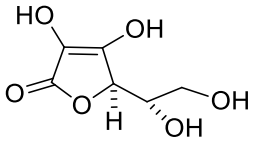 Ascorbic Acid	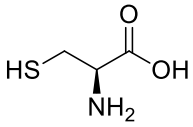 Cysteine	Microwave synthesis 130 °C, 5 min, 7 bar
	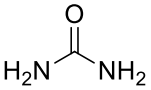 urea	
	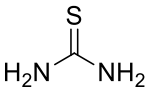	

	Thiourea	
	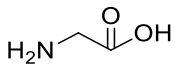 Glycine	

b) One pot single precursor-based synthesis of dual emissive C-dots

Carbon source	Doping materials	Reaction conditions
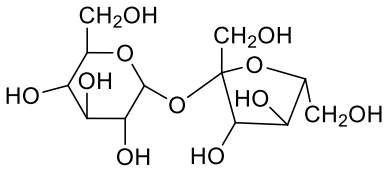 sucrose	Orthophosphoric acid (H_3PO_4) and sulfuric acid (H_2SO_4)	Microwave synthesis 150 °C, 10 min, 7 bar

c) Green synthesis of C-dots using organic waste

Citrus fruits peels were used to prepare C-dots by optimizing the time and temperature to obtain the specific emissive range and uniform size. The schematic presentation is mentioned in Fig. 1.2.

Fig. 1.2: Pictorial representation of the green synthesis of C-dots using fruit waste.

1.5 Techniques for characterizations

The nature and morphology of the prepared materials were characterized by the following techniques which are mentioned in details in Table 1.4.

Table 1.4: List of techniques used for the characterization of AuNPs and C-dots.

Techniques	Specification
UV-vis spectroscopy	Absorption properties of nanoparticles and Colorimetric sensing were done in dispersed phase on Champion UV-500 (AQ1205017) spectrophotometer.
Fourier transform infrared spectroscopy (FTIR-ATR)	Determination of functional groups present on the surface of AuNPs and C-dots were recorded on Fourier transform infrared spectroscopy-attenuated total reflectance (Agilent Resolution Pro-carry 660).
Particle size and Zeta potential	The surface charge and hydrodynamic size of material were recorded on Microtrac's dynamic light scattering (DLS), Nanotrac.
Photoluminescence spectroscopy (PL)	C-dots fluorescence behavior in the presence of foreign moieties was recorded on Perkin-Elmer (LS55).
High-resolution transmission electron microscopy (HRTEM)	The morphology of the materials was determined on TALOS F200S G2, 200 KeV, FEG, CMOS Camera 4K× 4K, In Column EDS detectors by drop-casting technique.
X-ray photoelectron spectroscopy (XPS)	The quantitative elemental composition and surface chemistry was done by XPS. The XPS was recorded on KRATOS Axis 165 (Shimadzu, UK) with Mg Kα radiation (1252.6 eV at 75 W).

1.6 Sensing mechanism of nanoprobes

a) SPR based sensing

Surface plasmon resonance (SPR) is the fundamental principle followed by many color-based biosensors. It is the standard tools for measuring adsorption of material onto planar metal

(typically gold or silver) surfaces or onto the surface of metal nanoparticles. When a light beam impinges onto a sensor (made from metal film coated on a glass slide) at a specific angle (resonance angle), the electrons in the metal film (called surface plasmons) are set to resonate with the light wave. The occurrence of this phenomenon is due to the resonant oscillation of conduction electrons at the interface between negative and positive permittivity material stimulated by incident light. The resonance results in the absorption of light which recorded from the detector as mentioned in Fig. 1.3.

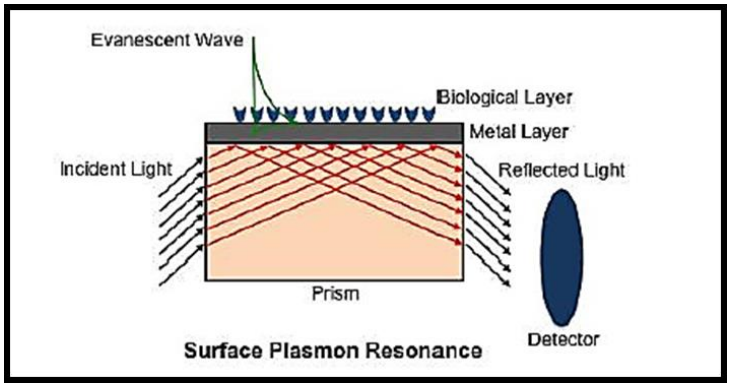

Fig. 1.3: Pictorial representation of the working principle of SPR sensing.

b) Sensing based on fluorescence quenching and enhancement of C-dots

This is a mechanism describing energy transfer between two light-sensitive molecules (chromophores). A donor chromophore, initially in its electronic excited state, may transfer energy to an acceptor chromophore through the nonradiative dipole-dipole coupling. The sensing ability of C-dots was measured in terms of energy transfer where it acts as a donor (electron-rich surface) and analyte 1 (electron-deficient species). This non-radiative process leads to a reduction in its fluorescence intensity. Till date, the interest towards specific and sensing get increased therefore fluorescence quenching based sensing is getting replaced with turn off/on-off methods in which another compatible analyte 2 is introduced that directly interfere with energy transfer mechanism and causes fluorescence enhancement as shown in Fig. 1.4.

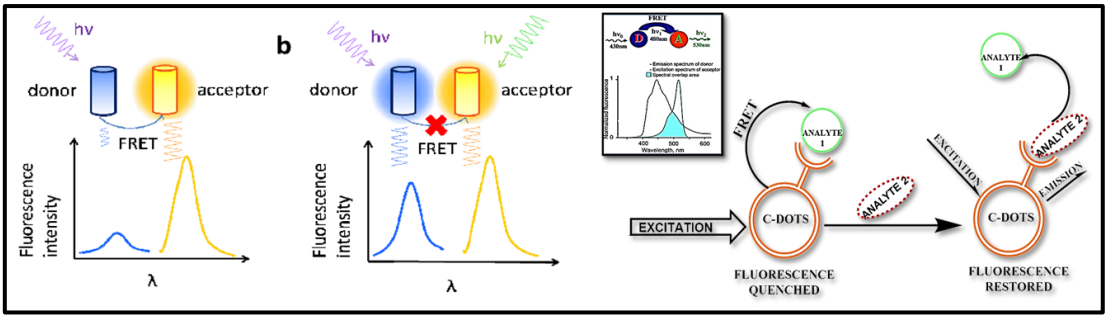

Fig. 1.4: Representation of turn-on/off mechanism based on FRET mechanism.

References

(1) Madueño, R.; Pineda, T.; Sevilla, J. M.; Blázquez, M. An Electrochemical Study of 6-Thioguanine Monolayers on a Mercury Electrode in Acid and Neutral Solutions. *J. Electroanal. Chem.* **2004**, *565* (2), 301–310. https://doi.org/10.1016/j.jelechem.2003.10.024.

(2) Rowland, K.; Lennard, L.; Lilleyman, J. S. High-Performance Liquid Chromatographic Assay of Methylthioguanine Nucleotide. *J. Chromatogr. B Biomed. Appl.* **1998**, *705* (1), 29–37. https://doi.org/10.1016/S0378-4347(97)00495-7.

(3) Mawatari, H.; Kato, Y.; Nishimura, S. I.; Sakura, N.; Ueda, K. Reversed-Phase High-Performance Liquid Chromatographic Assay Method for Quantitating 6-Mercaptopurine and Its Methylated and Non-Methylated Metabolites in a Single Sample. *J. Chromatogr. B Biomed. Appl.* **1998**, *716* (1–2), 392–396. https://doi.org/10.1016/S0378-4347(98)00329-6.

(4) Keuzenkamp-Jansen, C. W.; De Abreu, R. A.; Bökkerink, J. P. M.; Trijbels, J. M. F. Determination of Extracellular and Intracellular Thiopurines and Methylthiopurines by High-Performance Liquid Chromatography. *J. Chromatogr. B Biomed. Sci. Appl.* **1995**, *672* (1), 53–61. https://doi.org/10.1016/0378-4347(95)00206-X.

(5) Lennard, L.; Singleton, H. J. High-Performance Liquid Chromatographic Assay of the Methyl and Nucleotide Metabolites of 6-Mercaptopurine: Quantitation of Red Blood Cell 6-Thioguanine Nucleotide, 6-Thioinosinic Acid and 6-Methylmercaptopurine Metabolites in a Single Sample. *J. Chromatogr. B Biomed. Sci. Appl.* **1992**, *583* (1), 83–90. https://doi.org/10.1016/0378-4347(92)80347-S.

(6) Guha, N.; Loomis, D.; Grosse, Y.; Lauby-Secretan, B.; Ghissassi, F. El; Bouvard, V.;

Benbrahim-Tallaa, L.; Baan, R.; Mattock, H.; Straif, K. Carcinogenicity of Trichloroethylene, Tetrachloroethylene, Some Other Chlorinated Solvents, and Their Metabolites. *Lancet Oncol.* **2012**, *13* (12), 1192–1193. https://doi.org/10.1016/S1470-2045(12)70485-0.

(7) Lennard, L. Assay of 6-Thioinosinic Acid and 6-Thioguanine Nucleotides, Active Metabolites of 6-Mercaptopurine, in Human Red Blood Cells. *J. Chromatogr. B Biomed. Sci. Appl.* **1987**, *423* (C), 169–178. https://doi.org/10.1016/0378-4347(87)80340-7.

(8) March, G.; Nguyen, T. D.; Piro, B. Modified Electrodes Used for Electrochemical Detection of Metal Ions in Environmental Analysis. *Biosensors*. April 29, 2015, pp 241–275. https://doi.org/10.3390/bios5020241.

(9) Qian, Q.; Deng, J.; Wang, D.; Yang, L.; Yu, P.; Mao, L. Aspartic Acid-Promoted Highly Selective and Sensitive Colorimetric Sensing of Cysteine in Rat Brain. *Anal. Chem.* **2012**, *84* (21), 9579–9584. https://doi.org/10.1021/ac3024608.

(10) Zhao, W.; Chiuman, W.; Lam, J. C. F.; Brook, M. A.; Li, Y. Simple and Rapid Colorimetric Enzyme Sensing Assays Using Non-Crosslinking Gold Nanoparticle Aggregation. *Chem. Commun.* **2007**, No. 36, 3729–3731. https://doi.org/10.1039/b705335e.

(11) Sabela, M.; Balme, S.; Bechelany, M.; Janot, J. M.; Bisetty, K. A Review of Gold and Silver Nanoparticle-Based Colorimetric Sensing Assays. *Adv. Eng. Mater.* **2017**, *19* (12), 1–24. https://doi.org/10.1002/adem.201700270.

(12) Dayakar, T.; Venkateswara Rao, K.; Park, J.; Sadasivuni, K. K.; Ramachandra Rao, K.; Jaya rambabu, N. Non-Enzymatic Biosensing of Glucose Based on Silver Nanoparticles Synthesized from Ocimum Tenuiflorum Leaf Extract and Silver Nitrate. *Mater. Chem. Phys.* **2018**, *216*, 502–507. https://doi.org/10.1016/j.matchemphys.2018.05.046.

(13) Chegel, V.; Rachkov, O.; Lopatynskyi, A.; Ishihara, S.; Yanchuk, I.; Nemoto, Y.; Hill, J. P.; Ariga, K. Gold Nanoparticles Aggregation: Drastic Effect of Cooperative Functionalities in a Single Molecular Conjugate. *Journal of Physical Chemistry C*. February 2, 2012, pp 2683–2690. https://doi.org/10.1021/jp209251y.

(14) Prathna, T. C.; Chandrasekaran, N.; Mukherjee, A. Studies on Aggregation Behaviour of Silver Nanoparticles in Aqueous Matrices: Effect of Surface Functionalization and Matrix Composition. *Colloids Surfaces A Physicochem. Eng. Asp.* **2011**, *390* (1–3), 216–224. https://doi.org/10.1016/j.colsurfa.2011.09.047.

(15) Amendola, V.; Bakr, O. M.; Stellacci, F. A Study of the Surface Plasmon Resonance of Silver Nanoparticles by the Discrete Dipole Approximation Method: Effect of Shape, Size, Structure, and Assembly. *Plasmonics* **2010**, *5* (1), 85–97. https://doi.org/10.1007/s11468-009-9120-4.

(16) Wang, W.; Yang, M.; Wang, Z.; Yan, J.; Liu, C. Silver Nanoparticle Aggregates by Room Temperature Electron Reduction: Preparation and Characterization. *RSC Adv.* **2014**, *4* (108), 63079–63084. https://doi.org/10.1039/c4ra11803k.

(17) Takeuchi, Y.; Ida, T.; Kimura, K. Temperature Effect on Gold Nanodispersion in Organic Liquids. *Surf. Rev. Lett.* **1996**, *3* (1), 1205–1208. https://doi.org/10.1142/S0218625X96002175.

(18) Kreibig, U.; Genzel, L. Optical Absorption of Small Metallic Particles. *Surf. Sci.* **1985**, *156* (PART 2), 678–700. https://doi.org/10.1016/0039-6028(85)90239-0.

(19) Kim Thanh, N. T.; Rosenzweig, Z. Development of an Aggregation-Based Immunoassay for Anti-Protein A Using Gold Nanoparticles. *Anal. Chem.* **2002**, *74* (7), 1624–1628. https://doi.org/10.1021/ac011127p.

(20) Kundu, S.; Lau, S.; Liang, H. Shape-Controlled Catalysis by Cetyltrimethylammonium Bromide Terminated Gold Nanospheres, Nanorods, and Nanoprisms. *J. Phys. Chem. C* **2009**, *113* (13), 5150–5156. https://doi.org/10.1021/jp811331z.

(21) Kundu, S.; Peng, L.; Liang, H. A New Route to Obtain High-Yield Multiple-Shaped Gold Nanoparticles in Aqueous Solution Using Microwave Irradiation. *Inorg. Chem.* **2008**, *47* (14), 6344–6352. https://doi.org/10.1021/ic8004135.

(22) Wangoo, N.; Bhasin, K. K.; Boro, R.; Suri, C. R. Facile Synthesis and Functionalization of Water-Soluble Gold Nanoparticles for a Bioprobe. *Anal. Chim. Acta* **2008**, *610* (1), 142–148. https://doi.org/10.1016/j.aca.2008.01.033.

(23) Qi, M.; Tu, C.; Dai, Y.; Wang, W.; Wang, A.; Chen, J. A Simple Colorimetric Analytical Assay Using Gold Nanoparticles for Specific Detection of Tetracycline in Environmental Water Samples. *Anal. Methods* **2018**, *10* (27), 3402–3407. https://doi.org/10.1039/c8ay00713f.

(24) Chen, H.; Hu, W.; Li, C. M. Colorimetric Detection of Mercury(II) Based on 2,2′-Bipyridyl Induced Quasi-Linear Aggregation of Gold Nanoparticles. *Sensors Actuators, B Chem.* **2015**, *215*, 421–427. https://doi.org/10.1016/j.snb.2015.03.083.

(25) Quesada-González, D.; Jairo, G. A.; Blake, R. C.; Blake, D. A.; Merkoçi, A. Uranium (VI) Detection in Groundwater Using a Gold Nanoparticle/Paper-Based Lateral Flow Device. *Sci. Rep.* **2018**, *8* (1), 16157. https://doi.org/10.1038/s41598-018-34610-5.

(26) Pena-Pereira, F.; Lavilla, I.; Bendicho, C. Unmodified Gold Nanoparticles for In-Drop Plasmonic-Based Sensing of Iodide. *Sensors Actuators, B Chem.* **2017**, *242*, 940–948. https://doi.org/10.1016/j.snb.2016.09.161.

(27) Wu, Z. S.; Zhang, S. B.; Guo, M. M.; Chen, C. R.; Shen, G. L.; Yu, R. Q. Homogeneous, Unmodified Gold Nanoparticle-Based Colorimetric Assay of Hydrogen Peroxide. *Anal. Chim. Acta* **2007**, *584* (1), 122–128. https://doi.org/10.1016/j.aca.2006.11.003.

(28) Xia, F.; Zuo, X.; Yang, R.; Xiao, Y.; Kang, D.; Vallée-Bélisle, A.; Gong, X.; Yuen, J. D.; Hsu, B. B. Y.; Heeger, A. J.; et al. Colorimetric Detection of DNA, Small Molecules, Proteins, and Ions Using Unmodified Gold Nanoparticles and Conjugated Polyelectrolytes. *Proc. Natl. Acad. Sci. U. S. A.* **2010**, *107* (24), 10837–10841. https://doi.org/10.1073/pnas.1005632107.

(29) Zhao, W.; Lam, J. C. F.; Chiuman, W.; Brook, M. A.; Li, Y. Enzymatic Cleavage of Nucleic Acids on Gold Nanoparticles: A Generic Platform for Facile Colorimetric Biosensors. *Small* **2008**, *4* (6), 810–816. https://doi.org/10.1002/smll.200700757.

(30) Watanabe, S.; Yoshida, K.; Shinkawa, K.; Kumagawa, D.; Seguchi, H. Thioglucose-Stabilized Gold Nanoparticles as a Novel Platform for Colorimetric Bioassay Based on Nanoparticle Aggregation. *Colloids Surfaces B Biointerfaces* **2010**, *81* (2), 570–577. https://doi.org/10.1016/j.colsurfb.2010.07.061.

(31) Ghasemi, F.; Hormozi-Nezhad, M. R.; Mahmoudi, M. A Colorimetric Sensor Array for

Detection and Discrimination of Biothiols Based on Aggregation of Gold Nanoparticles. *Anal. Chim. Acta* **2015**, *882*, 58–67. https://doi.org/10.1016/j.aca.2015.04.011.

(32) Zhang, Y.; McKelvie, I. D.; Cattrall, R. W.; Kolev, S. D. Colorimetric Detection Based on Localised Surface Plasmon Resonance of Gold Nanoparticles: Merits, Inherent Shortcomings and Future Prospects. *Talanta*. Elsevier B.V. May 15, 2016, pp 410–422. https://doi.org/10.1016/j.talanta.2016.02.015.

(33) Alivisatos, A. P. Semiconductor Clusters, Nanocrystals, and Quantum Dots. *Science (80-.).* **1996**, *271* (5251), 933–937. https://doi.org/10.1126/science.271.5251.933.

(34) Qu, L.; Peng, X. Control of Photoluminescence Properties of CdSe Nanocrystals in Growth. *J. Am. Chem. Soc.* **2002**, *124* (9), 2049–2055. https://doi.org/10.1021/ja017002j.

(35) Shim, M.; Guyot-Sionnest, P. N-Type Colloidal Semiconductor Nanocrystals. *Nature* **2000**, *407* (6807), 981–983. https://doi.org/10.1038/35039577.

(36) Wang, Y.; Hu, R.; Lin, G.; Roy, I.; Yong, K. T. Functionalized Quantum Dots for Biosensing and Bioimaging and Concerns on Toxicity. *ACS Applied Materials and Interfaces*. April 24, 2013, pp 2786–2799. https://doi.org/10.1021/am302030a.

(37) Rong, Y.; Wu, C.; Yu, J.; Zhang, X.; Ye, F.; Zeigler, M.; Gallina, M. E.; Wu, I. C.; Zhang, Y.; Chan, Y. H.; et al. Multi-color Fluorescent Semiconducting Polymer Dots with Narrow Emissions and High Brightness. *ACS Nano* **2013**, *7* (1), 376–384. https://doi.org/10.1021/nn304376z.

(38) Wu, C.; Bull, B.; Szymanski, C.; Christensen, K.; McNeill, J. Multi-color Conjugated Polymer Dots for Biological Fluorescence Imaging. *ACS Nano* **2008**, *2* (11), 2415–2423. https://doi.org/10.1021/nn800590n.

(39) Zhao, Y. S.; Fu, H.; Peng, A.; Ma, Y.; Xiao, D.; Yao, J. Low-Dimensional Nanomaterials Based on Small Organic Molecules: Preparation and Optoelectronic Properties. *Adv. Mater.* **2008**, *20* (15), 2859–2876. https://doi.org/10.1002/adma.200800604.

(40) Kim, E.; Koh, M.; Lim, B. J.; Park, S. B. Emission Wavelength Prediction of a Full-

Color-Tunable Fluorescent Core Skeleton, 9-Aryl-1,2-Dihydropyrrolo[3,4-b]Indolizin-3-One. *J. Am. Chem. Soc.* **2011**, *133* (17), 6642–6649. https://doi.org/10.1021/ja110766a.

(41) Yao, D.; Zhao, S.; Guo, J.; Zhang, Z.; Zhang, H.; Liu, Y.; Wang, Y. Hydroxyphenyl-Benzothiazole Based Full Color Organic Emitting Materials Generated by Facile Molecular Modification. *J. Mater. Chem.* **2011**, *21* (11), 3568–3570. https://doi.org/10.1039/c1jm00009h.

(42) Zhou, Y.; Mintz, K. J.; Sharma, S. K.; Leblanc, R. M. Carbon Dots: Diverse Preparation, Application, and Perspective in Surface Chemistry. *Langmuir* **2019**, *35* (28), 9115–9132. https://doi.org/10.1021/acs.langmuir.9b00595.

(43) Peng, Z.; Han, X.; Li, S.; Al-Youbi, A. O.; Bashammakh, A. S.; El-Shahawi, M. S.; Leblanc, R. M. Carbon Dots: Biomacromolecule Interaction, Bioimaging and Nanomedicine. *Coordination Chemistry Reviews*. Elsevier B.V. July 15, 2017, pp 256–277. https://doi.org/10.1016/j.ccr.2017.06.001.

(44) Li, H.; Kang, Z.; Liu, Y.; Lee, S. T. Carbon Nanodots: Synthesis, Properties and Applications. *J. Mater. Chem.* **2012**, *22* (46), 24230–24253. https://doi.org/10.1039/c2jm34690g.

(45) Liu, W.; Li, C.; Ren, Y.; Sun, X.; Pan, W.; Li, Y.; Wang, J.; Wang, W. Carbon Dots: Surface Engineering and Applications. *Journal of Materials Chemistry B*. Royal Society of Chemistry 2016, pp 5772–5788. https://doi.org/10.1039/c6tb00976j.

(46) Yang, B.; Jelinek, R.; Kang, Z. Current Progress in Carbon Dots: Synthesis, Properties and Applications. *Mater. Chem. Front.* **2020**, *4* (5), 1287–1288. https://doi.org/10.1039/d0qm90015j.

(47) Chaudhary, S.; Umar, A.; Bhasin, K. K.; Singh, S. Applications of Carbon Dots in Nanomedicine. *Journal of Biomedical Nanotechnology*. American Scientific Publishers June 1, 2017, pp 591–637. https://doi.org/10.1166/jbn.2017.2390.

(48) Xiao, D.; Yuan, D.; He, H.; Lu, J. Microwave-Assisted One-Step Green Synthesis of Amino-Functionalized Fluorescent Carbon Nitride Dots from Chitosan. *Luminescence* **2013**, *28* (4), 612–615. https://doi.org/10.1002/bio.2486.

(49) Shore, A. Retraction: Amino Acid Derived Highly Luminescent, Heteroatom-Doped Carbon Dots for Label-Free Detection of Cd2+/Fe3+, Cell Imaging and Enhanced Antibacterial Activity (RSC Advances (2015) 5 (58141–58153) DOI: 10.1039/C5RA09525E). *RSC Advances*. 2018, p 39784. https://doi.org/10.1039/c8ra90093k.

(50) Singh, A.; Eftekhari, E.; Scott, J.; Kaur, J.; Yambem, S.; Leusch, F.; Wellings, R.; Gould, T.; Ostrikov, K.; Sonar, P.; et al. Carbon Dots Derived from Human Hair for Ppb Level Chloroform Sensing in Water. *Sustain. Mater. Technol.* **2020**, *25*, e00159. https://doi.org/10.1016/j.susmat.2020.e00159.

(51) Sachdev, A.; Gopinath, P. Green Synthesis of Multifunctional Carbon Dots from Coriander Leaves and Their Potential Application as Antioxidants, Sensors and Bioimaging Agents. *Analyst* **2015**, *140* (12), 4260–4269. https://doi.org/10.1039/c5an00454c.

(52) Amjadi, M.; Abolghasemi-Fakhri, Z.; Hallaj, T. Carbon Dots-Silver Nanoparticles Fluorescence Resonance Energy Transfer System as a Novel Turn-on Fluorescent Probe for Selective Determination of Cysteine. *J. Photochem. Photobiol. A Chem.* **2015**, *309*, 8–14. https://doi.org/10.1016/j.jphotochem.2015.04.016.

(53) Guo, D.; Wei, H. F.; Song, R. Bin; Fu, J.; Lu, X.; Jelinek, R.; Min, Q.; Zhang, J. R.; Zhang, Q.; Zhu, J. J. N,S-Doped Carbon Dots as Dual-Functional Modifiers to Boost Bio-Electricity Generation of Individually-Modified Bacterial Cells. *Nano Energy* **2019**, *63*. https://doi.org/10.1016/j.nanoen.2019.103875.

(54) Kim, T. H.; White, A. R.; Sirdaarta, J. P.; Ji, W.; Cock, I. E.; St John, J.; Boyd, S. E.; Brown, C. L.; Li, Q. Yellow-Emitting Carbon Nanodots and Their Flexible and Transparent Films for White LEDs. *ACS Appl. Mater. Interfaces* **2016**, *8* (48), 33102–33111. https://doi.org/10.1021/acsami.6b12113.

(55) Yuan, Y. H.; Liu, Z. X.; Li, R. S.; Zou, H. Y.; Lin, M.; Liu, H.; Huang, C. Z. Synthesis of Nitrogen-Doping Carbon Dots with Different Photoluminescence Properties by Controlling the Surface States. *Nanoscale* **2016**, *8* (12), 6770–6776. https://doi.org/10.1039/c6nr00402d.

(56) Holá, K.; Sudolská, M.; Kalytchuk, S.; Nachtigallová, D.; Rogach, A. L.; Otyepka, M.; Zbořil, R. Graphitic Nitrogen Triggers Red Fluorescence in Carbon Dots. *ACS Nano* **2017**, *11* (12), 12402–12410. https://doi.org/10.1021/acsnano.7b06399.

(57) Hill, S.; Galan, M. C. Fluorescent Carbon Dots from Mono- and Polysaccharides: Synthesis, Properties and Applications. *Beilstein Journal of Organic Chemistry*. Beilstein-Institut Zur Forderung der Chemischen Wissenschaften April 10, 2017, pp 675–693. https://doi.org/10.3762/bjoc.13.67.

(58) Swift, T. A.; Duchi, M.; Hill, S. A.; Benito-Alifonso, D.; Harniman, R. L.; Sheikh, S.; Davis, S. A.; Seddon, A. M.; Whitney, H. M.; Galan, M. C.; et al. Surface Functionalisation Significantly Changes the Physical and Electronic Properties of Carbon Nano-Dots. *Nanoscale* **2018**, *10* (29), 13908–13912. https://doi.org/10.1039/c8nr03430c.

(59) Huang, S.; Yang, E.; Yao, J.; Liu, Y.; Xiao, Q. Red Emission Nitrogen, Boron, Sulfur Co-Doped Carbon Dots for “on-off-on” Fluorescent Mode Detection of Ag+ Ions and L-Cysteine in Complex Biological Fluids and Living Cells. *Anal. Chim. Acta* **2018**, *1035*, 192–202. https://doi.org/10.1016/j.aca.2018.06.051.

(60) Zhao, C.; Li, X.; Cheng, C.; Yang, Y. Green and Microwave-Assisted Synthesis of Carbon Dots and Application for Visual Detection of Cobalt(II) Ions and PH Sensing. *Microchem. J.* **2019**, *147*, 183–190. https://doi.org/10.1016/j.microc.2019.03.029.

(61) Chen, S.; Liu, M. X.; Yu, Y. L.; Wang, J. H. Room-Temperature Synthesis of Fluorescent Carbon-Based Nanoparticles and Their Application in Multidimensional Sensing. *Sensors Actuators, B Chem.* **2019**, *288*, 749–756. https://doi.org/10.1016/j.snb.2019.03.067.

(62) Song, J.; Zhao, L.; Wang, Y.; Xue, Y.; Deng, Y.; Zhao, X.; Li, Q. Carbon Quantum Dots Prepared with Chitosan for Synthesis of CQDS/AuNPs for Iodine Ions Detection. *Nanomaterials* **2018**, *8* (12). https://doi.org/10.3390/NANO8121043.

(63) Panda, S.; Jadav, A.; Panda, N.; Mohapatra, S. A Novel Carbon Quantum Dot-Based Fluorescent Nanosensor for Selective Detection of Flumioxazin in Real Samples. *New J. Chem.* **2018**, *42* (3), 2074–2080. https://doi.org/10.1039/c7nj04358a.

(64) Das, R. K.; Mohapatra, S. Highly Luminescent, Heteroatom-Doped Carbon Quantum Dots for Ultrasensitive Sensing of Glucosamine and Targeted Imaging of Liver Cancer Cells. *J. Mater. Chem. B* **2017**, *5* (11), 2190–2197. https://doi.org/10.1039/c6tb03141b.

(65) Wei, J.; Ren, J.; Liu, J.; Meng, X.; Ren, X.; Chen, Z.; Tang, F. An Eco-Friendly, Simple, and Sensitive Fluorescence Biosensor for the Detection of Choline and Acetylcholine Based on C-Dots and the Fenton Reaction. *Biosens. Bioelectron.* **2014**, *52*, 304–309. https://doi.org/10.1016/j.bios.2013.09.006.

(66) Sun, C.; Zhang, Y.; Wang, P.; Yang, Y.; Wang, Y.; Xu, J.; Wang, Y.; Yu, W. W. Synthesis of Nitrogen and Sulfur Co-Doped Carbon Dots from Garlic for Selective Detection of Fe3+. *Nanoscale Res. Lett.* **2016**, *11* (1), 1–9. https://doi.org/10.1186/s11671-016-1326-8.

(67) Gedda, G.; Lee, C. Y.; Lin, Y. C.; Wu, H. F. Green Synthesis of Carbon Dots from Prawn Shells for Highly Selective and Sensitive Detection of Copper Ions. *Sensors Actuators, B Chem.* **2016**, *224*, 396–403. https://doi.org/10.1016/j.snb.2015.09.065.

(68) Dhenadhayalan, N.; Lin, K. C. Chemically Induced Fluorescence Switching of Carbon-Dots and Its Multiple Logic Gate Implementation. *Sci. Rep.* **2015**, *5*. https://doi.org/10.1038/srep10012.

(69) Basu, A.; Suryawanshi, A.; Kumawat, B.; Dandia, A.; Guin, D.; Ogale, S. B. Starch (Tapioca) to Carbon Dots: An Efficient Green Approach to an on-off-on Photoluminescence Probe for Fluoride Ion Sensing. *Analyst* **2015**, *140* (6), 1837–1841. https://doi.org/10.1039/c4an02340d.

(70) Romero, V.; Vila, V.; de la Calle, I.; Lavilla, I.; Bendicho, C. Turn–on Fluorescent Sensor for the Detection of Periodate Anion Following Photochemical Synthesis of Nitrogen and Sulphur Co–Doped Carbon Dots from Vegetables. *Sensors Actuators, B Chem.* **2019**, *280*, 290–297. https://doi.org/10.1016/j.snb.2018.10.064.

(71) Zhao, A.; Zhao, C.; Li, M.; Ren, J.; Qu, X. Ionic Liquids as Precursors for Highly Luminescent, Surface-Different Nitrogen-Doped Carbon Dots Used for Label-Free Detection of Cu2+/Fe3+ and Cell Imaging. *Anal. Chim. Acta* **2014**, *809*, 128–133. https://doi.org/10.1016/j.aca.2013.10.046.

(72) Shorie, M.; Kumar, V.; Sabherwal, P.; Ganguli, A. K. Carbon Quantum Dots-Mediated Direct Fluorescence Assay for the Detection of Cardiac Marker Myoglobin. *Current Science*. 2015, pp 1595–1596.

(73) Kaur, J.; Sharma, S.; Mehta, S. K.; Kansal, S. K. Highly Photoluminescent and pH Sensitive Nitrogen Doped Carbon Dots (NCDs) as a Fluorescent Sensor for the Efficient Detection of Cr (VI) Ions in Aqueous Media. *Spectrochim. Acta - Part A Mol. Biomol. Spectrosc.* **2020**, *227*. https://doi.org/10.1016/j.saa.2019.117572.

(74) Pan, D.; Zhang, J.; Li, Z.; Wu, C.; Yan, X.; Wu, M. Observation of PH-, Solvent-, Spin-, and Excitation-Dependent Blue Photoluminescence from Carbon Nanoparticles. *Chem. Commun.* **2010**, *46* (21), 3681–3683. https://doi.org/10.1039/c000114g.

(75) Ding, H.; Wei, J. S.; Zhang, P.; Zhou, Z. Y.; Gao, Q. Y.; Xiong, H. M. Solvent-Controlled Synthesis of Highly Luminescent Carbon Dots with a Wide Color Gamut and Narrowed Emission Peak Widths. *Small* **2018**, *14* (22). https://doi.org/10.1002/smll.201800612.

(76) Zhan, J.; Geng, B.; Wu, K.; Xu, G.; Wang, L.; Guo, R.; Lei, B.; Zheng, F.; Pan, D.; Wu, M. A Solvent-Engineered Molecule Fusion Strategy for Rational Synthesis of Carbon Quantum Dots with Multi-color Bandgap Fluorescence. *Carbon N. Y.* **2018**, *130*, 153–163. https://doi.org/10.1016/j.carbon.2017.12.075.

(77) Yuan, R.; Liu, J.; Xiang, W.; Liang, X. Red-Emitting Carbon Dots Phosphors: A Promising Red Color Convertor toward Warm White Light Emitting Diodes. *J. Mater. Sci. Mater. Electron.* **2018**, *29* (12), 10453–10460. https://doi.org/10.1007/s10854-018-9103-3.

Chapter-2

Size Dependent Properties of Gold Nanoparticles and Estimation of Its Sensing Efficacy Towards Thiopurines

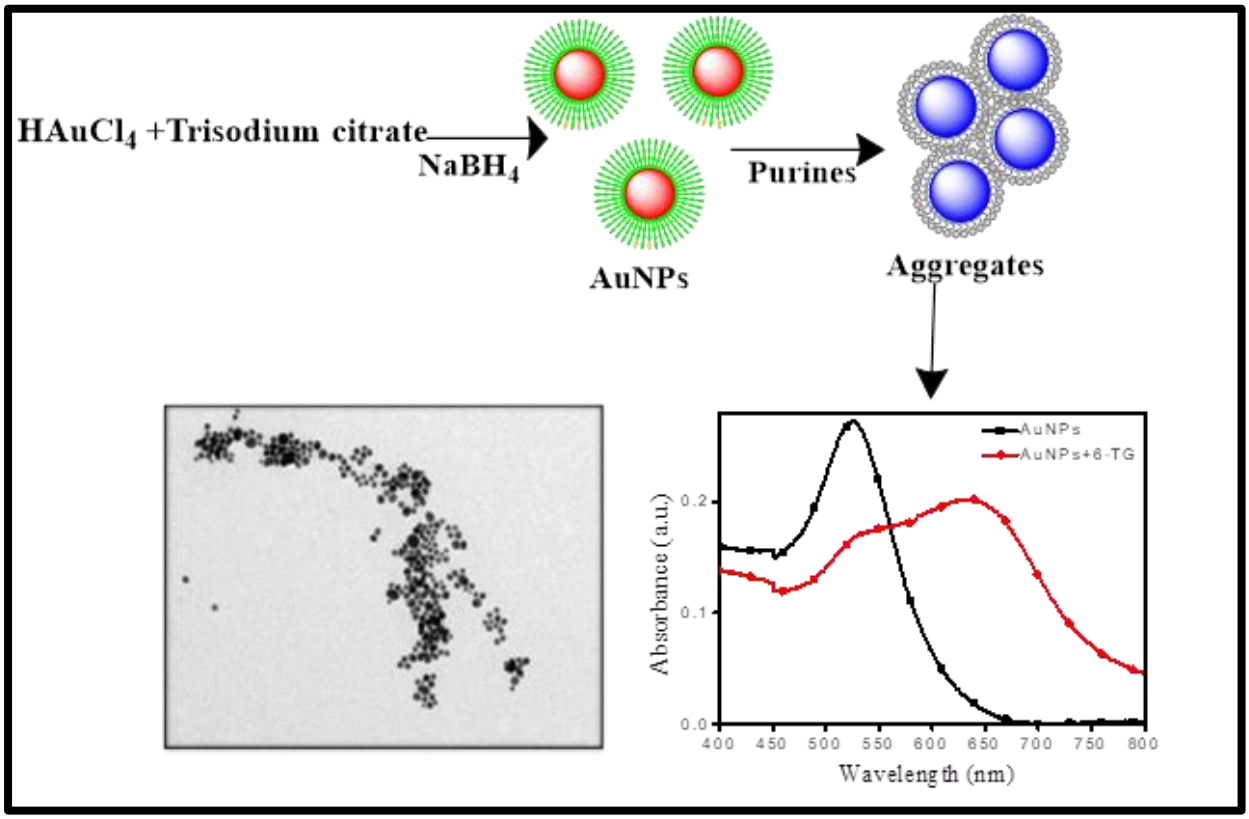

Highlights

- Fren's method was followed to synthesis of variable size of AuNPs.
- Impact of citrate capping on the particle size of AuNPs was evaluated.
- Interaction studies of thiopurines with different size AuNPs was done for quantitative analysis.

2.1 Introduction

Purine is a heterocyclic aromatic compound found in high concentration in meat and meat products, especially internal organs such as liver and kidney. They are well known in the body and perceived for primary two functions: (1) as building blocks for DNA (the primary genetic material in our cells) and (2) as substances that could be broken down to form a uric acid (which can potentially increase the risk of gout). The minimum intake of purine per day is in the range of 1430-1800 mg. Even in the field of pharmacy and biochemistry thiopurines exclusively show diverse applications. Some purines such as 6-thioguanine (6-TG), 6-mercaptopurine (6-MP) and azathioprine are used as a prodrug for the treatment of acute leukaemias and chronic myeloid leukaemia[1]. 6-TG is widely used as a chemotherapeutic drug for treatment of advanced stages of leukaemia[2,3]. 6–TG easily gets incorporated into the nucleic acid during synthesis and blocks further progression of the disease[4]. 6-TG is highly toxic and causes Thrombocytopenia, Anemia, Anorexia, Nausea and vomiting, Hepato-toxicity, etc[5,6]. Therefore it is very critical to maintain (2-3mg/kg/day for both paediatric and adults)[7] of the drug in plasma level to avoid high toxicity maintaining efficiency. To reduce unwanted side effects of cancer chemotherapeutic drug and to improve life quality of the patients and keeping adequate effectiveness, maintenance of steady drug concentration in the system is important. For this reason, periodic estimation of drugs/ drug metabolites concentrations in body fluid(s) like serum, plasma, urine, etc. is of immense importance. So, the proper and exact quantification of thiopurines in vegetables, pulses and drugs is required on urgent basis.

Several reported techniques have been accounted for the quantification of purines including voltammetry[8], fluorimetry[9], luminescence analysis[10], HPLC[11–14] and electrochemical strategy[15]. However, there are still a few points of confinement in these strategies. One critical point of confinement of HPLC and spectrometric techniques is that it lacks sufficient UV absorption and also need a suitable mobile phase and a reactant which obviously increased the cost and analytical complexity. Therefore, with the advancement of nanotechnology, other techniques have been developed such as surface plasmon resonance and electroanalytical methods to estimate the drug from the body fluid. But due to the requirement of sophisticated instrumentation, expensive reagents and cumbersome sample preparation other available methodology despite their good sensitivities, has not become very popular. Thus, the development of a new technique with high sensitivity, fast, high throughput and simple practical method for the determination of purine is still in a great demand.

Plasmonic nanoparticles (NPs) such as Au, Ag and Cu, etc. have optical properties which depend on their inter-particle distance and their SPR occurs in the visible region and due to this reason, they have gained incredible attention as colorimetric/optical sensors[16]. AuNPs is attaining intense attention scientifically and technically as a source of optical nanoprobe, because of its stability in meteorological conditions which allow them to show excellent biocompatibility with biomolecules and distance-dependence optical absorbance[17–21]. They also exhibit different colors range from red to purple, to blue and almost black due to the variation in the inter-particle distance of AuNPs[22–24]. This unusual phenomenon gives rise to a new analytical and sensing technique which leads to the development of Surface Enhanced Raman Scattering and enhancement in surface plasmon resonance immune sensing effect [25,26] because Au colloid monolayer can adsorb molecules in their closed space[27,28]. The presence of negative surface charge helps them in improving their binding efficiency with several biomolecules such as selective detection of DNA templates[29], polynucleotides[30,31], aminothiols and amino acid[17,32]. Unfortunately, there is still some complication in surface charge adjustment via, e.g., change of pH and salt concentration which may lead to loss of charge-based repulsive forces and that may bring variation in the quantitative determination of important biological moieties. Till now, different shapes of AuNPs were already used for sensing of 6-TG, but still, some study is yet to make on sensitivity and the interaction of different size AuNPs towards purines. This method will be better or comparable in the case of sensitivity and will involve less sample preparation and high output than the available methods. This research may open up a new avenue introducing nanomaterials into practical applications.

Here we have synthesised four different sizes AuNPs ranging from 8 nm to 30 nm to investigate the impact of purines on the surface chemistry of AuNPs together with pH through color change and SPR variation. The experimental result demonstrated the ability of this method and found to be quick, easy, effective and safe for quantitative detection of purines.

2.2 Experimental section

2.2.1 Chemical and materials

AR-Grade reagents were used for experimenting. Chloroauric acid ($HAuCl_4.3H_2O$) and Tri-sodium citrate were purchased from Aldrich. 6-MP and 6-TG were received from Tokyo Chemical Industry (TCI). Distilled water (18.2MΩ, Millipore) is used for the preparation of a stock solution of purines and different size AuNPs.

2.2.2 Preparation of gold nanoparticles

Size-controlled synthesis of AuNPs was done by modifying the Fren's method. 1250 µl of 10^{-2} M $HAuCl_4$ was added in 50 ml distilled water and the solution was heated at 97°C. Trisodium citrate (1%) was used as a reducing and stabilising agent for the conversion of Au^{+3} to Au^0. On addition of citrate to the boiling mixture of gold salt solution, the color starts changing from yellow to blue to purple to red[16]. Once the red color obtained, the solution kept at room temperature to cool down. Then a few drops of the $NaBH_4$ solution was added to it for the completion of the reaction (Au^{+3} to Au^0). Summarised information on the synthetic procedure, as well as verification of different sizes, is incorporated in Table 2.1.

Table 2.1: Details of different ratio of [$HAuCl_4$] / [citrate] and their color variation.

Sample name	Volume of $HAuCl_4$ 10^{-2}M (µl)	Volume of Citrate (1%) (µl)	Color	λ_{max} (nm)	Size of AuNPs from TEM images (± 3nm)
A	1250	2000	Dark red	521	8
B	1250	875	Red	525	13
C	1250	625	Pink	530	20
D	1250	400	Light Pink	535	30

2.2.3 Synthesis of thiopurines/AuNPs assemblies

The firstly different concentration of purine solutions was prepared from their stock solution (10^{-2} M). To sustain the stability of AuNPs and molecular structure of biomolecules pH of the gold solution was adjusted using HCl (10^{-2} M, 100 µl) to pH~4. Thiopurines/ AuNPs assemblies were prepared, with the addition of 30 µl of purine into 3000 µl AuNPs solution. Then the prepared mixture was analysed through UV-Vis spectroscopy to study their interaction with AuNPs [16]. The molecular structure of 6-MP and 6-TG was given in Fig. 2.1.

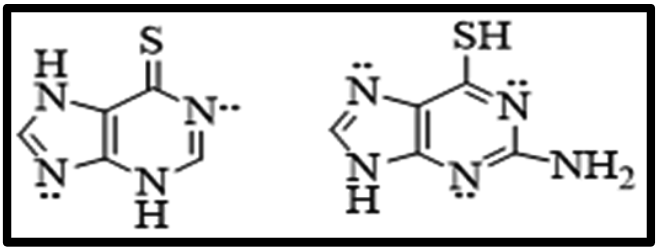

Fig. 2.1: Molecular structure of 6-Thioguanine (6-TG) and 6-Mercaptopurine (6-MP).

2.2.4 Instrumentation

The SPR of AuNPs was done using Champion UV-500 (AQ1205017) spectrophotometer and data analysed using software; Origin Pro 8. Fourier transform infrared spectroscopy-attenuated total reflectance (FTIR-ATR, Agilent Resolution Pro-carry 660) was recorded to know the purity of nano-material and their interactions with purines. Particle size and charge distribution were determined by Microtrac's dynamic light scattering (DLS), Nanotrac. For morphology and size determination, transmission electron microscopy (TEM) was done by drop-casting of 10 µl purified AuNPs dispersions on the carbon-coated copper grid and allowing them to dry in air for size determination using TEM operating at 200 KeV.

2.3 Result and discussion

2.3.1 Characterization studies of AuNPs

Four different sizes gold NPs (8-30 nm) have been synthesised to investigate the variation in the inter-particle distance of AuNPs during ligand exchange reaction by different purines. As NPs stability and particle size depending upon the surface charge, size-controlled AuNPs were achieved by varying the citrate ion concentration (Table 2.1). To analyse the size variation in AuNPs, UV-vis extinction spectra were recorded for each sample. It was observed that as the volume of citrate solution decreases (2000 µl to 400 µl), SPR shifts from 521 to 535 nm which is shown in Fig. 2.2. The red shifting of SPR was due to increment in the dipole-dipole interaction among AuNPs and dielectric constant of the medium i.e described in Mie scattering theory [33] and Maxwell-Garnett effective medium theory[16]. But on the addition of purines, the citrate layer gets disrupted that cause rapid particle aggregation and due to a decrease in the inter-particle distance, the SPR peak of AuNPs undergoes a red shift. According to Mie theory, this bathochromic shift occurred along the long axis of the AuNP chains due to longitudinal electronic plasma oscillation[34]. Also, upon the addition of purine to the citrate-stabilized gold particles, the color of all the AuNPs solutions becomes red to pink to blue indicating the formation of aggregates of AuNPs.

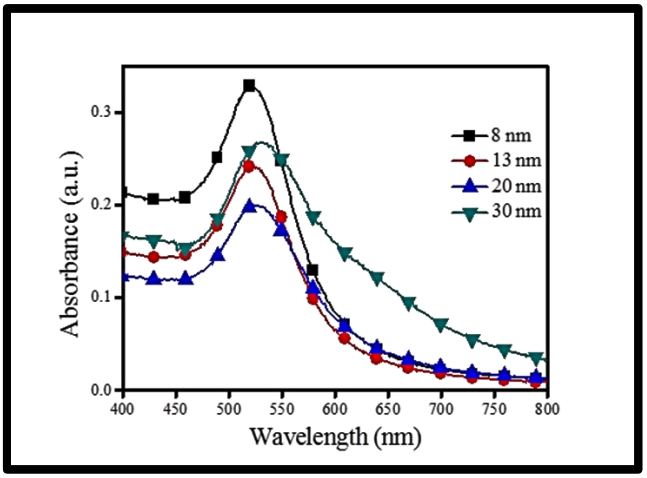

Fig. 2.2: UV-vis spectra for different size gold nanoparticles.

Surface zeta potential and average particle size were also recorded before and after the addition of purines in AuNPs which are listed in Table 2.2. High negative zeta potential (-32.1 mV) was observed for more citrate ion capped AuNPs which decreases the final size of the NPs. When purines were added to the colloidal AuNPs solution, their surface charge decreases due to placing exchange reaction [35] between purines and citrate ions. It is clear from the result that replacement of citrate ions with 6-TG molecules destabilised the NPs and leads to aggregation which was confirmed by the huge increase in average particle size (Table 2.2). It was found that average particle diameter increased on the addition of purines and more pronounced for larger particles. This rapid aggregation of AuNPs for larger size AuNPs is due to less negative surface charge and facile cross-linkage through sulphur and nitrogen between AuNPs and purines[34].

Table 2.2: Average diameter and zeta potential of AuNPs before and after the addition of purines.

Sample	Before addition of purines		After addition of purines	
	Diameter (nm)	Zeta-potential (mV)	Diameter (nm)	Zeta-potential (mV)
A	10	-32.1	70	-24.4
B	15	-24.7	115	-21.2
C	25	-20.4	150	-19.2
D	40	-17.5	200	-14.5

2.3.2 FTIR studies

To confirm the citrate capping and interaction of AuNPs with purines FTIR spectra were recorded in the spectral frame 400–4000 cm^{-1}. AuNPs show pronounced peak around 1500-1630 and 1305-1415 cm^{-1} due to the symmetric and asymmetric stretching vibration of COO^- [36] (Fig. 2.3) which justify the surface of AuNPs was functionalized with citrate moieties. The presence of surface-bound purines is justified when N–H stretch for free purines at 3100 cm^{-1} shifted to 3344 cm^{-1} for Au aggregates and S-H stretch/bending at 2338/600 cm^{-1} is disappeared (Fig. 2.4). The perceived observation showed that AuNPs have a stronger affinity for nitrogen and sulphur moieties. Even some pronounced peak of citrate moiety also disappears (Fig. 2.4). This confirms the interaction of purines with AuNPs and replacement of citrate moiety from the surface of AuNPs.

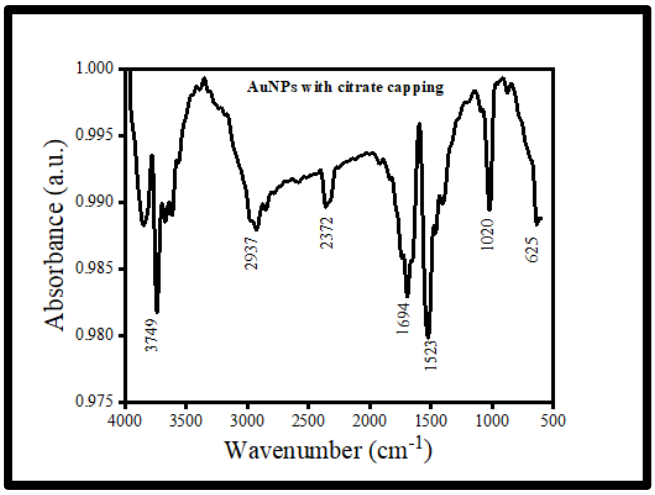

Fig. 2.3: FTIR spectra of citrate capped AuNPs

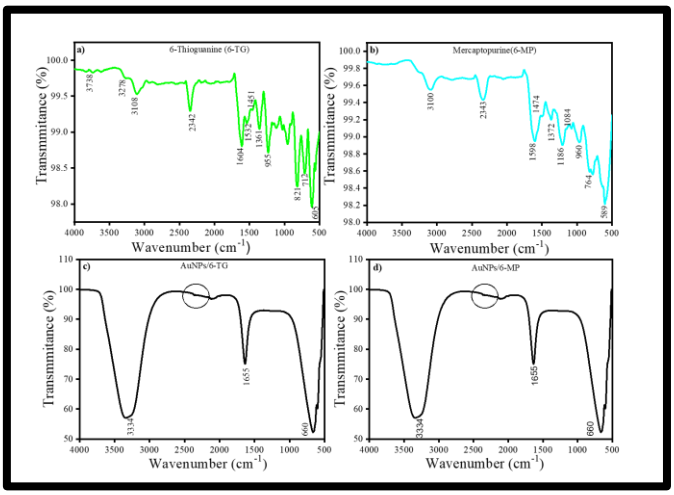

Fig. 2.4: FTIR spectra of a) pure 6-TG, b) pure 6-MP, c) 6-TG-induced and d) 6-MP induced gold nanoparticle aggregates at pH~4.

2.3.3 TEM studies

The synthesis process followed to obtain a broad range of AuNPs sizes that was observed from TEM images. The TEM images of citrate-capped AuNPs of four different sizes (8, 13, 20 and 30 nm) showed in Fig. 2.5, which confirms their mono-dispersity and non-aggregating nature. But upon addition of purines, AuNPs were aggregated which is shown in Fig. 2.6 From the TEM images, it is evident that there is no particular geometry of the aggregated particles is formed.

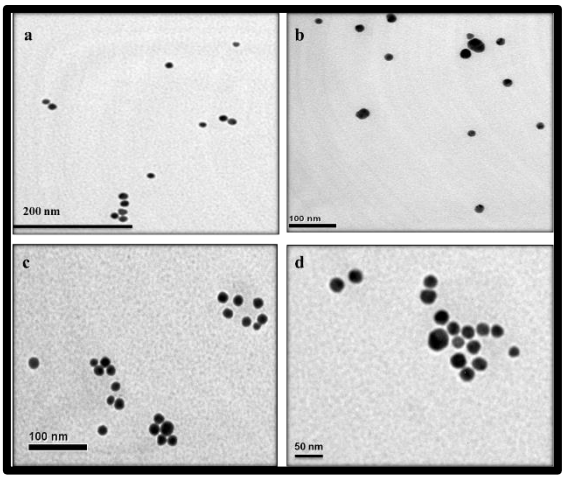

Fig. 2.5: TEM images of non-aggregated AuNPs a) 8 nm, b) 13 nm, c) 20 nm and d) 30 nm.

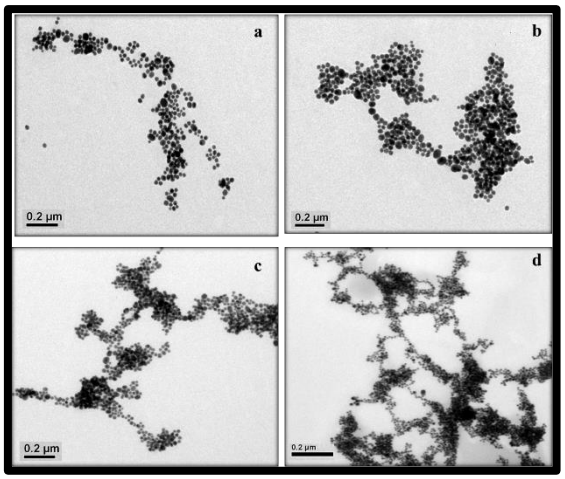

Fig. 2.6: TEM images for AuNPs aggregate A) 8 nm, B) 13 nm, C) 20 nm and D) 30 nm.

2.3.4 Stability and optimisation studies for sensing activity of AuNPs

The steadiness of colloidal nanoparticle systems is the key for proper applications in physical and biological disciplines which were based on Derjaguin-Laudua-Verwey-Overbeck (DLVO) theory [37]. It was found that citrate ions clouds around the AuNPs lead to $F_{ree} >> F_{ast}$ $_{Trac}$ due to negative surface charge that prevents their aggregation[16]. So, to study the effect of

pH and salt on their surface charge and its stability, UV-visible spectra were recorded at different pH and salt concentrations. When different volume (10-100 µl) of 0.1 M NaCl was added to AuNPs, the peak at 521 nm sustained (Fig. 2.7a.) but after 10-15 days, AuNPs aggregation starts in the presence of NaCl salt. Whereas in huge pH (4-12) range, the AuNPs are highly stable but at high acidic condition (pH <3) it leads to aggregation and the color change from red to purple to blue which was occurred due to surface charge neutralisation of AuNPs (Fig. 2.7b)[16]. After obtaining these outcomes, to sustain the stability of AuNPs fresh preparation is to be done and the only pH ~4 was advised to use for the detection of purines as at low pH, the binding efficiency of negatively charged AuNPs with protonated purines are enhanced.

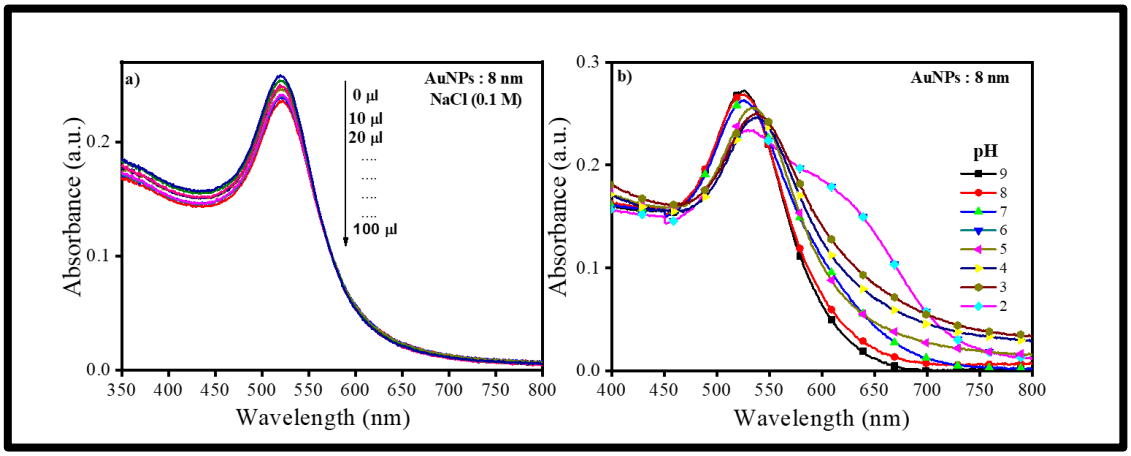

Fig. 2.7: UV-vis spectra to study the stability of gold nanoparticles at different a) volume of salt concentration and b) pH.

2.3.5 Kinetic study

2.3.5.1 Effect of reaction time

Kinetic studies were done to see the effect of purines on the inter-particle distance of AuNPs by measuring SPR. The absorption spectra for AuNPs and its mixture with purine were recorded at different time intervals. It was stated in Mie Theory [33] that single peak is attained due to the dipole plasma oscillation for AuNPs induced by an external field. When purines added to the colloidal solution of AuNPs, the inter-particle spacing between the particles decreases. With the increase of time, the first peak at 521 nm becomes weaker and the second peak at a longer wavelength (~700 nm) intensifies and red-shifted. But after 30 min peak variation get almost constant and blue color was obtained which confirms the completion of the place exchange reaction (Fig. 2.8).

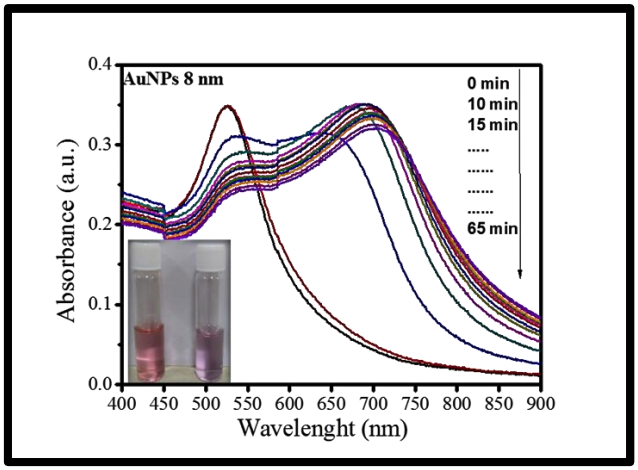

Fig. 2.8: Time-dependent UV-vis spectra recorded at various times after addition of purine (10 mM, 30 µl) in AuNPs (0.25 mM, 3 ml).

2.3.6 Quantitative detection of thiopurines

Morphology of AuNPs and optical properties vary with the concentration of biological moieties. To study the interaction and quantification of purines, the different molar ratio of [purines]/ [AuNPs] from 10^{-2}– 10^{-7} M were used. It was pragmatic that dipole plasmon of AuNPs shifted to higher λ_{max}, i.e. the intensity of the ~521 nm progressively weak and the shoulder crest nearly at ~700 nm overwhelms and showed a broad peak. Whereas with the decrease in some purines (10^{-2}-10^{-7} M) SPR peak position perceived at identical λ_{max}, i.e. 521 nm. This variation in the absorption spectrum of AuNPs and purines mixture was due to the change of inter-particle distance of AuNPs due to Au-S/Au-N interactions which get reduced for a dilute solution of purines[16,34]. When the different size of AuNPs was analysed with different concentrations of purine (10^{-2}– 10^{-7} M), it was found that larger size AuNPs (30 nm) was more sensitive towards purines even at their lower concentration (10^{-7} M), because large size AuNPs have small surface charge energy which triggers the aggregation process (Fig. 2.9 and 2.10). To analyse the sensitivity of AuNPs towards two different purines having similar functional groups, SPR peak displacement, $\Delta\lambda_{max}$ (between two dipole plasmon peaks) against particle size was plotted (Fig. 2.11). An almost linear increase in peak displacement against particle size is observed for 6-TG, but infinitesimal deviation for 6-MP. These investigations concluded that larger size AuNPs is more sensitive for purine molecule detection and the lower limit of detection is 10^{-7} M.

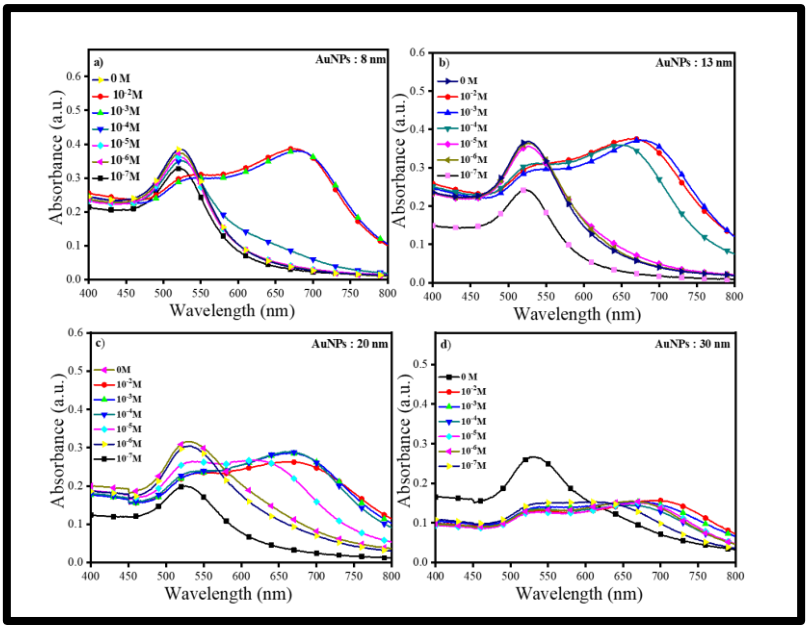

Fig. 2.9: UV-vis spectra of Au aggregates at various concentration of 6-TG at pH~4 using a) 8 nm, b) 13 nm, c) 20 nm and d) 30 nm AuNPs.

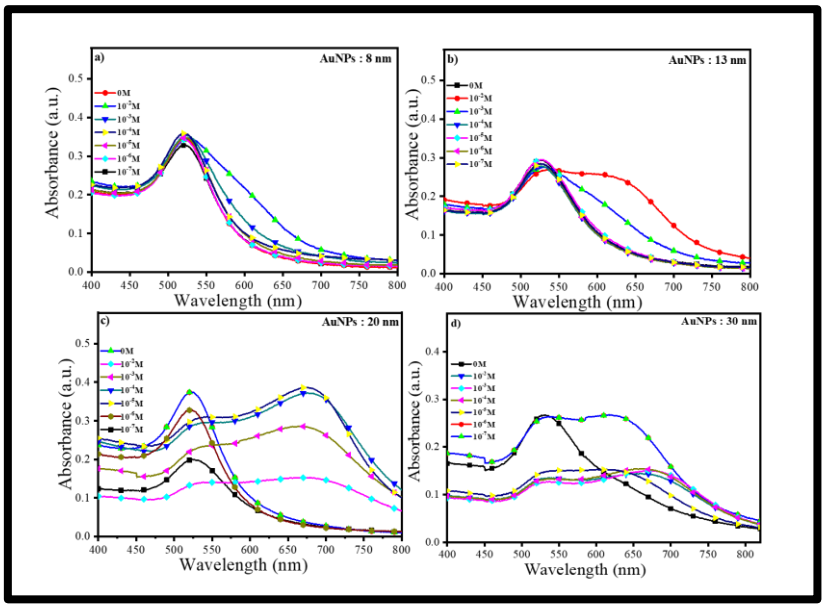

Fig. 2.10: UV-vis spectra of AuNPs aggregate at various concentration of 6-MP at pH~4 using a) 8 nm, b) 13 nm, c) 20 nm and d) 30 nm AuNPs.

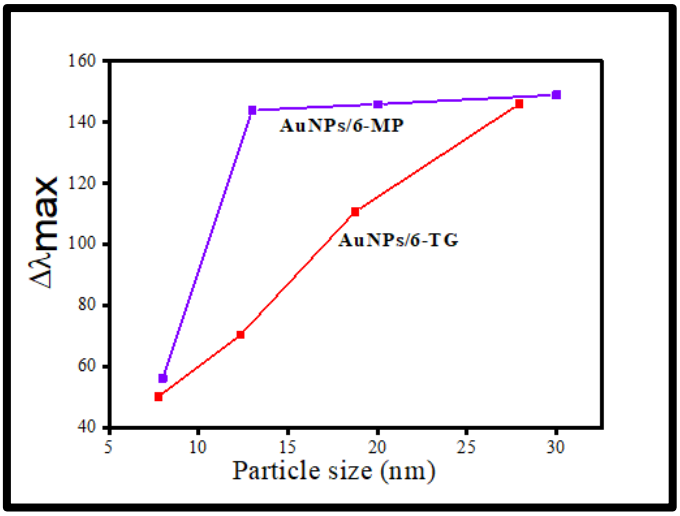

Fig. 2.11: Plot of $\Delta\lambda_{max}$ vs. particle size.

2.3.7 Comparison of different methods for sensing of thiopurines

A comparative study was done for detection of 6-TG with different known techniques by colorimetric/optical sensors (Table 2.3). It was found that our, as synthesised AuNPs are a highly efficient sensor for detection of purines and this system, may be used for several other biomolecules.

Table 2.3: A comparative account for the detection of 6-TG.

Methods	Detection system	Limit of detection (mM)	Reference
HPLC	Fluorescence	0.0027±0.02	38
DPSV	$[Fe(CN_6)]^{3-}$	0.2±0.0032	39
Spectrofluorometry	----	0.05±0.012	40
SEM	$Co(bpy)^{2+}$/ p-Aminophenol	0.12±0.0042	41,42
DPV	FDCCNTE	0.009±0.001	43

SPR	Different-Size AuNPs	10^{-4}	This work

References

(1) Lennard, L.; Lilleyman, J. S.; Van Loon, J.; Weinshilboum, R. M. Genetic Variation in Response to 6-Mercaptopurine for Childhood Acute Lymphoblastic Leukaemia. *Lancet* **1990**, *336* (8709), 225–229. https://doi.org/10.1016/0140-6736(90)91745-V.

(2) Al-Ghobashy, M. A.; Hassan, S. A.; Abdelaziz, D. H.; Elhosseiny, N. M.; Sabry, N. A.; Attia, A. S.; El-Sayed, M. H. Development and Validation of LC???MS/MS Assay for the Simultaneous Determination of Methotrexate, 6-Mercaptopurine and Its Active Metabolite 6-Thioguanine in Plasma of Children with Acute Lymphoblastic Leukemia: Correlation with Genetic Polymorphism. *J. Chromatogr. B Anal. Technol. Biomed. Life Sci.* **2016**, *1038*, 88–94. https://doi.org/10.1016/j.jchromb.2016.10.035.

(3) Munshi, P.; Lubin, M.; Bertino, J. 6-Thioguanine: A Drug with Unrealized Potential for Cancer Therapy. *Oncologist* **2014,** 19(7), 760-765.

(4) C.S., S. *Martindale: The Complete Drug Reference*; 2009.

(5) Oancea, I.; Png, C. W.; Das, I.; Lourie, R.; Winkler, I. G.; Eri, R.; Subramaniam, N.; Jinnah, H. A.; McWhinney, B. C.; Levesque, J.-P.; et al. A Novel Mouse Model of Veno-Occlusive Disease Provides Strategies to Prevent Thioguanine-Induced Hepatic Toxicity. *Gut* **2013**, *62* (4), 594–605. https://doi.org/10.1136/gutjnl-2012-302274.

(6) Tack, G. J.; Asseldonk, D. P.; Wanrooij, R. L. J.; Bodegraven, A. A.; Mulder, C. J. Tioguanine in the Treatment of Refractory Coeliac Disease - a Single Centre Experience. *Aliment. Pharmacol. Ther.* **2012**, *36* (3), 274–281. https://doi.org/10.1111/j.1365-2036.2012.05154.x.

(7) Fishman M; M, M.-O. *Cancer Chemotherapy Guidelines and Recomendations for Practice*; 1999.

(8) Madueño, R.; Pineda, T.; Sevilla, J. M.; Blázquez, M. An Electrochemical Study of 6-Thioguanine Monolayers on a Mercury Electrode in Acid and Neutral Solutions. *J.*

Electroanal. Chem. **2004**, *565* (2), 301–310. https://doi.org/10.1016/j.jelechem.2003.10.024.

(9) Rowland, K.; Lennard, L.; Lilleyman, J. S. High-Performance Liquid Chromatographic Assay of Methylthioguanine Nucleotide. *J. Chromatogr. B. Biomed. Sci. Appl.* **1998**, *705* (1), 29–37.

(10) Mawatari, H.; Kato, Y.; Nishimura, S. I.; Sakura, N.; Ueda, K. Reversed-Phase High-Performance Liquid Chromatographic Assay Method for Quantitating 6-Mercaptopurine and Its Methylated and Non-Methylated Metabolites in a Single Sample. *J. Chromatogr. B Biomed. Appl.* **1998**, *716* (1–2), 392–396. https://doi.org/10.1016/S0378-4347(98)00329-6.

(11) Keuzenkamp-Jansen, C. W.; De Abreu, R. A.; Bökkerink, J. P. M.; Trijbels, J. M. F. Determination of Extracellular and Intracellular Thiopurines and Methylthiopurines by High-Performance Liquid Chromatography. *J. Chromatogr. B Biomed. Sci. Appl.* **1995**, *672* (1), 53–61. https://doi.org/10.1016/0378-4347(95)00206-X.

(12) Lennard, L.; Singleton, H. J. High-Performance Liquid Chromatographic Assay of the Methyl and Nucleotide Metabolites of 6-Mercaptopurine: Quantitation of Red Blood Cell 6-Thioguanine Nucleotide, 6-Thioinosinic Acid and 6-Methylmercaptopurine Metabolites in a Single Sample. *J. Chromatogr. B Biomed. Sci. Appl.* **1992**, *583* (1), 83–90. https://doi.org/10.1016/0378-4347(92)80347-S.

(13) Lennard, L. Assay of 6-Thioinosinic Acid and 6-Thioguanine Nucleotides, Active Metabolites of 6-Mercaptopurine, in Human Red Blood Cells. *J. Chromatogr. B Biomed. Sci. Appl.* **1987**, *423* (C), 169–178. https://doi.org/10.1016/0378-4347(87)80340-7.

(14) Lennard, L. Assay of 6-Mercaptopurine in Human Plasma. *J. Chromatogr. B Biomed. Sci. Appl.* **1985**, *345*, 441–446. https://doi.org/10.1016/0378-4347(85)80186-9.

(15) Lavi, L. E.; Holcenberg, J. S. A Rapid and Sensitive High-Performance Liquid Chromatographic Assay for 6-Mercaptopurine Metabolites in Red Blood Cells. *Anal. Biochem.* **1985**, *144* (2), 514–521. https://doi.org/10.1016/0003-2697(85)90148-4.

(16) Basu, S.; Ghosh, S. K.; Kundu, S.; Panigrahi, S.; Praharaj, S.; Pande, S.; Jana, S.; Pal,

T. Biomolecule Induced Nanoparticle Aggregation: Effect of Particle Size on Interparticle Coupling. *J. Colloid Interface Sci.* **2007**, *313* (2), 724–734. https://doi.org/10.1016/j.jcis.2007.04.069.

(17) Zhong, Z.; Patskovskyy, S.; Bouvrette, P.; Luong, J. H. T.; Gedanken, A. The Surface Chemistry of Au Colloids and Their Interactions with Functional Amino Acids. *J. Phys. Chem. B* **2004**, *108* (13), 4046–4052. https://doi.org/10.1021/jp037056a.

(18) Lubomirsky, I.; Wang, T. Y.; Gartsman, K.; Connolly, S.; Fitzmaurice, D. Biologically Programmed Nanoparticle Assembly. *Adv. Mater.* **2000**, *12* (2), 147–150. https://doi.org/10.1002/(SICI)1521-4095(200001)12:2<147::AID-ADMA147>3.0.CO;2-U.

(19) Mrksich, M. A Surface Chemistry Approach to Studying Cell Adhesion. *Chem. Soc. Rev.* **2000**, *29* (4), 267–273. https://doi.org/10.1039/a705397e.

(20) Bright, R. M.; Walter, D. G.; Musick, M. D.; Jackson, M. a.; Allison, K. J.; Natan, M. J. Chemical and Electrochemical Ag Deposition onto Preformed Au Colloid Monolayers: Approaches to Uniformly-Sized Surface Features with Ag-Like Optical Properties. *Langmuir* **1996**, *12* (3), 810–817. https://doi.org/10.1021/la950429h.

(21) Alvarez, M. M.; Khoury, J. T.; Schaaff, T. G.; ShaFig. ullin, M. N.; Vezmar, I.; Whetten, R. L. Optical Absorption Spectra of Nanocrystal Gold Molecules. *J. Phys. Chem. B* **1997**, *101* (19), 3706–3712. https://doi.org/10.1021/jp962922n.

(22) Takeuchi, Y.; Ida, T.; Kimura, K. Temperature Effect on Gold Nanodispersion in Organic Liquids. *Surf. Rev. Lett.* **1996**, *3* (1), 1205–1208. https://doi.org/10.1142/S0218625X96002175.

(23) Kreibig, U.; Genzel, L. Optical Absorption of Small Metallic Particles. *Surf. Sci.* **1985**, *156* (PART 2), 678–700. https://doi.org/10.1016/0039-6028(85)90239-0.

(24) Thanh, N. T. K.; Rosenzweig, Z. Development of an Aggregation Based Immunoassay for Anti Protein a Using Gold Nanoparticles. *Abstr. Pap. Am. Chem. Soc.* **2002**, *223*, U74–U74.

(25) Andrew Lyon, L.; Musick, M. D.; Natan, M. J. Colloidal Au-Enhanced Surface Plasmon

Resonance Immunosensing. *Anal. Chem.* **1998**, *70* (24), 5177–5183. https://doi.org/10.1021/ac9809940.

(26) Musick, M. D.; Keating, C. D.; Lyon, L. A.; Botsko, S. L.; Pena, D. J.; Holliway, W. D.; McEvoy, T. M.; Richardson, J. N.; Natan, M. J. Metal Films Prepared by Stepwise Assembly. 2. Construction and Characterization of Colloidal Au and Ag Multilayers. *Chem. Mater.* **2000**, *12* (10), 2869–2881. https://doi.org/10.1021/cm990714c.

(27) Storhoff, J. J.; Mucic, R. C.; Mirkin, C. a. Strategies for Organizing Nanoparticles into Aggregate Structures and Functional Materials. *J. Clust. Sci.* **1997**, *8* (2), 179–216. https://doi.org/1040-7278/97/0600-0179.

(28) Freeman, R. G.; Grabar, K. C.; Allison, K. J.; Bright, R. M.; Davis, J. A.; Guthrie, A. P.; Hommer, M. B.; Jackson, M. A.; Smith, P. C.; Walter, D. G.; et al. Self-Assembled Metal Colloid Monolayers: An Approach to SERS Substrates. *Science (80-.).* **1995**, *267* (5204), 1629–1632. https://doi.org/10.1126/science.267.5204.1629.

(29) Taton, T.; Mirkin, C.; Letsinger, R. Scanometric DNA Array Detection with Nanoparticle Probes. *Science* **2000**, *289* (5485), 1757–1760. https://doi.org/10.1126/science.289.5485.1757.

(30) Storhoff, J. J.; Elghanian, R.; Mucic, R. C.; Mirkin, C. a; Letsinger, R. L. Article One-Pot Colorimetric Differentiation of Polynucleotides with Single Base Imperfections Using Gold Nanoparticle Probes One-Pot Colorimetric Differentiation of Polynucleotides with Single Base Imperfections Using Gold Nanoparticle Probes. *J. Am. Chem. Soc.* **1998**, *7863* (97), 1959–1964. https://doi.org/10.1021/ja972332i.

(31) Elghanian, R.; Storhoff, J. J.; Mucic, R. C.; Letsinger, R. L.; Mirkin, C. A. Selective Colorimetric Detection of Polynucleotides Properties of Gold Nanoparticles Selective Colorimetric Detection of Polynucleotides Based on the Distance-Dependent Optical Properties of Gold Nanoparticles. *Science (80-.).* **2010**, *1078* (1997), 1078–1081. https://doi.org/10.1126/science.277.5329.1078.

(32) Templeton, A. C.; Chen, S.; Gross, S. M.; Murray, R. W. Water-Soluble, Isolable Gold Clusters Protected by Tiopronin and Coenzyme A Monolayers. *Langmuir* **1999**, *15* (1), 66–76. https://doi.org/10.1021/la9808420.

(33) Physik, A. D. E. R.; Vol, N. (Beiträge Zur Optik Trüber Medien , Speziell Kolloidaller Metallösungen ; von Gustav Mie). *Ann. Phys.* **1908**, *25*, 1–52.

(34) Basu, S.; Pande, S.; Jana, S.; Bolisetty, S.; Pal, T. Controlled Interparticle Spacing for Surface-Modified Gold Nanoparticle Aggregates Controlled Interparticle Spacing for Surface-Modified Gold Nanoparticle Aggregates. *Society* **2008**, No. 13, 8276–8282. https://doi.org/10.1021/la8000784.

(35) Park, J.; Shumaker-parry, J. S. Structural Study of Citrate Layers on Gold Nanoparticles : Role of Intermolecular Interactions in Stabilizing Nanoparticles. *Langmuir* **2005**, *21* (21), 1–33. https://doi.org/10.1021/la0504560.

(36) Park, J. W.; Shumaker-Parry, J. S. Structural Study of Citrate Layers on Gold Nanoparticles: Role of Intermolecular Interactions in Stabilizing Nanoparticles. *J. Am. Chem. Soc.* **2014**, *136* (5), 1907–1921. https://doi.org/10.1021/ja4097384.

(37) Ghosh, S. K.; Pal, T. Interparticle Coupling Effect on the Surface Plasmon Resonance of Gold Nanoparticles: From Theory to Applications. *Chemical Reviews*. 2007, pp 4797–4862. https://doi.org/10.1021/cr0680282.

(38) Olesen, K. M.; Hansen, S. H.; Sidenius, U.; Schmiegelow, K. Determination of Leukocyte DNA 6-Thioguanine Nucleotide Levels by High-Performance Liquid Chromatography with Fluorescence Detection. *J. Chromatogr. B Anal. Technol. Biomed. Life Sci.* **2008**, *864* (1–2), 149–155. https://doi.org/10.1016/j.jchromb.2008.02.007.

(39) Warren, D. J.; Slørdal, L. A High-Performance Liquid Chromatographic Method for the Determination of 6-Thioguanine Residues in DNA Using Precolumn Derivatization and Fluorescence Detection. *Anal. Biochem.* **1993**, *215* (2), 278–283. https://doi.org/10.1006/abio.1993.1587.

(40) Thomas, A. Spectrofluorometric Determination of Thiopurines—I: 6-Thioguanine. *Talanta* **1976**, *23* (5), 383–386. https://doi.org/10.1016/0039-9140(76)80051-3.

(41) Wang, W.; Wang, S. F.; Xie, F. An Electrochemical Sensor of Non-Electroactive Drug 6-Thioguanine Based on the DsDNA/AET/Au. *Sensors Actuators, B Chem.* **2006**, *120* (1), 238–244. https://doi.org/10.1016/j.snb.2006.02.012.

(42) Mirmomtaz, E.; Ensafi, A. A.; Karimi-Maleh, H. Electrocatalytic Determination of 6-Tioguanine at a p-Aminophenol Modified Carbon Paste Electrode. *Electroanalysis* **2008**, *20* (18), 1973–1979. https://doi.org/10.1002/elan.200804273.

(43) Ensafi, A. A.; Karimi-Maleh, H. Modified Multiwall Carbon Nanotubes Paste Electrode as a Sensor for Simultaneous Determination of 6-Thioguanine and Folic Acid Using Ferrocenedicarboxylic Acid as a Mediator. *J. Electroanal. Chem.* **2010**, *640* (1–2), 75–83. https://doi.org/10.1016/j.jelechem.2010.01.010.

CHAPTER-3

Selective Detection of Fluoride Ions by Using Oxygen and Nitrogen Rich C-dots and its Logic Gate Implementation

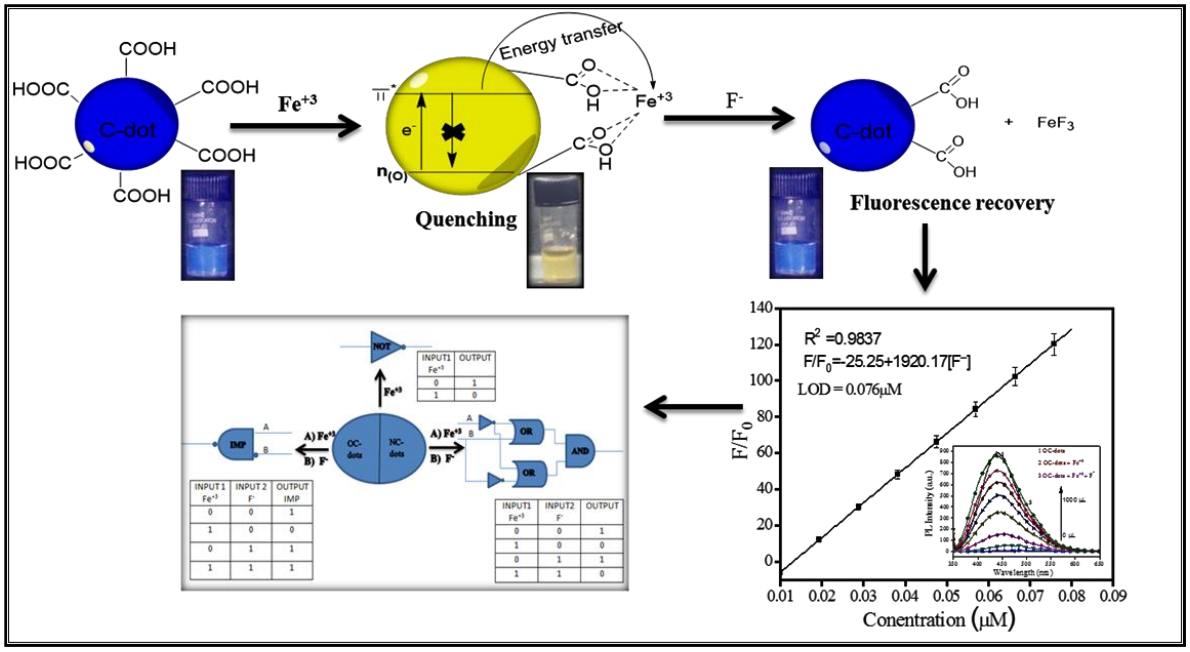

Highlights

- Nitrogen and oxygen-enriched C-dots were synthesized by green precursors.
- C-dots were acting as a nanoprobe for selective and sensitive detection of metal ions.
- Turn-on/-off PL property of C-dots was used for fluoride ion sensing.
- Designing of the logic gate was done to implement it in electronic devices.
- The efficiency of the probe was tested with real samples (tap/lake water).

3.1 Introduction

Heavy metal anions and cations (e.g. arsenic, iron, copper, fluoride, nitrates, and phosphates) are useful for a biological system. However, due to industrial growth and human activities, their content gets increased beyond their permissible limit which leads to a reduction of natural resources and ruthless effect on human health. Among all the heavy metals cations/anions, F^- ions (>1.5 mg/l) [1,2] are considered as one of the major water pollutants [1,3]. It shows several physiological changes in plants that affect their root, shoot and leaf elongation of crops which are not visible to naked eyes but that can affect the food production. Even their excess intake in the human body, it can damage bones, teeth, and kidney [2,4], inhibit IQ development of children [5–7]. So, there is a necessity for identifying the areas affected by these contaminants mainly F^- ions to help in treating the groundwater in such areas.

Several analytical methods e.g. potentiometric (ion-selective electrode [ISE]) [3], gas chromatographic (GC) [8], colorimetric [9], fluorometric, enzymatic, proton activation analysis [8] have been sanctioned by federal agencies and organizations such as Environmental Protection Agency (EPA), National Institute for Occupational Safety and Health (NIOSH) for the detection of F^- ions in the environment. Inclusively, all these techniques are not suitable as it requires sophisticated instrumentation, expensive reagents, cumbersome sample preparation, which increases the cost and analytical complexity of the sensing probe. The best alternative to overcome these problems is nano-sensors, as they have the ability for rapid, accurate, compact and portable determination of organic and inorganic moieties.

Several fluorescent nanomaterials are known such as semiconductor quantum dots (SQDs) that were used in detecting toxic ions due to their high stability, high extinction coefficient, and high photoluminescence quantum yield (PLQY) [10–15]. However, their applicability in the real sample is debatable due to their inherent toxicity [12,13]. Therefore, the newly emerging class of nano-carbons, i.e. C-dots [16–18] can be an ideal material to replace all the conventional fluorescent probes due to their high aqueous stability, high biocompatibility, and low toxicity. Due to its unique turn-on/turn-off PL property in the presence of foreign moieties [1,2,19,20], many scientists fabricated C-dots and its composites for the detection of several toxins. Dong *et al.* [21] have synthesized polyamine-functionalized C-dots for the

selective and sensitive detection of copper ions (LOD = 6 nM). Xu *et al.* [22] have detected food colouring dyes (tartrazine) by C-dots prepared from greener material (aloe) and their detection range found between 0.25 to 32.50 µM. Mohapatra *et al.* [2] have prepared a highly selective composite system using C-dots (fluorophore) and magnetically separable nickel ethylenediaminetetraacetic acid complex-bound silica-coated magnetite (fluoride receptor). The method was based on the exchange reaction between C-dots and F^- ions, which influence the binding of fluoride to the magnetic receptor with a minimum detection limit of 0.06 µM. Furthermore, Lui *et al.*[1] and Basu *et al*.[5] have prepared new improved C-dots/composites (e.g. zirconium-complex, tapioca, etc.) which were used in real samples to check their applicability in determining fluoride ions in environmental matrices. But all the above-mentioned processes, the material preparation was tedious and sensing principle was not explained which is important to understand and design sensing probes. All the aforementioned studies showed that there is a need to develop simple materials with a suitable explanation of their working mechanism. Different strategies were explored such as supramolecular recognition [23–25], hydrogen bonding [24,26], and Lewis acid-base interactions [24,27,28] to develop the low cost, non-hazardous and portable fluorescent probe which can be used in resourced laboratories and in the different environmental matrices.

Herein, we have emphasized on the green synthesis of C-dots using mosambi peels (*Citrus limetta*) as well as non-toxic precursors such as ascorbic acid /urea respectively to develop the turn-off/-on strategy for the detection of fluoride ions. Besides, OC-dots and NC-dots were implemented in different logic gate such as NOT, OR, IMP to design improved nano-electric devices. Subsequently, the sensing efficiency of the probe was tested in real samples and further compared with inductively coupled plasma atomic emission spectroscopy (ICP-AES) results.

3.2 Experimental section

3.2.1 Chemical and materials

Mosambi peels (*Citrus limetta*) were collected from a local fruit vendor. Other reagents like ascorbic acid, urea and dichloromethane were purchased from Sigma-Aldrich. Double distilled water (18.2 MΩ, Millipore) was used for the preparation of different C-dots and a stock solution of metal ions.

3.2.2 Preparation of C-dots

Microwave and ultrasonic routes were used to prepare the C-dots from mosambi peels and citric acid /urea respectively. Firstly, washed mosambi peels were dried in an oven (100 °C) for 24 hours and carbonized at 220 °C for 2 hours under air atmosphere. The carbonized powdered material (2 g) was sonicated at frequency of 30 kHz for 45 min to obtain a brown color suspension. To remove the organic impurities, washing was done for 5 times with dichloromethane. Finally, the purified suspension was filtrated with 0.2 μm membrane to obtain a yellow suspension of 2.28 mg/ml C-dots. The C-dots synthesized by this waste mosambi peel was named as OC-dots, where 'O' represents 'oxygen' enriched C-dots surface.

For the preparation of nitrogen-rich C-dots, 1 g ascorbic acid and 3 g urea were mixed in 15 ml of water and heated at 130 °C for 3 minutes in a microwave (50 W). The obtained mixture was kept to cool down and centrifuged at 9000 rpm for 10 min to eliminate suspended impurities to obtain the pure C-dots (3.2 mg/ml). The C-dots synthesized by these reagents was named as NC-dots, where 'N' represents 'nitrogen' enriched C-dots surface.

3.2.3 Determination of PLQY

The quantum yield (ϕ) for both OC-dots and NC-dots was evaluated by using quinine sulphate as a reference (from literature ϕ'=0.54) dissolved in 0.1M H_2SO_4 (refractive index $\acute{\eta}$=1.33). The integrated PL intensities and absorbency values were calculated for the reference quinine sulphate and both the C-dots were dissolved in deionised water ($\acute{\eta}'$=1.33) by subsequent equation-1:

$$\phi = \phi' \times (I/I') \times (A'/A) \times (\acute{\eta}^2/\acute{\eta}'^2) \qquad 1$$

Where 'φ' denotes as the quantum yield, 'φ_R' is PLQY of reference, 'I' as the integrated area of fluorescence intensity, 'A' as the absorbance value and 'η' as refractive index.

3.2.4 Methodology for detecting cations/anions

Stock solution (10^{-3} M) for different metal ions was prepared using metal salts like ferric nitrate, copper nitrate, nickel nitrate, lead nitrate, calcium nitrate, magnesium nitrate, and cadmium nitrate to study their interaction with different C-dots (OC-dots and NC-dots). Then the aqueous solution of metal ions was mixed with C-dots (4000 μl), which was kept for 10 min to study their PL quenching efficiency. Furthermore, to perform its PL recovery experiment with anions, (e.g. fluoride, chloride, phosphate, nitrate and sulphate, etc.) different amount of aqueous solution of anions (1 – 10 μM) was added into the mixture of C-dots and Fe^{3+} ions (4000 μl + 750 μl).

3.2.5 Analysis of fluoride ion in the real sample

Tap and lake water was collected from different cities (Patiala, Ludhiana) of Punjab, India to determine the sensitivity of the probe in a real sample. Firstly, the water samples were filtered with 0.22 µm syringe filter and the determination of heavy metals was done using ICP-AES. Then tap/lake water was spiked with different concentration (2-8 µM) of fluoride ions, to evaluate the sensing efficiency of the probe which was assessed through ICP-AES technique.

3.2.6 Instrumentation

The morphology and composition of the prepared C-dots were characterized by using high-resolution transmission electron microscopy (HRTEM) operating at 200 KeV. For HRTEM analysis, samples were prepared by drop-casting of 10 µl purified C-dots dispersions on the carbon-coated copper grid and allowing the excess of solvent to evaporate. The fluorescence emission spectra were collected by using LS-55 spectrofluorophotometer (Perkin Elmer). The hydrodynamic size and zeta potential was determined by Microtrac's dynamic light scattering (DLS), Nanotrac. Elemental analysis was done by CHN analyzer (Thermo scientific flash 2000). Fourier transform infrared spectroscopy-attenuated total reflectance (FTIR-ATR, Agilent Resolution Pro-carry 660) was recorded to know the different functional groups on the surface of two different C-dots.

3.3 Result and discussion

3.3.1 Characteristics of C-dots

The prepared OC-dots and NC-dots were characterized by HRTEM, FTIR, CHN analyzer and fluorescence spectrometry. Firstly, the formation of OC-dots and NC-dots was confirmed from its yellow color suspension and blue/ green fluorescence under the UV lamp. The stability of OC-dots and NC-dots were also evaluated. It was found that with the exposure of light for 30 minutes the PL intensity remain undisturbed for both OC-dots (λ_{em} =438 nm) and NC-dots (λ_{em} = 455 nm) shown in Fig. 3.1a & 3.1b. Even a high concentration of NaCl salt (0.1 M) does not show any effect on the stability of both C-dots which confirmed its reusability for the detection of fluoride ions (Fig. 3.1c). The quantum yield of both OC-dots and NC-dots was found 34% and 15% investigated w.r.t the reference, i.e. quinine sulphate.

The HRTEM images demonstrate that both the C-dots were partially monodispersed and spherical. The average diameters of OC-dots and NC-dots were 2 ± 0.50 and 4 ± 2 nm respectively, which is shown in Fig. 3.2a & 3.2b. The FTIR spectrum of OC-dots exhibits absorption peak at 3347 cm^{-1} (O-H stretching), 1638.5 cm^{-1} (O-H bending), 1744.5 cm^{-1}, 1638.5 cm^{-1} (C=O group), and 1512 cm^{-1} (C=C stretching of aromatic compounds). The NC-dots had sharp bands between 1000 and 1500 cm^{-1} due to –CO, -CH, -CN which confirmed the presence of different functional groups on the surface of C-dots (Fig. 3.3a & 3.3b). The CHN analysis was done to evaluate its elemental composition. According to the percentage distribution of elements mentioned in Table 3.1, NC-dots contained more nitrogen (30.4%) w.r.t OC-dots (6%), maybe due to the utilization of nitrogen-containing precursor in NC-dots, i.e. urea.

Table 3.1: Representation of elemental composition of OC-dots and NC-dots.

Material	Carbon (%)	Hydrogen (%)	Oxygen (%)	Nitrogen (%)
OC-dots	52.8	20.8	20.4	6
NC-dots	48.3	15.2	10.8	30.4

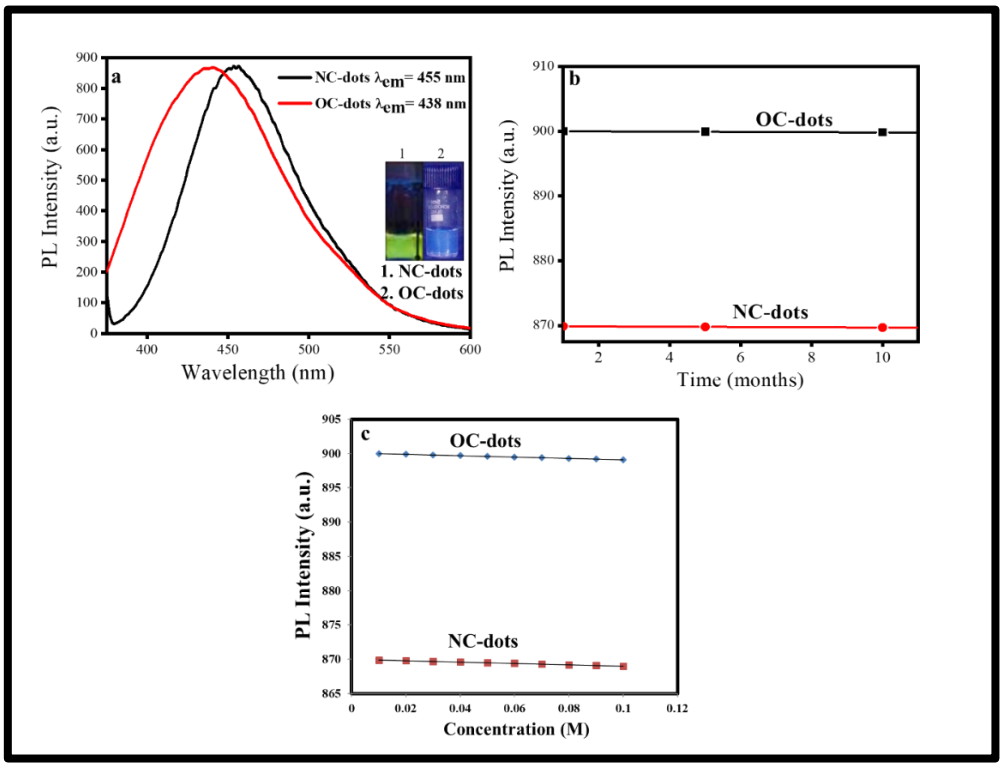

Fig. 3.1: Photoluminescence properties of C-dots a) PL intensity of different surface passivated C-dots, b) effect of light on PL intensity of C-dots and c) effect of different concentration of NaCl.

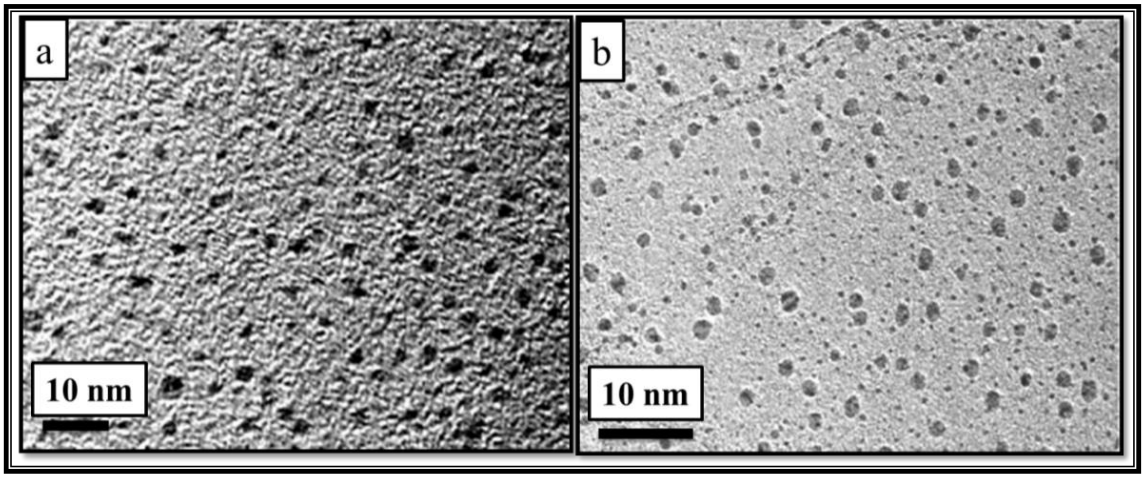

Fig. 3.2: HRTEM image of a) OC-dots prepared from mosambi peels and b) NC-dots prepared from ascorbic acid and urea.

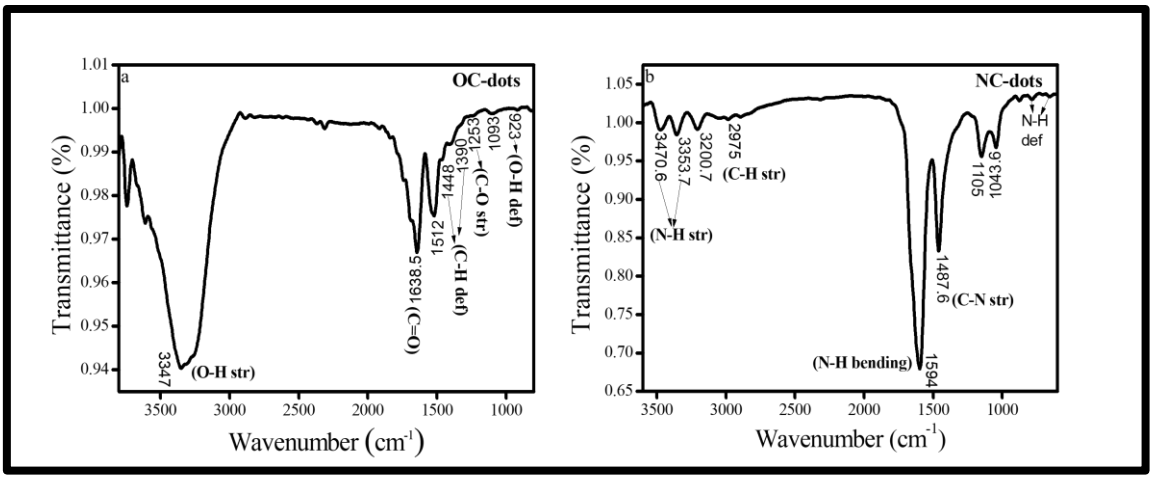

Fig. 3.3: FTIR spectra of a) OC-dots prepared from mosambi peels and b) NC-dots prepared from ascorbic acid and urea.

3.3.2 Optimization of reaction conditions for the detection of fluoride ions

The efficiency of the fluorescent probe depends on numerous parameters such as pH, temperature, excitation wavelength and a slit width of fluorescence spectroscopy. So, to enhance the sensitivity and selectivity of the sensing probe, there is a requirement to optimize the reaction conditions. Here, we have used different concentration and slit width to access the variation in its PL intensity. It was found that, 4 ml of C-dots with both the slit width 5 nm and 10 nm, exhibited maximum PL intensity (Fig. 3.4a and 3.4b). The effect of pH was also recorded for both the C-dots on its PL intensity (Fig. 3.4c & 3.4d). The results demonstrated that pH~6 was suitable for performing PL quenching and recovery experiment. Whereas, a highly acidic and basic condition found inappropriate due to protonation of carboxylic groups

and formation of $Fe(OH)_3$ [29,30], which result in weaker interaction of C-dots with Fe^{3+} ions and reduction in its sensing efficiency.

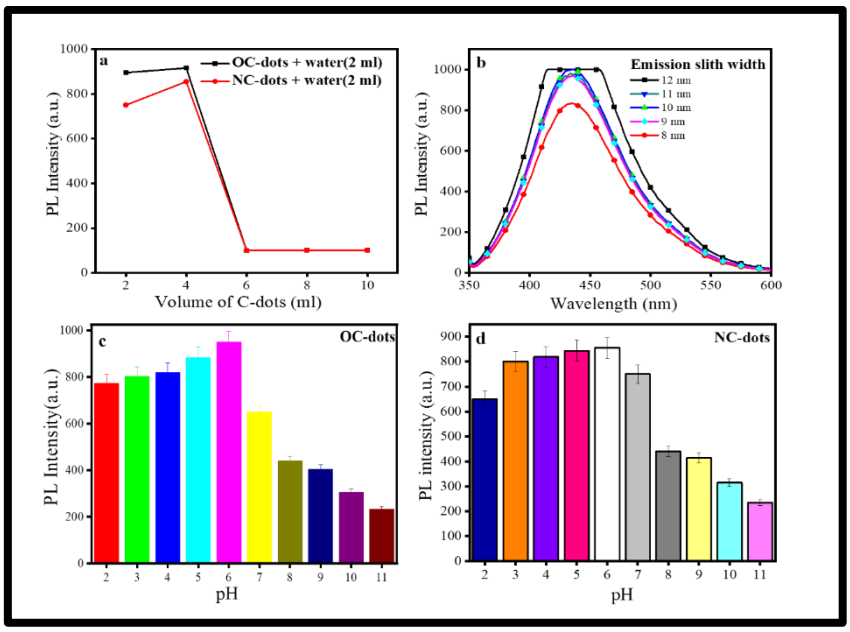

Fig. 3.4: Optimization of experimental conditions: a) effect of different quantity of C-dots, b) effect of emission slit width at constant excitation slit width, and c, d) effect of pH on the fluorescence intensity at λ_{ex}=340 and 350 nm for OC-dots and NC-dots respectively.

3.3.3 Selectivity of C-dots towards different cations

Selectivity is a crucial parameter to evaluate the performance of chemo-sensor. So, the interaction of different C-dots was examined with different metal ions (e.g. Fe^{3+}, Cu^{2+} Cd^{2+}, Zn^{2+}, Na^{+}, Ca^{2+}, Mg^{2+}, Pb^{2+}, Fe^{+2} and Ni^{2+}) by estimating the variation in its PL intensity. The experimental results revealed that Fe^{3+} ions exhibited maximum fluorescence quenching for both C-dots (~94.8%) due to strong interaction with carboxylic/amino/ hydroxyl groups on the surface of C-dots (Fig. 3.5). This quenching mechanism was explained based on hard-soft-acid–base (HSAB) principle, where Fe^{3+}ions was hard acid [30] and –COOH group acted as hard base which increased its affinity w.r.t to other cations. As Cu^{+2} ions belong to borderline metals, it also shows PL quenching to some extent among all other metal ions [31] (Fig. 3.6). So, these two specific cations (Fe^{3+} and Cu^{2+}) were used to perform recovery experiment (turn-on) with fluoride ions.

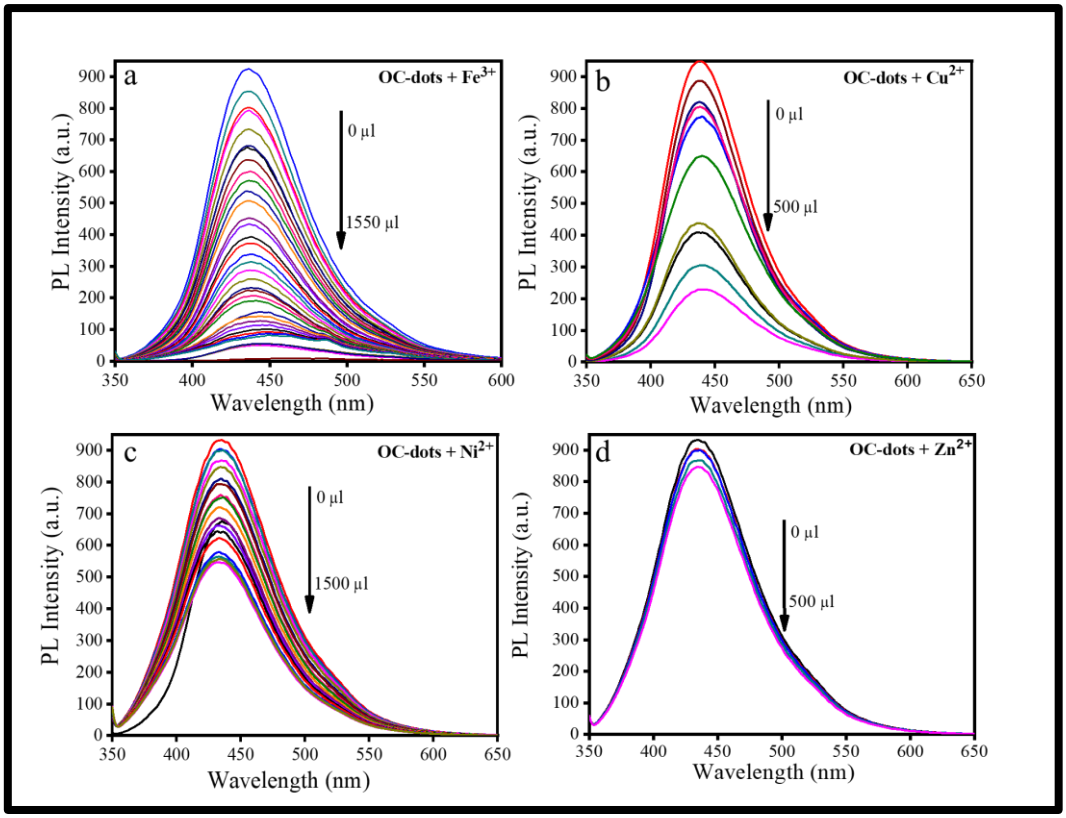

Fig. 3.5: Fluorescence quenching spectra of OC-dots in the presence of different ions.

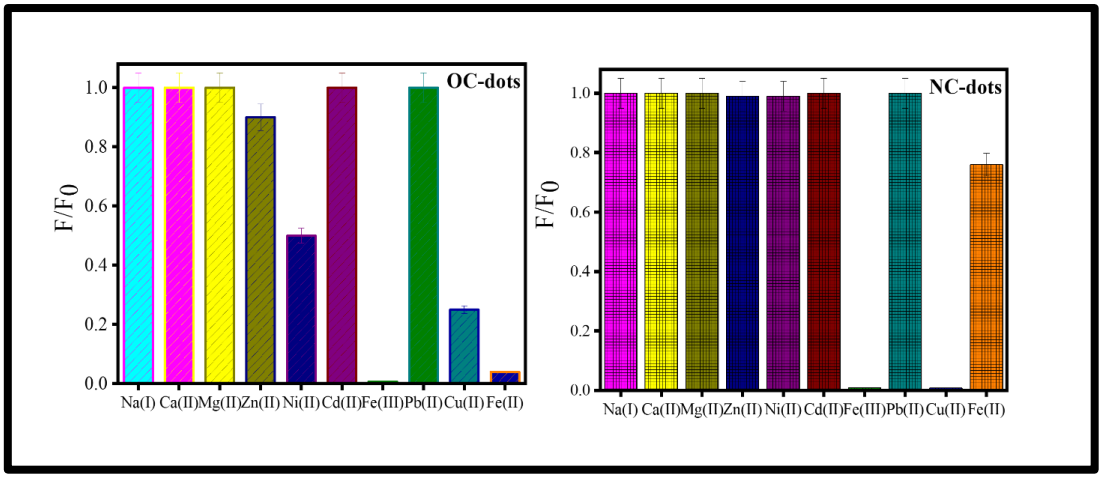

Fig. 3.6: Evaluation of fluorescence intensity for the selectivity of OC-dots/NC-dots towards different metal cations.

Further, the investigation for the sensitivity of C-dots with different concentration of ferric ions (0 to 0.4×10^{-5} M), the plot of F_0/F vs. quencher concentration was done according to Stern-Volmer equation, i.e.

$$F_0/F = 1+K_{SV}[Q]$$

Where F_0 and F are the fluorescence intensities of the fluorophore in the absence and presence of quencher Q, respectively, K_{SV} is the Stern Volmer constant (M^{-1}) and [Q] is the concentration of the quencher. To determine whether quenching is static or dynamic, the Stern-Volmer constant value was recorded at three different temperatures (25, 35 and 45˚C). There was no significant change found in the value of $K_{SV} = 38.22 \times 10^{-5}$ M^{-1} which indicated that the quenching process was static in nature (shown in Fig. 3.7).

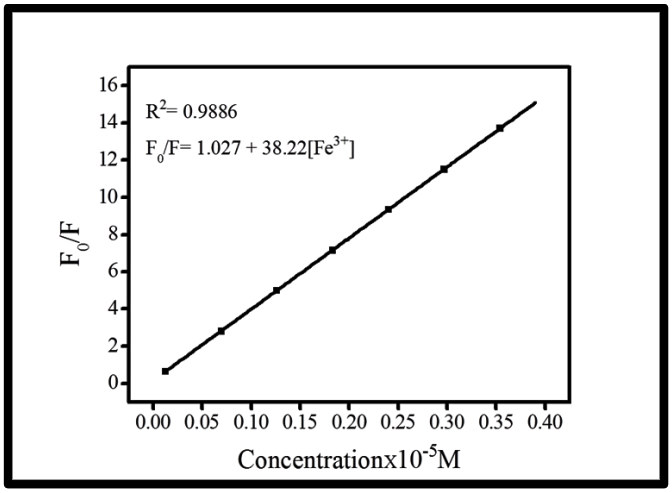

Fig. 3.7: Stern-Volmer plot F_0/F vs Quencher concentration (Fe^{+3} ions).

3.3.4 Turn-off/-on mechanism

The variation in photoluminescence intensity and zeta potential was studied for the foundation of conceivable sensing mechanism of the probe. To determine the sensing mechanism initially, the variation in photoluminescence intensity was estimated for both C-dots and ferric ion sensor system. It was found that in the presence of fluoride ions, the PL intensity was recovered only for the OC-dots, not for NC-dots (Fig. 3.8). This is due to the stronger affinity of free amino groups on the surface of NC-dots with ferric ions which results in an inhibition of FeF_3 complex formation [32]. From the CHN analysis, it was cleared that, the surface of NC-dots was nitrogen-rich (amino group) but OC-dots were oxygen-rich (carboxylic acid group). So, OC-dots and ferric ion mixture found sensitive for fluoride ions, based on the HSAB rule hard acid (Fe^{+3}) and hard base (F^-) showed more interaction which leads to the formation of a stable FeF_3 ionic compound with high lattice energy 5870 kJ mol^{-1} and responsible for its fluorescent enhancement (as OC-dots are free) [5].

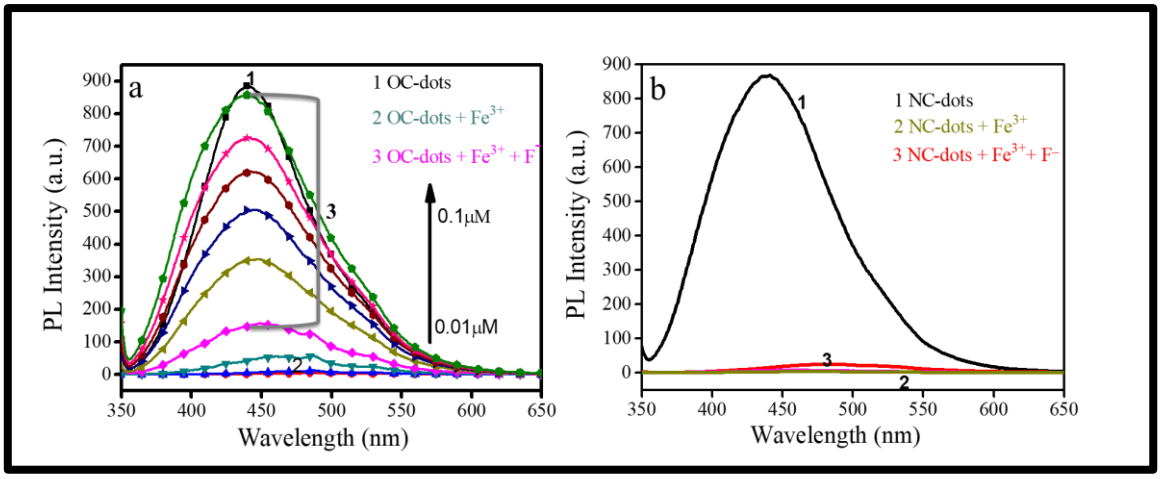

Fig. 3.8: Sensitivity of a) OC-dots and b) NC-dots towards F^- ion in the presence of Fe^{3+} ions.

Furthermore, the zeta potential was recorded for both the C-dots in the absence and presence of ferric and fluoride ions (Table 3.2). The results explained that the presence of Fe^{3+} ions in the ratio of 4:0.75 leads to a reduction in the zeta potential values for OC-dots (-30 ± 10 to -20 ± 2 mV) and NC-dots (-28 ± 5 to -10 ± 5 mV). This variation was due to the strong interaction of ferric ions with both C-dots, that reduces the inter-particle distance and leads to its aggregation. This aggregation process was further confirmed by a red-shift in the emission wavelength of C-dots (438 nm to 445.8 nm for OC-dots and 455 nm to 496.6 nm for NC-dots) which was shown in Fig. 3.5. Hence, from the obtained results it was clear that the fluorescence quenching of C-dots in the presence of ferric ions was due to both aggregations as well as energy transfer process (Scheme 3.1). Besides, the recovery in zeta potential values was also observed for OC-dots/NC-dots and ferric ion system in the presence of fluoride ions (-20 ± 2 to -26 ± 1 mV for OC-dots and -10 ± 5 to -15 ± 5 mV for NC-dots). These results indicated that OC-dots and ferric ion system was more sensitive toward fluoride ion and justified the aforementioned results of its photoluminescence [33] (Scheme 3.1).

Table 3.2: Zeta-potential of C-dots in the presence and absence of Fe^{+3} and F^- ions.

Concentration ratio (C-dots: Fe^{3+})	Zeta-potential (mV)	Concentration ratio (C-dots: Fe^{3+}:F^-)	Zeta potential (mV)
OC-dots (1:0) NC-dots (1:0)	-30 ± 10 -28 ± 5	OC-dots (1:0:0) NC-dots (1:0:0)	-30 ± 10 -28 ± 5

OC-dots (4:0.75) NC-dots (4:0.75)	-20 ± 2 -10 ± 5	OC-dots (4:0.75:1) NC-dots (4:0.75:1)	-26 ± 1 -15 ± 5
OC-dots (1:1) NC-dots (1:1)	-22 ± 2 -12 ± 5	OC-dots (1:1:1) NC-dots (1:1:1)	-23 ± 2 -13 ± 3

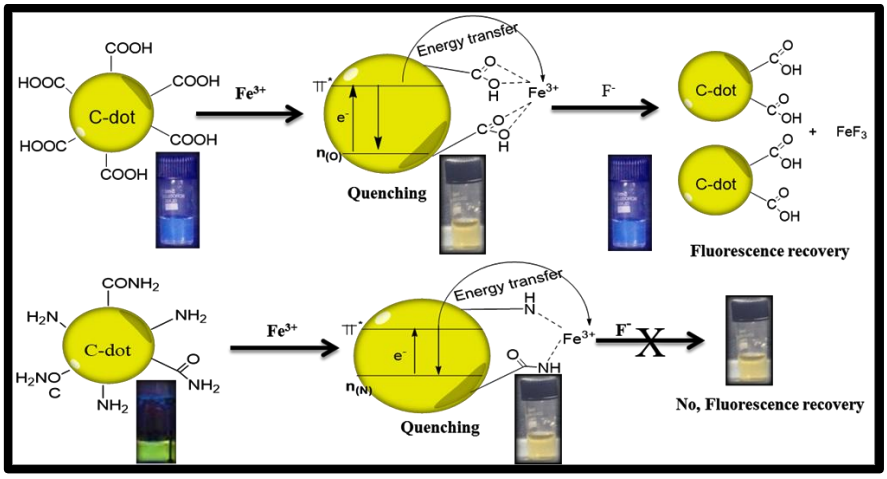

Scheme 3.1: Representation of the sensing mechanism of OC-dots and NC-dots for F- ions determination.

3.3.5 Selectivity of Fe^{3+} ions containing OC-dots towards F^- ions

To check the selectivity of the probe (OC-dots + Ferric ions) towards fluoride ion, the fluorescence recovery of OC-dots at 438 nm was studied in the presence of F- ions (1 µM) and other anions (20 µM) including fluoride (F^-), bromide (Br^-), sulphite (SO_3^{2-}), nitrite (NO_2^-), acetate (AcO^-), phosphate (PO_4^-), nitrate (NO_3^{2-}), sulphate (SO_4^{2-}) and chloride (Cl^-). The results indicated that only fluoride ions showed significant enhancement of fluorescence intensity at 438 nm. However, the larger size of anions could not cause a noticeable change in fluorescence intensity due to its less compatibility with Fe^{3+} ions for the formation of ionic compounds showed in Fig. 3.9.

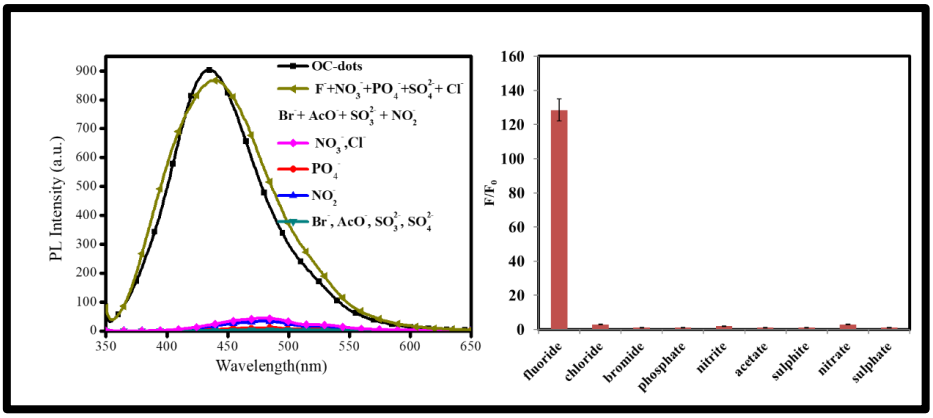

Fig. 3.9: Selectivity of OC-dots and Fe^{3+} ions system towards different metal anions.

3.3.6 Quantification of F^- ions with OC-dots and the Fe^{3+} ions system

To evaluate the stoichiometric response of the probe towards the fluoride ions, the reaction kinetics was measured between a mixture of OC-dots/Fe^{3+} and F^- ions (Fig. 3.10a). It was found that the fluorescence intensity increased with the reaction time. The whole process reached in equilibrium at about 1 min which confirmed the rapid interaction of sensing probe with F^- ions at room temperature. So, we selected 1 min as incubation time and studied the effect of concentration on fluorescence recovery for the quantitative determination of F^- ions. It was found that with the increase of F^- ions (0 to 1000 µl), the fluorescence intensity restored gradually and finally reached the maximum (Fig. 3.10a). To calculate the detecting limit of the probe, the plot between fluorescence enhancements, F/F_0 against concentration was done (Fig. 3.10b). The equation of the linear fitted curve, $F/F_0 = -11.262 + 1596.8[F^-]$ helped in determining the detection limit which was found 0.01 µM and regression coefficient was 0.9664, i.e. much lower than the previously reported results in the literature (Table 3.3).

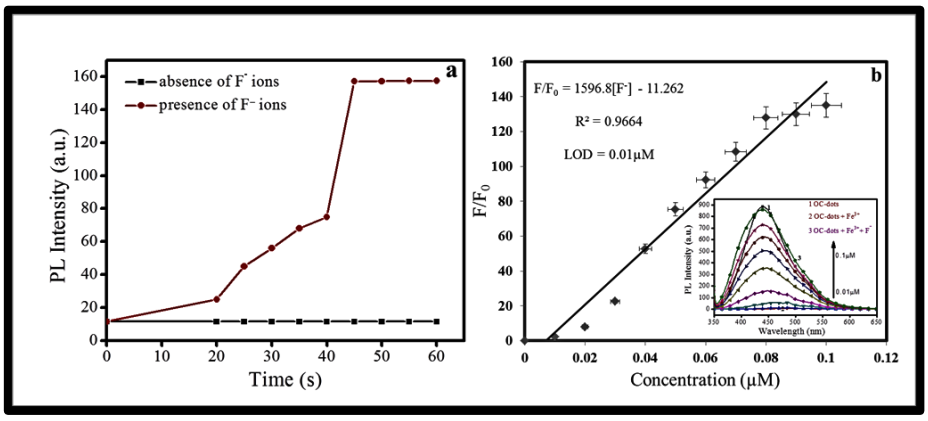

Fig. 3.10: a) Effect of time on the emission spectra of OC-dots-Fe^{3+} ion mixture in the absence and presence of fluoride ions and b) plot of PL intensity variation at λ_{em}=340 nm as a function of the concentration of F^- ions for the quantitative determination of F^- ions.

Table 3.3: Comparison of different sensing probe for detecting F^- ions based on the limit of detection (LOD).

Technique	Material/Apparatus	LOD	Ref
Spectrophotometer	Single beam spectrophotometer	2.38 µM	[34]
HPLC	UV	0.47 µM	[35]
Ion chromatography	ICP-MS	2.38 µM	[36]
Flow injection analysis	Spectro-fluorimeter	0.47 µM	[37]
Based on the release of AuNPs agglomeration dithiol linkers in the presence of inorganic	Fluoride colorimetric Chemosensor Gold nanoparticles (AuNPs)	120 µM	[38]
Interaction of L with F^- and acetate ions (AcO^-) results in enhanced ICT, leading to the prominent color change from yellow to orange-brown	Colorimetric and ratiometric chemosensor for detection of F^- and AcO^- ions/ Quinoline	0.067 µM	[39]
Ratio-metric fluorescence detection of fluoride ions	Lanthanide metal-organic framework	2 µM	[40]

Turn on/off fluorescence	Carbon-dots from mosambi peel	0.01 µM	In this work

After the completion of sensing experiment, the performance of logic gate functions (e.g. NOT, AND, IMP and OR) was determined based on the interaction between metal ions (Fe^{3+}) and anions (F^{-}) and C-dots. To execute the logic gate, the addition of metal ion (Fe^{3+}), and the anion (F^{-}) in C-dots kept as two-input, whereas variation in fluorescence intensity as an output signal for which four possible input combinations (0, 0; 1, 0; 0, 1; 1, 1) were used. The absence and association of these ionic inputs with C-dots defined as 0 and 1 states respectively. The output defined as 1 and 0 corresponds to strong and weak fluorescence response. NOT logic gate was used to study the variation in fluorescence intensity of C-dots with Fe^{3+} ions as an input signal. Addition of ferric ions quenched the fluorescence intensity of C-dots which indicate that the output is 0 (low). These results correlate with the function of the NOT logic gate.

Further, we have constructed the modified IMP logic gate in the presence of Fe^{3+} (fixed concentration) and F^{-} (varying concentration) as input 1 and 2 to the OC-dots. Primarily, individual inputs were used to examine their influence on C-dots and their corresponding output fluorescence intensity signal. The fluorescence intensity of OC-dots was quenched only in the presence of ferric ions whereas no effect was found on the addition of fluoride ions. Remarkably, in the presence of both inputs, the fluorescence intensity of C-dots was recovered by the addition of F^{-} (low or high concentration) which was quenched upon the addition of Fe^{3+} ions. This above-mentioned combination of two inputs correlates with the IMP logic gate behavior [41,42].

Similarly, we have constructed the combination of OR, AND, NOT logic gate in the presence of Fe^{3+} (fixed concentration) and F^{-} (varying concentration) ions as input 1 and 2 to the NC-dots. Primarily, individual inputs were used to examine their influence on C-dots and their corresponding output fluorescence intensity signal. It was detected that the fluorescence intensity of NC-dots was quenched in the presence of individual inputs of Fe^{3+} ions and remain the same in the presence of a low or high concentration of F^{-} ions. Unexpectedly, in the presence of both inputs (1, 1), the fluorescence intensity of NC-dots was remains quenched due to the strong coordination of Fe^{3+} ions with amino groups on the surface of NC-dots. These

results revealed that the different logic operation can be achieved by varying the concentration of metal ions as inputs (Fig. 3.11).

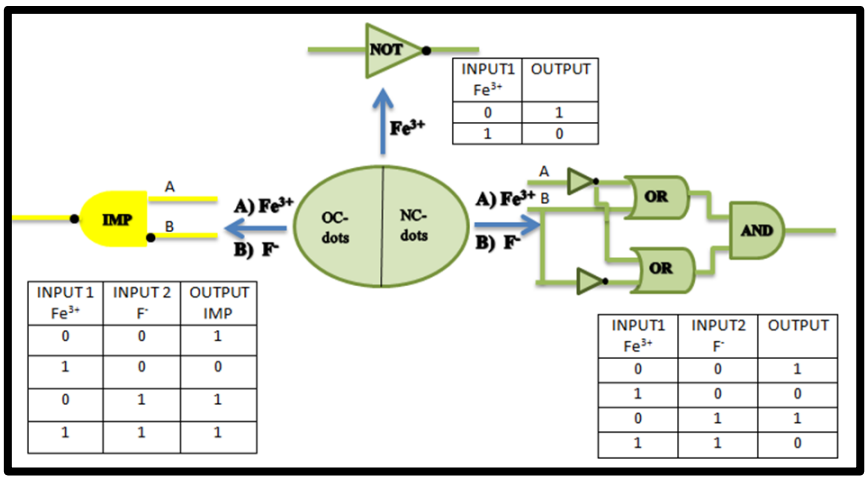

Fig. 3.11: Schematic representation of logic gate obtained for OC-dot/Fe^{3+}/F^- and NC-dots/ Fe^{3+}/F^-.

3.3.7 Method validation through real samples

To illustrate the practical applicability of our C-dots probe for selective detection of F^- ions, a certain concentration of F^- was added into the real samples including tap /lake water, and the real-time detection of F^- was carried out. The detailed results determined by our OC-dots based probe were shown in Table 3.4 which was also compared with the measured amount by ICP-AES technique. The results analyzed by both methods were very close and the % recoveries were in the satisfying range. The recovery of F^- was almost 99.0% for tap and lake water, suggesting that our OC-dots based probe was suited to detect F^- in real water samples.

Table 3.4: Detection of Fluoride ions using OC-dots probe and ICP-AES.

Sample	Concentration of F^- ions (µM)	ICP-AES(µM)	OC-dots	Recovery (%)
Tap water	2	1.89	1.988 ± 0.023	99
	4	3.89	4.052 ± 0.012	96
	6	5.99	5.781 ± 0.035	96
	8	8.0	7.832 ± 0.038	98

Lake water	2	1.79	1.978 ± 0.013	90.4
	4	3.58	3.998 ± 0.012	89.7
	6	5.53	6.011 ± 0.025	91
	8	7.99	8.232 ± 0.038	97

References

(1) Liu, J.-M.; Lin, L.-P.; Wang, X.-X.; Jiao, L.; Cui, M.-L.; Jiang, S.-L.; Cai, W.-L.; Zhang, L.-H.; Zheng, Z.-Y. Zr(H 2 O) 2 EDTA Modulated Luminescent Carbon Dots as Fluorescent Probes for Fluoride Detection. *Analyst* **2013**, *138* (1), 278–283. https://doi.org/10.1039/C2AN36055A.

(2) Mohapatra, S.; Sahu, S.; Nayak, S.; Ghosh, S. K. Design of Fe_3O_4@SiO_2@Carbon Quantum Dot Based Nanostructure for Fluorescence Sensing, Magnetic Separation, and Live Cell Imaging of Fluoride Ion. *Langmuir* **2015**, *31* (29), 8111–8120. https://doi.org/10.1021/acs.langmuir.5b01513.

(3) Chavali, R.; Gunda, N. S. K.; Naicker, S.; Mitra, S. K. Rapid Detection of Fluoride in Potable Water Using a Novel Fluorogenic Compound 7-O-Tert-Butyldiphenylsilyl-4-Methylcoumarin. *Anal. Chem. Res.* **2015**, *6*, 26–31. https://doi.org/10.1016/j.ancr.2015.10.003.

(4) Zheng, X.; Zhu, W.; Liu, D.; Ai, H.; Huang, Y.; Lu, Z. Highly Selective Colorimetric/Fluorometric Dual-Channel Fluoride Ion Probe, and Its Capability of Differentiating Cancer Cells. *ACS Appl. Mater. Interfaces* **2014**, *6* (11), 7996–8000. https://doi.org/10.1021/am501546h.

(5) Basu, A.; Suryawanshi, A.; Kumawat, B.; Dandia, A.; Guin, D.; Ogale, S. B. Starch (Tapioca) to Carbon Dots: An Efficient Green Approach to an on–off–on Photoluminescence Probe for Fluoride Ion Sensing. *Analyst* **2015**, *140* (6), 1837–1841. https://doi.org/10.1039/C4AN02340D.

(6) Cametti, M.; Rissanen, K. Highlights on Contemporary Recognition and Sensing of Fluoride Anion in Solution and in the Solid State. *Chem. Soc. Rev.* **2013**, *42* (5), 2016–

2038. https://doi.org/10.1039/c2cs35439j.

(7) Roy, A.; Datar, A.; Kand, D.; Saha, T.; Talukdar, P. A Fluorescent off–on NBD-Probe for F− Sensing: Theoretical Validation and Experimental Studies. *Org. Biomol. Chem.* **2014**, *12* (13), 2143. https://doi.org/10.1039/c3ob41886c.

(8) Yahyavi, H.; Kaykhaii, M.; Mirmoghaddam, M. Recent Developments in Methods of Analysis for Fluoride Determination. *Critical Reviews in Analytical Chemistry*. March 2016, pp 106–121. https://doi.org/10.1080/10408347.2014.985814.

(9) Yamaguchi, S.; Akiyama, S.; Tamao, K. Colorimetric Fluoride Ion Sensing by Boron-Containing π-Electron Systems. *J. Am. Chem. Soc.* **2001**, *123* (46), 11372–11375. https://doi.org/10.1021/ja015957w.

(10) Dekaliuk, M. O.; Viagin, O.; Malyukin, Y. V.; Demchenko, A. P. Fluorescent Carbon Nanomaterials: "Quantum Dots" or Nanoclusters? *Phys. Chem. Chem. Phys.* **2014**, *16* (30), 16075–16084. https://doi.org/10.1039/C4CP00138A.

(11) Demchenko, A. P.; Dekaliuk, M. O. The Origin of Emissive States of Carbon Nanoparticles Derived from Ensemble-Averaged and Single-Molecular Studies. *Nanoscale* **2016**, *8* (29), 14057–14069. https://doi.org/10.1039/C6NR02669A.

(12) Lou, Y.; Zhao, Y.; Zhu, J.-J. Ultrasensitive Optical Detection of Anions by Quantum Dots. *Nanoscale Horiz.* **2016**, *1* (2), 125–134. https://doi.org/10.1039/C5NH00039D.

(13) Singh, P.; Prabhune, A. A.; Tripathi, C. S. P.; Guin, D. Water-Soluble Photoluminescence On-Off-On Probe for Speedy and Selective Detection of Fluoride Ions. *ACS Sustain. Chem. Eng.* **2017**, *5* (1), 982–987. https://doi.org/10.1021/acssuschemeng.6b02296.

(14) Kumar, P.; Kumar, P.; Bharadwaj, L. M.; Paul, A. K.; Sharma, S. C.; Kush, P.; Deep, A. Aqueous Synthesis of L-Cysteine Stabilized Water-Dispersible CdS:Mn Quantum Dots for Biosensing Applications. *Bionanoscience* **2013**, *3* (2), 95–101. https://doi.org/10.1007/s12668-013-0078-5.

(15) Vashist, S.; Tewari, R.; Bajpai, R. Review of Quantum Dot Technologies for Cancer Detection and Treatment. *AZojono J Nanotechnolgy online* **2006**, *2*, 1–14.

https://doi.org/10.2240/azojono0113.

(16) Dhenadhayalan, N.; Lin, K. C.; Suresh, R.; Ramamurthy, P. Unravelling the Multiple Emissive States in Citric-Acid-Derived Carbon Dots. *J. Phys. Chem. C* **2016**, *120* (2), 1252–1261. https://doi.org/10.1021/acs.jpcc.5b08516.

(17) Wang, Y.; Hu, A. Carbon Quantum Dots: Synthesis, Properties and Applications. *J. Mater. Chem. C* **2014**, *2* (34), 6921. https://doi.org/10.1039/C4TC00988F.

(18) Sun, Y. P.; Zhou, B.; Lin, Y.; Wang, W.; Fernando, K. A. S.; Pathak, P.; Meziani, M. J.; Harruff, B. A.; Wang, X.; Wang, H.; et al. Quantum-Sized Carbon Dots for Bright and Colorful Photoluminescence. *J. Am. Chem. Soc.* **2006**, *128* (24), 7756–7757. https://doi.org/10.1021/ja062677d.

(19) Garg, D.; Mehta, A.; Mishra, A.; Basu, S. A Sensitive Turn on Fluorescent Probe for Detection of Biothiols Using MnO2@carbon Dots Nanocomposites. *Spectrochim. Acta Part A Mol. Biomol. Spectrosc.* **2017**. https://doi.org/10.1016/J.SAA.2017.11.041.

(20) Mehta, A.; D., P.; Thakur, A.; Basu, S. Enhanced Photocatalytic Water Splitting by Gold Carbon Dot Core Shell Nanocatalyst under Visible/Sunlight. *New J. Chem.* **2017**, *41* (11), 4573–4581. https://doi.org/10.1039/C7NJ00933J.

(21) Dong, Y.; Wang, R.; Li, G.; Chen, C.; Chi, Y.; Chen, G. Polyamine-Functionalized Carbon Quantum Dots as Fluorescent Probes for Selective and Sensitive Detection of Copper Ions. *Anal. Chem.* **2012**, *84* (14), 6220–6224. https://doi.org/10.1021/ac3012126.

(22) Xu, H.; Yang, X.; Li, G.; Zhao, C.; Liao, X. Green Synthesis of Fluorescent Carbon Dots for Selective Detection of Tartrazine in Food Samples. *J. Agric. Food Chem.* **2015**, *63* (30), 6707–6714. https://doi.org/10.1021/acs.jafc.5b02319.

(23) Schmidtchen, F. P.; Berger, M. Artificial Organic Host Molecules for Anions. *Chem. Rev.* **1997**, *97* (5), 1609–1646. https://doi.org/10.1021/cr9603845.

(24) Martínez-Máñez, R.; Sancenón, F. Fluorogenic and Chromogenic Chemosensors and Reagents for Anions. *Chem. Rev.* **2003**, *103* (11), 4419–4476. https://doi.org/10.1021/cr010421e.

(25) Kang, S. O.; Llinares, J. M.; Powell, D.; VanderVelde, D.; Bowman-James, K. New Polyamide Cryptand for Anion Binding. *J. Am. Chem. Soc.* **2003**, *125* (34), 10152–10153. https://doi.org/10.1021/ja034969+.

(26) Sui, B.; Kim, B.; Zhang, Y.; Frazer, A.; Belfield, K. D. Highly Selective Fluorescence Turn-on Sensor for Fluoride Detection. *ACS Appl. Mater. Interfaces* **2013**, *5* (8), 2920–2923. https://doi.org/10.1021/am400588w.

(27) Hudnall, T. W.; Kim, Y. M.; Bebbington, M. W. P.; Bourissou, D.; Gabbaï, F. P. Fluoride Ion Chelation by a Bidentate Phosphonium/Borane Lewis Acid. *J. Am. Chem. Soc.* **2008**, *130* (33), 10890–10891. https://doi.org/10.1021/ja804492y.

(28) Liu, X. Y.; Bai, D. R.; Wang, S. Zuschriften. *Angew. Chemie* **2006**, *118* (33), 5601–5604. https://doi.org/10.1002/ange.200601286.

(29) Huang, H.; Xu, Y.; Tang, C.-J.; Chen, J.-R.; Wang, A.-J.; Feng, J.-J. Facile and Green Synthesis of Photoluminescent Carbon Nanoparticles for Cellular Imaging. *New J. Chem.* **2014**, *38* (2), 784. https://doi.org/10.1039/c3nj01185b.

(30) Yan, F.; Zou, Y.; Wang, M.; Mu, X.; Yang, N.; Chen, L. Highly Photoluminescent Carbon Dots-Based Fluorescent Chemosensors for Sensitive and Selective Detection of Mercury Ions and Application of Imaging in Living Cells. *Sensors Actuators, B Chem.* **2014**, *192*, 488–495. https://doi.org/10.1016/j.snb.2013.11.041.

(31) Irving, B. H.; Williams, R. J. P. The Stability of Transition-Metal Complexes. *J. Chem. Soc.* **1953**, 3192–3210. https://doi.org/10.1039/JR9530003192.

(32) Fang, L.; Xu, Q.; Zheng, X.; Zhang, W.; Zheng, J.; Wu, M.; Wu, W. Soy Flour-Derived Carbon Dots: Facile Preparation, Fluorescence Enhancement, and Sensitive Fe3+ Detection. *J. Nanoparticle Res.* **2016**, *18* (8), 224. https://doi.org/10.1007/s11051-016-3521-z.

(33) Singhal, P.; Vats, B. G.; Jha, S. K.; Neogy, S. Green, Water-Dispersible Photoluminescent On-Off-On Probe for Selective Detection of Fluoride Ions. *ACS Appl. Mater. Interfaces* **2017**, *9* (24), 20536–20544. https://doi.org/10.1021/acsami.7b03346.

(34) Barghouthi, Z.; Amereih, S. Field Determination of Fluoride in Drinking Water Using a

Polymeric Aluminium Complex of 5-(2-Carboxyphenylazo)-8-Hydroxyquinoline Impregnated Paper. *Int. J. Environ. Anal. Chem.* **2013**, *93* (5), 565–577. https://doi.org/10.1080/03067319.2012.690147.

(35) Musijowski, J.; Szostek, B.; Koc, M.; Trojanowicz, M. Determination of Fluoride as Fluorosilane Derivative Using Reversed-Phase HPLC with UV Detection for Determination of Total Organic Fluorine. *J. Sep. Sci.* **2010**, *33* (17–18), 2636–2644. https://doi.org/10.1002/jssc.201000179.

(36) Bayón Montes, M.; Garcia Rodríguez, A.; García Alonso, J. I.; Sanz-Medel, A. Indirect Determination of Trace Amounts of Fluoride in Natural Waters by Ion Chromatography: A Comparison of on-Line Post-Column Fluorimetry and ICP-MS Detectors. *Analyst* **1999**, *124* (1), 27–31. https://doi.org/10.1039/a807079b.

(37) Takayanagi, T.; Yamashita, H.; Motomizu, S.; Musijowski, J.; Trojanowicz, M. Preconcentration and Decomposition of Perfluorinated Carboxylic Acids on an Activated Charcoal Cartridge with Sodium Biphenyl Reagent and Its Determination at Mg L-1 Level on the Basis of Flow Injection-Fluorimetric Detection of Fluoride Ion. *Talanta* **2008**, *74* (5), 1224–1230. https://doi.org/10.1016/j.talanta.2007.08.026.

(38) Gu, J. A.; Lin, Y. J.; Chia, Y. M.; Lin, H. Y.; Huang, S. T. Colorimetric and Bare-Eye Determination of Fluoride Using Gold Nanoparticle Agglomeration Probes. *Microchim. Acta* **2013**, *180* (9–10), 801–806. https://doi.org/10.1007/s00604-013-0972-0.

(39) Yadav, U. N.; Pant, P.; Sharma, D.; Sahoo, S. K.; Shankarling, G. S. Quinoline-Based Chemosensor for Fluoride and Acetate: A Combined Experimental and DFT Study. *Sensors Actuators, B Chem.* **2014**, *197*, 73–80. https://doi.org/10.1016/j.snb.2014.02.075.

(40) Yang, Z. R.; Wang, M. M.; Wang, X. S.; Yin, X. B. Boric-Acid-Functional Lanthanide Metal-Organic Frameworks for Selective Ratiometric Fluorescence Detection of Fluoride Ions. *Anal. Chem.* **2017**, *89* (3), 1930–1936. https://doi.org/10.1021/acs.analchem.6b04421.

(41) Guo, J. H.; Kong, D. M.; Shen, H. X. Design of a Fluorescent DNA IMPLICATION Logic Gate and Detection of Ag+ and Cysteine with Triphenylmethane Dye/G-

Quadruplex Complexes. *Biosens. Bioelectron.* **2010**, *26* (2), 327–332. https://doi.org/10.1016/j.bios.2010.08.020.

(42) Zhu, J.; Zhang, L.; Li, T.; Dong, S.; Wang, E. Enzyme-Free Unlabeled DNA Logic Circuits Based on Toehold-Mediated Strand Displacement and Split G-Quadruplex Enhanced Fluorescence. *Adv. Mater.* **2013**, *25* (17), 2440–2444. https://doi.org/10.1002/adma.201205360.

CHAPTER-4

Effect of Acids and Solvents on the Photoluminescence Properties of C-dots and Its Sensing Efficacy Towards Metal Ions

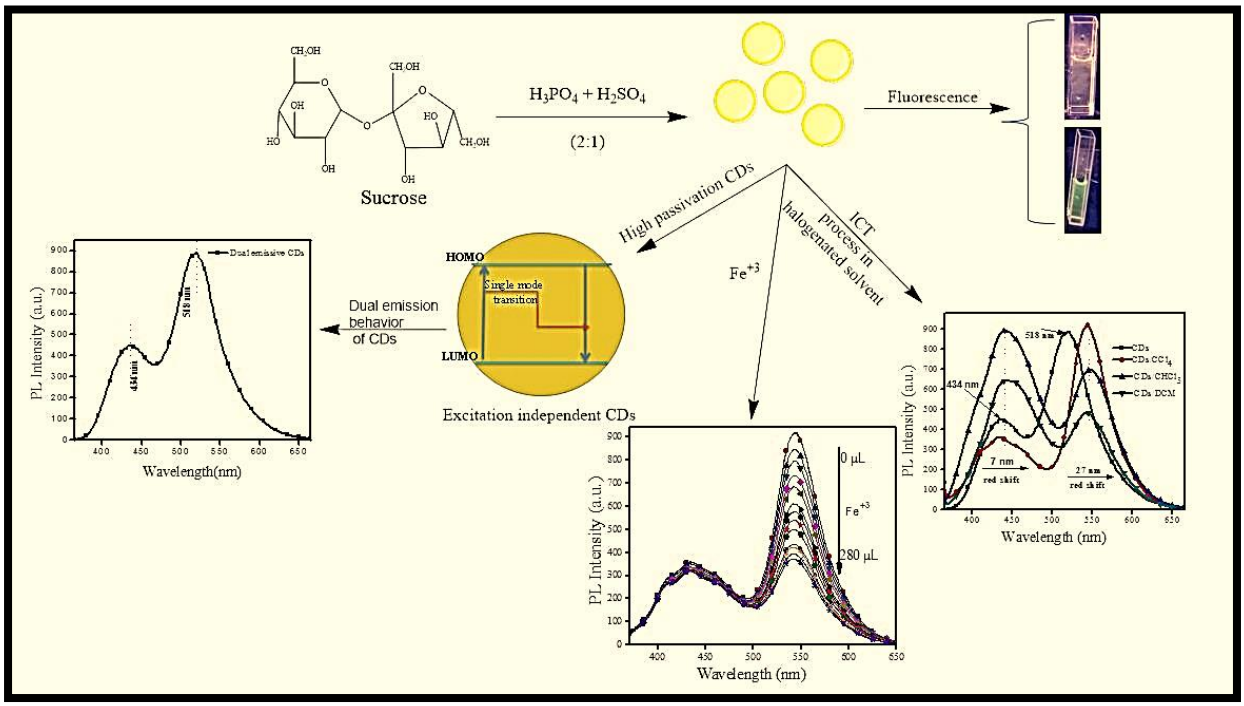

Highlights

- Single precursor salt was used for the synthesis of dual emissive carbon dots (C-dots).
- The optimized mixture of acids was used to tune the emission spectra of C-dots.
- The solvatochromic behaviors of C-dots in different solvents were explored.
- The C-dots were used for the selective detection of metal ions (Fe^{+3}) in the real samples.

4.1 Introduction

There was no long history for the discovery of carbon quantum dots (C-dots), but it occupies the prominent place in the field of luminescent nano-materials due to its high aqueous solubility, exceptional photoluminescence (PL) properties, favourable biocompatibility, chemical inertness and easy functionalization in respect to known organic fluorophores. Nowadays, the research focus is shifted towards the implications of luminescent C-dots. Still, to boost its utility in target-specific sensing and bio-imaging field, simplified eco-friendly strategies need to be introduced to tune its luminescence properties. This can be achieved by tailoring their intrinsic properties and modification of its surface design by conjugation of different functional groups on its surface [1,2].

Several different synthetic chemical and physical routes such as electrochemical [3], thermal treatment [4], hydrothermal or acidic oxidation [5], microwave [6], ultrasonic [7,8], cage-opening of fullerene [9], arc discharge [10], laser ablation [11], and plasma treatment [12] to fabricate luminescent C-dots were reported to fabricate multi-color C-dots. Many groups followed functionalization route to attain modified C-dots using boronic acid/aptamer as a precursor for the determination of metal cations [13,14] and glucose [15]. Dong *et al.*[2] functionalized C-dots using polyamine to tune its emissive properties and further used as nano-probe based on the inner filter effect for Cu^{+2} ion sensing. Even several moieties were also detected (such as Vitamin B_{12}, amino acids and dopamine, etc.) through the diverse strategies which include Foster Resonance Energy Transfer (FRET), Photoinduced Electron Transfer (PET), aggregation-caused quenching by coordination and reaction-induced fluorescence quenching using C-dots [16–20]. Besides, to make target specific sensor [12,21] many groups were also emphasizing on the extrinsic parameters such as dopants, solvents to tune its photoluminescence (PL) properties. Kwon *et al.* [22] used sulfur doping route to tune its electronic states and PL intensity in the longer wavelength regime. Moreover, reduction pathways were also followed by Zheng *et al.* [23] to obtain the long-range emissive (450 to 520 nm) C-dots. In recent studies, many researchers modified synthetic conditions, precursors and reagents (citric acid and formamide) to obtain excitation wavelength-dependent multi-color C-dots [24–27]. Likewise, Bao and co-workers, [28] modified the reaction time and temperature to prepare the new excitation independent series of C-dots. Ding *et al.* [29] used hydrothermal method to prepare the batch of multi-color C-dots from p-phenylenediamine and urea which showed blue to red emission (440-625 nm, Q.Y. 8.5-35%) at the single excitation wavelength. Some of the groups also used green materials to tune the emissive properties of C-dots [30,31]. These variations in emissive properties of C-dots were

achieved by several groups due to the modulation in the quantum size and surface states [29,32].

Nowadays to tune the emissive range of C-dots, more emphasis is given on the dispersive medium. Wu and co-workers reported a red-shift in the emission spectra (400 to 430 nm) for C-dots with the same excitation wavelength, dispersed in different solvents [4]. Even analogous results were reported for graphene quantum dots in different solvents with the emission range from 475 to 515 nm [33]. The tenacity for the development in its synthetic routes was to improve its efficacy for bio-imaging and bio-sensing. Overall, the above-mentioned advancements for preparing multi-color C-dots were found tedious, expensive and low yield. Thus, eco-friendly and cost-effective routes were required to attain long emissive range C-dots.

To execute these problems, some groups utilizing the combination of carbohydrates and acids to produce a series of C-dots [34]. Some significant reports were mentioned by Wee *et al.* [35] where they used the dehydrating agent (H_2SO_4), various protein and carbohydrate nanoparticles to produce C-dots. Likewise, other groups use different acids (H_3PO_4, HCl and HNO_3)[36] to attain green, yellow and red-emitting C-dots [37,38]. Though, the reported work was effective due to the utilization of low energy, basic laboratory glassware. Still, some experimental studies were required to justify the role of acids to attain dual emissive properties in them. Till now, solvatochromism studies for dual emissive C-dots was not explored [39,40].

Therefore, we have reported an eco-friendly route to attain dual emissive C-dots by using different carbohydrates with a combination of acids. Besides, its photophysical properties were discovered in different solvent systems. Successively, the sensing ability of C-dots was also explored with various metal ions in both aqueous and non-aqueous medium. The experimental studies revealed exceptional behavior for dual emissive C-dots in halogenated solvents, which exhibited a bathochromic shift in its emission spectra w.r.t the aqueous medium which has not been reported elsewhere.

4.2 Experimental section

4.2.1 Materials and characterization

Sucrose, fructose, glucose was purchased from Thermo Fisher Scientific, United States. Other basic chemical reagents like orthophosphoric acid, nitric acid, sulfuric acid, hydrochloric acid, ferric nitrate, ferrous nitrate, copper nitrate, zinc nitrate, magnesium nitrate, cadmium nitrate and nickel nitrate were purchased from Sigma Aldrich. Different kinds of solvents namely dichloromethane (CH_2Cl_2), chloroform ($CHCl_3$), carbon tetrachloride (CCl_4),

acetonitrile (ACN), dimethylformamide (DMF), methanol was purchased from Loba Chemie Pvt Ltd (spectrograde), India. All these reagents and carbohydrates were used directly by preparing their aqueous solution using distilled water (18.2 MΩ, Millipore). The C-dots were synthesized by using Multiwave-300 microwave synthesis reactor (Anton Paar, USA). The synthesized C-dots were characterized by High-resolution transmission electron microscope (HRTEM), (TALOS F200S G2, 200 KeV, FEG, CMOS Camera 4K x 4K, In Column EDS detectors) for the analysis of its surface morphology and particle size by using a drop-casting technique. Moreover, Fourier transform infrared spectroscopy-attenuated total reflectance (FTIR-ATR) Agilent Resolution Pro-carry 660) XPS, X-ray photoelectron microscopy and Energy-dispersive X-ray spectroscopy (EDX) techniques were carried out to know the better insight on the C-dots surface. LS-55 spectro-fluorophotometer (Perkin Elmer) was also used to study its optoelectronic properties.

4.2.2 Preparative method for dual emissive C-dots

The one-pot synthesis was followed to fabricate dual emissive C-dots. Firstly, 0.5g sucrose (0.15 M) was dissolved in 10 ml of distilled water followed by the addition of 100 µl concentrated sulfuric acid (H_2SO_4) and 200 µl of concentrated ortho-phosphoric acid (H_3PO_4) in the ratio of 1:2. The prepared mixture was transferred into the microwave glass vial and subjected to microwave heating at 130 °C for 10 min. After the completion of the reaction, the brown color colloidal solution was obtained. It was purified by centrifugation at 5000 rpm for 30 min to get yellow color C-dots and further, it passes through a syringe filter (0.22 µm) to get a homogeneous colloidal mixture which exhibited dual emissive properties (Scheme 4.1). The surface analysis and photoluminescence were also done to study its morphology and optical properties.

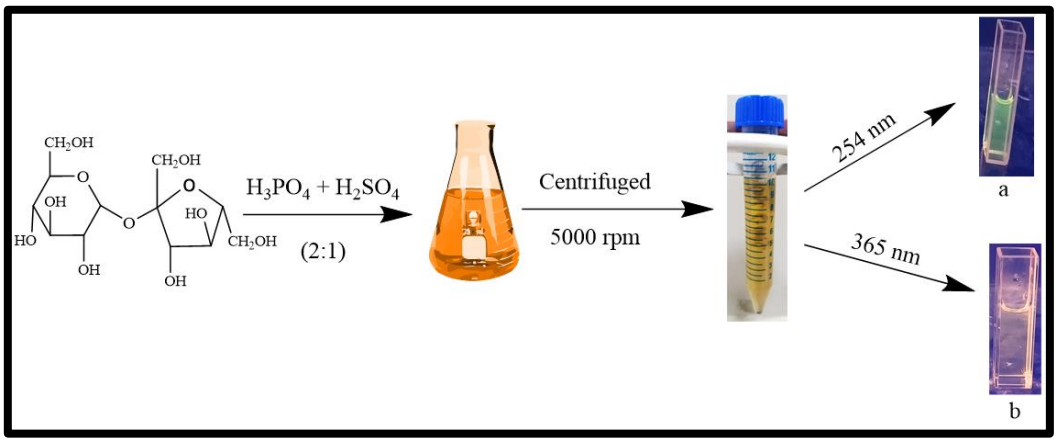

Scheme 4.1: Pictorial representation to synthesize the dual emissive C-dots.

4.2.3 Photoluminescence quantum yield (PLQY) measurements

The PLQY of all four NC-dots was evaluated using quinine sulphate (ϕ_r= 0.546) [37] as a reference solution dissolved in 0.01 M H_2SO_4 by subsequent equation-1:

$$\phi = \phi' \times (I/I') \times (A'/A) \times (\eta^2/\eta'^2) \quad 1$$

Where 'φ' denotes as the quantum yield, 'φ_R' is PLQY of reference, 'I' as the integrated area of fluorescence intensity, 'A' as the absorbance value and 'η' as refractive index.

4.2.4 Methodology for photoluminescence studies of dual emissive C-dots

To evaluate the solvatochromic and sensing behavior of C-dots firstly, C-dots was dispersed in different solvents (2 ml) and its emission spectra were evaluated in all different media respectively. Furthermore, the stock solution of metal salts like Mg^{2+}, Cu^{2+}, Zn^{2+}, Co^{2+}, Ni^{2+}, Fe^{3+} and Fe^{2+} (10^{-3} M) was prepared in distilled water which was added (10 µl) in a test tube and air-dried. Then, C-dots was dispersed in different solvents (2 ml) and added to the test tube. Afterwards, their interactions with C-dots in different solvent systems were analyzed by recording its PL emission spectra. To validate the sensing efficacy of C-dots, real samples (Ferric citrate tablets- 200 mg) were also analyzed by following the same above-mentioned protocol.

4.3 Result and discussion

4.3.1 The mechanism involved in the fabrication of dual emissive C-dots

In this protocol, major emphasis was given on acids for the activation of carbon particles and to modify the surface functional groups. In the synthesis of C-dots, both the acids (H_2SO_4 and H_3PO_4) play an independent role to tune its emission properties. H_3PO_4 helps to promote the carbonization of sucrose at slower kinetics to produce surface defects which cause red-shift [41–45] whereas, H_2SO_4 due to its stronger oxidizing ability generates O=C-O-H and C-O-H from C-H and its dehydrating property induces unsaturation from C-C, causing a blue shift in the emission spectra of C-dots [46,47]. Therefore, the acid mixture (H_2SO_4 + H_3PO_4) was chosen to produce dual emissive C-dots in a single step without using toxic reagents and to fix its discrete energy bandgap [48].

The preparative method for C-dots involves various steps. Initially, sucrose solution undergoes modifications through hydrolysis and dehydration to form furfural intermediates (such as hydroxyl methyl furfural) [49,50]. The intermediate was further polymerized, aromatized

[51,52] and subsequently undergoes the nucleation and particle growth process to attain the brownish colloidal solution [53] which was explained in detail in Scheme 4.2. Further, to confirm the dual emissive behavior in prepared C-dots, its aqueous solution was kept under the UV light irradiation where it showed green and yellow color emission at two different wavelengths (254 and 365 nm) (Scheme 4.1).

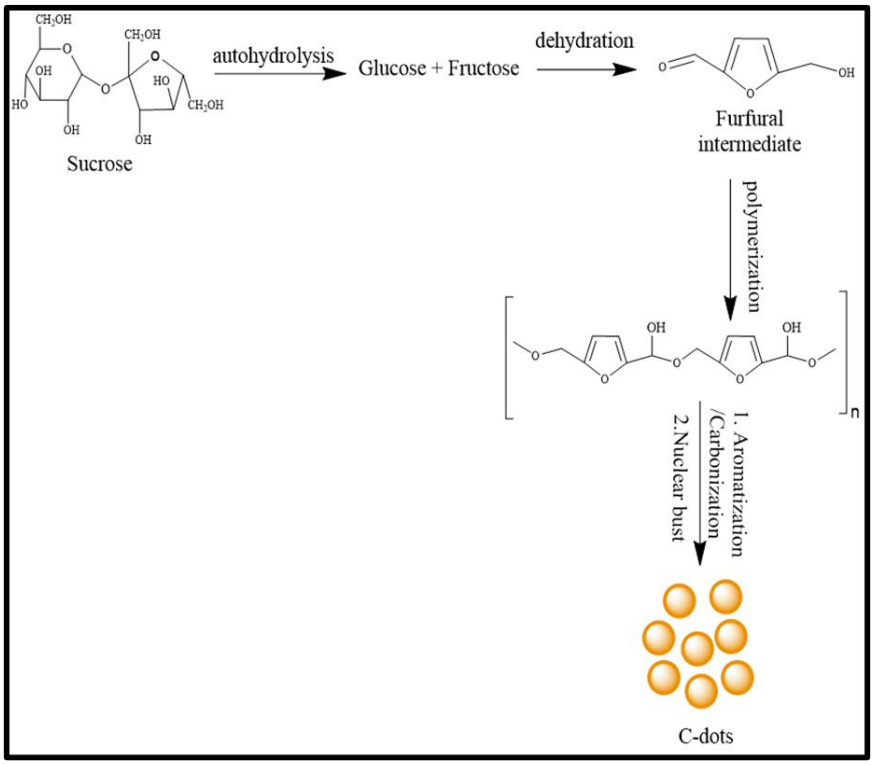

Scheme 4.2: Schematic presentation of the mechanism used to obtain dual emissive C-dots.

4.3.2 Optical properties and stability of dual emissive C-dots

The optical properties of dual emissive C-dots are shown in Fig. 4.1. Firstly, UV-vis spectrum was recorded, which showed the prominent absorption peak at ~284 nm, (which is due to the n-π* transition of C=O bond) and a weak shoulder band at ~227 nm. The weak band is attributed to the π-π*transition of the aromatic sp^2 bond [54] (Fig. 4.1a). PL spectra were also recorded to confirm the dual emission behavior of C-dots. It showed two emission peaks at 434 nm and 518 nm (Fig. 4.1b) by exciting the sample at 350 nm. This dual emission peak was attained due to the formation of discrete fixed energy gaps and the elimination of intermediate energy levels in C-dots induced with the help of acid mixtures [48]. Moreover, the synthesized dual emissive C-dots showed excitation independent behavior in comparison to the other reported multi-color C-dots [55] (shown in Fig. 4.1c). This unusual trend in C-dots was explained based on surface passivation as reported by Zhang *et al.* [56]. According to their interpretation,

the multi-mode absorptions were attained for low passivation C-dots due to the formation of different energy states, which was responsible for its excitation dependent PL property [35]. Moreover, the single transition mode developed in case of high passivation C-dots surface which generates excitation-independent PL [35]. So, from the aforementioned results, it has been concluded that a mixture of acids plays a vital role in the high surface passivation and development of single transition mode among C-dots.

It is necessary to investigate the solution conditions of C-dots before the utilization in various applications. pH is the main parameter that influences the emission properties of C-dots which needs to be studied. So, PL spectra of C-dots were recorded at different pH range from 2 to 9 (Fig. 4.1d). The study showed that C-dots attain equivalent PL intensity in the pH range from 2-6. But with the increment of pH towards the basic range, it shows high pH sensitivity due to the presence of several hetero-atoms (confirmed by EDX and XPS analysis) on its surface [57]. So, it can be used as an effective analytical tool in the pH range (2-6). Consequently, the PL spectra were recorded at different concentrations of KCl salt, which shows the constant response in the PL intensity and mixture appears to be homogeneous, i.e. no aggregation took place in the presence of concentrated K^+ cations and Cl^- anions (Fig. 4.2a) [47]. Besides, we have also analyzed C-dots under UV lamp irradiation for one hour which shows no change in its PL intensity (Fig. 4.2b). Therefore, the obtained results conclude that C-dots can be used in analytical application to quantify the analyte of interest without any interference of surrounding environment.

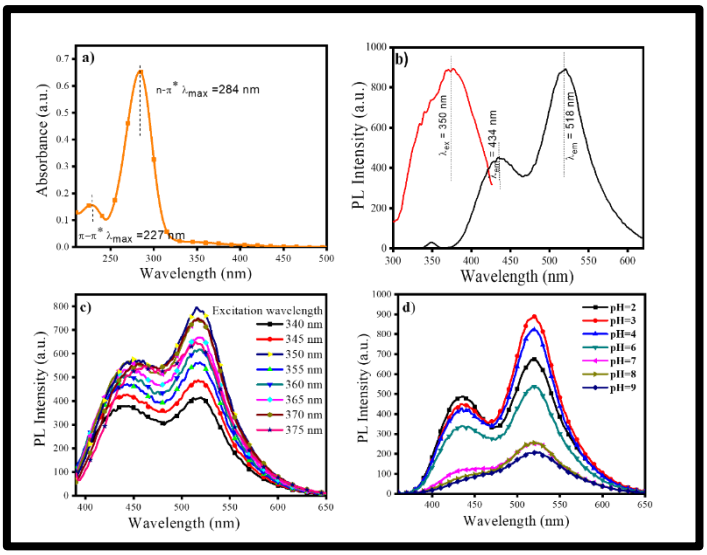

Fig. 4.1: Optical properties of dual emissive C-dots: a) UV-visible spectra, b) excitation and emission spectra (λ_{ex} = 350 nm), c) effect of excitation wavelength and d) effect of pH on its PL intensity.

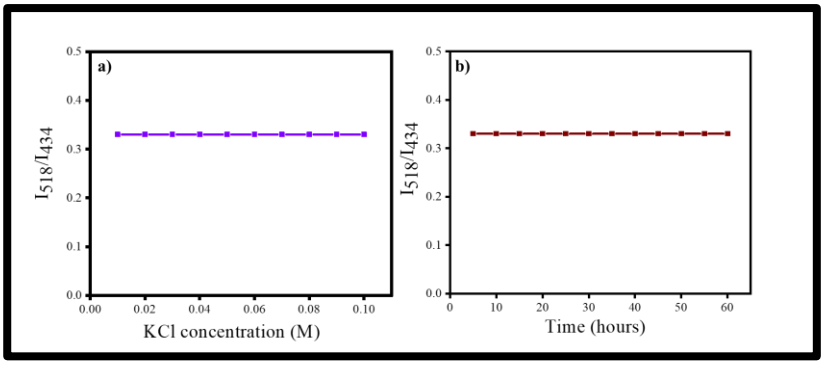

Fig. 4.2: PL intensity of dual emissive C-dots under a) different concentration of KCl salt and b) UV light exposure.

4.3.3 Characterization of dual emissive C-dots

The morphology and the size distribution of dual emissive C-dots were characterized by HRTEM, represented in Fig. 4.3. The HRTEM result justifies its partial mono-dispersed and spherical feature, with narrow particle size distribution ranging from 4-7 nm (average diameter of 4.6 nm). In Fig. 4.3b, the HRTEM image showed the lattice fringes with the d-spacing value of 0.24 nm which corresponds to (100) facet of graphitic C-dots. Furthermore, in the selected-area electron-diffraction (SAED) displayed a ring pattern with an inter-planar lattice spacing of 0.24 nm and the high crystallinity, which agrees with the (100) lattice spacing of graphitic C-dots (Fig. 4.3c) [58].

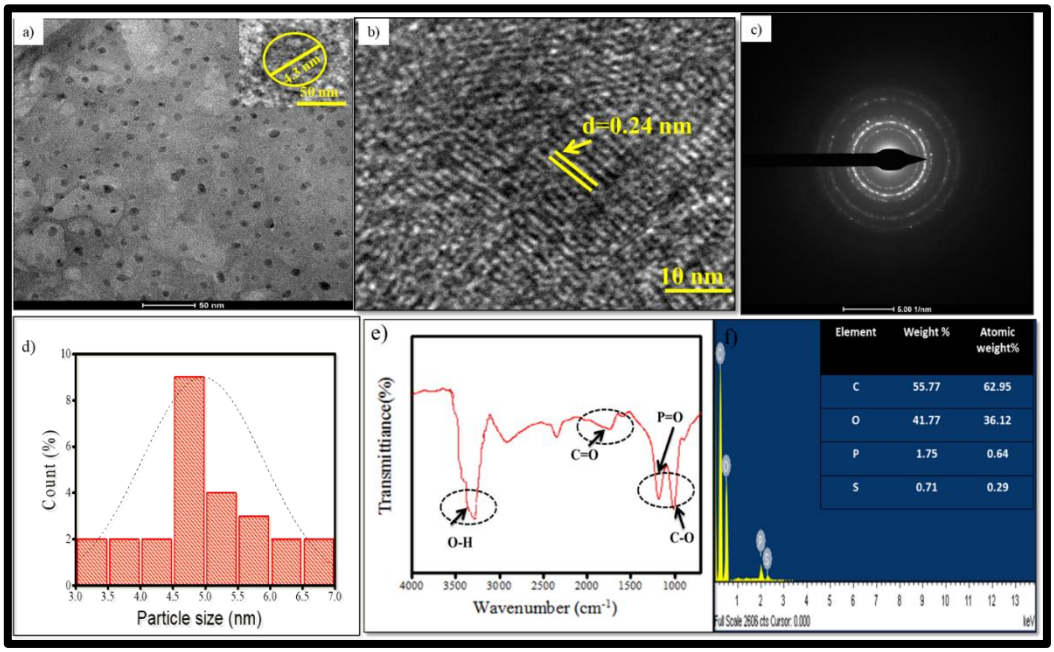

Fig. 4.3: Physico-chemical properties of dual emissive C-dots: a) HRTEM and the inset shows the particle size of individual C-dots, b) lattice fringes of individual C-dots, c) corresponding

selected-area electron-diffraction (SAED) pattern image, d) histogram distribution of particle size from HRTEM image, e) FTIR spectra of C-dots and f) energy dispersive spectra of C-dots.

The XPS studies were done to determine the surface chemical composition of dual emissive C-dots. The survey spectrum of XPS revealed that surface of C-dots primarily composed of C_{1s} (49.84%), O_{1s} (41.66%) and another small part was contributed by P_{2p} (6.47%), and S_{2p} (2.47%) (Fig. 4.4a). The high-resolution XPS data of C_{1s} were deconvoluted into four peaks at 284.6, 286.1, 287.9 and 288.9 eV, which represent the C_{1s} states exists in the C–C/C=C, C–S, C–O and C=O bonds respectively (Fig. 4.4b) [59]. The O_{1s} spectra showed two main peaks at 531.8 eV and 532.8 eV which indicates the presence of C=O and C-O respectively [60]. The P_{2p} spectrum (Fig. 4.4d) revealed the presence of P=O (133.1 eV) and P−C (134.1 eV) groups [61]. The S_{2p} spectrum (Fig. 4.4e) showed three major peaks at 167.8, 168.4 and 169.5 eV, corresponding to C–SO_x (x = 2, 3, 4) species respectively, which indicates that sulfur groups exist in sulfonate state on C-dots surface [62,63]. The surface state of C-dots was also elucidated through FTIR spectra mentioned in Fig. 4.3e. The spectral details show the broad peak at 3420 cm^{-1} associated with the O–H group and the sharp absorption peak at 1630 cm^{-1} which confirmed the presence of the carbonyl group on its surface. Besides, the spectra display two another peaks at 1162 and 1065 cm^{-1}, which confirmed the existence of P=O groups from phosphate or polyphosphates, and the O–C stretching vibration of P–O–C (aromatic), respectively [37]. This phosphate groups may be derived from the bidentate bonding between the [PO_4^{3-}] and –OH group on its surface [37]. Further, the presence of sulfur and phosphorus in C-dots was confirmed by EDX analysis, which demonstrates the presence of carbon, oxygen, sulfur, and phosphorus on its surface (Fig. 4.3f). These results indicated that C-dots surface comprises several hydrophilic and hetero groups on its surface which were responsible for its dual photoluminescence, high water solubility and aids in complex formation.

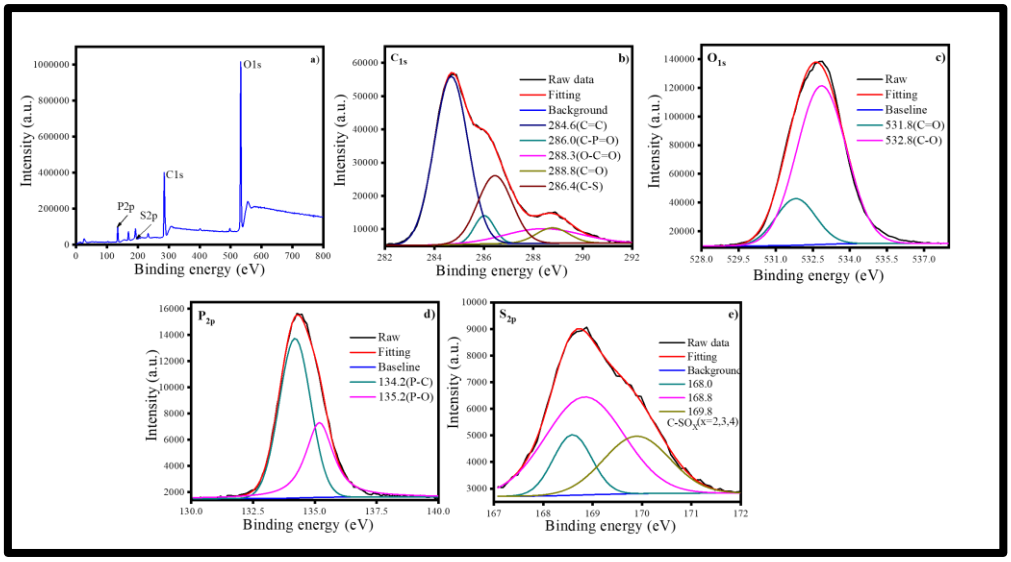

Fig. 4.4: XPS spectrum of dual emissive C-dots, a) survey spectrum, b) C_{1s}, c) O_{1s}, d) P_{2p} and e) S_{2p} deconvoluted spectrum.

4.3.4 Optimization of different carbon precursor, concentration and reaction time to fabricate dual emissive C-dots

Different sources of carbon and reaction time play a vital role to modify the PL behavior and morphology of C-dots. So, we used various precursors such as sucrose, fructose, and glucose in the presence of mixed acids (H_3PO_4 + H_2SO_4) to fabricate C-dots. The experimental results suggest that if the carbon precursors have similar functional groups present on it, then its conversion to C-dots in the presence of mixed acids exhibited consistent emission peaks at 434 nm and 518 nm as shown in Fig. 4.5a. Although, the PL peak intensity for sucrose found to be is highest among all the precursors. So, these results indicate that the different molar concentration of sucrose was preferred to attain the dual emissive C-dots. The experiments results suggest that acid-mediated sucrose-based C-dots exhibited the highest PL intensity at 0.15 M concentration of sucrose as shown in Fig. 4.5b.

Moreover, times studies were performed to evaluate the impact of reaction time rate on its PL properties. The result specifies that the maximum PL intensity for dual emissive C-dots was attained in ~8-10 min under microwave irradiation (Fig. 4.5), which is less than the reported methodology [48]. Thus, it is necessary to optimize the concentration of carbon source and reaction time for the development of dual emissive behavior C-dots in acidic conditions.

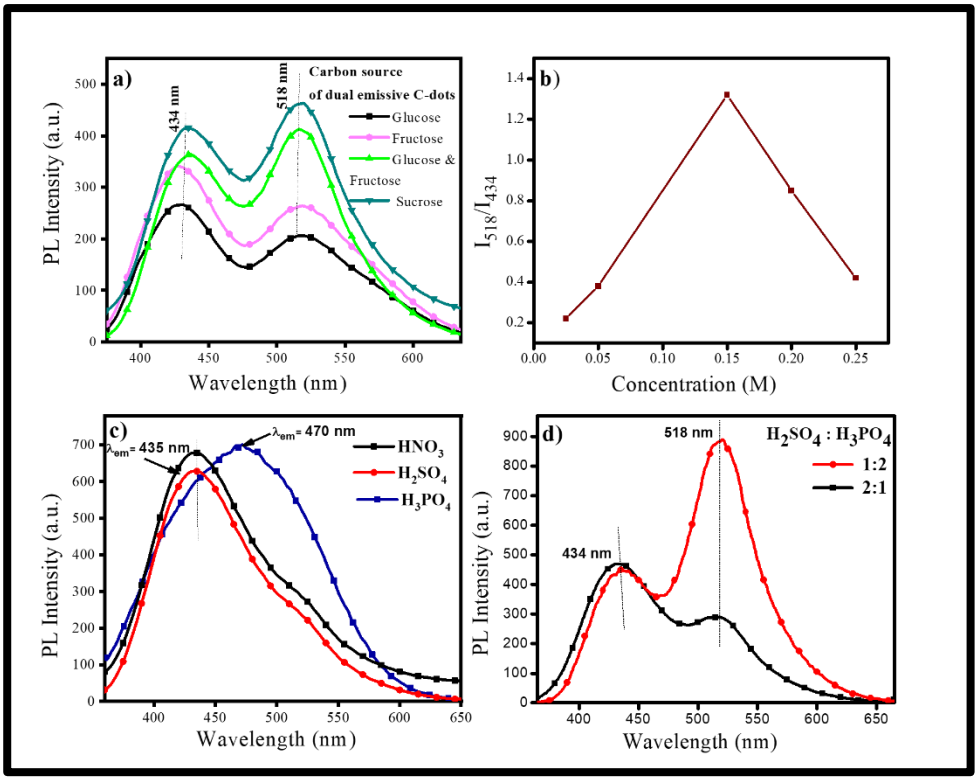

Fig. 4.5: The emission spectra of dual emissive C-dots: a) using different precursor, b) at various concentration of sucrose, c) in the presence of different acids and d) in the presence of mixed acids.

4.3.5 Effect of different acids on PL properties of C-dots

The particle size and functional groups present on the surface of C-dots play an important role to fetch difference in its emission properties. So, we used acids to modify its emissive sites to attain multi-color C-dots. To explain the significance of acids, H_3PO_4, H_2SO_4, HNO_3, and their combinations were used for the preparation of C-dots from sucrose precursor. At first, the individual effect of acids such as H_2SO_4, HNO_3 was studied, which showed significant single emission peak in the blue region (435 nm) as shown in Fig. 4.5c. However, the emission peak of the C-dots undergoes bathochromic shift (470 nm) in the presence of H_3PO_4. This distinct behaviour in emission properties of C-dots in the presence of different acids was originated from defects on its surface, which develops discrete surface states with an energy level between the π and π* states of the carbon double bond in the C-dots emission sites [48]. Dong *et al.* [38] reported that the presence of hetero-atoms modified the PL properties of C-dots. Similarly, Xu *et al.* [37] showed emission shift towards the red region is due to the phosphorus-doped C-dots. Based on these reports, we conclude that doping can create new energy levels or change their initial bandgap [64,65]**.** Because of that, we used a combination of

acids (H_2SO_4 + H_3PO_4) and studied its impact on the synthesis of C-dots by altering their ratios from 2:1 to 1:2 (Fig. 4.5d). The result indicates that the combination of acids in both conditions leads to induce dual emission peaks (434 nm and 518 nm) in C-dots. The existence of longer wavelength peak in C-dots attributed to the surface or edge functional group and the shorter emission wavelength was due to the presence of uniform sp^2 domains [47]. These characteristic features of dual emissive peaks in C-dots indicated that the mixed acids lead to the formation of intermediate energy level, i.e. not possible in their absence which helps to overcome the activation energy for better carbonization and emission intensity [48].

Even, the intensity of the dual emissive peaks also depends on the ratio of mixed acids for the formation of C-dots (Fig. 4.5d). The results revealed that the acid ratio of 1:2 (H_2SO_4 + H_3PO_4) helps to attain prominent emission peak at 518 nm w.r.t 2:1 (H_2SO_4 + H_3PO_4) because both acids have different pK_a value (H_3PO_4> H_2SO_4) [48]. If the concentration of H_2SO_4 gets increased, the carbonization process gets enhanced and converted the carbon precursor into non-fluorescent products [48]. Hence, a high concentration of H_3PO_4 is necessary for the formation of red emissive C-dots with appropriate PL intensity. So, the specific molar ratio (2:1) of acids was necessary for the fixation of emission wavelength to obtain dual PL characteristic in C-dots.

4.3.6 Solvatochromic studies of dual emissive C-dots

The surrounding medium of the C-dots also has a vital role to modulate the emission spectral behavior. So, to comprehend the better insight into the interaction of dual emissive C-dots with solvents, we have studied their photophysical properties. According to general trends, if the polarity of the surrounding medium increases the fluorescence active compounds exhibit bathochromic shifts in their emission spectra. However, in our case, the dual emissive C-dots undergoes hypsochromic emission shift in the presence of water (highly polar solvent). It has been observed that the first emission maxima appeared at 434 nm (shorter wavelength) along with a prominent peak at 518 nm (longer wavelength) (Fig. 4.6a). In presence of methanol, the shorter wavelength emission maxima appeared at 443 nm along with a band at 523 nm. In polar aprotic solvents (ACN and DMF), C-dots exhibit a bathochromic shift in emission spectra of both the emission maxima compared to that of water. Also, the longer wavelength emission maxima appeared as a shoulder band in polar aprotic solvents. These results justified that hypsochromic shift of C-dots in water compared to methanol, ACN, and DMF was due to the solvent-induced change of electronic ground state from less dipolar to more dipolar

chromophore [66]. Moreover, in the case of water, the longer wavelength emission maxima appear as a prominent peak, which is attributed to extensive hydrogen-bonding interactions, dipole-dipole interactions, and specific solute-solvent interactions. But, in other protic (methanol) and aprotic (ACN, DMF) solvents these types of specific interactions were less prominent due to which the longer wavelength emission maxima appears as a shoulder band (Fig. 4.6a).

Furthermore, it was observed that the polarity of the medium (Lippert Mataga (LM) model) is not always playing a significant role in solvatochromic shifts, there are some other factors such as polarizability (π^*), hydrogen bond accepting ability (HBA, β) and hydrogen bond donating ability (HBD, α) of solvents (Kamlet Taft (KT) model) also influences the PL properties of C-dots [67,68]. From the Kamlet-Taft parameter (Table 4.1), it was observed that the value of HBA parameter (β) is relatively larger in methanol, ACN and DMF as compared to that of water, which results in a hypsochromic shift in emission spectra of aqueous C-dots (shown in Table 4.2) [69].

Table 4.1: Values of Lippert, KT, polarity parameter and dielectric constant for various solvents.

Solvent System	Lippert parameter	KT model parameter [70]		
	Δf	π^*	α	β
H_2O	0.320	1.09	1.17	0.18
MeOH	0.310	0.60	0.93	0.62
DMF	0.275	0.275	0.88	0.69
ACN	0.305	0.75	0.19	0.31
CCl_4	0.011	0.55	0	0
$CHCl_3$	0.0135	0.58	0.44	0
CH_2Cl_2	0.219	0.82	0.13	0.10

Table 4.2: Detail of emission spectra for dual emissive C-dots in the presence of variant solvent systems.

Solvent system	Excitation wavelength (λ_{ex})	Emission wavelength (λ_{em})	
		λ_1	λ_2

H_2O	350 nm	434	518
MeOH		443	523
DMF		445	527
ACN		449	546
CCl_4		436	544
$CHCl_3$		440	546
CH_2Cl_2		443	543

Moreover, another unusual kind of emission spectrum was observed in the presence of halogenated solvents (CH_2Cl_2, $CHCl_3$, and CCl_4) (Fig. 4.6b). The dual emissive C-dots exhibit bathochromic emission in both the shorter and longer wavelengths, as well as both the emission maxima, appear as prominent peaks. This behavior was observed due to the formation of donor-π-acceptor interaction between sp^2 domain, electron-rich hetero-atoms on the surface of C-dots and halogenated solvents [71,72], that increases its ICT character in the excited state [73,74]. Similar results were reported by Ooyama *et al.* [75] where they observed a bathochromic shift in ICT bands of halogenated solvents with novel donor– π–acceptor type pyridinium dyes. Therefore, from the solvatochromic analysis, it can be concluded that the PL properties of dual emissive C-dots were dependent upon the nature of the solvents.

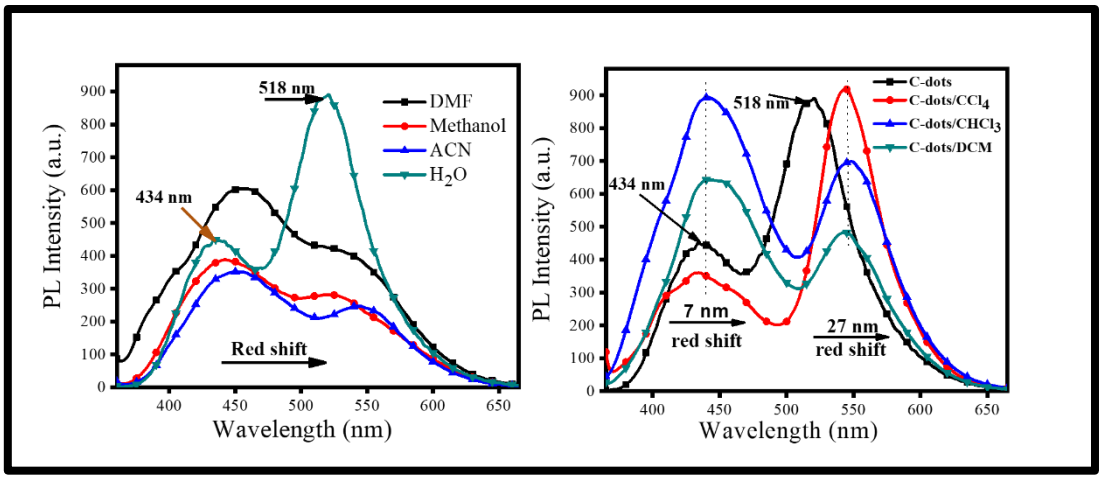

Fig. 4.6: Solvatochromism of dual emissive C-dots: a) non-halogenated and b) halogenated solvents.

4.3.7 Interaction of C-dots with different metal ions in aqueous and halogenated solvents

Here, we have also explored the efficacy of metal ions interaction with dual emissive C-dots in aqueous medium and halogenated solvents by determining the photoluminescence properties. The sensing efficacy of C-dots was evaluated in acidic conditions (pH~3) because with protonation of its surface causes weaker electrostatic interaction across all metal ions and promote selectivity towards metal ions that have higher charge and smaller size [47]. According to experimental analysis, it has been observed from Fig. 4.7 that C-dots undergoes fluorescence quenching with the gradual addition of Fe^{3+} ions.

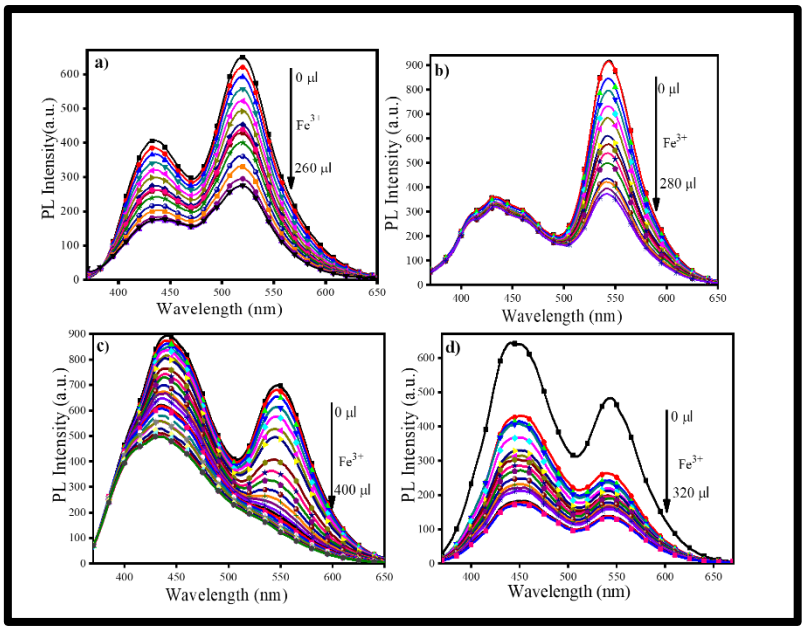

Fig. 4.7: Interaction studies of dual emissive C-dots with Fe^{3+} ions dispersed in a) H_2O, b) CCl_4, c) $CHCl_3$ and d) CH_2Cl_2 medium.

In water, chloroform, and CH_2Cl_2, C-dots steadily quenches at both the wavelength. But the extent of quenching efficiency at the longer wavelength is much more as compared to the shorter one because at longer wavelength more surface or edge functional groups (C=O, P=O and O-H, etc.) exist, which induces electrostatic interaction with Fe^{3+} ions [76]. This remarkable fluorescence response in a non-aqueous and aqueous medium in the presence of Fe^{3+} ions can be probably attributed because dual emissive C-dots have C=O/O-H on its surface that generates Fe^{3+}/C-dots complex which leads to electron transfer from its HOMO (singlet excited state) to the half field 3d orbital of Fe^{3+} ions and induces fluorescence quenching among C-dots through photoinduced electron transfer mechanism (PET) [77]. This quenching

mechanism of dual C-dots towards Fe^{3+} ions was justified by evaluating different kinds of the photophysical parameters such as PLQY (φ) and lifetime decay (τ_{av}), radiative (k_r) and non-radiative rate constant (k_{nr}) values, which was mentioned in Table 4.3.

Table 4.3: Effect of Fe^{3+} ions on various photophysical parameters of C-dots in different solvents.

System	φ	τ_{av} (ns)	k_r (ns^{-1})	k_{nr} (ns^{-1})	$\chi 2$
C-dots in water	0.50	0.319	1.567	1.567	1.16
C-dots in water + Fe^{3+}	0.27	0.284	0.951	2.570	1.20
C-dots in CCl_4	0.78	0.855	0.913	0.257	1.04
C-dots in CCl_4 + Fe^{3+}	0.34	0.498	0.683	1.325	1.18
C-dots in $CHCl_3$	0.86	1.132	0.760	0.124	1.21
C-dots in $CHCl_3$ + Fe^{3+}	0.31	0.756	0.410	0.913	1.16
C-dots in CH_2Cl_2	0.56	0.771	0.726	0.571	1.09
C-dots in CH_2Cl_2+ Fe^{3+}	0.14	0.508	0.276	1.693	1.04

The PLQY of C-dots in water, CCl_4, $CHCl_3$ and CH_2Cl_2 are 0.50, 078, 0.86 and 0.56 respectively. Presence of Fe^{3+} ions causes quenching of the PLQY of C-dots in all the studied solvent systems. The PLQY of C-dots in presence of water, CCl_4, $CHCl_3$ and CH_2Cl_2 are 0.27, 0.34, 0.31 and 0.14 respectively. Similarly, lifetime values of C-dots also confirm that in the presence of Fe^{3+} ions significantly quenching of the lifetime value occurs in different solvent systems (Table 4.3 and Fig. 4.8).

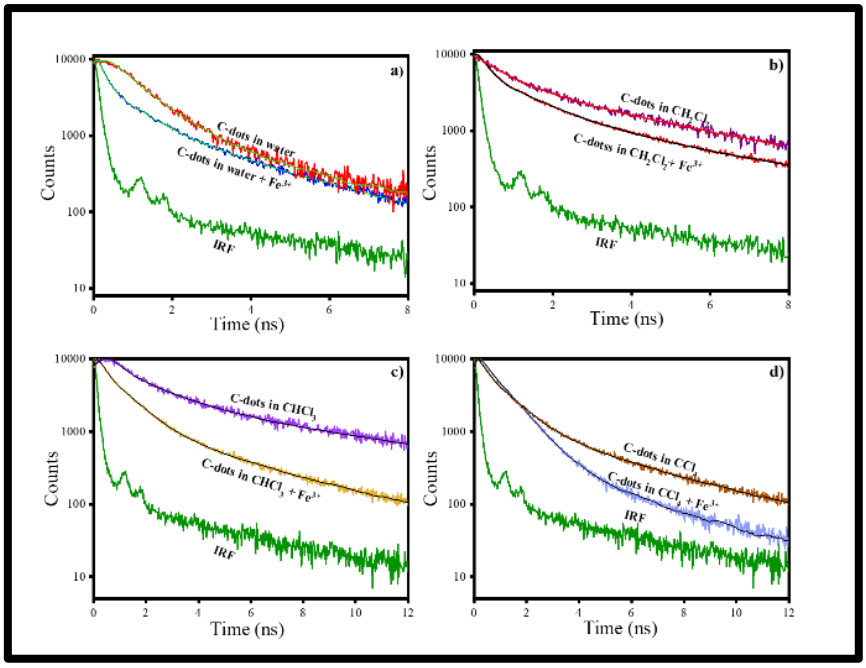

Fig. 4.8: Lifetime decay of dual emissive C-dots in the absence and presence of Fe^{3+} ions in different medium a) water, b) CH_2Cl_2, c) $CHCl_3$ and d) CCl_4.

Furthermore, the Stern-Volmer equation (2) was followed to evaluate the sensing efficiency of C-dots in various medium towards Fe^{3+} ions.

$$F_0/F = 1 + K_{SV}C \qquad (2)$$

Where F_0 is the initial fluorescence intensity in the absence of an analyte, F is the fluorescence intensity in the related concentrations of metal, K_{SV} is the Stern-Volmer constant and C is the concentration of metal ions. It was seen from the experimental results that; fluorescence quenching is in the order of $CHCl_3$ (K_{SV} = 0.077 × 10^{-6} M^{-1})>CCl_4 (K_{SV} = 0.063 × 10^{-6} M^{-1})>CH_2Cl_2 (K_{SV} = 0.044× 10^{-6} M^{-1})>H_2O (K_{SV} = 0.031× 10^{-6} M^{-1}) which is illustrated in Fig. 4.9. The performed experiments indicate that dual emissive C-dots in the different solvent system can act as a sensing probe for the metal ions.

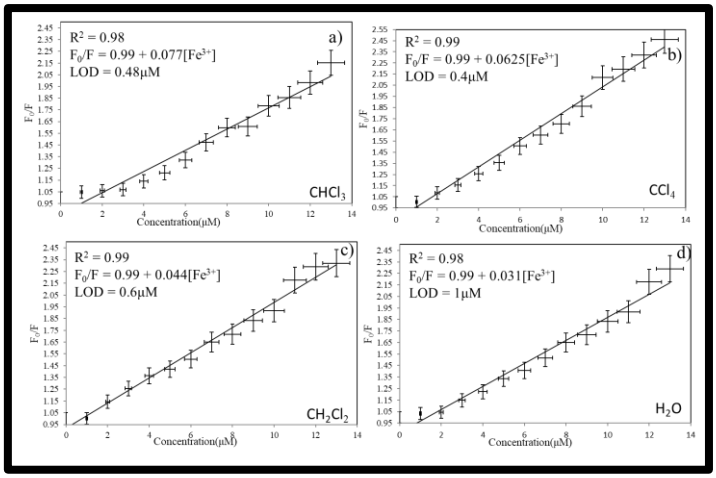

Fig. 4.9: Stern-Volmer plot between PL intensity of C-dots and Fe^{3+}ions concentrations in a different medium.

Moreover, the estimation for the selectivity of C-dots towards the Fe^{3+} ions in a different solvent system, we investigated its fluorescence response with other metal ions like Cu^{2+}, Zn^{2+}, Fe^{2+}, Cd^{2+}, Ni^{2+}, Mg^{2+}, i.e. shown in Fig. 4.10. The results showed no significant change in the fluorescence intensity of C-dots in the aforementioned metal ions except Fe^{3+} ions. The selectivity of Fe^{3+} ions leads to severe fluorescence quenching of carbon quantum dots due to the strong interaction of Fe^{3+} with the carboxylic/phosphate/hydroxyl/sulfur groups on the surfaces of the C-dots. This quenching mechanism can be explained by the hard-soft-acid-base (HSAB) principle, where Fe^{3+} ions act as hard acid and hetero atom-based surface-functionalized C-dots act as hard base [31]. Anjana *et al.* reported that significant electron transfer induced quenching of Fe^{3+} ions between hetero-atom rich C-dots also occurred due to its paramagnetic effect, higher charge density, smaller size and positive reduction potential [78]. Thus, it was justified that the dual emissive C-dots were highly selective and sensitive probe for Fe^{3+} ions in both aqueous and non-aqueous medium.

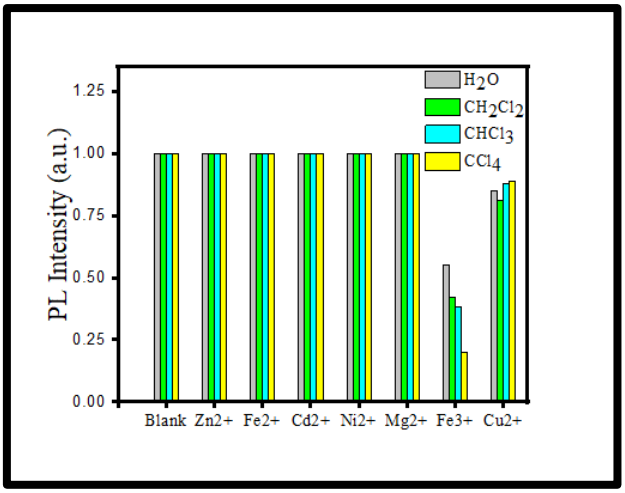

Fig. 4.10: Interference studies of metal ions with C-dots in the presence of the different solvent system.

Furthermore, to evaluate the efficacy of dual emissive C-dots its detection limit for Fe^{3+} ions was compared with several reported materials mentioned in Table 4.4. After the comparison, it was concluded that Fe^{3+} ions can be quantified effectively in any solvent medium using dual emissive C-dots.

Table 4.4: Comparison studies with different sensing probe for Fe^{3+} ions detection (in aqueous medium).

S. No.	Sensing probe for Fe^{3+} ions	LOD (μM)	Ref.
1.	Graphene quantum dots	0.09	[76]
2.	Banana derived C-dots	0.21	[79]
3.	DL Malic acid-derived C-dots	0.8	[80]
4.	N, S co-doped C-dots	0.017	[81]
5.	Mint leaves derived C-dots	0.37	[82]
5.	Acid mediated dual emissive C-dots	0.4	This work

4.3.8 Efficacy of dual emissive C-dots in the real sample sensing

The dual emissive C-dots found selective for Fe^{3+} ions in the both organic and aqueous medium. So, its PL spectra were recorded to study its effects in the real samples (Fe^{3+} ions in tablets and syrups). Different volume (0-250 μl) of Fe^{3+} ions was spiked in the real sample solution to maintain a suitable concentration of these ions. The results obtained from PL studies show that Fe^{3+} ions gradually decrease the PL intensity at λ_{em} = 543 nm. A similar trend was

also observed for standard samples. The accuracy was also evaluated by calculating its recovery % in the organic and aqueous phase to support the analytical results mentioned in Table 4.5. As a result, 99.8% recovery was obtained in the C-dots (organic and aqueous phase) for Fe^{3+} ions. Thus, this nano-probe can effectively use in the real samples for Fe^{3+} ions determination.

Table 4.5: Solvatochromic sensing efficiency of dual emissive C-dots in the real sample.

S.No.	Solvatochromic sensing system	The concentration of Fe^{3+} ions (µM)		Recovery (%)
		Added	Determined ± SD	
1	C-dots + CCl_4	20	19.60 ± 0.23	98.0
		20	19.93 ± 0.25	99.6
		20	19.89 ± 0.27	99.4
2	C-dots + $CHCl_3$	20	20.10 ± 0.39	100.5
		20	20.12 ± 0.37	100.6
		20	20.01± 0.42	100.0
3	C-dots + CH_2Cl_2	20	19.85± 0.29	99.2
		20	19.70 ± 0.31	98.5
		20	19.95 ± 0.33	99.7
5	C-dots + H_2O	20	19.90 ± 0.31	99.5
		20	19.90 ± 0.31	99.7
		20	19.80 ± 0.27	99.0

References

(1) Lim, S. Y.; Shen, W.; Gao, Z. Carbon Quantum Dots and Their Applications. *Chemical Society Reviews*. Royal Society of Chemistry December 8, 2015, pp 362–381. https://doi.org/10.1039/c4cs00269e.

(2) Dong, Y.; Wang, R.; Li, G.; Chen, C.; Chi, Y.; Chen, G. Polyamine-Functionalized Carbon Quantum Dots as Fluorescent Probes for Selective and Sensitive Detection of Copper Ions. *Anal. Chem.* **2012**, *84* (14), 6220–6224.

https://doi.org/10.1021/ac3012126.

(3) Zhao, Q.-L.; Zhang, Z.-L.; Huang, B.-H.; Peng, J.; Zhang, M.; Pang, D.-W. Facile Preparation of Low Cytotoxicity Fluorescent Carbon Nanocrystals by Electrooxidation of Graphite. *Chem. Commun.* **2008**, *0* (41), 5116. https://doi.org/10.1039/b812420e.

(4) Pan, D.; Zhang, J.; Li, Z.; Wu, C.; Yan, X.; Wu, M. Observation of PH-, Solvent-, Spin-, and Excitation-Dependent Blue Photoluminescence from Carbon Nanoparticles. *Chem. Commun.* **2010**, *46* (21), 3681–3683. https://doi.org/10.1039/c000114g.

(5) Liu, H.; Ye, T.; Mao, C. Fluorescent Carbon Nanoparticles Derived from Candle Soot. *Angew. Chemie - Int. Ed.* **2007**, *46* (34), 6473–6475. https://doi.org/10.1002/anie.200701271.

(6) Wang, Q.; Zheng, H.; Long, Y.; Zhang, L.; Gao, M.; Bai, W. Microwave-Hydrothermal Synthesis of Fluorescent Carbon Dots from Graphite Oxide. *Carbon N. Y.* **2011**, *49* (9), 3134–3140. https://doi.org/10.1016/j.carbon.2011.03.041.

(7) Li, H.; He, X.; Liu, Y.; Huang, H.; Lian, S.; Lee, S. T.; Kang, Z. One-Step Ultrasonic Synthesis of Water-Soluble Carbon Nanoparticles with Excellent Photoluminescent Properties. *Carbon N. Y.* **2011**, *49* (2), 605–609. https://doi.org/10.1016/j.carbon.2010.10.004.

(8) Lu, M.; Zhou, L. One-Step Sonochemical Synthesis of Versatile Nitrogen-Doped Carbon Quantum Dots for Sensitive Detection of Fe2+ Ions and Temperature in Vitro. *Mater. Sci. Eng. C* **2019**, *101*, 352–359. https://doi.org/10.1016/J.MSEC.2019.03.109.

(9) Lu, J.; Yeo, P. S. E.; Gan, C. K.; Wu, P.; Loh, K. P. Transforming C 60 Molecules into Graphene Quantum Dots. *Nat. Nanotechnol.* **2011**, *6* (4), 247–252. https://doi.org/10.1038/nnano.2011.30.

(10) Xu, X.; Ray, R.; Gu, Y.; Ploehn, H. J.; Gearheart, L.; Raker, K.; Scrivens, W. A. Electrophoretic Analysis and Purification of Fluorescent Single-Walled Carbon Nanotube Fragments. *J. Am. Chem. Soc.* **2004**, *126* (40), 12736–12737. https://doi.org/10.1021/ja040082h.

(11) Yang, S.; Zeng, H.; Zhao, H.; Zhang, H.; Cai, W. Luminescent Hollow Carbon Shells

and Fullerene-like Carbon Spheres Produced by Laser Ablation with Toluene. *J. Mater. Chem.* **2011**, *21* (12), 4432–4436. https://doi.org/10.1039/c0jm03475d.

(12) Jiang, H.; Chen, F.; Lagally, M. G.; Denes, F. S. New Strategy for Synthesis and Functionalization of Carbon Nanoparticles. *Langmuir* **2010**, *26* (3), 1991–1995. https://doi.org/10.1021/la9022163.

(13) Qian, Z. S.; Shan, X. Y.; Chai, L. J.; Chen, J. R.; Feng, H. A Fluorescent Nanosensor Based on Graphene Quantum Dots-Aptamer Probe and Graphene Oxide Platform for Detection of Lead (II) Ion. *Biosens. Bioelectron.* **2015**, *68*, 225–231. https://doi.org/10.1016/j.bios.2014.12.057.

(14) Cui, X.; Zhu, L.; Wu, J.; Hou, Y.; Wang, P.; Wang, Z.; Yang, M. A Fluorescent Biosensor Based on Carbon Dots-Labeled Oligodeoxyribonucleotide and Graphene Oxide for Mercury (II) Detection. *Biosens. Bioelectron.* **2015**, *63*, 506–512. https://doi.org/10.1016/j.bios.2014.07.085.

(15) Qu, Z. B.; Zhou, X.; Gu, L.; Lan, R.; Sun, D.; Yu, D.; Shi, G. Boronic Acid Functionalized Graphene Quantum Dots as a Fluorescent Probe for Selective and Sensitive Glucose Determination in Microdialysate. *Chem. Commun.* **2013**, *49* (84), 9830–9832. https://doi.org/10.1039/c3cc44393k.

(16) Feng, H.; Qian, Z. Functional Carbon Quantum Dots: A Versatile Platform for Chemosensing and Biosensing. *Chem. Rec.* **2018**, *18* (5), 491–505. https://doi.org/10.1002/tcr.201700055.

(17) Gao, X.; Du, C.; Zhuang, Z.; Chen, W. Carbon Quantum Dot-Based Nanoprobes for Metal Ion Detection. *Journal of Materials Chemistry C*. Royal Society of Chemistry 2016, pp 6927–6945. https://doi.org/10.1039/c6tc02055k.

(18) Gao, X.; Lu, Y.; Zhang, R.; He, S.; Ju, J.; Liu, M.; Li, L.; Chen, W. One-Pot Synthesis of Carbon Nanodots for Fluorescence Turn-on Detection of Ag + Based on the Ag + -Induced Enhancement of Fluorescence. *J. Mater. Chem. C* **2015**, *3* (10), 2302–2309. https://doi.org/10.1039/c4tc02582b.

(19) Zhang, R.; Chen, W. Nitrogen-Doped Carbon Quantum Dots: Facile Synthesis and Application as a "Turn-off" Fluorescent Probe for Detection of Hg2+ Ions. *Biosens.*

Bioelectron. **2014**, *55*, 83–90. https://doi.org/10.1016/j.bios.2013.11.074.

(20) Zu, F.; Yan, F.; Bai, Z.; Xu, J.; Wang, Y.; Huang, Y.; Zhou, X. The Quenching of the Fluorescence of Carbon Dots: A Review on Mechanisms and Applications. *Microchimica Acta*. Springer-Verlag Wien July 1, 2017, pp 1899–1914. https://doi.org/10.1007/s00604-017-2318-9.

(21) Yan, F.; Jiang, Y.; Sun, X.; Bai, Z.; Zhang, Y.; Zhou, X. Surface Modification and Chemical Functionalization of Carbon Dots: A Review. *Microchimica Acta*. Springer-Verlag Wien September 1, 2018. https://doi.org/10.1007/s00604-018-2953-9.

(22) Kwon, W.; Lim, J.; Lee, J.; Park, T.; Rhee, S.-W. Sulfur-Incorporated Carbon Quantum Dots with a Strong Long-Wavelength Absorption Band. *J. Mater. Chem. C* **2013**, *1* (10), 2002. https://doi.org/10.1039/c3tc00683b.

(23) Zheng, H.; Wang, Q.; Long, Y.; Zhang, H.; Huang, X.; Zhu, R. Enhancing the Luminescence of Carbon Dots with a Reduction Pathway. *Chem. Commun.* **2011**, *47* (38), 10650. https://doi.org/10.1039/c1cc14741b.

(24) Pan, L.; Sun, S.; Zhang, A.; Jiang, K.; Zhang, L.; Dong, C.; Huang, Q.; Wu, A.; Lin, H. Truly Fluorescent Excitation-Dependent Carbon Dots and Their Applications in Multi-color Cellular Imaging and Multidimensional Sensing. *Adv. Mater.* **2015**, *27* (47), 7782–7787. https://doi.org/10.1002/adma.201503821.

(25) Kailasa, S. K.; Ha, S.; Baek, S. H.; Phan, L. M. T.; Kim, S.; Kwak, K.; Park, T. J. Tuning of Carbon Dots Emission Color for Sensing of Fe 3+ Ion and Bioimaging Applications. *Mater. Sci. Eng. C* **2019**, *98*, 834–842. https://doi.org/10.1016/j.msec.2019.01.002.

(26) Li, S.; Jiang, J.; Yan, Y.; Wang, P.; Huang, G.; Kim, N. hoon; Lee, J. H.; He, D. Red, Green, and Blue Fluorescent Folate-Receptor-Targeting Carbon Dots for Cervical Cancer Cellular and Tissue Imaging. *Mater. Sci. Eng. C* **2018**, *93*, 1054–1063. https://doi.org/10.1016/J.MSEC.2018.08.058.

(27) Feng, H.; Qian, Z. Functional Carbon Quantum Dots: A Versatile Platform for Chemosensing and Biosensing. *Chem. Rec.* **2018**, *18* (5), 491–505. https://doi.org/10.1002/tcr.201700055.

(28) Bao, L.; Liu, C.; Zhang, Z.-L.; Pang, D.-W. Photoluminescence-Tunable Carbon Nanodots: Surface-State Energy-Gap Tuning. *Adv. Mater.* **2015**, *27* (10), 1663–1667. https://doi.org/10.1002/adma.201405070.

(29) Ding, H.; Yu, S.-B.; Wei, J.-S.; Xiong, H.-M. Full-Color Light-Emitting Carbon Dots with a Surface-State-Controlled Luminescence Mechanism. *ACS Nano* **2016**, *10* (1), 484–491. https://doi.org/10.1021/acsnano.5b05406.

(30) Mehta, A.; Mishra, A.; Kainth, S.; Basu, S. Carbon Quantum Dots/TiO2 Nanocomposite for Sensing of Toxic Metals and Photodetoxification of Dyes with Kill Waste by Waste Concept. *Mater. Des.* **2018**, *155*, 485–493. https://doi.org/10.1016/j.matdes.2018.06.015.

(31) Kainth, S.; Mehta, A.; Mishra, A.; Basu, S. Implementation of a Logic Gate by Chemically Induced Nitrogen and Oxygen Rich C-Dots for the Selective Detection of Fluoride Ions. *New J. Chem.* **2018**, *42* (14), 12162–12171. https://doi.org/10.1039/c8nj02041h.

(32) Jiang, K.; Sun, S.; Zhang, L.; Lu, Y.; Wu, A.; Cai, C.; Lin, H. Red, Green, and Blue Luminescence by Carbon Dots: Full-Color Emission Tuning and Multi-color Cellular Imaging. *Angew. Chemie - Int. Ed.* **2015**, *54* (18), 5360–5363. https://doi.org/10.1002/anie.201501193.

(33) Zhu, S.; Zhang, J.; Qiao, C.; Tang, S.; Li, Y.; Yuan, W.; Li, B.; Tian, L.; Liu, F.; Hu, R.; et al. Strongly Green-Photoluminescent Graphene Quantum Dots for Bioimaging Applications. *Chem. Commun.* **2011**, *47* (24), 6858. https://doi.org/10.1039/c1cc11122a.

(34) Ray, S. C.; Saha, A.; Jana, N. R.; Sarkar, R. Fluorescent Carbon Nanoparticles: Synthesis, Characterization, and Bioimaging Application. *J. Phys. Chem. C* **2009**, *113* (43), 18546–18551. https://doi.org/10.1021/jp905912n.

(35) Wee, S. S.; Ng, Y. H.; Ng, S. M. et al *Talanta* **2013**, *116*, 71–76. https://doi.org/10.1016/J.TALANTA.2013.04.081.

(36) Bhunia, S. K.; Saha, A.; Maity, A. R.; Ray, S. C.; Jana, N. R. Carbon Nanoparticle-Based Fluorescent Bioimaging Probes. *Sci. Rep.* **2013**, *3* (1), 1473.

https://doi.org/10.1038/srep01473.

(37) Xu, Z.-Q.; Yang, L.-Y.; Fan, X.-Y.; Jin, J.-C.; Mei, J.; Peng, W.; Jiang, F.-L.; Xiao, Q.; Liu, Y. Low Temperature Synthesis of Highly Stable Phosphate Functionalized Two Color Carbon Nanodots and Their Application in Cell Imaging. *Carbon N. Y.* **2014**, *66*, 351–360. https://doi.org/10.1016/j.carbon.2013.09.010.

(38) Dong, Y.; Pang, H.; Yang, H. Bin; Guo, C.; Shao, J.; Chi, Y.; Li, C. M.; Yu, T. Carbon-Based Dots Co-Doped with Nitrogen and Sulfur for High Quantum Yield and Excitation-Independent Emission. *Angew. Chemie Int. Ed.* **2013**, *52* (30), 7800–7804. https://doi.org/10.1002/anie.201301114.

(39) Sciortino, A.; Marino, E.; Dam, B. van; Schall, P.; Cannas, M.; Messina, F. Solvatochromism Unravels the Emission Mechanism of Carbon Nanodots. *J. Phys. Chem. Lett.* **2016**, *7* (17), 3419–3423. https://doi.org/10.1021/acs.jpclett.6b01590.

(40) Reckmeier, C. J.; Wang, Y.; Zboril, R.; Rogach, A. L. Influence of Doping and Temperature on Solvatochromic Shifts in Optical Spectra of Carbon Dots. *J. Phys. Chem. C* **2016**, *120* (19), 10591–10604. https://doi.org/10.1021/acs.jpcc.5b12294.

(41) Crosby, G. A.; Demas, J. N. Measurement of Photoluminescence Quantum Yields. Review. *J. Phys. Chem.* **1971**, *75* (8), 991–1024. https://doi.org/10.1021/j100678a001.

(42) Puziy, A. M.; Poddubnaya, O. I.; Martínez-Alonso, A.; Suárez-García, F.; Tascón, J. M. D. Synthetic Carbons Activated with Phosphoric - Acid I. Surface Chemistry and Ion Binding Properties. *Carbon N. Y.* **2002**, *40* (9), 1493–1505. https://doi.org/10.1016/S0008-6223(01)00317-7.

(43) Puziy, A. M.; Poddubnaya, O. I.; Gawdzik, B.; Sobiesiak, M.; Tsyba, M. M. Phosphoric Acid Activation—Functionalization and Porosity Modification. *Appl. Surf. Sci.* **2007**, *253* (13), 5736–5740. https://doi.org/10.1016/J.APSUSC.2006.12.034.

(44) Puziy, A. M.; Poddubnaya, O. I.; Ziatdinov, A. M. On the Chemical Structure of Phosphorus Compounds in Phosphoric Acid-Activated Carbon. *Appl. Surf. Sci.* **2006**, *252* (23), 8036–8038. https://doi.org/10.1016/j.apsusc.2005.10.044.

(45) Puziy, A. M.; Poddubnaya, O. I.; Martínez-Alonso, A.; Suárez-García, F.; Tascón, J.

M. D. Surface Chemistry of Phosphorus-Containing Carbons of Lignocellulosic Origin. *Carbon N. Y.* **2005**, *43* (14), 2857–2868. https://doi.org/10.1016/J.CARBON.2005.06.014.

(46) Hu, Y.; Yang, J.; Tian, J.; Jia, L.; Yu, J. S. Waste Frying Oil as a Precursor for One-Step Synthesis of Sulfur-Doped Carbon Dots with PH-Sensitive Photoluminescence. *Carbon N. Y.* **2014**, *77*, 775–782. https://doi.org/10.1016/j.carbon.2014.05.081.

(47) Chang, M. M. F.; Ginjom, I. R.; Ngu-Schwemlein, M.; Ng, S. M. Synthesis of Yellow Fluorescent Carbon Dots and Their Application to the Determination of Chromium(III) with Selectivity Improved by PH Tuning. *Microchim. Acta* **2016**, *183* (6), 1899–1907. https://doi.org/10.1007/s00604-016-1819-2.

(48) Loi, E.; Ng, R. W. C.; Chang, M. M. F.; Fong, J. F. Y.; Ng, Y. H.; Ng, S. M. One-Pot Synthesis of Carbon Dots Using Two Different Acids and Their Respective Unique Photoluminescence Property. *Luminescence* **2017**, *32* (1), 114–118. https://doi.org/10.1002/bio.3157.

(49) Ryu, J.; Suh, Y. W.; Suh, D. J.; Ahn, D. J. Hydrothermal Preparation of Carbon Microspheres from Mono-Saccharides and Phenolic Compounds. *Carbon N. Y.* **2010**, *48* (7), 1990–1998. https://doi.org/10.1016/j.carbon.2010.02.006.

(50) Kwon, W.; Do, S.; Rhee, S.-W. Formation of Highly Luminescent Nearly Monodisperse Carbon Quantum Dots via Emulsion-Templated Carbonization of Carbohydrates. *RSC Adv.* **2012**, *2* (30), 11223. https://doi.org/10.1039/c2ra22186a.

(51) Sakaki, T.; Shibata, M.; Miki, T.; Hirosue, H.; Hayashi, N. Reaction Model of Cellulose Decomposition in Near-Critical Water and Fermentation of Products. *Bioresour. Technol.* **1996**, *58* (2), 197–202. https://doi.org/10.1016/S0960-8524(96)00099-5.

(52) Chen, B.; Li, F.; Li, S.; Weng, W.; Guo, H.; Guo, T.; Zhang, X.; Chen, Y.; Huang, T.; Hong, X.; et al. Large Scale Synthesis of Photoluminescent Carbon Nanodots and Their Application for Bioimaging. *Nanoscale* **2013**, *5* (5), 1967–1971. https://doi.org/10.1039/c2nr32675b.

(53) Li, H.; Ming, H.; Liu, Y.; Yu, H.; He, X.; Huang, H.; Pan, K.; Kang, Z.; Lee, S.-T.

Fluorescent Carbon Nanoparticles: Electrochemical Synthesis and Their PH Sensitive Photoluminescence Properties. *New J. Chem.* **2011**, *35* (11), 2666. https://doi.org/10.1039/c1nj20575g.

(54) Luo, Z.; Lu, Y.; Somers, L. A.; Johnson, A. T. C. High Yield Preparation of Macroscopic Graphene Oxide Membranes. *J. Am. Chem. Soc.* **2009**, *131* (3), 898–899. https://doi.org/10.1021/ja807934n.

(55) Zhang, Z.; Zhang, J.; Chen, N.; Qu, L. Graphene Quantum Dots: An Emerging Material for Energy-Related Applications and Beyond. *Energy Environ. Sci.* **2012**, *5* (10), 8869. https://doi.org/10.1039/c2ee22982j.

(56) Li, X.; Zhang, S.; Kulinich, S. A.; Liu, Y.; Zeng, H. Engineering Surface States of Carbon Dots to Achieve Controllable Luminescence for Solid-Luminescent Composites and Sensitive Be2+ Detection. *Sci. Rep.* **2015**, *4* (1), 4976. https://doi.org/10.1038/srep04976.

(57) Zhao, C.; Li, X.; Cheng, C.; Yang, Y. Green and Microwave-Assisted Synthesis of Carbon Dots and Application for Visual Detection of Cobalt(II) Ions and PH Sensing. *Microchem. J.* **2019**, *147*, 183–190. https://doi.org/10.1016/j.microc.2019.03.029.

(58) Jeong, Y.; Moon, K.; Jeong, S.; Koh, W. G.; Lee, K. Converting Waste Papers to Fluorescent Carbon Dots in the Recycling Process without Loss of Ionic Liquids and Bioimaging Applications. *ACS Sustain. Chem. Eng.* **2018**, *6* (4), 4510–4515. https://doi.org/10.1021/acssuschemeng.8b00353.

(59) Chen, Y.; Wu, Y.; Weng, B.; Wang, B.; Li, C. Facile Synthesis of Nitrogen and Sulfur Co-Doped Carbon Dots and Application for Fe(III) Ions Detection and Cell Imaging. *Sensors Actuators, B Chem.* **2016**, *223*, 689–696. https://doi.org/10.1016/j.snb.2015.09.081.

(60) Li, J.; Ma, S.; Xiao, X.; Zhao, D. The One-Step Preparation of Green-Emissioned Carbon Dots through Hydrothermal Route and Its Application. *J. Nanomater.* **2019**, *2019*, 1–10. https://doi.org/10.1155/2019/8628354.

(61) Shi, B.; Su, Y.; Zhang, L.; Huang, M.; Liu, R.; Zhao, S. Nitrogen and Phosphorus Co-Doped Carbon Nanodots as a Novel Fluorescent Probe for Highly Sensitive Detection

of Fe3+ in Human Serum and Living Cells. *ACS Appl. Mater. Interfaces* **2016**, *8* (17), 10717–10725. https://doi.org/10.1021/acsami.6b01325.

(62) Ding, H.; Wei, J. S.; Xiong, H. M. Nitrogen and Sulfur Co-Doped Carbon Dots with Strong Blue Luminescence. *Nanoscale* **2014**, *6* (22), 13817–13823. https://doi.org/10.1039/c4nr04267k.

(63) Yang, G.; Wan, X.; Su, Y.; Zeng, X.; Tang, J. Acidophilic S-Doped Carbon Quantum Dots Derived from Cellulose Fibers and Their Fluorescence Sensing Performance for Metal Ions in an Extremely Strong Acid Environment. *J. Mater. Chem. A* **2016**, *4* (33), 12841–12849. https://doi.org/10.1039/c6ta05943k.

(64) Wu, Z. L.; Liu, Z. X.; Yuan, Y. H. Carbon Dots: Materials, Synthesis, Properties and Approaches to Long-Wavelength and Multi-color Emission. *Journal of Materials Chemistry B*. The Royal Society of Chemistry May 31, 2017, pp 3794–3809. https://doi.org/10.1039/c7tb00363c.

(65) Yan, F.; Sun, Z.; Zhang, H.; Sun, X.; Jiang, Y.; Bai, Z. The Fluorescence Mechanism of Carbon Dots, and Methods for Tuning Their Emission Color: A Review. *Microchimica Acta*. Springer Vienna August 29, 2019, p 583. https://doi.org/10.1007/s00604-019-3688-y.

(66) Reichardt, C. Solvatochromic Dyes as Solvent Polarity Indicators. *Chem. Rev.* **1994**, *94* (8), 2319–2358. https://doi.org/10.1021/cr00032a005.

(67) Song, W.; Duan, W.; Liu, Y.; Ye, Z.; Chen, Y.; Chen, H.; Qi, S.; Wu, J.; Liu, D.; Xiao, L.; et al. Ratiometric Detection of Intracellular Lysine and PH with One-Pot Synthesized Dual Emissive Carbon Dots. *Anal. Chem.* **2017**, *89* (24), 13626–13633. https://doi.org/10.1021/acs.analchem.7b04211.

(68) Qu, S.; Zhou, D.; Li, D.; Ji, W.; Jing, P.; Han, D.; Liu, L.; Zeng, H.; Shen, D. Toward Efficient Orange Emissive Carbon Nanodots through Conjugated Sp2-Domain Controlling and Surface Charges Engineering. *Adv. Mater.* **2016**, *28* (18), 3516–3521. https://doi.org/10.1002/adma.201504891.

(69) Jones, S. S.; Sahatiya, P.; Badhulika, S. One Step, High Yield Synthesis of Amphiphilic Carbon Quantum Dots Derived from Chia Seeds: A Solvatochromic

Study. *New J. Chem.* **2017**, *41* (21), 13130–13139. https://doi.org/10.1039/c7nj03513f.

(70) Abraham, M. H.; Grellier, P. L.; Abboud, J.-L. M.; Doherty, R. M.; Taft, R. W. Solvent Effects in Organic Chemistry — Recent Developments. *Can. J. Chem.* **2006**, *66* (11), 2673–2686. https://doi.org/10.1139/v88-420.

(71) Yamaguchi, K.; Murai, T.; Tsuchiya, Y.; Miwa, Y.; Kutsumizu, S.; Sasamori, T.; Tokitoh, N. Pyridinium 5-Aminothiazoles: Specific Photophysical Properties and Vapochromism in Halogenated Solvents. *RSC Adv.* **2017**, *7* (29), 18132–18135. https://doi.org/10.1039/C7RA01896G.

(72) Mataga, N.; Kaifu, Y.; Koizumi, M. Solvent Effects upon Fluorescence Spectra and the Dipolemoments of Excited Molecules. *Bull. Chem. Soc. Jpn.* **1956**, *29* (4), 465–470. https://doi.org/10.1246/bcsj.29.465.

(73) Cigáň, M.; Donovalová, J.; Szöcs, V.; Gašpar, J.; Jakusová, K.; Gáplovský, A. 7-(Dimethylamino)Coumarin-3-Carbaldehyde and Its Phenylsemicarbazone: TICT Excited State Modulation, Fluorescent H-Aggregates, and Preferential Solvation. *J. Phys. Chem. A* **2013**, *117* (23), 4870–4883. https://doi.org/10.1021/jp402627a.

(74) Chatterjee, A.; Seth, D. Photophysical Properties of 7-(Diethylamino)Coumarin-3-Carboxylic Acid in the Nanocage of Cyclodextrins and in Different Solvents and Solvent Mixtures. *Photochem. Photobiol.* **2013**, *89*, 280–293. https://doi.org/10.1111/php.12000.

(75) Ooyama, Y.; Asada, R.; Inoue, S.; Komaguchi, K.; Imae, I.; Harima, Y. Solvatochromism of Novel Donor–π–Acceptor Type Pyridinium Dyes in Halogenated and Non-Halogenated Solvents. *New J. Chem.* **2009**, *33* (11), 2311. https://doi.org/10.1039/b9nj00332k.

(76) Ju, J.; Chen, W. Synthesis of Highly Fluorescent Nitrogen-Doped Graphene Quantum Dots for Sensitive, Label-Free Detection of Fe (III) in Aqueous Media. *Biosens. Bioelectron.* **2014**, *58*, 219–225. https://doi.org/10.1016/j.bios.2014.02.061.

(77) Pramanik, A.; Biswas, S.; Kumbhakar, P. Solvatochromism in Highly Luminescent Environmental Friendly Carbon Quantum Dots for Sensing Applications: Conversion of Bio-Waste into Bio-Asset. *Spectrochim. Acta - Part A Mol. Biomol. Spectrosc.*

2018, *191*, 498–512. https://doi.org/10.1016/j.saa.2017.10.054.

(78) Anjana, R. R.; Anjali Devi, J. S.; Jayasree, M.; Aparna, R. S.; Aswathy, B.; Praveen, G. L.; Lekha, G. M.; Sony, G. S,N-Doped Carbon Dots as a Fluorescent Probe for Bilirubin. *Microchim. Acta* **2018**, *185* (1). https://doi.org/10.1007/s00604-017-2574-8.

(79) Vikneswaran, R.; Ramesh, S.; Yahya, R. Green Synthesized Carbon Nanodots as a Fluorescent Probe for Selective and Sensitive Detection of Iron(III) Ions. *Mater. Lett.* **2014**, *136*, 179–182. https://doi.org/10.1016/j.matlet.2014.08.063.

(80) Lu, W.; Gong, X.; Nan, M.; Liu, Y.; Shuang, S.; Dong, C. Comparative Study for N and S Doped Carbon Dots: Synthesis, Characterization and Applications for Fe3+ Probe and Cellular Imaging. *Anal. Chim. Acta* **2015**, *898*, 116–127. https://doi.org/10.1016/j.aca.2015.09.050.

(81) Bolm, C.; Legros, J.; Le Paih, J.; Zani, L. Iron-Catalyzed Reactions in Organic Synthesis. *Chem. Rev.* **2004**, *104* (12), 6217–6254. https://doi.org/10.1021/cr040664h.

(82) Raveendran, V.; Suresh Babu, A. R.; Renuka, N. K. Mint Leaf Derived Carbon Dots for Dual Analyte Detection of Fe(III) and Ascorbic Acid. *RSC Adv.* **2019**, *9* (21), 12070–12077. https://doi.org/10.1039/c9ra02120e.

CHAPTER-5

Impact of Different Nitrogen Surface Passivation in C-dots and Its Sensing Efficacy Towards Picric Acid and Creatinine

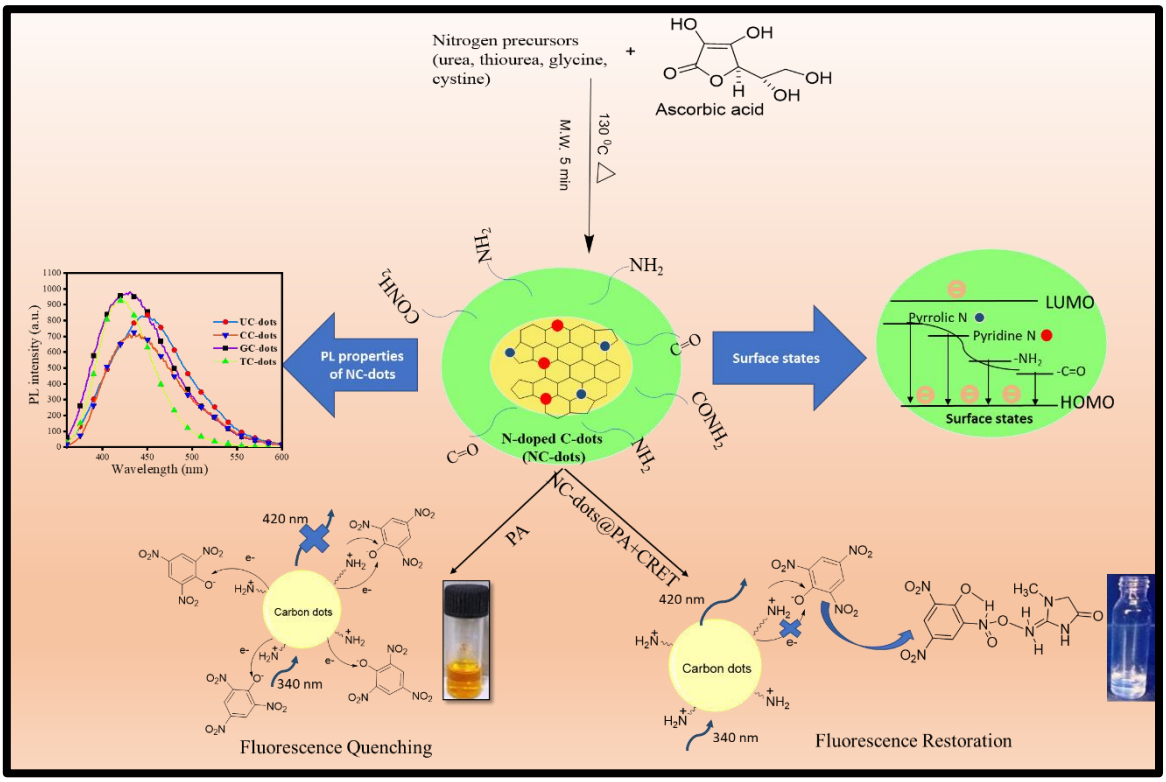

Highlights

1. Rapid microwave synthesis of nitrogen precursor dependent carbon dots (NC-dots).
2. Modulation of physio-chemical and fluorescence properties of NC-dots using different nitrogen passivating agent.
3. Determination of the interaction efficacy of nitrogen passivated NC-dots towards 2,4,6 trinitrophenol (PA).
4. Turn off-on PL properties of NC-dots was applied for selective/sensitivity detection of creatinine.
5. Method validation of proposed route using real samples.

5.1 Introduction

Photoluminescence (PL) active materials seek great attention in the field of chemo/bio-sensing, bio-imaging and drug delivery. There were several varieties of classical fluorophore like quantum dots (QDs), organic fluorophores which were known as an analytical tool for toxic and important biological moieties. Nowadays zero-dimensional carbon dots (C-dots) have attracted as most promising attention as a novel fluorescent nanomaterial in the field of the biosensor, energy, drug delivery, bio-imaging and catalysis. The C-dots have paid great attention in research due to their several splendid properties such as tunable PL properties, multi-colored emission, excellent chemical stability, low cost, facile preparation and ease of functionalization. In this context, C-dots are regarded as most important green materials with excellent water solubility, low toxicity, excellent biocompatibility as compared with other conventional classical fluorophores, semiconductor quantum dots [1–3]. The fundamental factor for exhibiting photoluminescence (PL) property of C-dots is due to the presence of molecular and core state and their surface groups[2], which are responsible for variation in the bandgap, particle size as well as tunable emissive properties.

Numerous traditional strategies were reported in the literature to prepare the C-dots such as strong acidic electrochemical oxidation, microwave-assisted synthesis, hydrothermal treatment and ultrasonic methods [4–7]. Even, researchers were also succeeding towards various cost-effective amendments such as carbonization of various natural biomass as a carbon precursor-like milk, fruit juice, peels and coffee grounds, etc. to attain different properties of C-dots [5,8–11]. The major components in C-dots contain carbon (C) and oxygen (O) as the prominent element and showed blue fluorescence with low quantum yield (PLQY) which often limits its application and development [12]. Thus, there is a requirement of surface modification or functionalization to boost its biosensing efficacy.

Several parameters control the optical properties of C-dots, i.e. synthetic routes, the types of precursor and passivating agents. The simplest way to tune the PL properties of C-dots was through surface state mechanism by interacting carbon skeleton with different neighboring atoms using various passivating agents [2,13–16]. The involvement of diverse surface elements eliminates or suppress the original O-states in the C-dots, facilitate the radiative recombination which leads to the rise in its PLQY and tunable bandgap energy.

Among numerous elements utilization of nitrogen precursor as passivating agent plays a crucial role in tuning its PL properties due to comparable atomic size as carbon atoms, which is adjusted easily in the carbon skeleton [17–19]. It originates multiple nitrogen species in the structure of C-dots such as amino, pyrrole, pyridine and graphite type in which only amino form distributed on its surface and other exhibited at their centre and edge of its graphene skeleton. These four types of nitrogen species contribute invariant form towards its optical properties. Non-amino groups produce surface defects in its molecular core which finally cause PL enhancement whereas graphitic nitrogen modulates its color emitting properties. Overall, nitrogen doping modulates the chemical reactivity, surface and electronic properties and cause a bathochromic shift in emission wavelength of C-dots [20,21].

Few synthetic routes were reported in literature where different nitrogen-containing precursor was used to prepare NC-dots. Ding *et al* prepared multi-color NC-dots using p-phenylenediamine and urea as precursor [22]. They separated eight different types of NC-dots through silica chromatography, which exhibited variation of their emission wavelength in the range of blue to red emission (440-625 nm) and their PLQY values (8.5-35%) [22]. Many researchers also utilized variant nitrogen-containing precursors such as ammonium citrate [23], a mixture of glucose and ammonium hydroxide [24], citric acid and branched poly(ethylenimine) [24] and ethylenediamine to prepare different NC-dots. These different nitrogen-containing precursors cause quantum-confinement and red-edge effect in the NC-dots, which modulate their electronic properties. Apart from that, amino rich precursors such as o-phenyl-diamine and 4-aminobutyric acid were also reported for yellow emissive NC-dots, which was implemented to detect fluoroquinolones derivatives via fluorescence sensing approach [25]. Likewise, Song *et al* explored dual emissive NC-dots by using single nitrogen precursor (a mixture of o-phenyl-diamine and ortho-phosphoric acid) for the intercellular detection of lysine [26]. Many other nitrogen sources such as 1,2,4 triaminobenzene were also utilized to prepare NC-dots, which was used for the cell-imaging and bifunctional sensing [27]. The necessity to develop these dual emissive/multi-color C-dots was to establish sensing methodology based on their ratio-metric approaches, which eliminates the fluctuation of the excitation source, local environmental change and variation of the concentration of the probe to improve their sensitivity towards different toxic moieties [28,29].

Among variant, hazardous materials, 2,4,6-trinitrophenol (picric acid, PA) found explosive due to the existence of electrophilic nitro groups and high-water solubility. Immense

evidence for its quantification was known with graphene quantum dots[30], hydrophilic and hydrophobic C-dots [31,32]. Due to excited state electron transfer/charge transfer interaction, C-dots exhibited high PL response (significant quenching) for PA [32,33]. In biochemistry, PA is also used as an analytical tool for the determination of creatinine which is known as Jaffe's reaction. The abnormal level of creatinine (37-250 mg/dL) present in blood and urine obstruct proper about the kidney functioning, causes the renal disease, muscular dystrophy and myasthenia [34,35]. Therefore, monitoring of creatinine in biological samples of the patient is becoming a major concern in these days. Many sensing strategies were reported for the detection of creatinine. Parmar and co-workers followed a colorimetric based evaluation of creatinine using picric acid capped silver nanoparticles[36]. Gluten stabilized fluorescent gold quantum cluster was used as a fluorophore to quantify the amount of creatinine in the blood samples[35]. All the reported methods have certain limitations w.r.t their experimental method, cost-effectiveness, selectivity and sensitivity towards creatinine. In this context, there is a necessity to quantify the amount of creatinine in a simple, straight forward and cost-effective approach. So far, to the best of our knowledge, no work has been reported with NC-dots@PA system for the detection and quantification of creatinine through fluorescence turn-off-on approach.

Herein, we have examined the impact of different nitrogen precursors such as urea, thiourea, cysteine and glycine on the physio-chemical and photoluminescence properties of NC-dots. Besides, chemical composition was evaluated using Fourier transform infrared spectroscopy and X-ray photoelectron spectroscopy techniques. Finally, we assess the effect of different surface groups on the PLQY, fluorescence lifetime of NC-dots and to authenticate the role of different nitrogen precursor towards biomolecule sensing. Moreover, the implementation of different interconnecting molecular logic gate (IMP, AND, OR) was applied to design the nano-senor.

5.2 Experimental section

5.2.1 Materials and characterization

Thiourea, urea, cysteine, glycine and ascorbic acid were purchased from Loba Chemie Pvt Ltd (spectrograde), India. All these reagents were used directly by preparing their aqueous solution using distilled water (18.2 MΩ, Millipore). The NC-dots were synthesized by using Multiwave-300 microwave synthesis reactor (Anton Paar, USA). LS-55 spectro-

fluorophotometer (Perkin Elmer) was used to study its optoelectronic properties. The fluorescence lifetime decay for NC-dots in the presence and absence of the analyte will be collected by time-correlated single-photon counting (TCSPC) measurements using delta-flex modular fluorescence lifetime system (HORIBA Scientific) with light-emitting diode (LED) light source (340 nm) with instrument response function (IRF) ~200 ps. The synthesized NC-dots were also characterized by High-resolution transmission electron microscope (HRTEM), (TALOS F200S G2, 200 KeV, FEG, CMOS Camera 4Kx 4K, In Column EDS detectors) for the analysis of its surface morphology and particle size by using a drop-casting technique. Moreover, Fourier transform infrared spectroscopy-attenuated total reflectance (FTIR-ATR, Agilent Resolution Pro-carry 660) XPS, X-ray photoelectron microscopy and Energy-dispersive X-ray spectroscopy (EDX) techniques were carried out to know the better insight on the NC-dots surface.

5.2.2 Synthesis of NC-dots

The microwave-assisted synthesis was followed to attain nitrogen-doped carbon dots (NC-dots) using different nitrogen precursors such as urea, thiourea, glycine, cysteine and carbon source as ascorbic acid which are abbreviated as UC-dots, TC-dots, GC-dots and CC-dots respectively. Firstly, ascorbic acid and respective nitrogen-containing precursors were dissolved in 10 ml of distilled water and kept for 5 min at 130 ^{0}C in microwave synthesizer. Afterwards, the obtained yellowish-brown solution was purified by centrifugation at 5000 rpm and the supernatant was passed through filter membranes of 0.22 μm to obtain pure NC-dots.

5.2.3 Experimental procedure for fluorescence quenching of NC-dots and PA

We have analyzed the fluorescence emission spectra of all the synthesized NC-dots (UC-dots, GC-dots, TC-dots and CC-dots) using LS-50 Perkin Elmer spectrofluorometer. Primarily, 100 μl of NC-dots from the prepared stock solution was pipette out in a 2 ml cuvette, rest volume was marked by distilled water and their emission spectra were recorded at λ_{ex} = 340 nm. To the same cuvette containing NC-dots, the respective amount of PA solution was gradually added from the prepared stock solution and their emission spectra were collected. The addition of PA solution was continued till the maximum fluorescence quenching achieved.

5.2.4 Determination of PLQY

The PLQY of all four NC-dots was evaluated using quinine sulphate (ϕ_r= 0.546) [37] as a reference solution dissolved in 0.01 M H_2SO_4 by subsequent equation-1:

$$\varphi = \varphi_r \times (I/I_r) \times (A_r/A) \times (\eta^2/\eta^2_r) \qquad 1$$

Where 'φ', 'φ_r' denotes as PLQY of the sample and reference, 'I' as the integrated area of fluorescence intensity, 'A' as the absorbance value and 'η' as refractive index.

5.2.5 Determination of quenching constant

The quenching constant of different NC-dots in the presence of PA was evaluated using the following Stern-Volmer equation:

$$\frac{F_0}{F} = 1 + K_{SV}[Q] \qquad 2$$

The parameters namely F_0 and F represent the fluorescence intensity in the absence and presence of PA respectively. Q is the concentration of PA. K_{SV} represents the Stern Volmer quenching constant. The determination of the K_{SV} value was done from the slope obtained from the plot of F_0/F vs [Q].

5.2.6 Determination of binding constant

The interaction studies between NC-dots with PA were determined using 1:1 stoichiometry of the Benesi-Hildebrand equation as follow [38]:

$$\frac{1}{F_0 - F} = \frac{1}{F_1 - F} + \frac{1}{K_1[A]_0(F_1 - F)} \qquad 3$$

Where F_0 and F are the fluorescence intensities of NC-dots in the absence and presence of PA. F_1 is the fluorescence intensity for the 1:1 complex. Therefore, the B-H plot of $1/(F_0 - F)$ vs. $1/[A]_0$ should give a straight line. From the slope and intercept of the line, the binding constant (K_1) values for different NC-dots have been estimated.

5.2.7 Experimental procedure to detect creatinine based on fluorescence restoration

The fluorescence of prepared NC-dots@PA systems was explored for the quantification of creatinine (CRET). The efficacy of this nanoprobe was evaluated based on ligand replacement and fluorescence restoration approach (turn-on). To the NC-dots@PA system,

1mM stock solution of CRET was gradually added and the respective fluorescence spectra were recorded at the same excitation wavelength (λ_{ex} = 340 nm). The addition of CRET results in the fluorescence enhancement of NC-dots@PA from which we have further quantified its detection limit using the equation:

$$\text{LOD} = \frac{3\theta}{slope} \qquad 4$$

Where 'θ' is the standard deviation and slope obtained from the respective plot.

5.2.8 Sensing of creatinine detection in urine

The urine sample was collected from laboratory co-workers, were stored at 4 ^{0}C and discarded after 24 h. The urine samples were centrifuged for 30 min at 4000 rpm and filtered using a syringe filter (0.44 µm). Aliquots of the urine samples (3 ml) were treated as similar like calibration standards and the fluorescent intensity at 450 nm was monitored.

5.3 Results and discussion

5.3.1 Size and surface composition of different NC-dots

The size and morphology for different NC-dots were characterized through HRTEM analysis. The HRTEM images indicated that all the NC-dots were spherical and monodispersed with a diameter range of 5-8 nm (Fig. 5.1). The lattice fringes of all four NC-dots showed the spacing of 0.22 nm (Fig. 5.1), i.e. corresponding to the (100) in-plane lattice fringe of graphene that justified that sp^2 carbon skeleton was present in NC-dots [39]. The surface composition for all four NC-dots was assessed by using FTIR shown in Fig. 5.1e. In FTIR spectra, the intense band appeared at 3583 cm^{-1}, which is assigned for the N-H stretching vibrations (pyrrolic nitrogen). The band at 2081 cm^{-1} represent N-H stretching vibration and band at 1635 cm^{-1} assigned for pyrrolic, pyridinic, and chemisorbed nitrogen [40]. The other bands appeared at 1386 and 1129 cm^{-1} assigned for C-N (graphitic nitrogen) and C-O stretching [40,41]. The attained bands reveal that all four NC-dots were functionalized with variant hydrophilic groups which give the primary idea to understand the interactions between NC-dots and PA. The surface states and composition in NC-dots was also characterized by XPS. The full spectra are shown in Fig. 5.1f, reveal that all four NC-dots were composed of same elements C, N, O having variant ratio. The C1s band was de-convoluted into four peaks at 284.8, 286.1, 287.2 and 288.5 eV, which are assigned to C=C/C−C, C−N/C−O, C=N and C=O/−CONH− respectively (Fig.

5.2 and Table 5.1). The N1s band was also split into three peaks, corresponding to pyridinic N (398.4 eV), amino N (399.2 eV) and pyrrolic N (400.2 eV) as mentioned in Table 5.2 and Fig. 5.2. In the O 1s spectrum, two peaks were found at 531.2 and 533.0 eV, revealing the existence of C−O and C=O (Fig. 5.2 and Table 5.3). The contribution of each several surface groups was calculated from their de-convoluted spectra. The evaluation revealed that the content of C=O/-CONH- surface groups exists as in the order of UC-dots>CC-dots~GC-dots>TC-dots whereas the content of non-amino groups exists in the order of TC-dots>CC-dots~GC-dots>UC-dots. These results specify that NC-dots exhibited variant nitrogen surface groups and degree of oxidation that induces red-shift in its emissive spectra [41]. The existence of these different surface groups content ratio can be a helpful tool to tune the selectivity of NC-dots towards toxin biomolecules.

Table 5.1: XPS data analysis of C 1s spectra of different NC-dots.

NC-dots	U**C-dots**	C**C-dots**	G**C-dots**	T**C-dots**
C-C/C=C	60%	41%	40%	65%
C-N/C-O	22%	42%	45%	21%
C=O/-CONH-	18%	15%	14%	13%

Table 5.2: XPS data analysis of the N 1s spectra of different NC-dots.

NC-dots	U**C-dots**	C**C-dots**	G**C-dots**	T**C-dots**
Pyridinic N	15%	6%	7%	5%
Amino N	----	13%	15%	41%
Pyrrolic N	85%	79%	78 %	53%

Table 5.3: XPS data analysis of O 1s spectra of different NC-dots.

NC-dots	U**C-dots**	C**C-dots**	G**C-dots**	T**C-dots**
C-O	40%	43%	49%	53%
C=O	60%	57%	51%	47%

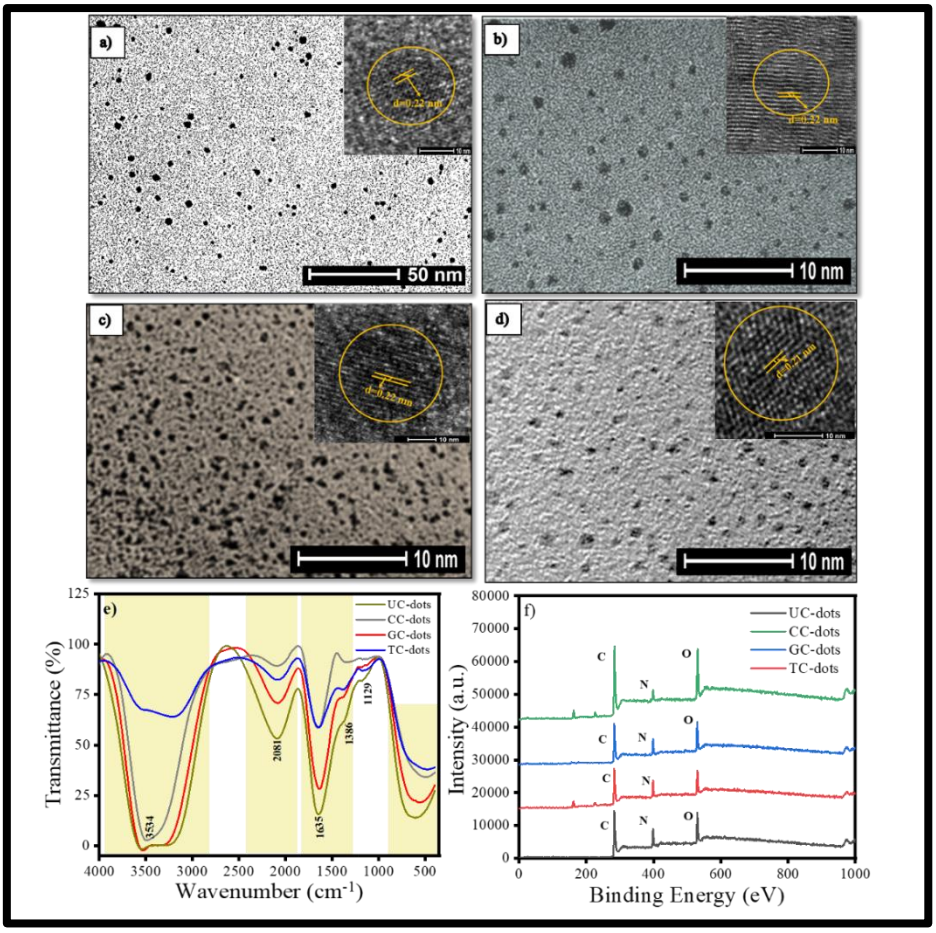

Fig. 5.1: Particle size, surface compositions and elements a) UC-dots, b) CC-dots, c) GC-dots, d) TC-dots, e) FTIR, and f) XPS spectra.

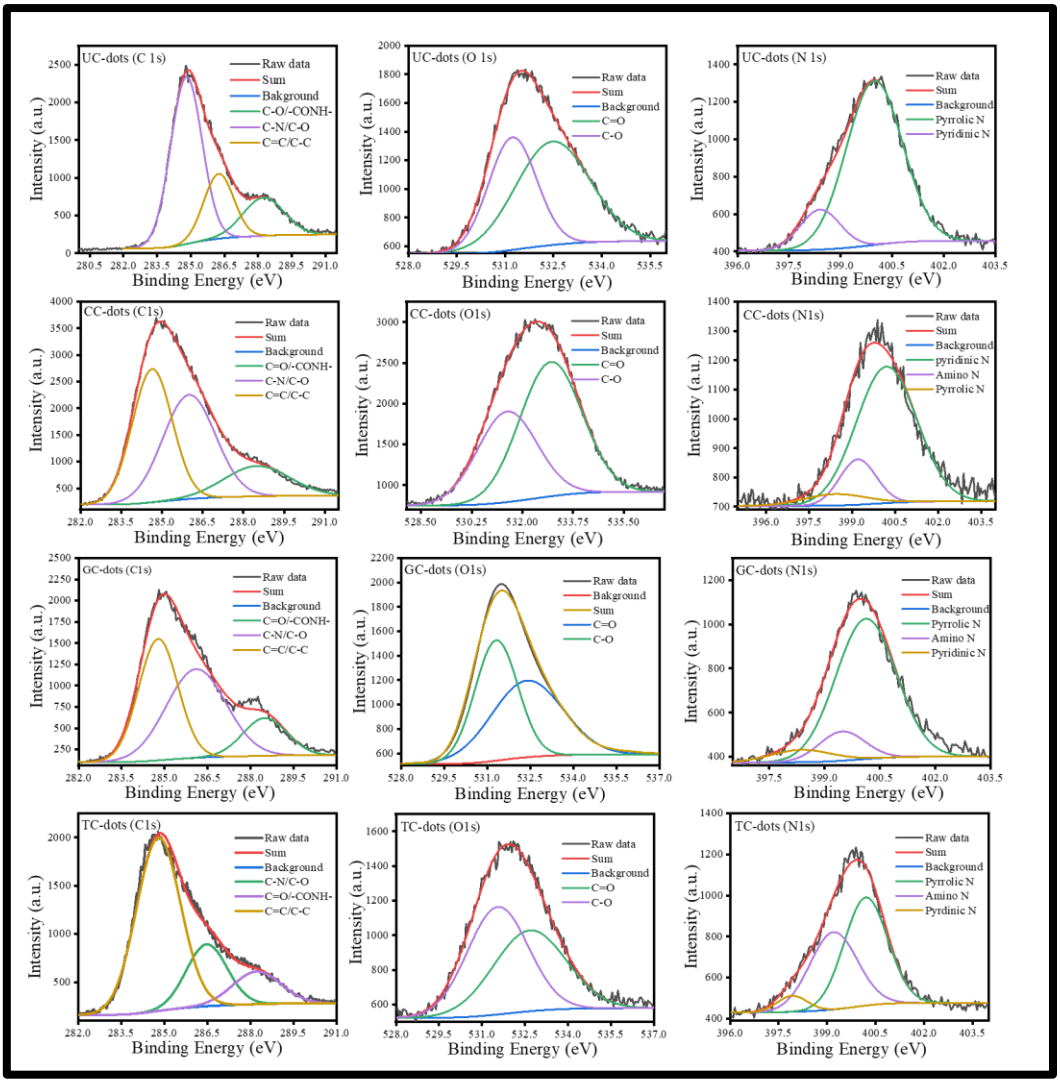

Fig. 5.2: Deconvoluted XPS spectra of C 1s O 1s and N 1s for: a) UC-dots, b) CC-dots, c) GC-dots, and d) TC-dots.

5.3.2 Fluorescence studies of different NC-dots

The PL spectra of all the NC-dots were assessed at λ_{ex} = 340 nm. The experimental results indicated that the emission wavelength lies in the range from 412-436 nm that undergoes red shift, i.e. UC-dots>CC-dots~GC-dots>TC-dots (Fig. 5.3a). This distinct emission behavior among NC-dots occurs due to the deformation in its plane that decreases their bandgap energy, which is caused by various surface groups such as -$CONH_2$, different nitrogen species (pyridinic, pyrrolic and amino) [2]. However, the emission spectra of NC-dots were also recorded at the different excitation wavelength, ranges from 340-390 nm (Fig. 5.3b and 5.4). The experimental studies revealed that the PL peak position undergoes a bathochromic shift in their emission wavelength from 400 to 460 nm and found dependent on the excitation wavelength.

This feature of NC-dots arises mainly due to the presence of various surface states such as C-H, C=O, C-NH_2 and C-OH (supported by XPS and FTIR analysis) [42,43].

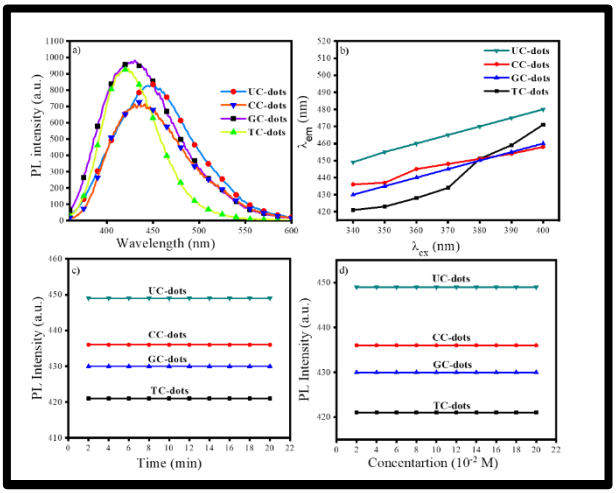

Fig. 5.3: Fluorescence studies of NC-dots: a) emission properties of different NC-dots at λ_{ex} =340nm, b) emission behavior at the different excitation wavelength, c) impact of UV irradiation and d) different ionic strength of NaCl on their PL properties.

PLQY is also one of the most inherent fluorescence properties of a fluorophore. So, we have calculated the PLQY values using quinine sulphate as a reference (ϕ_r = 0.546) in equation-1 (section-5.2.4) for UC-dots, CC-dots, GC-dots and TC-dots which are found 58%, 51%, 51% and 31% respectively due to the higher nitrogen content enter carbon core and form a pyrrolic structure which effectively improves PLQY (evaluated in XPS analysis). These results were justified from previous reports where hetero-atoms and surface passivation can enhance the PLQY of C-dots w.r.t pure carbon and oxygen-rich C-dots. [2,41,44,45].

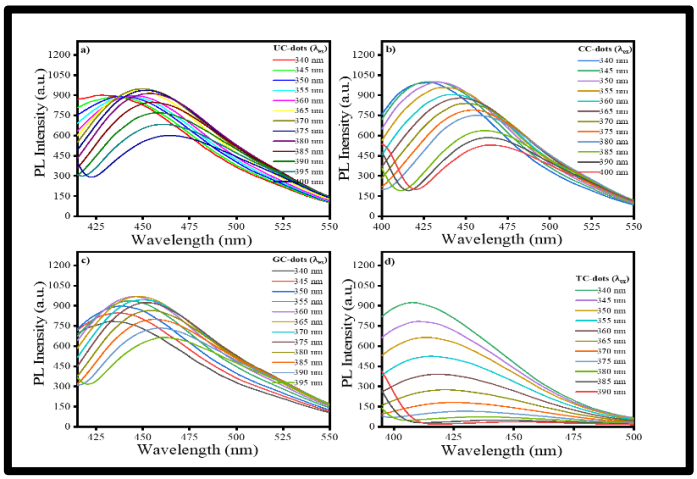

Fig. 5.4: Effect of excitation wavelength on emission spectra: a) UC-dots, b) CC-dots, c) GC-dots, and d) TC-dots.

The photostability of NC-dots was also assessed from the PL studies under UV irradiation and at different ionic strengths of NaCl salt. The studies revealed that after the exposure of continuous UV-Lamp irradiation for 20 min, it did not disturb the emission spectra which signify its good anti-photobleaching property. Even, in the presence of different ionic strength (NaCl) its emission peak did not get disturbed which guarantees their sensing applicability in the biological and aquatic system (Fig. 5.3c and Fig. 5.3d).

5.3.3 Effect of pH on different NC-dots

The effect of pH plays a vital role in controlling the sensing efficacy of probe towards biomolecules and metal ions. It has been found that the PL intensity of different NC-dots remains almost unaltered by variations of the pH values (Fig. 5.5). This result reflects that protonation and deprotonation have minimal impact on the electronic transition of NC-dots. Therefore, it can be demonstrated that NC-dots have a good potential candidate to use in biological system [46].

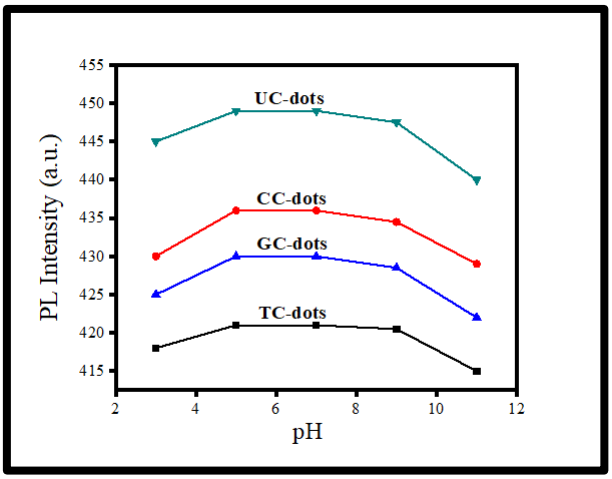

Fig. 5.5: Effect of pH on the emission spectra of NC-dots.

5.3.4 Interaction studies of different NC-dots with PA

We have performed the fluorescence quenching study to explore the interaction of PA with four different NC-dots. The experimental showed a remarkable reduction in PL intensity among all NC-dots on the addition of PA. This observed phenomenon occurred due to the excited-state electron-transfer from electron-rich species on NC-dots surface to the electron-deficient PA [43]. Moreover, to evaluate its quenching efficacy, Stern-Volmer quenching experiment was performed to calculate Stern-Volmer quenching constant values (K_{SV}) at three different pH ~4, 7 and 9 (Fig. 5.6) using equation 2. The experimental results indicated that all

four NC-dots showed a higher rate of quenching constant at pH=7 w.r.t other pH values. This observed behavior is due to the formation of anion-cation pair *via* strong electrostatic interaction between the nitrogen-rich surface of NC-dots and PA and the absence of deprotonation and protonation of PA which frequently occurs at lower and higher pH values [47]. Additionally, the experiment studies revealed that among all four NC-dots, UC-dots and CC-dots showed similar quenching efficiency, with K_{SV}~0.27× 10^5 M^{-1} whereas, for TC-dots, GC-dots have similar K_{SV}~0.42 × 10^5 M^{-1} values. These small variations in their K_{SV} were observed due to the different content ratio of nitrogen species which changes their probability for electrostatic interaction (formation of anion and cation pair) with PA.

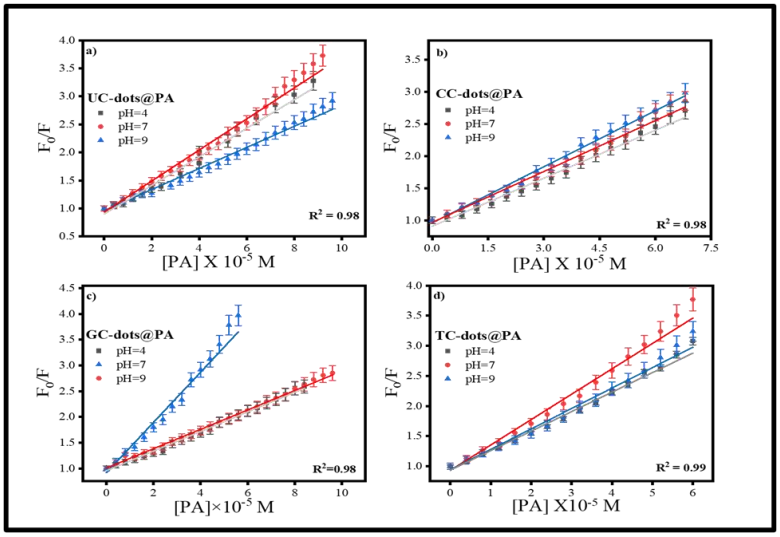

Fig. 5.6: Stern-Volmer plot for a) UC-dots, b) CC-dots, c) GC-dots and d) TC-dots at three different pH in the presence of PA.

Subsequently, the binding efficacy for PA was also evaluated from the B-H plot and binding constant using equation-3. At pH=7, all four NC-dots exhibited excellent binding w.r.t pH = 4 and 9 with a binding constant of 1.79×10^7, 2×10^7, 2.66×10^7 and 2.85×10^7 M^{-1} for UC-dots, CC-dots GC-dots and TC-dots respectively as shown in Fig. 5.7. This apparent rise in this binding efficacy from UC-dots to TC-dots towards PA occurs due to the existence of variant content ratio of amino surface groups. Thus, all experimental studies revealed that different nitrogen sources can be a useful route to modulate the selectivity of NC-dots for the detection of the biomolecules.

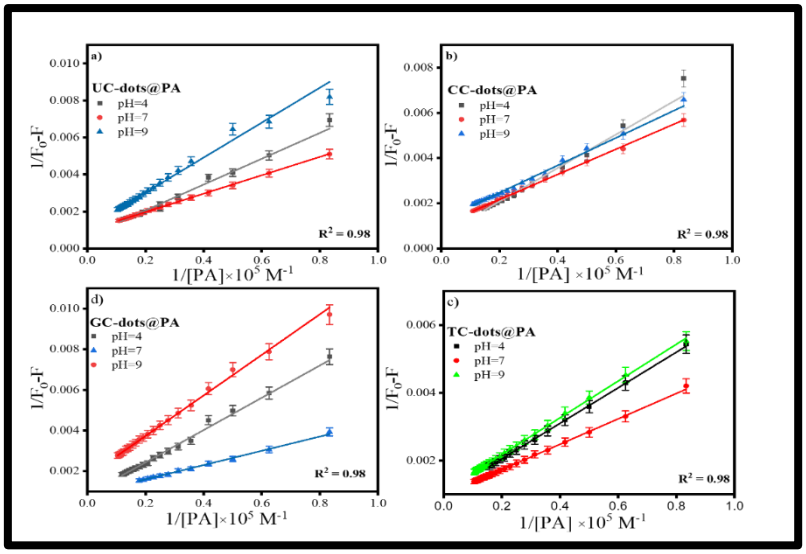

Fig. 5.7: B-H plot to evaluate the binding constant for a) UC-dots, b) CC-dots, c) GC-dots and d) TC-dots with PA at different concentration.

5.3.5 Establishment of PL sensing method for creatinine

Jaffe reaction was used as a reference tool to evaluate the NC-dots@PA system for the CRET quantification based on fluorescence restoration mechanism. To study the interaction between CRET and NC-dots@PA, the medium was adjusted at pH = 9 by Tris HCl buffer (0.001 M) as Jaffe's reaction took place only at basic condition, even electrostatic interactions get also reduced between NC-dots and PA that can be attributed to its rapid fluorescence recovery. It was found that addition of CRET solution to different NC-dots@PA results in enhancement of the fluorescence intensity (Fig. 5.8a). Moreover, the color of the solution was also changed from yellow to orange-red which confirmed the formation of red Jaffe chromogen (Inset of Fig. 5.8b) [48]. The fluorescence recovery was also calculated for NC-dots, the UC-dots@PA exhibited maximum PL restoration (50%) whereas minimum (29%) for TC-dots@PA in the presence of CRET (Fig. 5.8c). These variations in the phenomenon were observed due to the difference in the ratio of amino groups on its surface (Table 5.1 and 5.2) as it enhances its association with PA through hydrogen bonding, which causes hindrance in the PA and CRET complex formation (shown in Scheme 5.1). These results symbolized that less amino rich NC-dots@PA system can be used as effective colorimetric as well as the fluorometric device for creatinine detection.

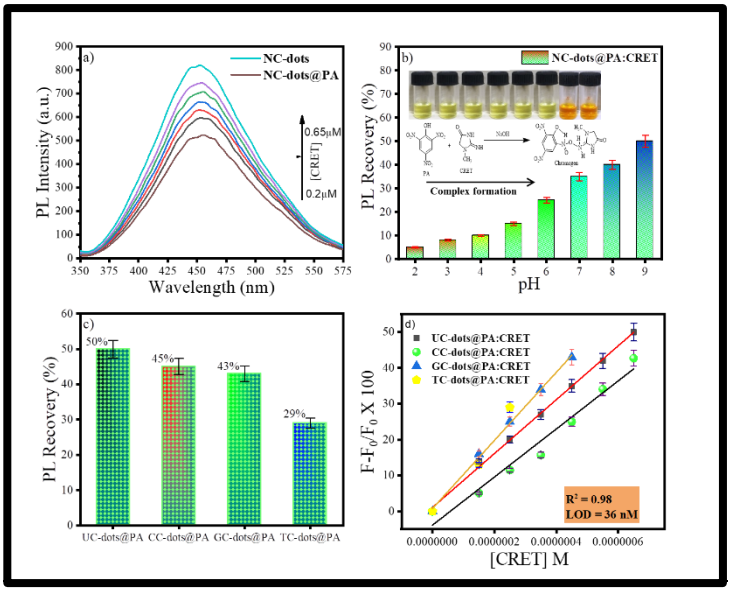

Fig. 5.8: Fluorescence behavior of NC-dots@PA in the presence of CRET: a) impact of different concentration of CRET on its PL intensity, b) effect of pH on its PL recovery, c) % PL recovery of different NC-dots@PA and, d) plot $F\text{-}F_0/F_0$ vs [CRET].

Furthermore, to validate its selectivity, its linear response was recorded by successive addition of CRET at a different concentration ranging from 0-0.65 µM (Fig. 5.8d). The results showed a good linear relationship between the PL signal ranging from 0.2-0.65 µM with a detection limit of 36 nM, i.e. calculated using eq-4. These experimental details indicated that prepared systems showed considerable selective response towards creatinine.

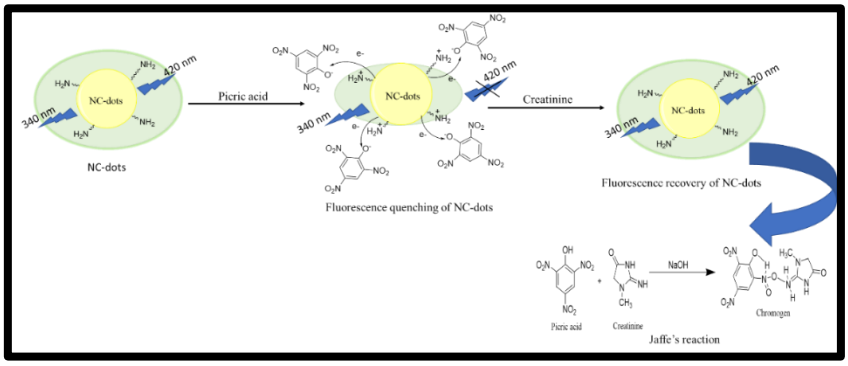

Scheme 5.1: Turn-off-on mechanism of NC-dots@PA in the presence of CRET.

5.3.6 Estimation of the selectivity for NC-dots@PA towards creatinine

The selectivity and sensitivity of the prepared nanosensor were validated through interference studies. Several relevant biological molecules like fructose (Frct), glucose (Glu), galactose (Gla), cysteine (Cys), glutathione (GSH), glycine (Gys) and metal ions like Fe^{+3}, Mg^{+2}, Zn^{+2}, Ca^{+2}, citrate was chosen to study the efficacy of the NC-dots@PA system by

maintaining their same concentration. The evaluated result indicates that foreign moieties showed no significant interaction with NC-dots@PA system and does not cause any hindrance in its PL recovery for creatinine (Fig. 5.9).

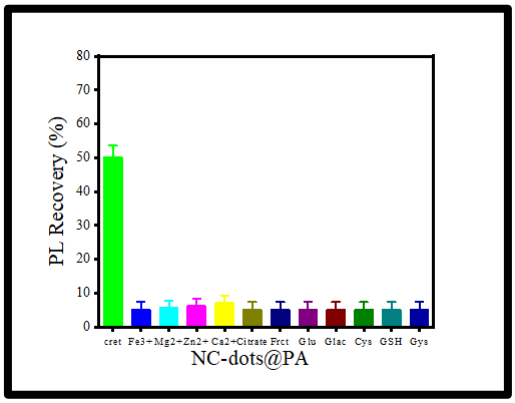

Fig. 5.9: Interference studies of NC-dots@PA to evaluate the sensing efficacy towards creatinine.

Furthermore, the effectiveness of the prepared probe was justified by comparing some current methods and detecting probes mentioned in Table 5.4. These studies indicate that our probe is cost-effective, green and show almost similar sensing applicability in comparison to expensive and colorimetric based techniques.

Table 5.4: Comparison of the efficacy of various analytical methods with the current method.

Methods	Detection system	Limit of detection	Reference
Colorimetric	Au@BSA	0.0084 µM	[49]
Colorimetric (Paper-based sensor)	Jaffe reaction	70.2 µM	[50]
Amperometric	----------	0.041 µM	[51]
Fluorometric	1,8 napthalimide (FCD-Pd complex)	0.30 µM	[52]
Fluorometric	Gluten-stabilized fluorescent gold quantum Cluster	0.002 µM	[53]
Fluorometric	N-doped carbon dots	36 nM	Current work

5.3.7 Time-resolved PL measurements of NC-dots in the presence of PA and creatinine

Time-resolved measurement was recorded for NC-dots at their respective emission wavelength by exciting the samples at λ_{ex} = 340 nm (Fig. 6). The average PL lifetime found in the range of 1-2 ns which is very close to the previously reported values [54]. Further to validate the interaction of PA with different NC-dots, the lifetime decay studies were recorded in the presence and absence of PA (Fig. 5.10). The outcomes displayed a significant decline in its average lifetime values upon the addition of the PA solution (21 mM, 150µL) and showed dynamic quenching characteristics (Fig. 5.10 and Table 5.5).

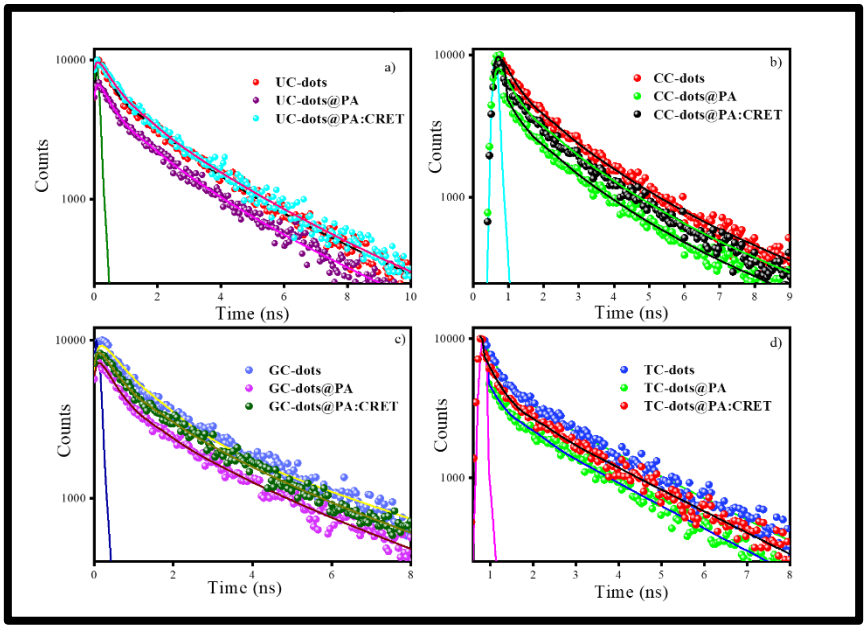

Fig. 5.10: Time resolved spectra for a) UC-dots, b) CC-dots, c) GC-dots and d) TC-dots in the absence and presence of PA and CRET.

Moreover, from these average lifetimes and PLQY values of NC-dots, radiative (k_r) or non-radiative decay rate (k_{nr}) was calculated by the following equations:

$$k_r = \frac{\phi}{\tau} \qquad 5$$

$$k_{nr} = \frac{1-\phi}{\tau} \qquad 6$$

Where ϕ is the quantum yield and τ_{av} is the average lifetime of the respective systems. Further, it is evident from the Table 5.5 that in the presence of PA, non-radiative decay rate (k_{nr}) gets enhanced w.r.t to radiative decay (k_r) for NC-dots which confirms that PA significantly

quenched its fluorescence. Additionally, the rate of electron transfer from NC-dots to PA and PA+CRET has also been calculated using the following equation:

$$k_{ET} = \frac{1}{\tau_{DA}} - \frac{1}{\tau_D} \qquad 7$$

Where, τ_D and τ_{DA} represents the average lifetime values of NC-dots, PA and PA+CRET respectively. It has been found that the rate of electron transfer became maximum for TC-dots (~0.76 ns) whereas minimum for UC-dots (~0.1 ns) in the presence of PA. This difference of the k_{ET} values arises due to the ratio of the amino groups on its surface as found from XPS analysis. Moreover, in the presence of CRET, the energy transfer process gets decline for NC-dots@PA system which justify that fluorescence restoration mechanism takes place (Scheme 5.1) due to the formation of a picric-creatinine complex.

Table 5.5: Photophysical parameters of NC-dots in the presence and absence of PA and CRET.

Systems	Φ	τ_{av}(ns)	k_r ($\times 10^9$ s^{-1})	k_{nr} ($\times 10^9$ s^{-1})	k_{ET} ($\times 10^9$ s^{-1})
UC-dots	0.58	2.12	0.27	0.23	-
UC-dots+PA	0.25	1.74	0.17	0.4	0.1
UC-dots+PA+CRET	0.48	1.9	0.25	0.27	0.05
CC-dots	0.51	1.63	0.31	0.34	-
CC-dots+PA	0.25	1.33	0.24	0.58	0.14
CC-dots+PA+CRET	0.38	1.51	0.25	0.41	0.05
GC-dots	0.51	1.71	0.31	0.31	-
GC-dots+PA	0.22	1.39	0.18	0.52	0.13
GC-dots +PA+CRET	0.39	1.55	0.25	0.39	0.06
TC-dots	0.31	1.08	0.37	0.56	-
TC-dots+PA	0.20	0.59	0.25	1.44	0.76
TC-dots+PA+CRET	0.26	0.97	0.26	0.77	0.1

5.3.8 Strategy to design molecular logic gate

The three inputs based molecular logic gates were also designed based on the turn-off-on response of NC-dots@PA towards creatinine. We define “0” and “1” as binary inputs of the

logic gates for the presence and absence of analytes, respectively. The output signal of logic gate depends on the PL intensity of NC-dots in which "0" refers to fluorescence quenching and "1" for non-quenching fluorescence. Three different IMP, OR and AND gates were evaluated for the relation of the following PL behavior for NC-dots with PA and creatinine respectively. The results specify that only three inputs combination, i.e. NC-dots (100), NC-dots/creatinine (101) and NC-dots/PA/creatinine (111) found suitable to validate the aforementioned fluorescence enhancement (output = 1) (Scheme 5.2). So, this system can be used as a portable device simulating the fluorescence induced signals into logic gate models.

Input (NC-dots)	Input2 (PA)	Input 3 (CRET)	Output (λ_{em})
0	0	0	0
0	1	0	0
0	0	1	0
1	0	0	1
1	1	0	0
1	0	1	1
0	1	1	0
1	1	1	1

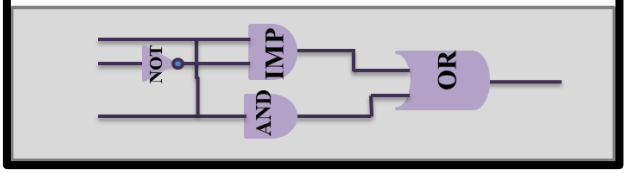

Scheme 5.2: Description of truth table and design of the molecular logic gate.

5.3.9 Real sample analysis for method validation

To validate the proposed method for the detection of creatinine, fluorescence recovery analyses were performed with the real system. The urine samples were spiked with a suitable amount of standard creatinine solution. The probe showed a similar response as the prepared standards with 90% recovery, i.e. determined using calibration curve mentioned in Table-5.6. These findings suggest that the developed methodology can be used as a selective tool to detect creatinine in real samples.

Table 5.6: Sensing efficiency of dual emissive NC-dots@PA in the real sample.

Spiked samples	Creatinine added (μM)	Creatinine found (μM)	Recovery (%)
1	0	0	0
2	0.22	0.26	84
3	0.28	0.32	87
4	0.36	0.4	90
5	0.42	0.5	84

References

(1) Ray, S. C.; Saha, A.; Jana, N. R.; Sarkar, R. Fluorescent Carbon Nanoparticles: Synthesis, Characterization, and Bioimaging Application. *J. Phys. Chem. C* **2009**, *113* (43), 18546–18551. https://doi.org/10.1021/jp905912n.

(2) Yan, F.; Sun, Z.; Zhang, H.; Sun, X.; Jiang, Y.; Bai, Z. The Fluorescence Mechanism of Carbon Dots, and Methods for Tuning Their Emission Color: A Review. *Microchimica Acta*. 2019. https://doi.org/10.1007/s00604-019-3688-y.

(3) Dalal, C.; Jana, N. R. Riboflavin-Terminated, Multivalent Quantum Dot as Fluorescent Cell Imaging Probe. *Langmuir* **2019**, *35* (35), 11380–11388. https://doi.org/10.1021/acs.langmuir.9b01168.

(4) Li, H.; Kang, Z.; Liu, Y.; Lee, S.-T. Carbon Nanodots: Synthesis, Properties and Applications. https://doi.org/10.1039/c2jm34690g.

(5) Kainth, S.; Mehta, A.; Mishra, A.; Basu, S. Implementation of a Logic Gate by Chemically Induced Nitrogen and Oxygen Rich C-Dots for the Selective Detection of Fluoride Ions. *New J. Chem.* **2018**, *42* (14), 12162–12171. https://doi.org/10.1039/c8nj02041h.

(6) Bhunia, S. K.; Saha, A.; Maity, A. R.; Ray, S. C.; Jana, N. R. Carbon Nanoparticle-Based Fluorescent Bioimaging Probes. *Sci. Rep.* **2013**, *3* (1), 1473. https://doi.org/10.1038/srep01473.

(7) Ali, H.; Ghosh, S.; Jana, N. R. Fluorescent Carbon Dots as Intracellular Imaging Probes. *WIREs Nanomedicine and Nanobiotechnology* **2020**. https://doi.org/10.1002/wnan.1617.

(8) Park, S. Y.; Lee, H. U.; Park, E. S.; Lee, S. C.; Lee, J. W.; Jeong, S. W.; Kim, C. H.; Lee, Y. C.; Huh, Y. S.; Lee, J. Photoluminescent Green Carbon Nanodots from Food-Waste-Derived Sources: Large-Scale Synthesis, Properties, and Biomedical Applications. *ACS Appl. Mater. Interfaces* **2014**, *6* (5), 3365–3370. https://doi.org/10.1021/am500159p.

(9) Wang, L.; Zhou, H. S. Green Synthesis of Luminescent Nitrogen-Doped Carbon Dots from Milk and Its Imaging Application. *Anal. Chem.* **2014**, *86* (18), 8902–8905. https://doi.org/10.1021/ac502646x.

(10) Kainth, S.; Mehta, A.; Mishra, A.; Basu, S. Implementation of a Logic Gate by Chemically Induced Nitrogen and Oxygen Rich C-Dots for the Selective Detection of Fluoride Ions. *New J. Chem.* **2018**, *42* (14), 12162–12171. https://doi.org/10.1039/c8nj02041h.

(11) Ghosh, S.; Ali, H.; Jana, N. R. Water Dispersible Red Fluorescent Carbon Nanoparticles via Carbonization of Resorcinol. *ACS Sustain. Chem. Eng.* **2019**, *7* (14), 12629–12637. https://doi.org/10.1021/acssuschemeng.9b02710.

(12) Yan, F.; Sun, Z.; Zhang, H.; Sun, X.; Jiang, Y.; Bai, Z. The Fluorescence Mechanism of Carbon Dots, and Methods for Tuning Their Emission Color: A Review. *Microchimica Acta*. Springer Vienna August 29, 2019, p 583. https://doi.org/10.1007/s00604-019-3688-y.

(13) D'Angelis do E. S. Barbosa, C.; Corrêa, J. R.; Medeiros, G. A.; Barreto, G.; Magalhães, K. G.; de Oliveira, A. L.; Spencer, J.; Rodrigues, M. O.; Neto, B. A. D. Carbon Dots (C-Dots) from Cow Manure with Impressive Subcellular Selectivity Tuned by Simple Chemical Modification. *Chem. - A Eur. J.* **2015**, *21* (13), 5055–5060. https://doi.org/10.1002/chem.201406330.

(14) Teng, X.; Ma, C.; Ge, C.; Yan, M.; Yang, J.; Zhang, Y.; Morais, P. C.; Bi, H. Green Synthesis of Nitrogen-Doped Carbon Dots from Konjac Flour with "off-on" Fluorescence by Fe 3+ and l-Lysine for Bioimaging. *J. Mater. Chem. B* **2014**, *2* (29), 4631–4639. https://doi.org/10.1039/c4tb00368c.

(15) Sciortino, L.; Sciortino, A.; Popescu, R.; Schneider, R.; Gerthsen, D.; Agnello, S.; Cannas, M.; Messina, F. Tailoring the Emission Color of Carbon Dots through Nitrogen-Induced Changes of Their Crystalline Structure. *J. Phys. Chem. C* **2018**, *122* (34), 19897–19903. https://doi.org/10.1021/acs.jpcc.8b04514.

(16) Jana, J.; Ganguly, M.; Chandrakumar, K. R. S.; Rao, G. M.; Pal, T. Boron Precursor-Dependent Evolution of Differently Emitting Carbon Dots. *Langmuir* **2017**, *33* (2), 573–584. https://doi.org/10.1021/acs.langmuir.6b04100.

(17) Wang, L.; Cao, H. X.; Pan, C. G.; He, Y. S.; Liu, H. F.; Zhou, L. H.; Li, C. Q.; Liang, G. X. A Fluorometric Aptasensor for Bisphenol a Based on the Inner Filter Effect of Gold Nanoparticles on the Fluorescence of Nitrogen-Doped Carbon Dots. *Microchim. Acta* **2019**, *186* (1). https://doi.org/10.1007/s00604-018-3153-3.

(18) Wu, W. C.; Chen, H. Y. T.; Lin, S. C.; Chen, H. Y.; Chen, F. R.; Chang, H. T.; Tseng, F. G. Nitrogen-Doped Carbon Nanodots Prepared from Polyethylenimine for Fluorometric Determination of Salivary Uric Acid. *Microchim. Acta* **2019**, *186* (3). https://doi.org/10.1007/s00604-019-3277-0.

(19) Liu, Y.; Tang, X.; Deng, M.; Cao, Y.; Li, Y.; Zheng, H.; Li, F.; Yan, F.; Lan, T.; Shi, L.; et al. Nitrogen Doped Graphene Quantum Dots as a Fluorescent Probe for Mercury(II) Ions. *Microchim. Acta* **2019**, *186* (3). https://doi.org/10.1007/s00604-019-3249-4.

(20) Wang, Y.; Zhuang, Q.; Ni, Y. Facile Microwave-Assisted Solid-Phase Synthesis of Highly Fluorescent Nitrogen-Sulfur-Codoped Carbon Quantum Dots for Cellular Imaging Applications. *Chem. - A Eur. J.* **2015**, *21* (37), 13004–13011. https://doi.org/10.1002/chem.201501723.

(21) Zhang, H.; Chen, Y.; Liang, M.; Xu, L.; Qi, S.; Chen, H.; Chen, X. Solid-Phase Synthesis of Highly Fluorescent Nitrogen-Doped Carbon Dots for Sensitive and Selective Probing Ferric Ions in Living Cells. *Anal. Chem* **2014**, *86*. https://doi.org/10.1021/ac502446m.

(22) Ding, H.; Yu, S. B.; Wei, J. S.; Xiong, H. M. Full-Color Light-Emitting Carbon Dots with a Surface-State-Controlled Luminescence Mechanism. *ACS Nano* **2016**, *10* (1), 484–491. https://doi.org/10.1021/acsnano.5b05406.

(23) Yang, Z.; Xu, M.; Liu, Y.; He, F.; Gao, F.; Su, Y.; Wei, H.; Zhang, Y. Nitrogen-Doped, Carbon-Rich, Highly Photoluminescent Carbon Dots from Ammonium Citrate. *Nanoscale* **2014**, *6* (3), 1890–1895. https://doi.org/10.1039/c3nr05380f.

(24) Ma, Z.; Ming, H.; Huang, H.; Liu, Y.; Kang, Z. One-Step Ultrasonic Synthesis of Fluorescent N-Doped Carbon Dots from Glucose and Their Visible-Light Sensitive Photocatalytic Ability. *New J. Chem.* **2012**, *36* (4), 861–864. https://doi.org/10.1039/c2nj20942j.

(25) Lu, W.; Jiao, Y.; Gao, Y.; Qiao, J.; Mozneb, M.; Shuang, S.; Dong, C.; Li, C. Z. Bright Yellow Fluorescent Carbon Dots as a Multifunctional Sensing Platform for the Label-Free Detection of Fluoroquinolones and Histidine. *ACS Appl. Mater. Interfaces* **2018**, *10* (49), 42915–42924. https://doi.org/10.1021/acsami.8b16710.

(26) Song, W.; Duan, W.; Liu, Y.; Ye, Z.; Chen, Y.; Chen, H.; Qi, S.; Wu, J.; Liu, D.; Xiao, L.; et al. Ratiometric Detection of Intracellular Lysine and PH with One-Pot Synthesized Dual Emissive Carbon Dots. *Anal. Chem.* **2017**, *89* (24), 13626–13633. https://doi.org/10.1021/acs.analchem.7b04211.

(27) Jiang, K.; Sun, S.; Zhang, L.; Wang, Y.; Cai, C.; Lin, H. Bright-Yellow-Emissive N-Doped Carbon Dots: Preparation, Cellular Imaging, and Bifunctional Sensing. *ACS Appl. Mater. Interfaces* **2015**, *7* (41), 23231–23238. https://doi.org/10.1021/acsami.5b07255.

(28) He, Y.; Yu, Z.; He, J.; Zhang, H.; Liu, Y.; Lei, B. Ratiometric and Selective Fluorescent Sensor for Fe(III) and Bovine Serum Albumin Based on Energy Transfer. *Sensors Actuators, B Chem.* **2018**, *262*, 228–235. https://doi.org/10.1016/j.snb.2018.01.242.

(29) Han, Z.; Nan, D.; Yang, H.; Sun, Q.; Pan, S.; Liu, H.; Hu, X. Carbon Quantum Dots Based Ratiometric Fluorescence Probe for Sensitive and Selective Detection of Cu2+ and Glutathione. *Sensors Actuators, B Chem.* **2019**, *298*, 126842. https://doi.org/10.1016/j.snb.2019.126842.

(30) Kaur, M.; Mehta, S. K.; Kansal, S. K. A Fluorescent Probe Based on Nitrogen Doped Graphene Quantum Dots for Turn off Sensing of Explosive and Detrimental Water Pollutant, TNP in Aqueous Medium. *Spectrochim. Acta - Part A Mol. Biomol. Spectrosc.* **2017**, *180*, 37–43. https://doi.org/10.1016/j.saa.2017.02.035.

(31) Li, J.; Zhang, L.; Li, P.; Zhang, Y.; Dong, C. One Step Hydrothermal Synthesis of Carbon Nanodots to Realize the Fluorescence Detection of Picric Acid in Real Samples. *Sensors Actuators, B Chem.* **2018**, *258*, 580–588. https://doi.org/10.1016/j.snb.2017.11.096.

(32) Cheng, F.; An, X.; Zheng, C.; Cao, S. Green Synthesis of Fluorescent Hydrophobic Carbon Quantum Dots and Their Use for 2,4,6-Trinitrophenol Detection. *RSC Adv.* **2015**, *5* (113), 93360–93363. https://doi.org/10.1039/c5ra19029k.

(33) Deng, X.; Wu, D. Highly Sensitive Photoluminescence Energy Transfer Detection for 2,4,6-Trinitrophenol Using Photoluminescent Carbon Nanodots. *RSC Adv.* **2014**, *4* (79), 42066–42070. https://doi.org/10.1039/c4ra06683a.

(34) Hanif, S.; John, P.; Gao, W.; Saqib, M.; Qi, L.; Xu, G. Chemiluminescence of Creatinine/H2O2/Co2+ and Its Application for Selective Creatinine Detection. *Biosens. Bioelectron.* **2016**, *75*, 347–351. https://doi.org/10.1016/j.bios.2015.08.053.

(35) Mathew, M. S.; Joseph, K. Green Synthesis of Gluten-Stabilized Fluorescent Gold Quantum Clusters: Application As Turn-On Sensing of Human Blood Creatinine. *ACS Sustain. Chem. Eng.* **2017**, *5* (6), 4837–4845. https://doi.org/10.1021/acssuschemeng.7b00273.

(36) Parmar, A. K.; Valand, N. N.; Solanki, K. B.; Menon, S. K. Picric Acid Capped Silver Nanoparticles as a Probe for Colorimetric Sensing of Creatinine in Human Blood and Cerebrospinal Fluid Samples. *Analyst* **2016**, *141* (4), 1488–1498. https://doi.org/10.1039/c5an02303c.

(37) Crosby, G. A.; Demas, J. N. Measurement of Photoluminescence Quantum Yields. Review. *J. Phys. Chem.* **1971**, *75* (8), 991–1024. https://doi.org/10.1021/j100678a001.

(38) Benesi, H. A.; Hildebrand, J. H. A Spectrophotometric Investigation of the Interaction of Iodine with Aromatic Hydrocarbons. *J. Am. Chem. Soc.* **1949**, *71* (8), 2703–2707. https://doi.org/10.1021/ja01176a030.

(39) Atchudan, R.; Edison, T. N. J. I.; Sethuraman, M. G.; Lee, Y. R. Efficient Synthesis of Highly Fluorescent Nitrogen-Doped Carbon Dots for Cell Imaging Using Unripe Fruit Extract of Prunus Mume. *Appl. Surf. Sci.* **2016**, *384*, 432–441. https://doi.org/10.1016/j.apsusc.2016.05.054.

(40) Lazar, P.; Mach, R.; Otyepka, M. Spectroscopic Fingerprints of Graphitic, Pyrrolic, Pyridinic, and Chemisorbed Nitrogen in N-Doped Graphene. *J. Phys. Chem. C* **2019**, *123* (16), 10695–10702. https://doi.org/10.1021/acs.jpcc.9b02163.

(41) Liu, C.; Wang, R.; Wang, B.; Deng, Z.; Jin, Y.; Kang, Y.; Chen, J. Orange, Yellow and Blue Luminescent Carbon Dots Controlled by Surface State for Multi-color Cellular Imaging, Light Emission and Illumination. *Microchim. Acta* **2018**, *185* (12). https://doi.org/10.1007/s00604-018-3072-3.

(42) Ramanan, V.; Thiyagarajan, S. K.; Raji, K.; Suresh, R.; Sekar, R.; Ramamurthy, P. Outright Green Synthesis of Fluorescent Carbon Dots from Eutrophic Algal Blooms for in Vitro Imaging. *ACS Sustain. Chem. Eng.* **2016**, *4* (9), 4724–4731. https://doi.org/10.1021/acssuschemeng.6b00935.

(43) Fan, Y. Z.; Zhang, Y.; Li, N.; Liu, S. G.; Liu, T.; Li, N. B.; Luo, H. Q. A Facile Synthesis of Water-Soluble Carbon Dots as a Label-Free Fluorescent Probe for Rapid, Selective and Sensitive Detection of Picric Acid. *Sensors Actuators, B Chem.* **2017**, *240*, 949–955. https://doi.org/10.1016/j.snb.2016.09.063.

(44) Liu, H.; Zhang, Y.; Liu, J. H.; Hou, P.; Zhou, J.; Huang, C. Z. RSC Advances Preparation of Nitrogen-Doped Carbon Dots with High Quantum Yield from Bombyx Mori Silk for Fe (III) Ions Detection †. **2017**, 50584–50590. https://doi.org/10.1039/c7ra10130a.

(45) Khan, W. U.; Wang, D.; Zhang, W.; Tang, Z.; Ma, X.; Ding, X.; Du, S.; Wang, Y. High Quantum Yield Green-Emitting Carbon Dots for Fe(III) Detection, Biocompatible Fluorescent Ink and Cellular Imaging. *Sci. Rep.* **2017**, *7* (1), 1–9. https://doi.org/10.1038/s41598-017-15054-9.

(46) Li, H.; Ming, H.; Liu, Y.; Yu, H.; He, X.; Huang, H.; Pan, K.; Kang, Z.; Lee, S.-T. Fluorescent Carbon Nanoparticles: Electrochemical Synthesis and Their PH Sensitive Photoluminescence Properties. *New J. Chem.* **2011**, *35* (11), 2666. https://doi.org/10.1039/c1nj20575g.

(47) Niu, Q.; Gao, K.; Lin, Z.; Wu, W. Amine-Capped Carbon Dots as a Nanosensor for Sensitive and Selective Detection of Picric Acid in Aqueous Solution via Electrostatic Interaction. *Anal. Methods* **2013**, *5* (21), 6228–6233. https://doi.org/10.1039/c3ay41275j.

(48) Brandt, P. W. A Study of the Mechanism of Pinocytosis. *Exp. Cell Res.* **1958**, *15* (2), 300–313. https://doi.org/10.1016/0014-4827(58)90032-6.

(49) Chaudhari, K.; Xavier, P. L.; Pradeep, T. Understanding the Evolution of Luminescent Gold Quantum Clusters in Protein Templates. *ACS Nano* **2011**, *5* (11), 8816–8827. https://doi.org/10.1021/nn202901a.

(50) Tambaru, D.; Rupilu, R. H.; Nitti, F.; Gauru, I.; Suwari. Development of Paper-Based Sensor Coupled with Smartphone Detector for Simple Creatinine Determination. In *AIP Conference Proceedings*; 2017; Vol. 1823, p 20095. https://doi.org/10.1063/1.4978168.

(51) Benkert, A.; Scheller, F.; Schössler, W.; Hentschel, C.; Micheel, B.; Behrsing, O.; Scharte, G.; Stöcklein, W.; Warsinke, A. Development of a Creatinine ELISA and an Amperometric Antibody-Based Creatinine Sensor with a Detection Limit in the Nanomolar Range. *Anal. Chem.* **2000**, *72* (5), 916–921. https://doi.org/10.1021/ac9909047.

(52) Pal, S.; Lohar, S.; Mukherjee, M.; Chattopadhyay, P.; Dhara, K. A Fluorescent Probe for the Selective Detection of Creatinine in Aqueous Buffer Applicable to Human Blood Serum. *Chem. Commun.* **2016**, *52* (94), 13706–13709. https://doi.org/10.1039/c6cc07291g.

(53) Mathew, M. S.; Joseph, K. Green Synthesis of Gluten-Stabilized Fluorescent Gold Quantum Clusters: Application As Turn-On Sensing of Human Blood Creatinine. *ACS Sustain. Chem. Eng.* **2017**, *5* (6), 4837–4845. https://doi.org/10.1021/acssuschemeng.7b00273.

(54) Bhattacharya, A.; Chatterjee, S.; Khorwal, V.; Mukherjee, T. K. Luminescence Turn-on/off Sensing of Biological Iron by Carbon Dots in Transferrin. *Phys. Chem. Chem. Phys.* **2016**, *18* (7), 5148–5158. https://doi.org/10.1039/c5cp05890b.

CONCLUSION

The theme of the thesis was planned accordingly to obtain various sizes, target specific label-free sensor using SPR active and fluorescent nanomaterials (AuNPs and C-dots). In the experimental work, we emphasized different precursor to acquiring long-range emissive C-dots and a different ratio of capping agent for the variable size of AuNPs. The studies revealed that the variant size of the SPR active nanoprobe can modulate its selectivity for the biomolecules. The bigger size probe detects the biomolecules up-to lower limit range, as analysed for thiopurines and variant size citrate capped AuNPs.

Another strategy related with fluorescent properties of C-dots which was tuned using different nitrogen dopants such as urea, thiourea, cysteine and glycine which persuade diverse surface species (pyrrolic, pyridinic and amino) that fetch revolution to induce high PLQY and long emissive range. Among the prepared nitrogen-doped C-dots, those have surfaced with a higher degree of oxidation, pyrrole and pyridinic rich exhibited excellent selectivity for creatinine (LOD = 36 nM). Even, biomass such as citrus peels was picked as a carbon source to prepare oxygen-rich C-dots which was used as an off-on fluorescent probe for fluoride ions and showed the excellent detection limit of 0.01 μM. Furthermore, based on the different pK_a values, a combination of H_2SO_4 + H_3PO_4 acids were used for the single-step synthesis of dual emissive C-dots. Then, solvatochromic behavior and metal ion interaction were explored for the dual emissive C-dots. They exhibited a bathochromic shift in emission spectra in the halogenated rich solvent medium due to the evolution of ICT character and intensified interaction with Fe^{+3} ions. Design of molecular logic gate was established to upsurge its prospect in electronic devices Overall, these experimental approaches revealed that different precursor and pH medium can be facile and cheap route in modulating emissive range and selectivity of C-dots. These different C-dots has a bright future to be useful material in fluorescent inks, remote sensor and bioimager for sustainable and ecological progress.

FUTURE PERSPECTIVES

- The physicists and physical chemists can work on the photophysical properties of different C-dots based on theoretical explanations to obtain green energy systems or green electronics.
- Development of different morphology of SPR active materials can be done using different capping agents for target-specific sensing.

- These nanoprobes can be used in remote sensing through proper implementation of logic gates.
- Simple and facile methods need to be developed to tune the C-dots emission range towards NIR region to utilize them for deep bioimaging of tissue and cells.

List of Publications

1. **Kainth, S.**, Maity, B., & Basu, S. **(2020)**. Deciphering the interaction of solvents with dual emissive carbon dots: A photoluminescence study and its response for different metal ions. *Materials Science and Engineering: C*, *108*, 110443. https://doi.org/10.1016/j.msec.2019.110443 **(IF = 4.959) ISSN: 0928-4931**

2. **Kainth, S.**, & Basu, S. **(2018)**. Quantitative Detection of Thiopurines by Inter-particle Distance-Dependent Properties of Gold Nanoparticles. *Plasmonics*, *13*(5), 1785-1793.https://doi.org/10.1007/s11468-018-0692-8 **(IF = 2.926) ISSN: 1557-1963**

3. **Kainth, S**., Mehta, A., Mishra, A., & Basu, S. **(2018)**. Implementation of a logic gate by chemically induced nitrogen and oxygen rich C-dots for the selective detection of fluoride ions *New Journal of Chemistry*, *42*(14), 12162-12171.https://doi.org/10.1039/C8NJ02041H **(IF = 3.069) ISSN: 1369-9261**

4. **Kainth, S.**, Maity, B., & Basu, S. Impact of Different Nitrogen Surface Passivation in Carbon-Dots and Its Sensing Efficacy Towards Picric Acid and Creatinine. *Journal of Material Chemistry C.* (**Under Review**)

Other Publications

1. Mishra, A., Mehta, A., **Kainth, S.**, & Basu, S. **(2018)**. Effect of g-C3N4 loading on TiO_2/Bentonite nanocomposites for efficient heterogeneous photocatalytic degradation of industrial dye under visible light. *Journal of Alloys and Compounds*, *764*, 406-415. https://doi.org/10.1016/j.jallcom.2018.06.089 **(IF = 4.175) ISSN: 0925-8388**
2. Mishra, A., Mehta, A., **Kainth, S.**, & Basu, S. **(2018)**. Effect of different plasmonic metals on photocatalytic degradation of volatile organic compounds (VOCs) by bentonite/M- TiO_2 nanocomposites under UV/visible light. *Applied Clay Science*, *153*, 144- 153.https://doi.org/10.1016/j.clay.2017.11.040 **(IF = 3.890) ISSN: 0169-1317**
3. Mehta, A., Mishra, A., **Kainth, S.**, & Basu, S. **(2018)**. Carbon quantum dots/TiO_2 nanocomposite for sensing of toxic metals and photodetoxification of dyes with kill waste by waste concept. *Materials & Design*, *155*, 485-493.https://doi.org/10.1016/j.matdes.2018.06.015 **(IF =5.770) ISSN: 0264-1275**
4. Mishra, A., Mehta, A., **Kainth, S.,** & Basu, S. **(2018)**. A comparative study on the effect of different precursors for synthesis and efficient photocatalytic activity of gC_3N_4/TiO_2/bentonite nanocomposites. *Journal of materials science*, *53*(18), 13126-13142. https://doi.org/10.1007/s10853-018-2565-0 **(IF = 3.442) ISSN: 0022-2461**

Paper presented in Conference/Workshop attended

Poster Presentation

- **5th International Conference on Advanced Nanomaterial & Nanotechnology** organized by Centre of Nanotechnology **Indian Institute of Technology Guwahati**, Assam, India. (December-2017)

Oral Presentation

- UGC Sponsored **10th National Conference on recent advances in Chemical and Environmental Sciences (RACES-2019)** organized by **Multan Mal Modi College**, Patiala. (April-2019)

Workshop

- Electroceramics **Summer School** "Process and properties of Electro-ceramics for Energy applications" organized by the **University of Hasselt, Belgium**. (July-2018)

Achievement

- **Young Scientist Award** in UGC Sponsored 10th National Conference on recent advances in Chemical and Environmental Sciences **(RACES-2019).**

Publications

Materials Science & Engineering C 108 (2020) 110443

Contents lists available at ScienceDirect

Materials Science & Engineering C

journal homepage: www.elsevier.com/locate/msec

Deciphering the interaction of solvents with dual emissive carbon dots: A photoluminescence study and its response for different metal ions

Shagun Kainth, Banibrata Maity*, Soumen Basu*

School of Chemistry and Biochemistry, Thapar Institute of Engineering & Technology, Patiala 147004, India

ARTICLE INFO

Keywords:
Dual emissive CDs
Acidic carbonization
Solvatochromism
Sensing
Metal ions

ABSTRACT

Carbon-based fluorescent quantum dots exhibited tunable photoluminescence (PL) property which is mainly dependent on its excitation wavelength which is an important factor required for optoelectronic and sensing applications. Here, we have established a microwave-based synthesis of dual emissive carbon quantum dots (CDs) using mixed-acid (H_3PO_4 + H_2SO_4) and mono/disaccharides as carbon precursor. In aqueous medium, CDs showed dual emission peaks at 434 nm and 518 nm, which exhibited excitation independent fluorescence property with particle size in the range of 4–7 nm. Furthermore, its photophysical properties were explored in different solvents. The astonishing bathochromic shift was observed in its emission wavelengths with the decrease in polarity of the solvents. Moreover, the metal sensing efficacy of CDs was explored in these solvent systems. It exhibited utmost selectivity for Fe(III) ions in both the organic and aqueous medium with maximum and minimum detecting limit of 1 μM and 0.4 μM respectively. These experimental results were also validated through real samples (Ferric citrate tablets 200 mg) and it showed excellent metal ion sensing accuracy for CDs in different media. The fundamental motive of this work was to explain the role of the mixed acid for the development of dual emissive CDs using a single precursor. The solvatochromic and sensing properties of CDs were explored in various solvents, which could be useful for sensing applications.

1. Introduction

There was no long history for the discovery of carbon quantum dots (CDs), but it occupies the prominent place in the field of luminescent nano-materials due to its high aqueous solubility, exceptional photoluminescence (PL) properties, favourable biocompatibility, chemical inertness and easy functionalization in respect to known organic fluorophores. Nowadays, the research focus is shifted towards the implications of luminescent CDs. Still, to boost its utility in target-specific sensing and bio-imaging field, simplified eco-friendly strategies need to be introduced to tune its luminescence properties. This can be achieved by tailoring their intrinsic properties and modification of its surface design by conjugation of different functional groups on its surface [1,2].

Several different synthetic chemical and physical routes such as electrochemical [3], thermal treatment [4], hydrothermal or acidic oxidation [5], microwave [6], ultrasonic [7,8], cage-opening of fullerene [9], arc discharge [10], laser ablation [11], and plasma treatment [12] to fabricate luminescent CDs was reported to fabricate multicolour CDs. Many groups followed functionalization route to attain modified CDs using boronic acid/aptamer as a precursor for the determination of metal cations [13,14] and glucose [15]. Chi et al. [2] functionalized CDs using polyamine to tune its emissive properties and further used as nano-probe based on the inner filter effect for Cu^{+2} ion sensing. Even several moieties were also detected (such as Vitamin B_{12}, amino acids and dopamine etc.) through the diverse strategies which include foster resonance energy transfer (FRET), photoinduced electron transfer (PET), aggregation-caused quenching by coordination and reaction-induced fluorescence quenching using CDs [16–20]. In addition, to make target specific sensor [12,21] many groups were also giving emphasis on extrinsic parameters such as dopants, solvents to tune its photoluminescence (PL) properties. Park et al. [22] used sulfur doping route to tune its electronic states and PL intensity in the longer wavelength regime. Moreover, reduction pathways were also followed by Dong et al. [23] to obtain the long-range emissive (450 to 520 nm) CDs. In recent studies, many researchers modified synthetic conditions, precursors and reagents (citric acid and formamide) to obtain excitation wavelength-dependent multicolour CDs [24–27]. Likewise, Pang and co-workers [28] modified the reaction time and temperature to prepare the new excitation independent series of CDs. Ding et al. [29] used hydrothermal method to prepare the batch of multicolour CDs from *p*-phenylenediamine and urea which showed blue to red emission (440–625 nm, Q.Y. 8.5–35%) at the single excitation wavelength. Some

* Corresponding authors.
E-mail addresses: banibrata.maity@thapar.edu (B. Maity), soumen.basu@thapar.edu (S. Basu).

https://doi.org/10.1016/j.msec.2019.110443
Received 10 May 2019; Received in revised form 8 November 2019; Accepted 15 November 2019
Available online 18 November 2019
0928-4931/

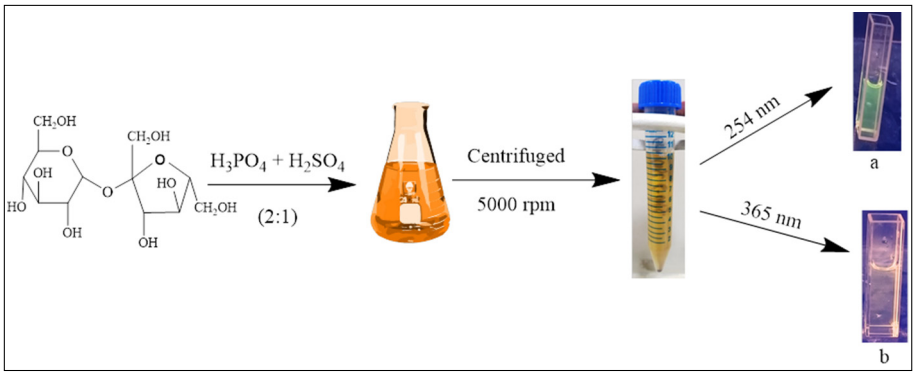

Scheme 1. Pictorial representation to synthesized the dual emissive CDs.

of the groups also used green materials to tune the emissive properties of CDs [30,31]. These variations in emissive properties of CDs were achieved by several groups due to the modulation in the quantum size and surface states [29,32].

Nowadays to tune the emissive range of CDs, more emphasis is given on the dispersive medium. Wu and coworkers reported a red-shift in the emission spectra (400 to 430 nm) for CDs with the same excitation wavelength, dispersed in different solvents [4]. Even analogous results were reported for graphene quantum dots in different solvents with the emission range from 475 to 515 nm [33]. The tenacity for the development in its synthetic routes was to improve its efficacy for bio-imaging and bio-sensing. Overall, the above-mentioned advancements for preparing multicolour CDs were found tedious, expensive and low yield. Thus, eco-friendly and cost-effective routes were required to attain long emissive range CDs.

To execute these problems, some groups utilizing the combination of carbohydrates and acids to produce a series of CDs [34]. Some significant reports were mentioned by Wee et al. [35,36] where they used the dehydrating agent (H_2SO_4), various protein and carbohydrate nanoparticles to produce CDs. Likewise, other groups use different acids (H_3PO_4, HCl and HNO_3) [37] to attain green, yellow and red-emitting CDs [38,39]. Though, the reported work was effective due to the utilization of low energy, basic laboratory glassware. Still, some experimental studies were required to justify the role of acids to attain dual emissive properties in them. Till now, solvatochromism studies for dual emissive CDs were not explored [40,41].

Therefore, we have reported an eco-friendly route to attain dual emissive CDs by using different carbohydrates with a combination of acids. In addition, its photophysical properties were discovered in different solvent systems. Successively, the sensing ability of CDs was also explored with various metal ions in both aqueous and non-aqueous medium. The experimental studies revealed exceptional behavior for dual emissive CDs in halogenated solvents, which exhibited a bathochromic shift in its emission spectra w.r.t the aqueous medium which has not been reported elsewhere.

2. Experimental sections

2.1. Materials and characterization

Sucrose, fructose, glucose was purchased from Thermo Fisher Scientific, United States. Other basic chemical reagents like orthophosphoric acid, nitric acid, sulfuric acid, hydrochloric acid, ferric nitrate, ferrous nitrate, copper nitrate, zinc nitrate were purchased from Sigma Aldrich. Different kinds of solvents namely dichloromethane (CH_2Cl_2), chloroform ($CHCl_3$), carbon tetrachloride (CCl_4), acetonitrile (ACN), dimethylformamide (DMF), methanol was purchased from Loba Chemie Pvt. Ltd. (spectrograde), India. All these reagents and carbohydrates were used directly by preparing their aqueous solution using distilled water (18.2 MΩ·cm, Millipore). The CDs were synthesized by using Multiwave-300 microwave synthesis reactor (Anton Paar, USA). The synthesized CDs were characterized by High-resolution transmission electron microscope (HRTEM), (TALOS F200S G2, 200 KV, FEG, CMOS Camera 4K × 4K, In Column EDS detectors) for the analysis of its surface morphology and particle size by using a drop-casting technique. Moreover, AT-IR spectroscopy (Agilent Resolution Pro-carry 660) XPS, X-ray photoelectron microscopy and Energy-dispersive X-ray spectroscopy (EDX) techniques were carried out to know the better insight on the CDs surface. LS-55 spectro-fluorophotometer (Perkin Elmer) was also used to study its optoelectronic properties.

2.2. Preparative method for dual emissive CDs

The one-pot synthesis was followed to fabricate dual emissive CDs. Firstly, 0.5 g sucrose (0.15 M) was dissolved in 10 ml of distilled water followed by the addition of 100 μl concentrated sulfuric acid (H_2SO_4) and 200 μl of concentrated ortho-phosphoric acid (H_3PO_4) in the ratio of 1:2. The prepared mixture was transferred into the microwave glass vial and subjected to microwave heating at 130 °C for 10 min. After the completion of the reaction, the brown colour colloidal solution was obtained. It was purified by centrifugation at 5000 rpm for 30 min to get yellow colour CDs and further it pass through a syringe filter (0.22 μm) to get a homogeneous colloidal mixture which exhibited dual emissive properties (Scheme 1). The surface analysis and photoluminescence were also done to study its morphology and optical properties.

2.3. Photoluminescence quantum yield (PLQY) measurements

To evaluate the PLQY for dual emissive CDs firstly, the reference fluorophore, quinine sulfate solution was prepared in 0.01 M H_2SO_4 (φ_R = 0.546) [42]. The concentration was set accordingly to set its absorbance below 0.1 to minimize the inner filter effect. The absorbance of CDs was also measured and its integrated fluorescence intensity area was calculated from the spectrum. The calculation for PLQY was done on the basis of Eq. (1).

$$\varphi = \varphi_R \times (I/I_R) \times (A_R/A) \times (\eta^2/\eta^2_R) \quad (1)$$

where 'φ' denotes as the quantum yield, 'φ_R' is PLQY of reference, 'I' as the integrated area of fluorescence intensity, 'A' as the absorbance value and 'η' as refractive index.

2.4. Methodology for photoluminescence studies of dual emissive CDs

To evaluate the solvatochromic and sensing behavior of CDs firstly, CDs was dispersed in different solvents (2 ml) and its emission spectra were evaluated in all different media respectively. Furthermore, the stock solution of metal salts like Mg(II), Cu(II), Zn(II), Co(II), Ni(II), Fe

(III) and Fe(II) (10^{-3} M) was prepared in distilled water which was added (10 μl) in a test tube and air-dried. Then, CDs was dispersed in different solvents (2 ml) and added to the test tube. Afterward, their interactions with CDs in different solvent systems were analyzed by recording its PL emission spectra. To validate the sensing efficacy of CDs, real samples (Ferric citrate tablets - 200 mg) were also analyzed by following the same above mentioned protocol.

3. Result and discussions

3.1. The mechanism involved in the fabrication of dual emissive CDs

In this protocol, major emphasis was given on acids for the activation of carbon particles and to modify the surface functional groups. In the synthesis of CDs, both the acids (H_2SO_4 and H_3PO_4) play an independent role to tune its emission properties. H_3PO_4 helps to promote the carbonization of sucrose at slower kinetics to produce surface defects which cause red-shift [43–46] whereas, H_2SO_4 due to its stronger oxidizing ability generates O═C−O−H and C−O−H from C−H and its dehydrating property induces unsaturation from C−C, causing a blue shift in the emission spectra of CDs [47,48]. Therefore, the acid mixture (H_2SO_4 + H_3PO_4) was chosen to produce dual emissive CDs in a single step without using toxic reagents and to fix its discrete energy band gap [49].

The preparative method for CDs involves various steps. Initially, sucrose solution undergoes modifications through hydrolysis and dehydration to form furfural intermediates (such as hydroxyl methyl furfural) [50,51]. The intermediate was further polymerized, aromatized [52,53] and subsequently undergoes the nucleation and particle growth process to attain the brownish colloidal solution [54] which was explained in detail in Scheme 2. Further, to confirm the dual emissive behavior in prepared CDs, its aqueous solution was kept under the UV light irradiation where it showed green and yellow colour emission at two different wavelengths (254 and 365 nm) (Scheme 1).

3.2. Optical properties and stability of dual emissive CDs

The optical properties of dual emissive CDs are shown in Fig. 1. Firstly, UV–Vis spectrum was recorded, which showed prominent absorption peak at ~284 nm, (which is due to the n-π* transition of C═O bond) and a weak shoulder band at ~227 nm. The weak band is attributed to the π-π*transition of the aromatic sp^2 bond [55] (Fig. 1a). PL spectra were also recorded to confirm the dual emission behavior of CDs. It showed two emission peaks at 434 nm and 518 nm (Fig. 1b) by exciting the sample at 350 nm. This dual emission peak was attained due to the formation of discrete fixed energy gaps and the elimination of intermediate energy levels in CDs induced with the help of acid mixtures [49]. Moreover, the synthesized dual emissive CDs showed excitation independent behavior in comparison to the other reported multi-colour CDs [56] (shown in Fig. 1c). This unusual trend in CDs was explained on the basis of surface passivation as reported by Zeng et al. [57]. According to their interpretation, the multi-mode absorptions were attained for low passivation CDs due to the formation of different energy states, which was responsible for its excitation dependent PL property [35]. Moreover, the single transition mode developed in case of high passivation CDs surface which generates excitation-independent PL [35]. So, from the aforementioned results it has been concluded that a mixture of acids plays a vital role in the high surface passivation and development of single transition mode among CDs.

It is necessary to investigate the solution conditions of CDs before the utilization in various applications. pH is the main parameter that influences the emission properties of CDs which needs to be studied. So, PL spectra of CDs were recorded at different pH range from 2 to 9 (Fig. 1d). The study showed that CDs attain equivalent PL intensity in the pH range from 2 to 6. But with the increment of pH towards the basic range, it shows high pH sensitivity due to the presence of several hetero-atoms (confirmed by EDX and XPS analysis) on its surface [58]. So, it can be used as an effective analytical tool in the pH range (2–6). Consequently, the PL spectra were recorded at different concentrations of KCl salt, which shows the constant response in the PL intensity and mixture appears to be homogeneous i.e. no aggregation took place in

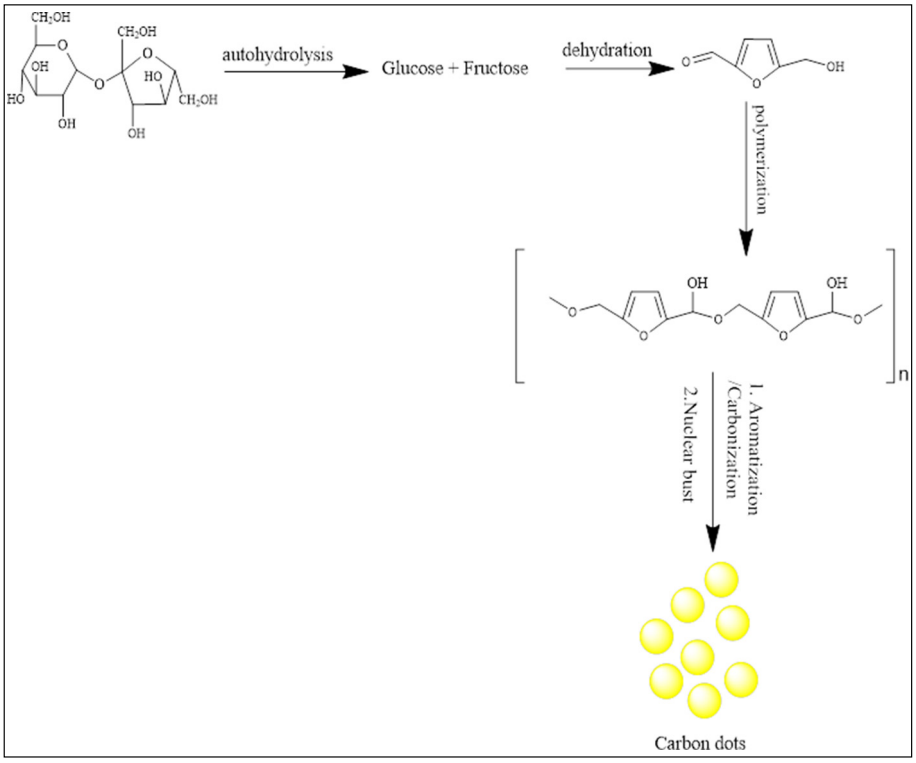

Scheme 2. Schematic presentation of mechanism used to obtain dual emissive CDs.

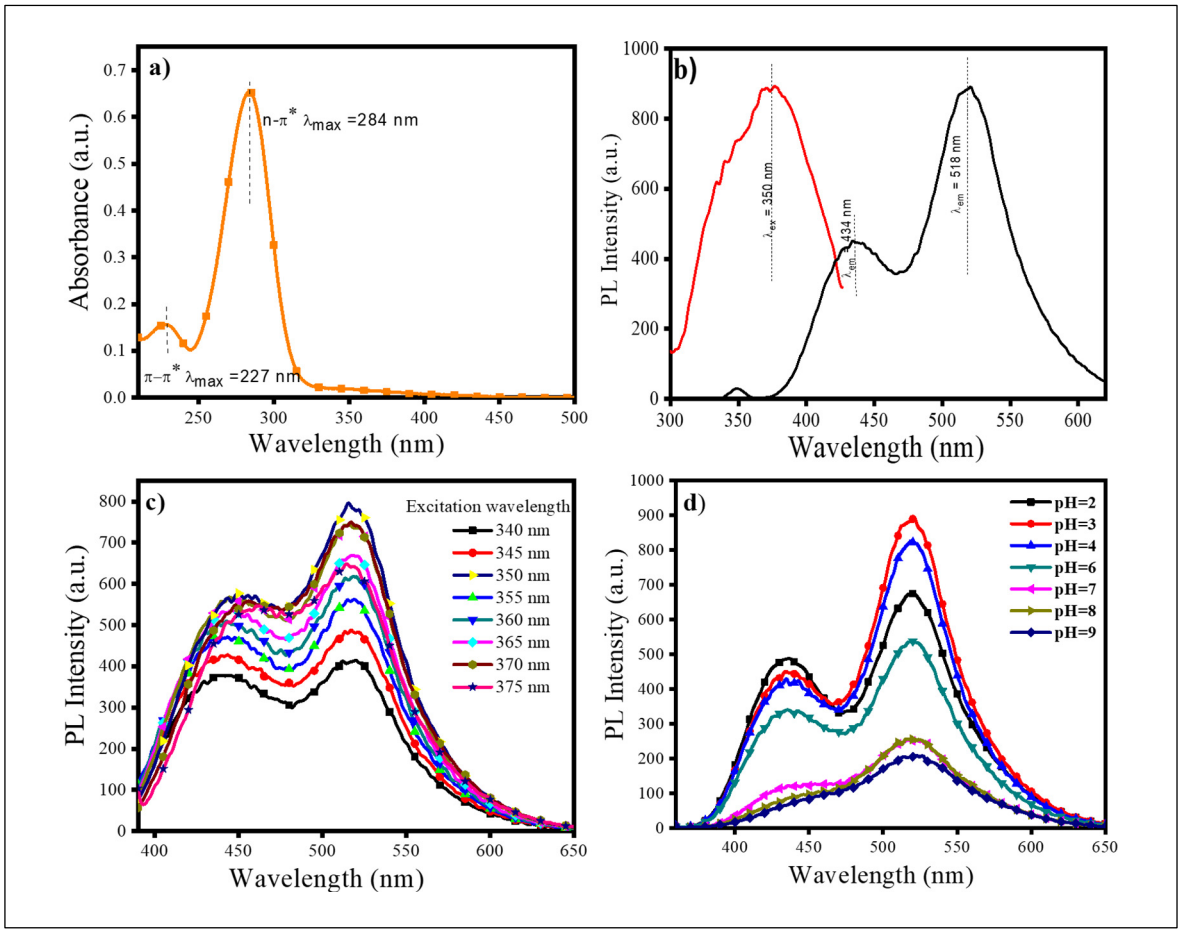

Fig. 1. Optical properties of dual emissive CDs: a) UV–visible spectra, b) excitation and emission spectra (λ_{ex} = 350 nm), c) effect of excitation wavelength and d) effect of pH on its PL intensity.

the presence of concentrated K^+ cations and Cl^- anions (Fig. S1a) [48]. In addition, we have also analyzed CDs under UV lamp irradiation for 1 h which shows no change in its PL intensity (Fig. S1b). Therefore, the obtained results conclude that CDs can be used in analytical application to quantify the analyte of interest without any interference of surrounding environment.

3.3. Characterization of dual emissive CDs

The morphology and the size distribution of dual emissive CDs were characterized by HRTEM, represented in Fig. 2. The HRTEM result justifies its partial mono-dispersed and spherical feature, with narrow particle size distribution ranging from 47 nm (average diameter of 4.6 nm). In Fig. 2b, the HRTEM image showed the lattice fringes with d-spacing value of 0.24 nm which corresponds to (100) facet of graphitic CDs. Furthermore, in the selected-area electron-diffraction (SAED) displayed a ring pattern with an inter-planar lattice spacing of 0.24 nm and the high crystallinity, which agrees with the (100) lattice spacing of graphitic CDs (Fig. 2c) [59].

The XPS studies were done to determine the surface chemical composition of dual emissive CDs. The survey spectrum of XPS revealed that surface of CDs primarily composed of C_{1s} (49.84%), O_{1s} (41.66%) and another small part was contributed by P_{2p} (6.47%), and S_{2p} (2.47%) (Fig. S3a). The high-resolution XPS data of C_{1s} were deconvoluted into four peaks at 284.6, 286.1, 287.9 and 288.9 eV, which represent the C_{1s} states exists in the C–C/C=C, C–S, C–O and C=O bonds respectively (Fig. S3b) [60]. The O_{1s} spectra showed two main peaks at 531.8 eV and 532.8 eV which indicates the presence of C=O and C–O respectively [61]. The P_{2p} spectrum (Fig. S3d) revealed the presence of P=O (133.1 eV) and P–C (134.1 eV) groups [62]. The S_{2p} spectrum (Fig. S3e) showed three major peaks at 167.8, 168.4 and 169.5 eV, corresponding to C–SO_x (x = 2, 3, 4) species respectively, which indicates that sulfur groups exist in sulfonate state on CDs surface [63,64]. The surface state of CDs was also elucidated through AT-IR spectra mentioned in Fig. 2e. The spectral details show the broad peak at 3420 cm^{-1} associated with the O–H group and the sharp absorption peak at 1630 cm^{-1} which confirmed the presence of the carbonyl group on its surface. In addition, the spectra display two another peaks at 1162 and 1065 cm^{-1}, which confirmed the existence of P=O groups from phosphate or polyphosphates, and the O–C stretching vibration of P–O–C (aromatic), respectively [38]. This phosphate groups may be derived from the bidentate bonding between the [PO_4^{3-}] and –OH group on its surface [38]. Further, the presence of sulfur and phosphorus in CDs was confirmed by EDX analysis, which demonstrates the presence of carbon, oxygen, sulfur, and phosphorus on its surface (Fig. 2f). These results indicated that CDs surface comprises several hydrophilic and hetero groups on its surface which were responsible for its dual photoluminescence, high water solubility and aids in complex formation.

3.4. Optimization of different carbon precursor, concentration and reaction time to fabricate dual emissive CDs

Different sources of carbon and reaction time play a vital role to modify the PL behavior and morphology of CDs. So, we used various precursors such as sucrose, fructose, and glucose in the presence of

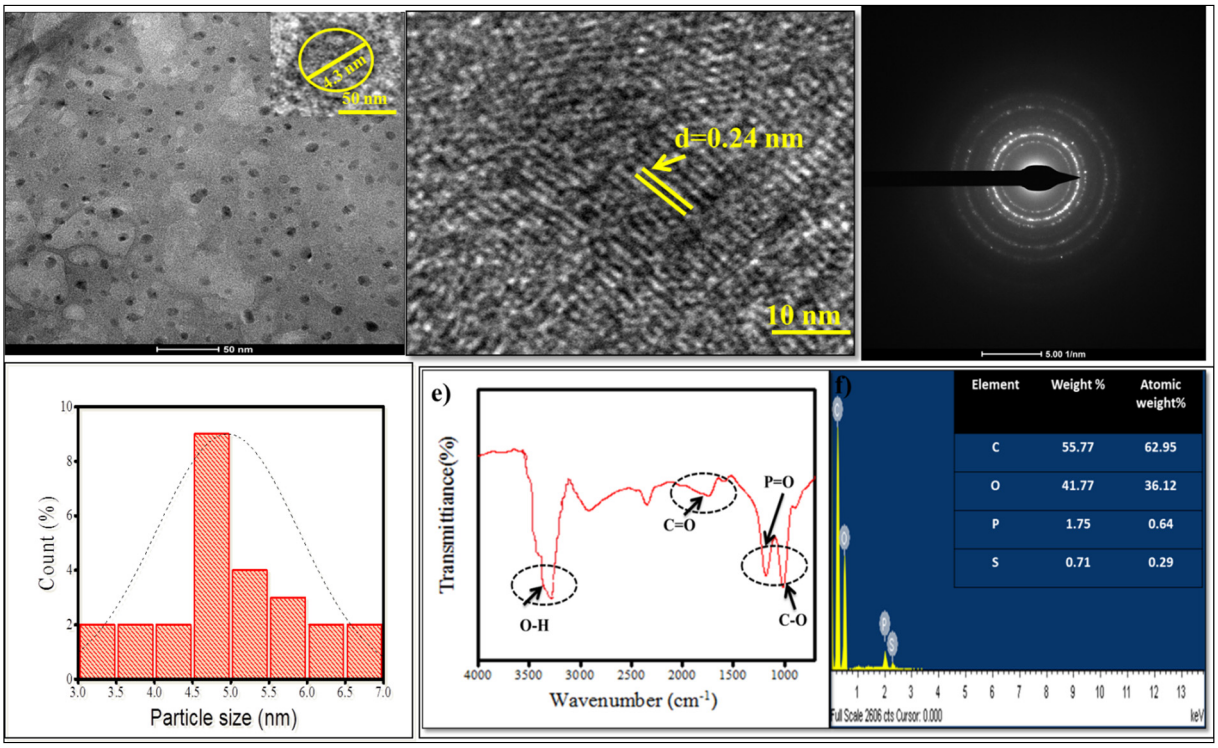

Fig. 2. Physico-chemical properties of dual emissive CDs: a) HRTEM and inset shows the particle size of individual CDs, b) lattice fringes of individual CDs, c) corresponding selected-area electron-diffraction (SAED) pattern image, d) histogram distribution of particle size from HRTEM image, e) AT-IR spectra of CDs and f) energy dispersive spectra of CDs.

mixed acids (H_3PO_4 + H_2SO_4) to fabricate CDs. The experimental results suggest that if the carbon precursors have similar functional groups present on it, then its conversion to CDs in the presence of mixed acids exhibited consistent emission peaks at 434 nm and 518 nm as shown in Fig. 3a. Although, the PL peak intensity for sucrose found to be is highest among all the precursors. So, from these results different molar concentration of sucrose was chosen to attain the dual emissive CDs. The experiments result specifies that acid-mediated sucrose-based CDs exhibited the highest PL intensity at 0.15 M concentration of sucrose as shown in Fig. 3b.

Moreover, times studies were performed to evaluate the impact of reaction time rate on its PL properties. The result specifies that the maximum PL intensity for dual emissive CDs was attained in ~8–10 min under microwave irradiation (Fig. S2), which is less than the reported methodology [49]. Thus, it is necessary to optimize the concentration of carbon source and reaction time for the development of dual emissive behavior CDs in acidic conditions.

3.5. Effect of different acids on PL properties of CDs

The particle size and functional groups present on the surface of CDs play an important role to fetch difference in its emission properties. So, we used acids to modify its emissive sites to attain multicolour CDs. To explain the significance of acids, H_3PO_4, H_2SO_4, HNO_3, and their combinations were used for the preparation of CDs from sucrose precursor. At first, the individual effect of acids such as H_2SO_4, HNO_3 was studied, which showed significant single emission peak in the blue region (435 nm) as shown in Fig. 3c. However, the emission peak of CDs undergoes bathochromic shift (470 nm) in the presence of H_3PO_4. This distinct behavior in emission properties of CDs in the presence of different acids was originated from defects on its surface, which develops discrete surface states with an energy level between the π and π* states of the carbon double bond in the CDs emission sites [49]. Dong et al. [39] reported that the presence of hetero-atoms modified the PL properties of CDs. Similarly, Xu et al. [38] showed emission shift towards the red region is due to the phosphorus-doped CDs. Based on these reports, we conclude that doping can create new energy levels or change their initial band gap [65,66]. In view of that, we used a combination of acids (H_2SO_4 + H_3PO_4) and studied its impact on the synthesis of CDs by altering their ratios from 2:1 to 1:2 (Fig. 3d). The result indicates that the combination of acids in both conditions leads to induce dual emission peaks (434 nm and 518 nm) in CDs. The existence of longer wavelength peak in CDs attributed to the surface or edge functional group and the shorter emission wavelength was due to the presence of uniform sp^2 domains [48]. These characteristic features of dual emissive peaks in CDs indicated that the mixed acids lead to the formation of intermediate energy level i.e. not possible in their absence which helps to overcome the activation energy for better carbonization and emission intensity [49].

Even, the intensity of the dual emissive peaks also depends on the ratio of mixed acids for the formation of CDs (Fig. 3d). The results revealed that the acid ratio of 1:2 (H_2SO_4 + H_3PO_4) helps to attain prominent emission peak at 518 nm w.r.t 2:1 (H_2SO_4 + H_3PO_4), because both acids have different pK_a value (H_3PO_4 > H_2SO_4) [49]. If the concentration of H_2SO_4 gets increased, the carbonization process gets enhanced and converted the carbon precursor into non-fluorescent products [49]. Hence, high concentration of H_3PO_4 is necessary for the formation red emissive CDs with appropriate PL intensity. So, fixation of a particular molar ratio (2:1) of acids was necessary to enhance the photophysical properties of CDs.

3.6. Solvatochromic studies of dual emissive CDs

The surrounding medium of the CDs also has a vital role to modulate the emission spectral behavior. So, to comprehend the better insight into the interaction of dual emissive CDs with solvents, we have studied their photophysical properties. According to general trends, if the polarity of the surrounding medium increases the fluorescence

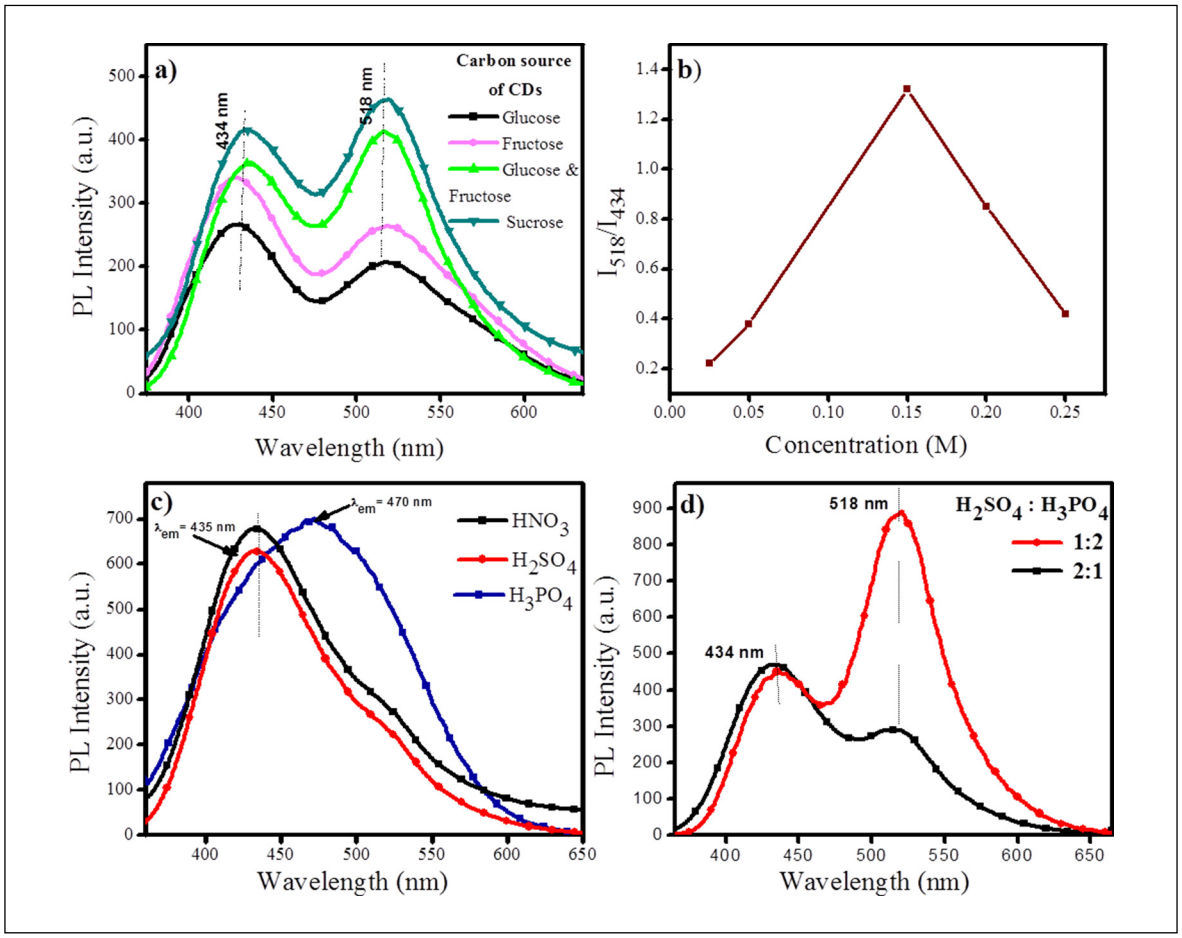

Fig. 3. The emission spectra of dual emissive CDs: a) using different precursor, b) at various concentration of sucrose, c) in the presence of different acids and d) in the presence of mixed acids.

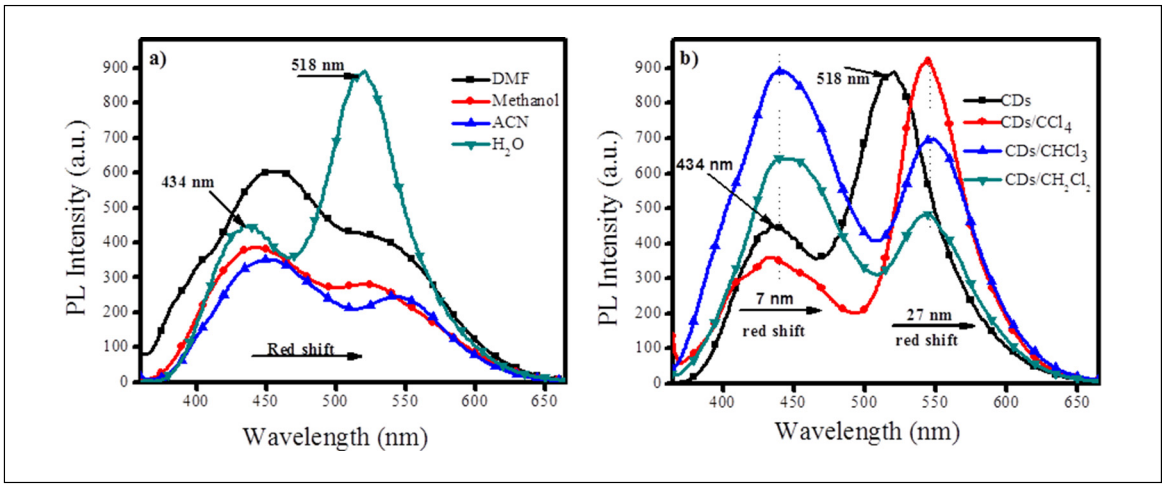

Fig. 4. Solvatochromism of dual emissive CDs: a) non-halogenated and b) halogenated solvents.

active compounds exhibit bathochromic shifts in their emission spectra. However, in our case, the dual emissive CDs undergoes hypsochromic emission shift in the presence of water (highly polar solvent). It has been observed that the first emission maxima appeared at 434 nm (shorter wavelength) along with a prominent peak at 518 nm (longer wavelength) (Fig. 4a). In presence of methanol, the shorter wavelength emission maxima appeared at 443 nm along with a band at 523 nm. In polar aprotic solvents (ACN and DMF), CDs exhibit a bathochromic shift in emission spectra of both the emission maxima compared to that of water. Also, the longer wavelength emission maxima appeared as a shoulder band in polar aprotic solvents. These results justified that hypsochromic shift of CDs in water compared to methanol, ACN, and DMF was due to the solvent-induced change of electronic ground state from less dipolar to more dipolar chromophore [67]. Moreover, in the case of water, the longer wavelength emission maxima appear as a prominent peak, which is attributed to extensive hydrogen-bonding

Table 1
Detail of emission spectra for dual emissive CDs in the presence of variant solvent systems.

Solvent system	Excitation wavelength (λ_{ex})	Emission wavelength (λ_{em})	
		λ_1	λ_2
H_2O	350 nm	434	518
MeOH		443	523
DMF		445	527
ACN		449	546
CCl_4		436	544
$CHCl_3$		440	546
CH_2Cl_2		443	543

interactions, dipole-dipole interactions, and specific solute-solvent interactions. But, in other protic (methanol) and aprotic (ACN, DMF) solvents these types of specific interactions were less prominent due to which the longer wavelength emission maxima appears as a shoulder band (Fig. 4a).

Furthermore, it was observed that the polarity of the medium (Lippert Mataga (LM) model) is not always playing a significant role in solvatochromic shifts, there are some other factors such as polarizability (π^*), hydrogen bond accepting ability (HBA, β) and hydrogen bond donating ability (HBD, α) of solvents (Kamlet Taft (KT) model) also influences the PL properties of CDs [68,69]. From the Kamlet-Taft parameter (Table ST1), it was observed that the value of HBA parameter (β) is relatively larger in methanol, ACN and DMF as compared to that of water, which results in a hypsochromic shift in emission spectra of aqueous CDs (shown in Table 1) [70].

Moreover, another unusual kind of emission spectrum was observed in the presence of halogenated solvents (CH_2Cl_2, $CHCl_3$, and CCl_4) (Fig. 4b). The dual emissive CDs exhibit bathochromic emission in both the shorter and longer wavelengths, as well as both the emission maxima, appear as prominent peaks. This behavior was observed due to the formation of donor-π-acceptor interaction between sp^2 domain, electron-rich hetero-atoms on the surface of CDs and halogenated solvents [71,72], that increases its ICT character in the excited state [73,74]. Similar results were reported by Ooyama et al. [75] where they observed a bathochromic shift in halogenated solvents through the D-π-A interaction mechanism. Therefore, from the solvatochromic analysis, it can be concluded that the dual emissive CDs are dependent upon the nature of the solvents.

3.7. Interaction of CDs with different metal ions in aqueous and halogenated solvents

Here, we have also explored the efficacy of metal ions interaction with dual emissive CDs in aqueous medium and halogenated solvents by determining the photoluminescence properties. The sensing efficacy of CDs was evaluated in acidic conditions (pH ~3) because with protonation of its surface causes weaker electrostatic interaction across all metal ions and promote selectivity towards metal ions that have higher charge and smaller size [48]. According to experimental analysis, it has been observed from Fig. 5 that CDs undergoes fluorescence quenching with the gradual addition of Fe(III) ion. In water, chloroform, and CH_2Cl_2, CDs steadily quenches at both the wavelength. But the extent of quenching efficiency at the longer wavelength is much more as compared to the shorter one because at longer wavelength more surface or edge functional groups (C═O, P═O and O−H etc.) exist, which induces electrostatic interaction with Fe(III) [76]. This remarkable fluorescence response in a non-aqueous and aqueous medium in the presence of Fe (III) can be probably attributed because dual emissive CDs have C═O/O−H on its surface that generates Fe(III)/CDs complex which leads to electron transfer from its HOMO (singlet excited state) to the half field 3d orbital of Fe(III) ions and induce fluorescence quenching among CDs through photoinduced electron transfer mechanism (PET) [77]. This quenching mechanism of dual CDs towards Fe(III) was justified by evaluating different kinds of the photophysical parameters such as PLQY (φ_f) and lifetime decay (τ_f), radiative (k_r) and non-radiative rate constant (k_{nr}) values, which was mentioned in Table ST2. The PLQY of CDs in water, CCl_4, $CHCl_3$ and CH_2Cl_2 are 0.50, 078, 0.86 and 0.56 respectively. Presence of Fe(III) ions causes quenching of the PLQY of CDs in all the studied solvent systems. The PLQY of CDs in presence of water, CCl_4, $CHCl_3$ and CH_2Cl_2 are 0.27, 0.34, 0.31 and 0.14 respectively. Similarly, lifetime values of CDs also confirms that in presence of Fe(III) ion significantly quenching of the lifetime value occurs in different solvent systems (Table ST2 and Fig. S4).

Furthermore, Stern-Volmer equation was followed to evaluate the sensing efficiency of CDs in various medium towards Fe(III) ions.

$$F_0/F = 1 + K_{SV}C$$

where F_0 is the initial fluorescence intensity in the absence of analyte, F is the fluorescence intensity in the related concentrations of metal, K_{SV} is the Stern-Volmer constant and C is the concentration of metal ions. It was seen from the experimental results that; fluorescence quenching is in the order of $CHCl_3$ ($K_{SV} = 0.077 \times 10^{-6}\ M^{-1}$) > CCl_4 ($K_{SV} = 0.063 \times 10^{-6}\ M^{-1}$) > CH_2Cl_2 ($K_{SV} = 0.044 \times 10^{-6}\ M^{-1}$) > H_2O ($K_{SV} = 0.031 \times 10^{-6}\ M^{-1}$) which is illustrated in Fig. S5. The performed experiments indicate that dual emissive CDs in the different solvent system can act as sensing probe for the metal ions.

Moreover, the estimation for the selectivity of CDs towards the Fe (III) ion in a different solvent system, we investigated its fluorescence response with other metal ions like Cu(II), Zn(II), Fe(II), Cd(II), Ni(II), Mg(II) i.e. shown in Fig. S6. The results showed no significant change in the fluorescence intensity of CDs in aforementioned metal ions except Fe(III) ions. The selectivity of Fe(III) lead to severe fluorescence quenching of carbon quantum dots due to strong interaction of Fe(III) with the carboxylic/phosphate/hydroxyl/sulfur groups on the surfaces of the CDs. This quenching mechanism can be explained by the hard-soft-acid-base (HSAB) principle, where Fe(III) act as hard acid and hetero atom based surface functionalized CDs act as hard base [31]. Anjana et al. also reported that significant electron transfer induced quenching of Fe(III) ions was observed for hetero-atom based CDs due to its paramagnetic effect, higher charge density, smaller size and positive reduction potential [78]. Thus, it was justified that the dual emissive CDs were highly selective and sensitive probe for Fe(III) ions in both aqueous and non-aqueous medium. To evaluate the efficacy of dual emissive CDs its detection limit for Fe(III) ions was compared with several reported materials mentioned in Table 2. After the comparison, it was concluded that the prepared system was cost-effective sensing probe for Fe(III) ions.

3.8. Efficacy of dual emissive CDs in the real sample sensing

The dual emissive CDs found selective for Fe(III) ions in both organic and aqueous medium. So, its PL spectra were recorded to study its effects in the real samples (Fe(III) ions in tablets and syrups). Different volume (0-250 μl) of Fe(III) ions was spiked in the real sample solution to maintain a suitable concentration of these ions. The results obtained from PL studies show that Fe(III) ions gradually decrease the PL intensity at λ_{em} = 543 nm. Similar trend was also observed for standard samples. The accuracy was also evaluated by calculating its recovery % in the organic and aqueous phase to support the analytical results mentioned in Table 3. As a result, 99.8% recovery was obtained in the CDs (organic and aqueous phase) for Fe(III) ions. Thus, this nano-probe can effectively use in the real samples for Fe(III) ions determination.

4. Conclusion

In summary, we demonstrated a single step microwave technique

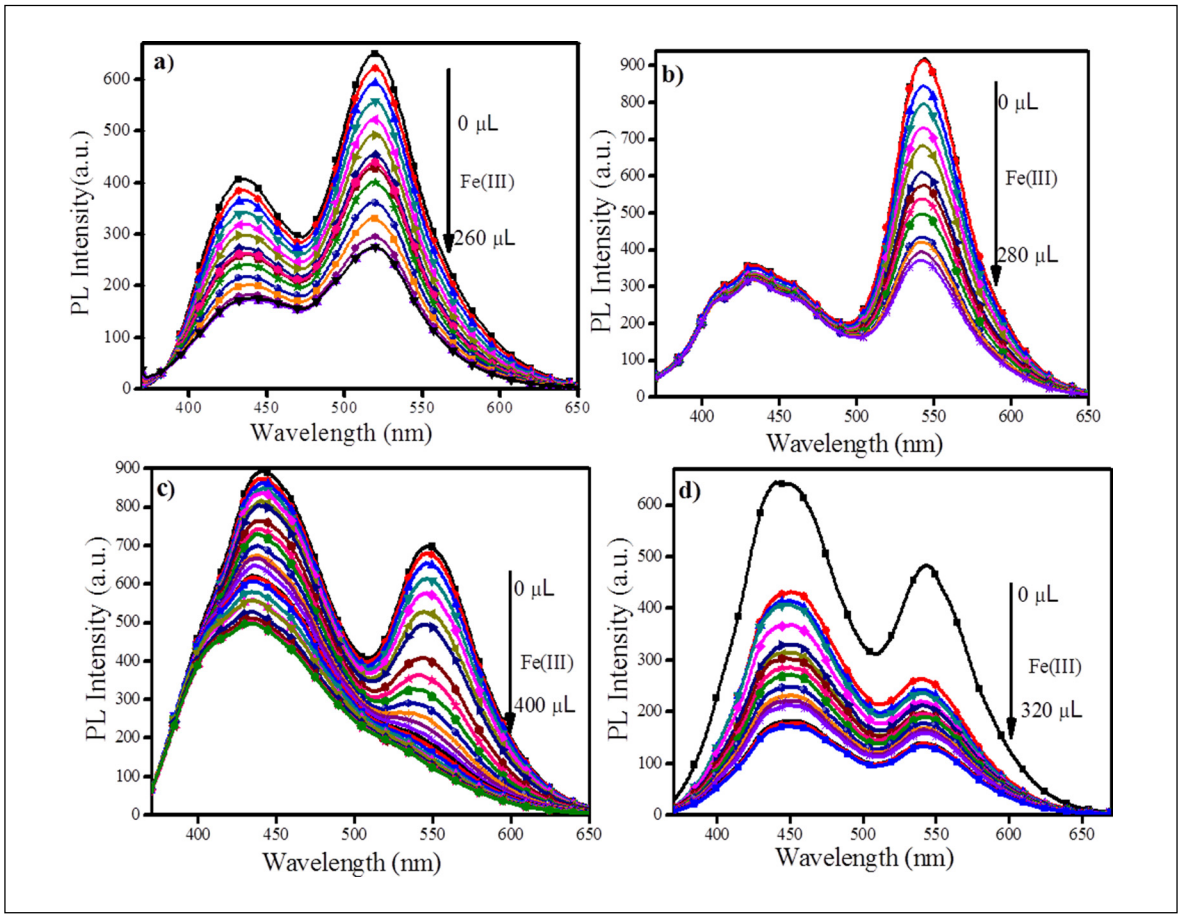

Fig. 5. Interaction studies of dual emissive CDs with Fe(III) ions dispersed in a) H_2O, b) CCl_4, c) $CHCl_3$ and d) CH_2Cl_2 medium.

Table 2
Comparison studies with different sensing probe for Fe(III) ions detection (in aqueous medium).

S. no.	Sensing probe for Fe(III)	LOD (μM)	Ref.
1.	Graphene quantum dots	0.09	[76]
2.	Banana derived CDs	0.21	[79]
3.	DL malic acid derived CDs	0.8	[80]
4.	N, S co-doped CDs	0.017	[81]
5.	Mint leaves derived CDs	0.37	[82]
5.	Acid mediated dual emissive CDs	0.4	This work

Table 3
Solvatochromic sensing efficiency of dual emissive CDs in the real sample.

S. no.	Solvatochromic sensing system	The concentration of Fe(III) ions (μM)		Recovery (%)
		Added	Determined ± SD	
1	CDs + CCl_4	20	19.60 ± 0.23	98.0
		20	19.93 ± 0.25	99.6
		20	19.89 ± 0.27	99.4
2	CDs + $CHCl_3$	20	20.10 ± 0.39	100.5
		20	20.12 ± 0.37	100.6
		20	20.01 ± 0.42	100.0
3	CDs + CH_2Cl_2	20	19.85 ± 0.29	99.2
		20	19.70 ± 0.31	98.5
		20	19.95 ± 0.33	99.7
5	CDs + H_2O	20	19.90 ± 0.31	99.5
		20	19.90 ± 0.31	99.7
		20	19.80 ± 0.27	99.0

followed up by mixed-acid based reaction with sucrose to obtain dual emissive CDs. Discussion of its synthetic mechanism was also stated in details, which indicates that acids play a vital role to induce dual emission behavior of CDs. The morphology and surface functionality of dual emissive CDs was confirmed by HRTEM, XPS, EDX and AT-IR techniques. Its optical properties were also analyzed in a variety of solvents, which showed emission dependent behavior as solvent medium plays vital role in modifying the molecular and surface states of CDs. The dual emissive CDs displayed unusual bathochromic shift in emission spectra in the presence of halogenated solvents. Therefore, metal ions sensing was explored in different solvent media. The experiments revealed that CDs have remarkable interaction with Fe(III) ions in comparison to other metal ions in different solvent media. This high selectivity and sensitivity were perceived due to the presence of vacant 3d-orbitals of Fe(III) and the electron-rich hetero-atoms/groups on the surface of dual emissive CDs. Overall, this accomplished work specifies that the empirical nature of solvents influence the emissive response of CDs. So, for effective sensing applications, it can be used as alternative nano-sensors.

Author contribution

S.B. and B.M jointly planned the research and supervised the work. S.K. and S.B. synthesized and characterized CDs. S.K. and B.M. optimized the reaction, solvatochromic study, and applications. All the authors jointly edited the manuscript.

Declaration of competing interest

The authors don't have any conflict of interest in the publication of

the manuscript.

Acknowledgements

The authors are thankful to CSIR (grant no: 01 (2955)/18/EMR-II) for financial help. The authors are also thankful to Centre for Nano and Soft Matter Sciences, Bengaluru for HRTEM analysis, and Dr. Vijay Luxami, SCBC, TIET for fluorescence lifetime facility and Sprint Testing Solutions-Mumbai for XPS facility.

Appendix A. Supplementary data

Supplementary data to this article can be found online at https://doi.org/10.1016/j.msec.2019.110443.

References

[1] S.Y. Lim, W. Shen, Z. Gao, Carbon quantum dots and their applications, Chem. Soc. Rev. 44 (2015) 362–381, https://doi.org/10.1039/c4cs00269e.
[2] Y. Dong, R. Wang, G. Li, C. Chen, Y. Chi, G. Chen, Polyamine-functionalized carbon quantum dots as fluorescent probes for selective and sensitive detection of copper ions, Anal. Chem. 84 (2012) 6220–6224, https://doi.org/10.1021/ac3012126.
[3] Q.-L. Zhao, Z.-L. Zhang, B.-H. Huang, J. Peng, M. Zhang, D.-W. Pang, Facile preparation of low cytotoxicity fluorescent carbon nanocrystals by electrooxidation of graphite, Chem. Commun. 0 (2008) 5116, https://doi.org/10.1039/b812420e.
[4] D. Pan, J. Zhang, Z. Li, C. Wu, X. Yan, M. Wu, Observation of pH-, solvent-, spin-, and excitation-dependent blue photoluminescence from carbon nanoparticles, Chem. Commun. 46 (2010) 3681–3683, https://doi.org/10.1039/c000114g.
[5] H. Liu, T. Ye, C. Mao, Fluorescent carbon nanoparticles derived from candle soot, Angew. Chem. Int. Ed. 46 (2007) 6473–6475, https://doi.org/10.1002/anie.200701271.
[6] Q. Wang, H. Zheng, Y. Long, L. Zhang, M. Gao, W. Bai, Microwave-hydrothermal synthesis of fluorescent carbon dots from graphite oxide, Carbon N. Y. 49 (2011) 3134–3140, https://doi.org/10.1016/j.carbon.2011.03.041.
[7] H. Li, X. He, Y. Liu, H. Huang, S. Lian, S.T. Lee, Z. Kang, One-step ultrasonic synthesis of water-soluble carbon nanoparticles with excellent photoluminescent properties, Carbon N. Y. 49 (2011) 605–609, https://doi.org/10.1016/j.carbon.2010.10.004.
[8] M. Lu, L. Zhou, One-step sonochemical synthesis of versatile nitrogen-doped carbon quantum dots for sensitive detection of Fe2+ ions and temperature in vitro, Mater. Sci. Eng. C 101 (2019) 352–359, https://doi.org/10.1016/J.MSEC.2019.03.109.
[9] J. Lu, P.S.E. Yeo, C.K. Gan, P. Wu, K.P. Loh, Transforming C-60 molecules into graphene quantum dots, Nat. Nanotechnol. 6 (2011) 247–252, https://doi.org/10.1038/nnano.2011.30.
[10] X. Xu, R. Ray, Y. Gu, H.J. Ploehn, L. Gearheart, K. Raker, W.A. Scrivens, Electrophoretic analysis and purification of fluorescent single-walled carbon nanotube fragments, J. Am. Chem. Soc. 126 (2004) 12736–12737, https://doi.org/10.1021/ja040082h.
[11] S. Yang, H. Zeng, H. Zhao, H. Zhang, W. Cai, Luminescent hollow carbon shells and fullerene-like carbon spheres produced by laser ablation with toluene, J. Mater. Chem. 21 (2011) 4432–4436, https://doi.org/10.1039/c0jm03475d.
[12] H. Jiang, F. Chen, M.G. Lagally, F.S. Denes, New strategy for synthesis and functionalization of carbon nanoparticles, Langmuir 26 (2010) 1991–1995, https://doi.org/10.1021/la9022163.
[13] Z.S. Qian, X.Y. Shan, L.J. Chai, J.R. Chen, H. Feng, A fluorescent nanosensor based on graphene quantum dots-aptamer probe and graphene oxide platform for detection of lead (II) ion, Biosens. Bioelectron. 68 (2015) 225–231, https://doi.org/10.1016/j.bios.2014.12.057.
[14] X. Cui, L. Zhu, J. Wu, Y. Hou, P. Wang, Z. Wang, M. Yang, A fluorescent biosensor based on carbon dots-labeled oligodeoxyribonucleotide and graphene oxide for mercury (II) detection, Biosens. Bioelectron. 63 (2015) 506–512, https://doi.org/10.1016/j.bios.2014.07.085.
[15] Z.B. Qu, X. Zhou, L. Gu, R. Lan, D. Sun, D. Yu, G. Shi, Boronic acid functionalized graphene quantum dots as a fluorescent probe for selective and sensitive glucose determination in microdialysate, Chem. Commun. 49 (2013) 9830–9832, https://doi.org/10.1039/c3cc44393k.
[16] H. Feng, Z. Qian, Functional carbon quantum dots: a versatile platform for chemosensing and biosensing, Chem. Rec. 18 (2018) 491–505, https://doi.org/10.1002/tcr.201700055.
[17] X. Gao, C. Du, Z. Zhuang, W. Chen, Carbon quantum dot-based nanoprobes for metal ion detection, J. Mater. Chem. C 4 (2016) 6927–6945, https://doi.org/10.1039/c6tc02055k.
[18] X. Gao, Y. Lu, R. Zhang, S. He, J. Ju, M. Liu, L. Li, W. Chen, One-pot synthesis of carbon nanodots for fluorescence turn-on detection of Ag+ based on the Ag+-induced enhancement of fluorescence, J. Mater. Chem. C 3 (2015) 2302–2309, https://doi.org/10.1039/c4tc02582b.
[19] R. Zhang, W. Chen, Nitrogen-doped carbon quantum dots: facile synthesis and application as a “turn-off” fluorescent probe for detection of Hg2+ ions, Biosens. Bioelectron. 55 (2014) 83–90, https://doi.org/10.1016/j.bios.2013.11.074.
[20] F. Zu, F. Yan, Z. Bai, J. Xu, Y. Wang, Y. Huang, X. Zhou, The quenching of the fluorescence of carbon dots: a review on mechanisms and applications, Microchim. Acta 184 (2017) 1899–1914, https://doi.org/10.1007/s00604-017-2318-9.
[21] F. Yan, Y. Jiang, X. Sun, Z. Bai, Y. Zhang, X. Zhou, Surface modification and chemical functionalization of carbon dots: a review, Microchim. Acta 185 (2018), https://doi.org/10.1007/s00604-018-2953-9.
[22] W. Kwon, J. Lim, J. Lee, T. Park, S.-W. Rhee, Sulfur-incorporated carbon quantum dots with a strong long-wavelength absorption band, J. Mater. Chem. C 1 (2013) 2002, https://doi.org/10.1039/c3tc00683b.
[23] H. Zheng, Q. Wang, Y. Long, H. Zhang, X. Huang, R. Zhu, Enhancing the luminescence of carbon dots with a reduction pathway, Chem. Commun. 47 (2011) 10650, , https://doi.org/10.1039/c1cc14741b.
[24] L. Pan, S. Sun, A. Zhang, K. Jiang, L. Zhang, C. Dong, Q. Huang, A. Wu, H. Lin, Truly fluorescent excitation-dependent carbon dots and their applications in multicolor cellular imaging and multidimensional sensing, Adv. Mater. 27 (2015) 7782–7787, https://doi.org/10.1002/adma.201503821.
[25] S.K. Kailasa, S. Ha, S.H. Baek, L.M.T. Phan, S. Kim, K. Kwak, T.J. Park, Tuning of carbon dots emission color for sensing of Fe3+ ion and bioimaging applications, Mater. Sci. Eng. C 98 (2019) 834–842, https://doi.org/10.1016/j.msec.2019.01.002.
[26] S. Li, J. Jiang, Y. Yan, P. Wang, G. Huang, N. hoon Kim, J.H. Lee, D. He, Red, green, and blue fluorescent folate-receptor-targeting carbon dots for cervical cancer cellular and tissue imaging, Mater. Sci. Eng. C 93 (2018) 1054–1063, https://doi.org/10.1016/J.MSEC.2018.08.058.
[27] H. Zhao, D. Gao, X. Liu, D. Jiang, Y. Zhu, X. Chen, H. Luo, H. Fan, X. Zhang, Exploring of multicolor emissive carbon dots with novel double emission mechanism, Sensors Actuators, B Chem. 277 (2018) 373–380, https://doi.org/10.1016/j.snb.2018.09.031.
[28] L. Bao, C. Liu, Z.-L. Zhang, D.-W. Pang, Photoluminescence-tunable carbon nanodots: surface-state energy-gap tuning, Adv. Mater. 27 (2015) 1663–1667, https://doi.org/10.1002/adma.201405070.
[29] H. Ding, S.-B. Yu, J.-S. Wei, H.-M. Xiong, Full-color light-emitting carbon dots with a surface-state-controlled luminescence mechanism, ACS Nano 10 (2016) 484–491, https://doi.org/10.1021/acsnano.5b05406.
[30] A. Mehta, A. Mishra, S. Kainth, S. Basu, Carbon quantum dots/TiO2 nanocomposite for sensing of toxic metals and photodetoxification of dyes with kill waste by waste concept, Mater. Des. 155 (2018) 485–493, https://doi.org/10.1016/j.matdes.2018.06.015.
[31] S. Kainth, A. Mehta, A. Mishra, S. Basu, Implementation of a logic gate by chemically induced nitrogen and oxygen rich C-dots for the selective detection of fluoride ions, New J. Chem. 42 (2018) 12162–12171, https://doi.org/10.1039/c8nj02041h.
[32] K. Jiang, S. Sun, L. Zhang, Y. Lu, A. Wu, C. Cai, H. Lin, Red, green, and blue luminescence by carbon dots: full-color emission tuning and multicolor cellular imaging, Angew. Chem. Int. Ed. 54 (2015) 5360–5363, https://doi.org/10.1002/anie.201501193.
[33] S. Zhu, J. Zhang, C. Qiao, S. Tang, Y. Li, W. Yuan, B. Li, L. Tian, F. Liu, R. Hu, H. Gao, H. Wei, H. Zhang, H. Sun, B. Yang, Strongly green-photoluminescent graphene quantum dots for bioimaging applications, Chem. Commun. 47 (2011) 6858, https://doi.org/10.1039/c1cc11122a.
[34] S.C. Ray, A. Saha, N.R. Jana, R. Sarkar, Fluorescent carbon nanoparticles: synthesis, characterization, and bioimaging application, J. Phys. Chem. C 113 (2009) 18546–18551, https://doi.org/10.1021/jp905912n.
[35] S.S. Wee, Y.H. Ng, S.M. Ng, Synthesis of fluorescent carbon dots via simple acid hydrolysis of bovine serum albumin and its potential as sensitive sensing probe for lead (II) ions, Talanta 116 (2013) 71–76, https://doi.org/10.1016/J.TALANTA.2013.04.081.
[36] S.F. Chin, S.N.A.M. Yazid, S.C. Pang, S.M. Ng, Facile synthesis of fluorescent carbon nanodots from starch nanoparticles, Mater. Lett. 85 (2012) 50–52, https://doi.org/10.1016/J.MATLET.2012.06.082.
[37] S.K. Bhunia, A. Saha, A.R. Maity, S.C. Ray, N.R. Jana, Carbon nanoparticle-based fluorescent bioimaging probes, Sci. Rep. 3 (2013) 1473, https://doi.org/10.1038/srep01473.
[38] Z.-Q. Xu, L.-Y. Yang, X.-Y. Fan, J.-C. Jin, J. Mei, W. Peng, F.-L. Jiang, Q. Xiao, Y. Liu, Low temperature synthesis of highly stable phosphate functionalized two color carbon nanodots and their application in cell imaging, Carbon N. Y. 66 (2014) 351–360, https://doi.org/10.1016/j.carbon.2013.09.010.
[39] Y. Dong, H. Pang, H. Bin Yang, C. Guo, J. Shao, Y. Chi, C.M. Li, T. Yu, Carbon-based dots co-doped with nitrogen and sulfur for high quantum yield and excitation-independent emission, Angew. Chem. Int. Ed. 52 (2013) 7800–7804, https://doi.org/10.1002/anie.201301114.
[40] A. Sciortino, E. Marino, B. van Dam, P. Schall, M. Cannas, F. Messina, Solvatochromism unravels the emission mechanism of carbon nanodots, J. Phys. Chem. Lett. 7 (2016) 3419–3423, https://doi.org/10.1021/acs.jpclett.6b01590.
[41] C.J. Reckmeier, Y. Wang, R. Zboril, A.L. Rogach, Influence of doping and temperature on solvatochromic shifts in optical spectra of carbon dots, J. Phys. Chem. C 120 (2016) 10591–10604, https://doi.org/10.1021/acs.jpcc.5b12294.
[42] G.A. Crosby, J.N. Demas, Measurement of photoluminescence quantum yields. Review, J. Phys. Chem. 75 (1971) 991–1024, https://doi.org/10.1021/j100678a001.
[43] A.M. Puziy, O.I. Poddubnaya, A. Martínez-Alonso, F. Suárez-García, J.M.D. Tascón, Synthetic carbons activated with phosphoric - acid I. Surface chemistry and ion binding properties, Carbon N. Y. 40 (2002) 1493–1505, https://doi.org/10.1016/S0008-6223(01)00317-7.
[44] A.M. Puziy, O.I. Poddubnaya, B. Gawdzik, M. Sobiesiak, M.M. Tsyba, Phosphoric acid activation—functionalization and porosity modification, Appl. Surf. Sci. 253 (2007) 5736–5740, https://doi.org/10.1016/J.APSUSC.2006.12.034.
[45] A.M. Puziy, O.I. Poddubnaya, A.M. Ziatdinov, On the chemical structure of

phosphorus compounds in phosphoric acid-activated carbon, Appl. Surf. Sci. 252 (2006) 8036–8038, https://doi.org/10.1016/j.apsusc.2005.10.044.
[46] A.M. Puziy, O.I. Poddubnaya, A. Martínez-Alonso, F. Suárez-García, J.M.D. Tascón, Surface chemistry of phosphorus-containing carbons of lignocellulosic origin, Carbon N. Y. 43 (2005) 2857–2868, https://doi.org/10.1016/J.CARBON.2005.06.014.
[47] Y. Hu, J. Yang, J. Tian, L. Jia, J.S. Yu, Waste frying oil as a precursor for one-step synthesis of sulfur-doped carbon dots with pH-sensitive photoluminescence, Carbon N. Y. 77 (2014) 775–782, https://doi.org/10.1016/j.carbon.2014.05.081.
[48] M.M.F. Chang, I.R. Ginjom, M. Ngu-Schwemlein, S.M. Ng, Synthesis of yellow fluorescent carbon dots and their application to the determination of chromium(III) with selectivity improved by pH tuning, Microchim. Acta 183 (2016) 1899–1907, https://doi.org/10.1007/s00604-016-1819-2.
[49] E. Loi, R.W.C. Ng, M.M.F. Chang, J.F.Y. Fong, Y.H. Ng, S.M. Ng, One-pot synthesis of carbon dots using two different acids and their respective unique photo-luminescence property, Luminescence 32 (2017) 114–118, https://doi.org/10.1002/bio.3157.
[50] J. Ryu, Y.W. Suh, D.J. Suh, D.J. Ahn, Hydrothermal preparation of carbon micro-spheres from mono-saccharides and phenolic compounds, Carbon N. Y. 48 (2010) 1990–1998, https://doi.org/10.1016/j.carbon.2010.02.006.
[51] W. Kwon, S. Do, S.-W. Rhee, Formation of highly luminescent nearly monodisperse carbon quantum dots via emulsion-templated carbonization of carbohydrates, RSC Adv. 2 (2012) 11223, , https://doi.org/10.1039/c2ra22186a.
[52] T. Sakaki, M. Shibata, T. Miki, H. Hirosue, N. Hayashi, Reaction model of cellulose decomposition in near-critical water and fermentation of products, Bioresour. Technol. 58 (1996) 197–202, https://doi.org/10.1016/S0960-8524(96)00099-5.
[53] B. Chen, F. Li, S. Li, W. Weng, H. Guo, T. Guo, X. Zhang, Y. Chen, T. Huang, X. Hong, S. You, Y. Lin, K. Zeng, S. Chen, Large scale synthesis of photoluminescent carbon nanodots and their application for bioimaging, Nanoscale 5 (2013) 1967–1971, https://doi.org/10.1039/c2nr32675b.
[54] H. Li, H. Ming, Y. Liu, H. Yu, X. He, H. Huang, K. Pan, Z. Kang, S.-T. Lee, Fluorescent carbon nanoparticles: electrochemical synthesis and their pH sensitive photo-luminescence properties, New J. Chem. 35 (2011) 2666, https://doi.org/10.1039/c1nj20575g.
[55] Z. Luo, Y. Lu, L.A. Somers, A.T.C. Johnson, High yield preparation of macroscopic graphene oxide membranes, J. Am. Chem. Soc. 131 (2009) 898–899, https://doi.org/10.1021/ja807934n.
[56] Z. Zhang, J. Zhang, N. Chen, L. Qu, Graphene quantum dots: an emerging material for energy-related applications and beyond, Energy Environ. Sci. 5 (2012) 8869, https://doi.org/10.1039/c2ee22982j.
[57] X. Li, S. Zhang, S.A. Kulinich, Y. Liu, H. Zeng, Engineering surface states of carbon dots to achieve controllable luminescence for solid-luminescent composites and sensitive Be2+ detection, Sci. Rep. 4 (2015) 4976, https://doi.org/10.1038/srep04976.
[58] C. Zhao, X. Li, C. Cheng, Y. Yang, Green and microwave-assisted synthesis of carbon dots and application for visual detection of cobalt (II) ions and pH sensing, Microchem. J. 147 (2019) 183–190, https://doi.org/10.1016/j.microc.2019.03.029.
[59] Y. Jeong, K. Moon, S. Jeong, W.G. Koh, K. Lee, Converting waste papers to fluor-escent carbon dots in the recycling process without loss of ionic liquids and bioi-maging applications, ACS Sustain. Chem. Eng. 6 (2018) 4510–4515, https://doi.org/10.1021/acssuschemeng.8b00353.
[60] Y. Chen, Y. Wu, B. Weng, B. Wang, C. Li, Facile synthesis of nitrogen and sulfur co-doped carbon dots and application for Fe(III) ions detection and cell imaging, Sensors Actuators B Chem. 223 (2016) 689–696, https://doi.org/10.1016/j.snb.2015.09.081.
[61] J. Li, S. Ma, X. Xiao, D. Zhao, The one-step preparation of green-emissioned carbon dots through hydrothermal route and its application, J. Nanomater. 2019 (2019) 1–10, https://doi.org/10.1155/2019/8628354.
[62] B. Shi, Y. Su, L. Zhang, M. Huang, R. Liu, S. Zhao, Nitrogen and phosphorus co-doped carbon nanodots as a novel fluorescent probe for highly sensitive detection of Fe3+ in human serum and living cells, ACS Appl. Mater. Interfaces 8 (2016) 10717–10725, https://doi.org/10.1021/acsami.6b01325.
[63] H. Ding, J.S. Wei, H.M. Xiong, Nitrogen and sulfur co-doped carbon dots with strong blue luminescence, Nanoscale 6 (2014) 13817–13823, https://doi.org/10.1039/c4nr04267k.
[64] G. Yang, X. Wan, Y. Su, X. Zeng, J. Tang, Acidophilic S-doped carbon quantum dots derived from cellulose fibers and their fluorescence sensing performance for metal ions in an extremely strong acid environment, J. Mater. Chem. A 4 (2016) 12841–12849, https://doi.org/10.1039/c6ta05943k.
[65] Z.L. Wu, Z.X. Liu, Y.H. Yuan, Carbon dots: materials, synthesis, properties and approaches to long-wavelength and multicolor emission, J. Mater. Chem. B 5 (2017) 3794–3809, https://doi.org/10.1039/c7tb00363c.
[66] F. Yan, Z. Sun, H. Zhang, X. Sun, Y. Jiang, Z. Bai, The fluorescence mechanism of carbon dots, and methods for tuning their emission color: a review, Microchim. Acta 186 (2019) 583, https://doi.org/10.1007/s00604-019-3688-y.
[67] C. Reichardt, Solvatochromic dyes as solvent polarity indicators, Chem. Rev. 94 (1994) 2319–2358, https://doi.org/10.1021/cr00032a005.
[68] W. Song, W. Duan, Y. Liu, Z. Ye, Y. Chen, H. Chen, S. Qi, J. Wu, D. Liu, L. Xiao, C. Ren, X. Chen, Ratiometric detection of intracellular lysine and pH with one-pot synthesized dual emissive carbon dots, Anal. Chem. 89 (2017) 13626–13633, https://doi.org/10.1021/acs.analchem.7b04211.
[69] S. Qu, D. Zhou, D. Li, W. Ji, P. Jing, D. Han, L. Liu, H. Zeng, D. Shen, Toward efficient orange emissive carbon nanodots through conjugated sp 2-domain con-trolling and surface charges engineering, Adv. Mater. 28 (2016) 3516–3521, https://doi.org/10.1002/adma.201504891.
[70] S.S. Jones, P. Sahatiya, S. Badhulika, One step, high yield synthesis of amphiphilic carbon quantum dots derived from chia seeds: a solvatochromic study, New J. Chem. 41 (2017) 13130–13139, https://doi.org/10.1039/c7nj03513f.
[71] K. Yamaguchi, T. Murai, Y. Tsuchiya, Y. Miwa, S. Kutsumizu, T. Sasamori, N. Tokitoh, Pyridinium 5-aminothiazoles: specific photophysical properties and vapochromism in halogenated solvents, RSC Adv. 7 (2017) 18132–18135, https://doi.org/10.1039/C7RA01896G.
[72] N. Mataga, Y. Kaifu, M. Koizumi, Solvent effects upon fluorescence spectra and the dipole moments of excited molecules, Bull. Chem. Soc. Jpn. 29 (1956) 465–470, https://doi.org/10.1246/bcsj.29.465.
[73] M. Cigáň, J. Donovalová, V. Szöcs, J. Gašpar, K. Jakusová, A. Gáplovský, 7-(Dimethylamino)coumarin-3-carbaldehyde and its phenylsemicarbazone: TICT ex-cited state modulation, fluorescent H-aggregates, and preferential solvation, J. Phys. Chem. A 117 (2013) 4870–4883, https://doi.org/10.1021/jp402627a.
[74] A. Chatterjee, D. Seth, Photophysical properties of 7-(diethylamino)coumarin-3-carboxylic acid in the nanocage of cyclodextrins and in different solvents and sol-vent mixtures, Photochem. Photobiol. 89 (2013) 280–293, https://doi.org/10.1111/php.12000.
[75] Y. Ooyama, R. Asada, S. Inoue, K. Komaguchi, I. Imae, Y. Harima, Solvatochromism of novel donor–π–acceptor type pyridinium dyes in halogenated and non-halogenated solvents, New J. Chem. 33 (2009) 2311, https://doi.org/10.1039/b9nj00332k.
[76] J. Ju, W. Chen, Synthesis of highly fluorescent nitrogen-doped graphene quantum dots for sensitive, label-free detection of Fe (III) in aqueous media, Biosens. Bioelectron. 58 (2014) 219–225, https://doi.org/10.1016/j.bios.2014.02.061.
[77] A. Pramanik, S. Biswas, P. Kumbhakar, Solvatochromism in highly luminescent environmental friendly carbon quantum dots for sensing applications: conversion of bio-waste into bio-asset, Spectrochim. Acta A Mol. Biomol. Spectrosc. 191 (2018) 498–512, https://doi.org/10.1016/j.saa.2017.10.054.
[78] R.R. Anjana, J.S. Anjali Devi, M. Jayasree, R.S. Aparna, B. Aswathy, G.L. Praveen, G.M. Lekha, G. Sony, S, N-doped carbon dots as a fluorescent probe for bilirubin, Microchim. Acta 185 (2018), https://doi.org/10.1007/s00604-017-2574-8.
[79] R. Vikneswaran, S. Ramesh, R. Yahya, Green synthesized carbon nanodots as a fluorescent probe for selective and sensitive detection of iron (III) ions, Mater. Lett. 136 (2014) 179–182, https://doi.org/10.1016/j.matlet.2014.08.063.
[80] W. Lu, X. Gong, M. Nan, Y. Liu, S. Shuang, C. Dong, Comparative study for N and S doped carbon dots: synthesis, characterization and applications for Fe3+ probe and cellular imaging, Anal. Chim. Acta 898 (2015) 116–127, https://doi.org/10.1016/j.aca.2015.09.050.
[81] C. Bolm, J. Legros, J. Le Paih, L. Zani, Iron-catalyzed reactions in organic synthesis, Chem. Rev. 104 (2004) 6217–6254, https://doi.org/10.1021/cr040664h.
[82] V. Raveendran, A.R. Suresh Babu, N.K. Renuka, Mint leaf derived carbon dots for dual analyte detection of Fe (III) and ascorbic acid, RSC Adv. 9 (2019) 12070–12077, https://doi.org/10.1039/c9ra02120e.

NJC

PAPER

View Article Online
View Journal

Cite this: DOI: 10.1039/c8nj02041h

Implementation of a logic gate by chemically induced nitrogen and oxygen rich C-dots for the selective detection of fluoride ions†

Shagun Kainth, Akansha Mehta, Amit Mishra and Soumen Basu *

Received 28th April 2018,
Accepted 12th June 2018

DOI: 10.1039/c8nj02041h

rsc.li/njc

The widespread pollution of fluoride ions in the environment badly affects the ecological system due to their high toxicity, mobility and the difficulty of their degradation. So, there is a need to design an environmentally friendly, highly selective and sensitive probe for their detection. Here, we have used natural ingredients (*e.g.* mosambi peels (*Citrus limetta*), L-ascorbic acid and urea) and mild reaction conditions to synthesize oxygen and nitrogen-rich fluorescent C-dots, named as OC-dots and NC-dots, respectively. We have proposed a turn-off/-on strategy for the specific recognition and quantification of F^- ions. Initially, based on the fluorescence resonance energy transfer (FRET) mechanism, the selectivities of both types of C-dots were investigated towards ten different cations. Both types of C-dot were found to be selective for only Fe^{3+}. The sensitivity of the OC-dot/NC-dot–Fe^{3+} system was also evaluated for fluoride ion detection and it was found that the OC-dot–Fe^{3+} ion mixture was only selective for F^- ions. The detection limit of the nanoprobe was found to be 0.01 μM, lower than the fluoride toxicity level defined by the U.S. Environmental Protection Agency (>1.5 ppm). The efficiency of the nanoprobe was compared using inductively coupled plasma atomic emission spectroscopy on real samples. The C-dot sensors were operated as different logic gates at the molecular level. All of the experimental data indicated that this probe is green, economical, quick and selective and can be used for establishing chemical logic gates for the detection of F^-.

1. Introduction

Heavy metals and their counteranions and cations (*e.g.* arsenic, iron, copper, fluorides, nitrates, and phosphates) play useful roles in biological systems. However, due to industrial growth and human activities, their environmental presence has been increased beyond the permissible limit, which has led to a reduction in natural resources and a negative effect on human health. Among all the heavy metal countercations/anions, F^- ions (>1.5 mg L^{-1})[1,2] are considered to be one of the major pollutants of water.[1,3] When fluoride polluted water is used on crops, it results in several physiological changes in plants that affect their root, shoot and leaf elongation, which are not visible to the naked eye, but can affect food production. In addition, an excessive intake of fluoride in the human body can damage bones, teeth, and the kidneys,[2,4] and also inhibit IQ development in children.[5–7] Therefore, it is necessary to identify the areas affected by these contaminants, mainly in the form of F^- ions, and help to treat the groundwater in such areas.

Several analytical methods, *e.g.* potentiometric (using an ion selective electrode [ISE]),[3] gas chromatographic (GC),[8] colorimetric,[9] fluorometric, enzymatic, and proton activation analysis,[8] have been used by federal agencies and organizations, such as the Environmental Protection Agency (EPA) and the National Institute for Occupational Safety and Health (NIOSH), for the detection of F^- ions in the environment. However, not all of these techniques are suitable for use as they often require sophisticated instrumentation, expensive reagents, and cumbersome sample preparation, which increase the cost and analytical complexity of the sensing probe. The best alternative to overcome these problems is the use of nanosensors, as they can be used for the rapid, accurate, compact and portable determination of organic and inorganic moieties.

Several fluorescent nanomaterials are already known, such as semiconductor quantum dots (SQDs), and have been used to detect toxic ions, due to their high stability, high extinction coefficients, and high photoluminescence (PL) yields.[10–13] However, their applicability towards real samples is debatable due to their inherent toxicity.[12,13] Therefore, the newly emerging class of nano-carbons, *i.e.* C-dots,[14–16] can be used as an ideal

School of Chemistry and Biochemistry, Thapar Institute of Engineering & Technology, Patiala-147004, India. E-mail: soumen.basu@thapar.edu

† Electronic supplementary information (ESI) available: (i) The evaluation of the fluorescence intensity for the selectivity of OC-dots/NC-dots towards different metal cations, (ii) the Stern–Volmer plot of F_0/F *vs.* Quencher concentration (Fe^{3+} ions) and (iii) Fig. S3: the fluorescence intensity of the OC-dots upon the addition of different anions. See DOI: 10.1039/c8nj02041h

material to replace all of the conventional fluorescent probes, due to their high aqueous stability, high biocompatibility, and low toxicity. Due to their unique turn-on/turn-off PL properties in the presence of foreign moieties,[1,2,17,18] many scientists have fabricated C-dots and their composites for the detection of several toxins. Dong *et al.*[19] synthesized polyamine-functionalized C-dots for the selective and sensitive detection of copper ions (LOD = 6 nM). Xu *et al.*[20] detected food colouring dyes (tartrazine) using C-dots prepared from a green material (aloe) and their detection range was found to be between 0.25 and 32.50 μM. Mohapatra *et al.*[2] prepared a highly selective composite system using C-dots (as the fluorophore) and magnetically separable nickel ethylenediaminetetraacetic acid complex-bound silica-coated magnetite (as the fluoride receptor). The method used was based on the exchange reaction between C-dots and F^- ions, which influences the binding of fluoride to the magnetic receptor with a minimum detection limit of 0.06 μM. Furthermore, Lui *et al.*[1] and Basu *et al.*[5] prepared new improved C-dots/composites (*e.g.* zirconium-complex, tapioca, *etc.*) and used these towards real samples to check their applicability in determining fluoride ions in environmental matrices. However, in all of the abovementioned processes, the material preparation was tedious and the sensing principle was not explained, which is important for the understanding and design of sensing probes. All of the aforementioned studies showed that there is a need to develop simple materials, accompanied by a suitable explanation of their working mechanism. Different strategies were explored, such as supramolecular recognition,[21–23] hydrogen bonding,[22,24] and Lewis acid–base interactions,[22,25,26] to develop low cost, non-hazardous and portable fluorescent probes that can be used in resourced laboratories and in different environmental matrices.

Here, in this work, we have put emphasis on the green synthesis of C-dots from mosambi peels (*Citrus limetta*), as well as from non-toxic precursors (ascorbic acid/urea) under mild conditions and a turn-off/-on strategy was followed for the detection of fluoride ions. Moreover, OC-dots and NC-dots were implemented in different logic gates such as NOT, OR, and IMP to design improved nanoelectric devices. The sensing efficiency of the probe was also tested in real samples and further compared with inductively coupled plasma atomic emission spectroscopic (ICP-AES) results.

2. Experimental

2.1. Chemical and materials

Mosambi peels (*Citrus limetta*) were collected from a local fruit vendor. Other reagents, such as ascorbic acid, urea and dichloromethane, were purchased from Sigma-Aldrich. Double distilled water was used for the preparation of different C-dots and the stock solutions of metal ions.

2.2. Preparation of C-dots

Microwave and ultrasonic routes were used to prepare the C-dots from mosambi peels and citric acid/urea, respectively. First, washed mosambi peels were dried in an oven (100 °C) for 24 hours and carbonized at 220 °C for 2 hours in air. The resulting carbonized powdered material (2 g) was sonicated for 45 min to obtain a brown coloured suspension. To remove organic impurities, the suspension was washed 5 times with dichloromethane. Finally, the purified suspension was filtered using a 0.2 μm membrane to obtain a 2.28 mg mL^{-1} yellow suspension of C-dots. The C-dots synthesized using these waste mosambi peels were named OC-dots, where the 'O' represents an 'oxygen' enriched C-dot surface.

For the preparation of nitrogen-rich C-dots, 1 g of ascorbic acid and 3 g of urea were mixed in 15 mL of water and heated at 130 °C for 3 minutes in a microwave. The obtained mixture was allowed to cool down and was centrifuged at 9000 rpm for 10 min to eliminate suspended impurities and obtain pure C-dots (3.2 mg mL^{-1}). The C-dots synthesized using these reagents were named NC-dots, where 'N' represents a 'nitrogen' enriched C-dot surface.

2.3. Quantum yield measurement

The quantum yields (ϕ) of both the OC-dots and NC-dots were evaluated using quinine sulphate as a reference (from literature ϕ' = 0.54) dissolved in 0.1 M H_2SO_4 (refractive index $\eta' = 1.33$). The integrated PL intensities I', I and absorbency values A', A were calculated for the reference quinine sulphate and both types of C-dots dissolved in deionised water $(\eta' = 1.33)$.

$$\phi = \phi' \times (I/I') \times (A'/A) \times \left(\eta'^2 \Big/ \eta'^2\right)$$

2.4. Methodology for detecting cations/anions

Stock solution (10^{-3} M) of different metal ions were prepared using metal salts such as ferric nitrate, copper nitrate, nickel nitrate, lead nitrate, calcium nitrate, magnesium nitrate, and cadmium nitrate to study their interaction with different C-dots (OC-dots and NC-dots). Then, the aqueous metal ion solutions were mixed with C-dots (4000 μL), and after 10 min were used to study their PL quenching efficiency. Furthermore, to measure the PL recovery of different anions, (*e.g.* fluoride, chloride, phosphate, nitrate and sulphate), different amounts of aqueous anion solutions (1–10 μM) were added into a mixture of C-dots and Fe^{3+} ions (4000 μL + 750 μL).

2.5. Analysis of F^- ions in real samples

Tap and lake water samples were collected from different cities (Patiala, Ludhiana) in the Punjab, India to determine the sensitivity of the probe in real samples. Firstly, the water samples were filtered using a 0.22 μm syringe filter and the determination of heavy metals was done using ICP-AES. Then the tap/lake water was spiked with different concentrations (2–8 μM) of fluoride ions, to evaluate the sensing efficiency of the probe, which was assessed using ICP-AES.

2.6. Instrumentation

The morphology and composition of the prepared C-dots were characterized using high-resolution transmission electron

microscopy (HRTEM) operating at 200 kV. For HRTEM analysis, samples were prepared by drop casting 10 μL purified C-dots dispersions on a carbon-coated copper grid and allowing the excess solvent to evaporate. The fluorescence emission spectra were collected using a LS-55 spectrofluorophotometer (PerkinElmer). Charge distributions were determined using Microtrac dynamic light scattering (DLS) apparatus, Nanotrac. Elemental analysis was done using a CHN analyzer (Thermoscientific flash 2000). Attenuated total reflectance infrared spectroscopy (AT-IR) was recorded to determine the nature of the different functional groups on the surface of the two different types of C-dots using an Agilent Resolution Pro-carry 660.

3. Result and discussion

3.1. Characteristics of C-dots

The prepared OC-dots and NC-dots were characterized by HRTEM, AT-IR, CHN microanalysis and fluorescence spectroscopy. Firstly, the formation of OC-dots and NC-dots was confirmed from their yellow colour suspensions and blue/green fluorescence under a UV lamp. The stabilities of the OC-dots and NC-dots were also evaluated. It was found that upon the exposure of light for 30 minutes the PL intensity remained undisturbed for both the OC-dots (λ_{em} = 438 nm) and NC-dots (λ_{em} = 455 nm), as shown in Fig. 1a and b. Even at a high concentration of NaCl salt (0.1 M), there does not appear to be any effect on the stability of both types of C-dots, which confirms their reusability for the detection of fluoride ions (Fig. 1c). The quantum yields of both the OC-dots and NC-dots were found to be 34% and 15% investigated with respect to the reference, *i.e.* quinine sulphate. The HRTEM images show that both types of C-dots are partially monodispersed and spherical. The average diameters of the OC-dots and NC-dots were found to be 2 ± 0.5 nm and 4 ± 2 nm, respectively, which is shown in Fig. 2a and b. The AT-IR spectrum of the OC-dots exhibits absorption peaks at 3347 cm^{-1} (O–H stretching), 1638.5 cm^{-1} (O–H bending), 1744.5 cm^{-1}, 1638.5 cm^{-1} (C═O groups), and 1512 cm^{-1} (C═C stretching of aromatic compounds). The spectrum of the NC-dots features sharp bands between 1000 and 1500 cm^{-1} due to –CO, –CH, –CN, which confirmed the presence of different functional groups on the surface of the C-dots (Fig. 3a and b). CHN analysis was done to evaluate their elemental compositions. According to the percentage distribution of elements shown in Table 1, the NC-dots contain more nitrogen (30.4%) than the OC-dots (6%), which may be due to the use of a nitrogen-containing precursor used in the preparation of the NC-dots, *i.e.* urea.

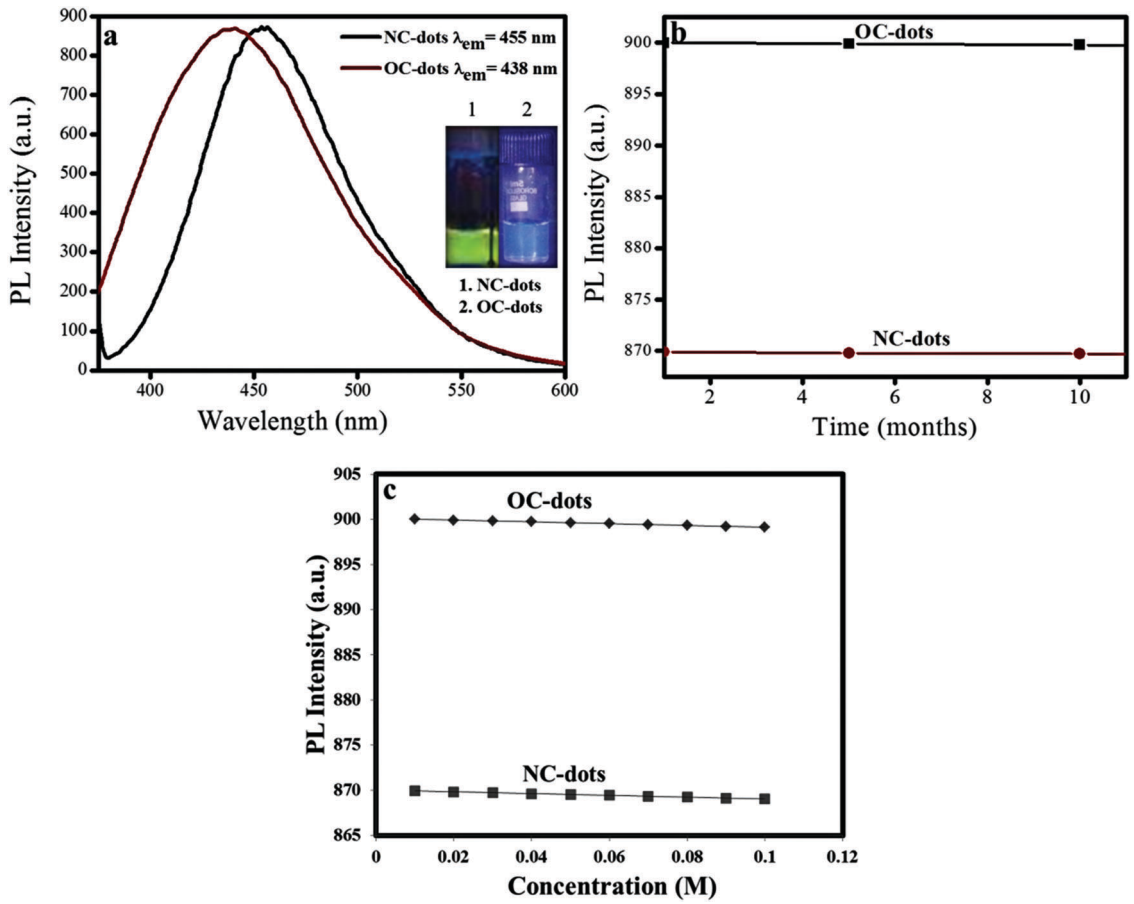

Fig. 1 Photoluminescence properties of C-dots. (a) The PL intensities of different surface passivated C-dots, (b) the effect of light on the PL intensity of the C-dots and (c) the effect of different concentrations of NaCl.

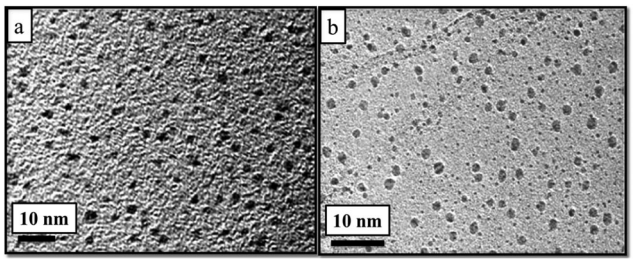

Fig. 2 HRTEM images of (a) OC-dots prepared from mosambi peels and (b) NC-dots prepared from ascorbic acid and urea.

3.2. Optimization of the reaction conditions for the detection of fluoride ions

The efficiency of the fluorescent probe depends on numerous parameters, such as pH, temperature, excitation wavelength and the slit width used in the fluorescence spectroscopic measurements. So, to enhance the sensitivity and selectivity of the sensing probe, there is a requirement to optimize the reaction conditions. Here, we have used different concentrations and slit widths to access the variation in the PL intensity. It was found that 4 mL of C-dots with both 5 and 10 nm slit widths exhibited the maximum PL intensity (Fig. 4a and b). The effect of pH on the PL intensity was also investigated for both types of C-dots (Fig. 4c and d). The results demonstrated that pH ~ 6 was suitable for performing PL quenching and recovery experiments, whereas highly acidic and basic conditions were found to be inappropriate due to the protonation of carboxylic groups and formation of $Fe(OH)_3$,[27,28] which result in a weaker interaction of the C-dots with Fe^{3+} ions and a reduction in their sensing efficiency.

3.3. Selectivity of the C-dots towards different cations

Selectivity is a crucial parameter for evaluating the performance of a chemosensor. So, the interactions of the two different types of C-dots were examined with different metal ions (*e.g.* Fe^{3+}, Cu^{2+}, Cd^{2+}, Zn^{2+}, Na^{+}, Ca^{2+}, Mg^{2+}, Pb^{2+}, Fe^{2+} and Ni^{2+}) by estimating the variation in their PL intensity. The experimental

Table 1 The elemental compositions of the OC-dots and NC-dots

Material	Carbon (%)	Hydrogen (%)	Oxygen (%)	Nitrogen (%)
OC-dots	52.8	20.8	20.4	6
NC-dots	48.3	15.2	10.8	30.4

results revealed that Fe^{3+} ions exhibited maximum fluorescence quenching for both types of C-dots (~94.8%) due to strong interactions with the carboxylic/amino/hydroxyl groups on the surfaces of the C-dots (Fig. 5). This quenching mechanism can be explained on the basis of the hard–soft acid–base (HSAB) principle, where Fe^{3+} acts as a hard acid[28] and the –COOH group acts as a hard base, which increases its affinity with respect to the other cations. As Cu^{2+} ions belong to the borderline metals, they also show PL quenching to some extent among all the other metal ions[29] (see Fig. S1 in ESI†). So, these two specific cations (Fe^{3+} and Cu^{2+}) were used to perform recovery experiments (turn-on) with fluoride ions.

With this aim, the sensitivities of the C-dots with different concentrations of ferric ions (0 to 0.4×10^{-5} M) were investigated, and the plot of F_0/F *vs.* quencher concentration was obtained using the Stern–Volmer equation, *i.e.*

$$F_0/F = 1 + K_{SV}[Q],$$

where F_0 and F are the fluorescence intensities of the fluorophore in the absence and presence of quencher Q, respectively, K_{SV} is the Stern–Volmer constant (M^{-1}) and [Q] is the concentration of the quencher. In order to determine whether the quenching was static or dynamic, the Stern–Volmer constant value was recorded at three different temperatures (25, 35 and 45 °C). There was no significant change found in the value of K_{SV} = 38.22, indicating that the quenching process was constant in nature, as shown in Fig. S2 (ESI†).

3.4. Turn-off/-on mechanism

The variations in the photoluminescence intensities and zeta potentials were studied with the aim of providing a foundation for elucidating the sensing mechanism of the probe. To determine the

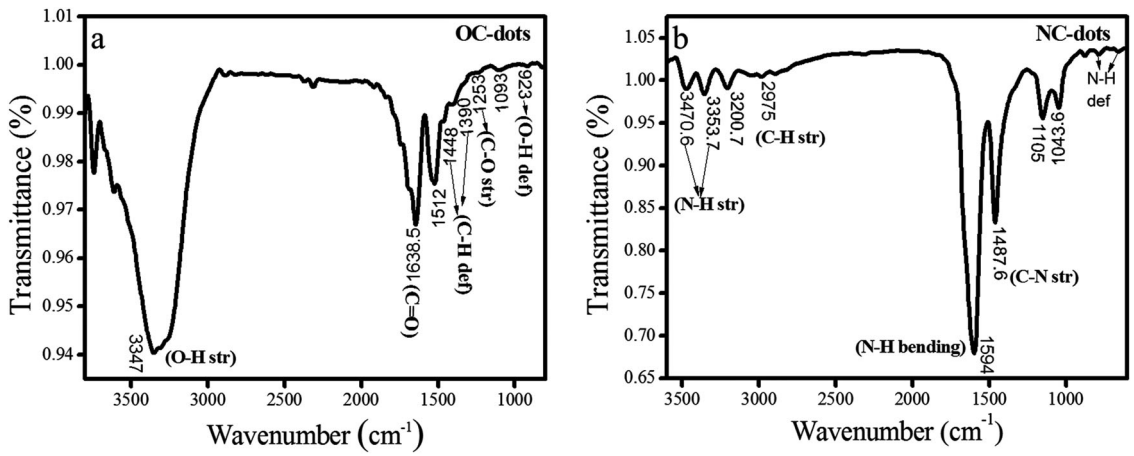

Fig. 3 AT-IR spectra of (a) OC-dots prepared from mosambi peels and (b) NC-dots prepared from ascorbic acid and urea.

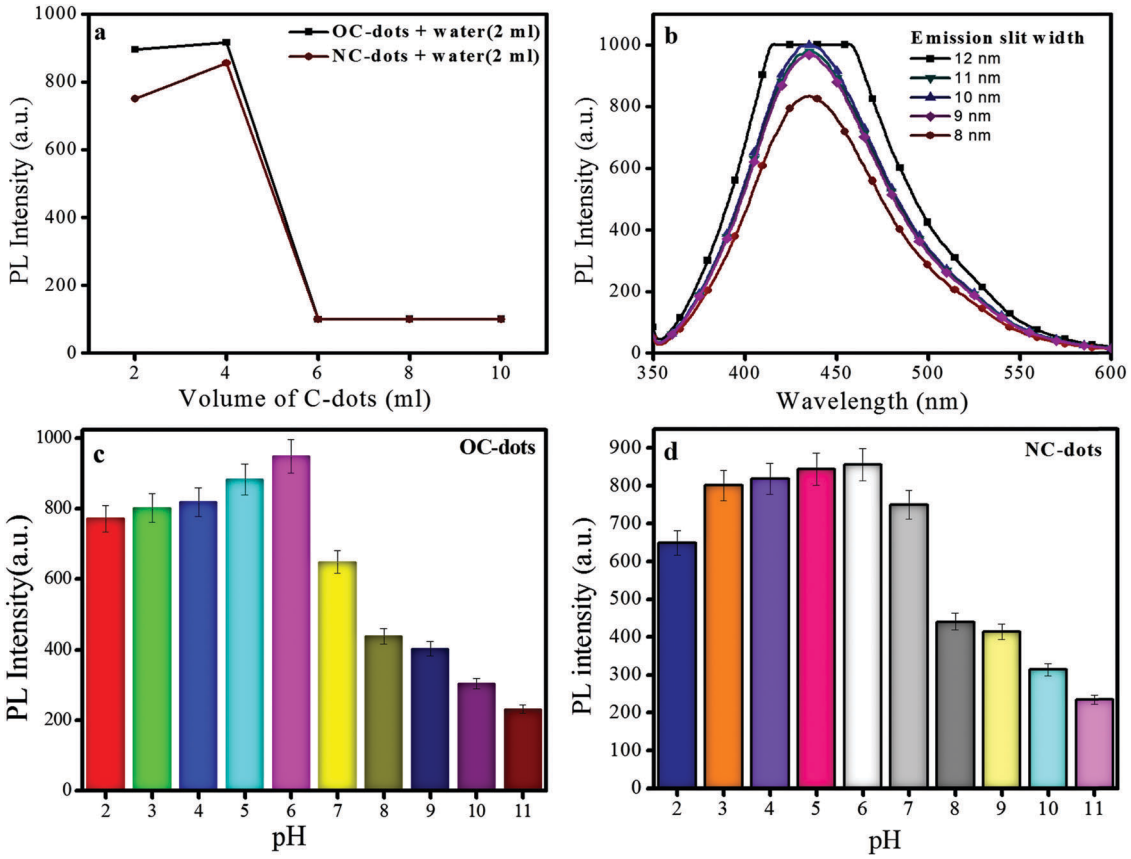

Fig. 4 Optimization of the experimental conditions: (a) the effect of different amounts of C-dots, (b) the effect of emission slit width at a constant excitation slit width, and (c and d) the effect of pH on the fluorescence intensity at λ_{ex} = 340 and 350 nm for the OC-dots and NC-dots, respectively.

initial sensing mechanism, the variations in the photoluminescence intensities were estimated for both types of C-dots and the ferric ion sensor system. It was found that in the presence of fluoride ions, the PL intensity was recovered only for the OC-dots, not for the NC-dots (Fig. 6). This is due to the stronger affinity of the free amino groups on the surface of the NC-dots with the ferric ions, which results in an inhibition of FeF_3 complex formation.[30] From the CHN analysis, it was clear that the surface of the NC-dots were nitrogen rich (amino groups), whereas the OC-dots were oxygen rich (carboxylic acid groups). So, the OC-dot and ferric ion mixture was found to be sensitive to fluoride ions, based on the HSAB rule that a hard acid (Fe^{3+}) and hard base (F^-) interact more, which leads to the formation of a stable FeF_3 ionic compound with a high lattice energy of 5870 kJ mol^{-1}, responsible for the fluorescence enhancement (as the OC-dots are free).[5] Furthermore, zeta potentials were recorded for both types of C-dots in the absence and presence of ferric and fluoride ions (Table 2). The results show that the presence of Fe^{3+} ions in the ratio of 4 : 0.75 leads to a reduction in the zeta potential values for the OC-dots (-30 ± 10 to -20 ± 2 mV) and NC-dots (-28 ± 5 to -10 ± 5 mV). This variation was due to the strong interaction of ferric ions with both types of C-dots, which reduces the inter-particle distance and leads to aggregation. This aggregation process was further confirmed by a red shift in the emission wavelength of the C-dots (438 nm to 445.8 nm for the OC-dots and 455 nm to 496.6 nm for the NC-dots), which is shown in Fig. 5. Hence, from the obtained results, it was clear that the fluorescence quenching of the C-dots in the presence of ferric ions was due to both aggregation, as well as an energy transfer process (Scheme 1). In addition, a recovery in the zeta potential values was also observed for the OC-dot/NC-dot and ferric ion system in the presence of fluoride ions (-20 ± 2 to -26 ± 1 mV for the OC-dots and -10 ± 5 to -15 ± 5 mV for the NC-dots). These results indicated that the OC-dot and ferric ion system was more sensitive toward fluoride ions and confirmed the aforementioned photoluminescence results[31] (Scheme 1).

3.5. Selectivity of ferric ions containing OC-dots towards F^- ions

To check the selectivity of the probe (OC-dots + ferric ions) towards fluoride ions, the fluorescence recovery of OC-dots at 438 nm was studied in the presence of F^- ions (1 μM) and other anions (20 μM), including phosphate, nitrate, sulphate and chloride ions. The results indicated that only fluoride ions showed a significant enhancement in the fluorescence intensity at 438 nm. However, the larger size of the anions did not result in any obvious change in the fluorescence intensity due to less compatibility with the Fe^{3+} ions in the formation of ionic compounds, as shown in Fig. S3 (ESI†). So, this sensing probe

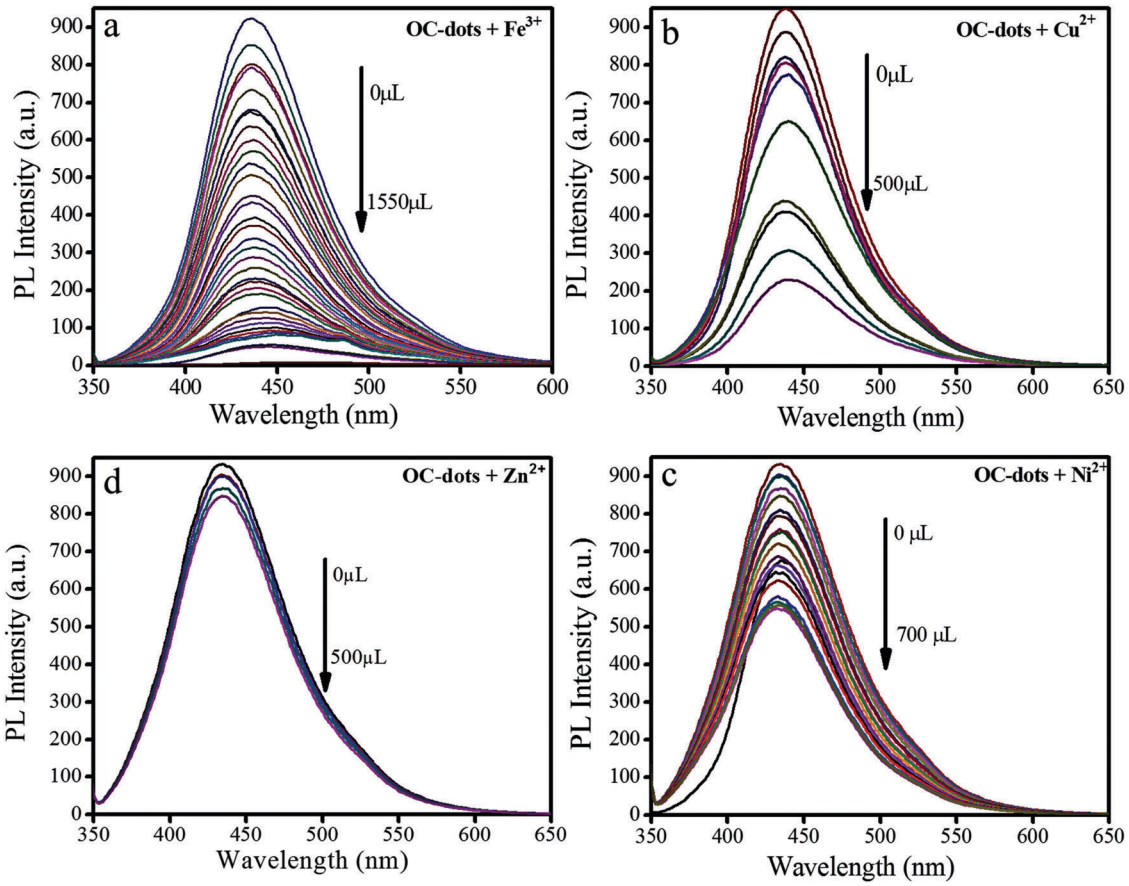

Fig. 5 Fluorescence quenching spectra of the OC-dots in the presence of different ions.

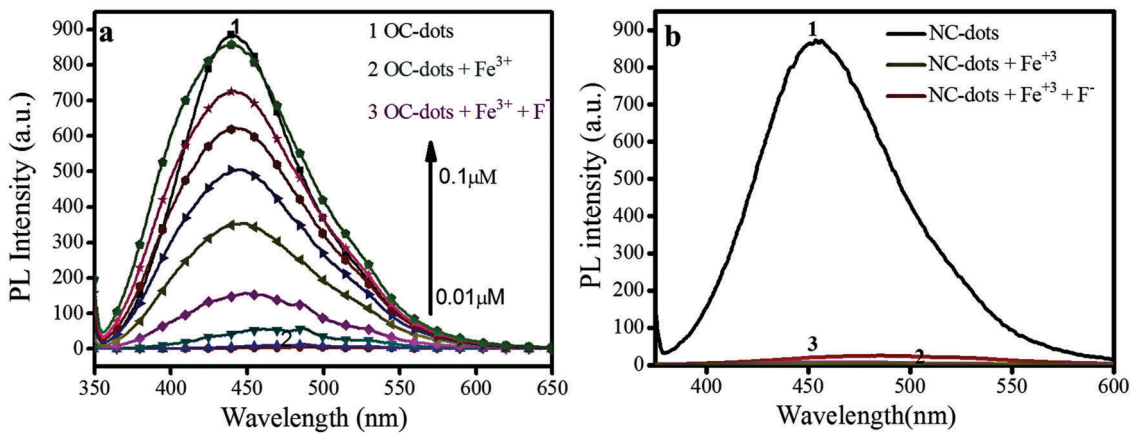

Fig. 6 Sensitivity of (a) the OC-dots and (b) the NC-dots towards F^- ions in the presence of Fe^{3+} ions.

can be used for the selective and quantitative analysis of fluoride ions.

3.6. Quantification of fluoride ions using the OC-dots and ferric ion system

To evaluate the stoichiometric response of the probe towards fluoride ions, the reaction kinetics were measured between a mixture of OC-dots/Fe^{3+} and F^- ions (Fig. 7a). It was found that the fluorescence intensity increased with the reaction time. The whole process reached equilibrium in about 1 min, which confirmed the rapid interaction of the sensing probe with the F^- ions at room temperature. So, we selected 1 min as an incubation time and studied the effect of the concentration on the fluorescence recovery for the quantitative determination of F^- ions. It was found that upon an increase in the concentration of F^- ions (0 to 1000 μL), the fluorescence intensity was

Table 2 Zeta-potential of C-dots in the presence and absence of Fe^{3+} and F^-

Concentration ratio (C-dots : Fe^{3+})	Zeta-potential (mV)	Concentration ratio (C-dots : Fe^{3+} : F^-)	Zeta potential (mV)
OC-dots (1 : 0)	−30 ± 10	OC-dots (1 : 0 : 0)	−30 ± 10
NC-dots (1 : 0)	−28 ± 5	NC-dots (1 : 0 : 0)	−28 ± 5
OC-dots (4 : 0.75)	−20 ± 2	OC-dots (4 : 0.75 : 1)	−26 ± 1
NC-dots (4 : 0.75)	−10 ± 5	NC-dots (4 : 0.75 : 1)	−15 ± 5
OC-dots (1 : 1)	−22 ± 2	OC-dots (1 : 1 : 1)	−23 ± 2
NC-dots (1 : 1)	−12 ± 5	NC-dots (1 : 1 : 1)	−13 ± 3

gradually restored and finally reached a maximum (Fig. 7a). To calculate the detecting limit of the probe, the fluorescence enhancement, F/F_0, was plotted against the concentration (Fig. 7b). The equation of the linear fitted curve, $F/F_0 = -11.262 + 1596.8[F^-]$, helped to determine the detection limit, which was found to be 0.01 μM, with a regression coefficient of 0.9664, *i.e.* much lower than the previously reported results in the literature (Table 3).

After the completion of the sensing experiments, the performance of a few logic gate functions (*e.g.* NOT, AND, IMP and OR) were determined on the basis of the interaction between the metal ions (Fe^{3+}) and anions (F^-) and C-dots. To execute the logic gates, the addition of metal ions (Fe^{3+}), and anions (F^-) in C-dots were used as the two inputs, whereas the variation in the fluorescence intensity was used as an output signal for which four possible input combinations (0, 0; 1, 0; 0, 1; 1, 1) were used. The absence and association of these ionic inputs in terms of the C-dots were defined as the 0 and 1 states, respectively. The outputs defined as 1 and 0 correspond to strong and weak fluorescence response. The NOT logic gate was used to study the variation in the fluorescence intensity of the

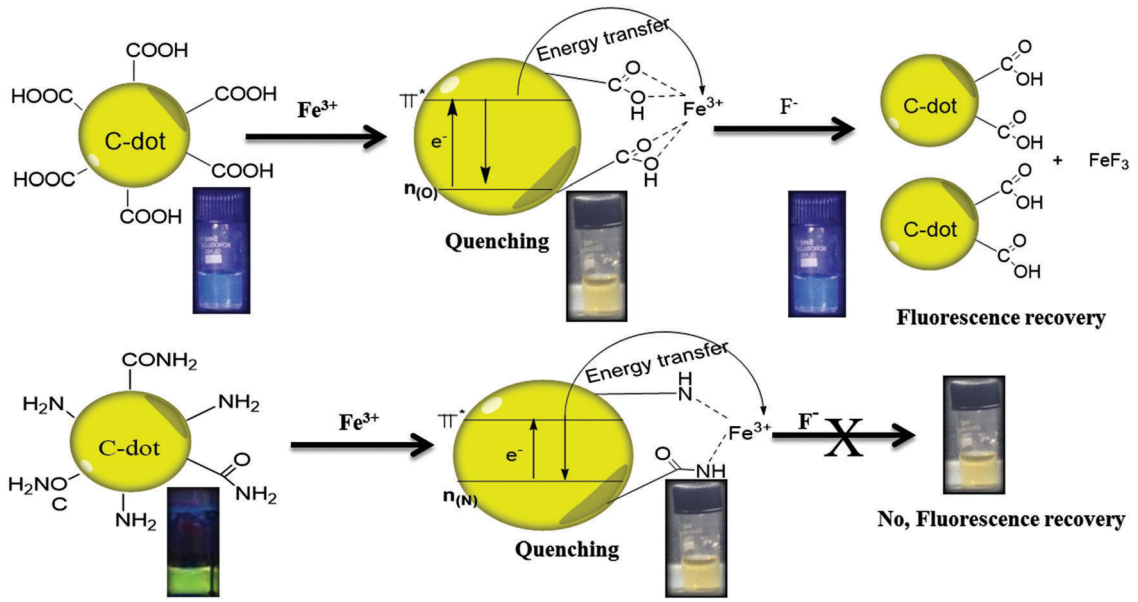

Scheme 1 Representation of the sensing mechanism of OC-dots and NC-dots for fluoride ion determination.

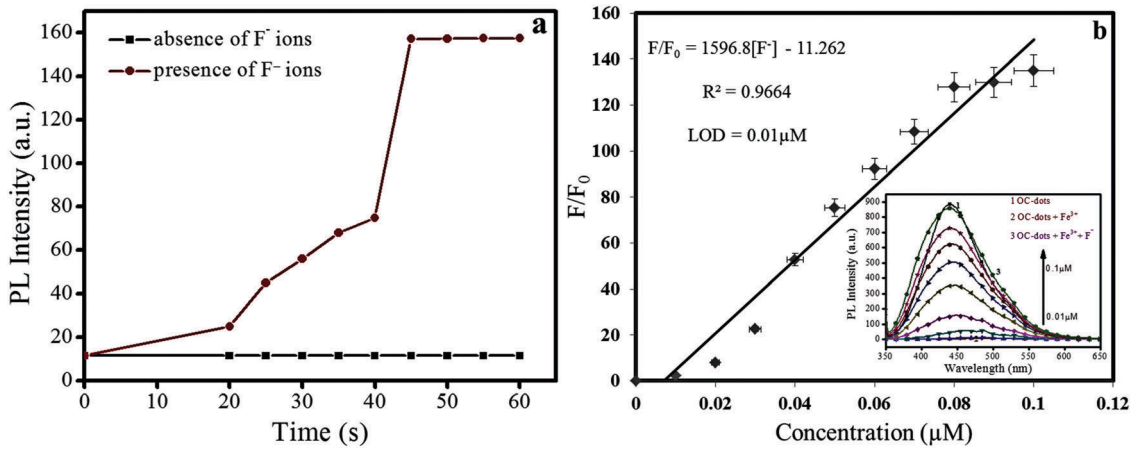

Fig. 7 (a) Effect of time on the emission spectra of the OC-dots–Fe^{3+} ion mixture in the absence and presence of fluoride ions and (b) the plot of the PL intensity variation at λ_{em} = 340 nm as a function of the concentration of F^- ions for the quantitative determination of F^- ions.

Table 3 Comparison of different sensing probes for the detection of F^- ions based on the LOD

Technique	Material/apparatus	LOD (μM)	Ref.
Spectrophotometer	Single beam spectrophotometer	2.38	32
HPLC	UV	0.47	33
Ion chromatography	ICP-MS	2.38	34
Flow injection analysis	Spectrofluorimeter	0.47	35
Based on the release of AuNP agglomerated dithiol linkers in the presence of inorganic fluoride ions	Fluoride colorimetric chemosensor gold nanoparticles (AuNP)	120	36
Interaction of L with F^- and AcO^- results in enhanced ICT, leading to a prominent colour change from yellow to orange-brown	Colorimetric and ratiometric chemosensor for the detection of F^- and AcO^- ions/quinoline	0.067	37
Ratiometric fluorescence detection of fluoride ions	Lanthanide metal–organic framework	2	38
Turn on/off fluorescence	Carbon-dots from mosambi peel	0.01	This work

C-dots with Fe^{3+} ions as an input signal. The addition of ferric ions quenched the fluorescence intensity of the C-dots, resulting in an output of 0 (low). These results correlate with the function of the NOT logic gate.

Furthermore, we constructed a modified IMP logic gate in the presence of Fe^{3+} (fixed concentration) and F^- (varying concentration) as inputs 1 and 2 to the OC-dots. Primarily, individual inputs were used to examine their influence on the C-dots and their corresponding output fluorescence intensity signal. The fluorescence intensity of the OC-dots was quenched only in the presence of ferric ions, whereas no effect was observed upon the addition of fluoride ions. Remarkably, in the presence of both inputs, the fluorescence intensity of the C-dots was recovered by the addition of F^- (low or high concentration), which was quenched upon the addition of Fe^{3+} ions. This abovementioned combination of the two inputs correlates with IMP logic gate behaviour.[39,40]

Similarly, we constructed a combination of OR, AND, NOT logic gates in the presence of Fe^{3+} (fixed concentration) and F^- (varying concentration) as inputs 1 and 2 to the NC-dots. Primarily, individual inputs were used to examine their influence on the C-dots and their corresponding output fluorescence intensity signal. It was detected that the fluorescence intensity of the NC-dots was quenched in the presence of the individual input of Fe^{3+} and remained the same in the presence of a low or high concentration of F^-. Unexpectedly, in the presence of both inputs (1, 1), the fluorescence intensity of the NC-dots remained quenched due to the strong coordination of Fe^{3+} ions with amino groups on the surface of the NC-dots. These results reveal that different logic operations can be achieved by varying the concentration of the metal ions used as inputs (Fig. 8).

3.7. Method validation using real samples

To illustrate the practical applicability of our C-dot probes for the selective detection of F^- ions, a certain concentration of F^- was added into real samples of tap/lake water, and the real-time detection of F^- was carried out. The detailed results determined using our OC-dot based probe are shown in Table 4, which were also compared with the measured amount from ICP-AES. The results analyzed by both methods were very close and the % recoveries were in the satisfactory range. The recovery of F^- was almost 99.0% for the tap and lake water, suggesting that our OC-dot based probe was suitable for using to detect F^- in real water samples.

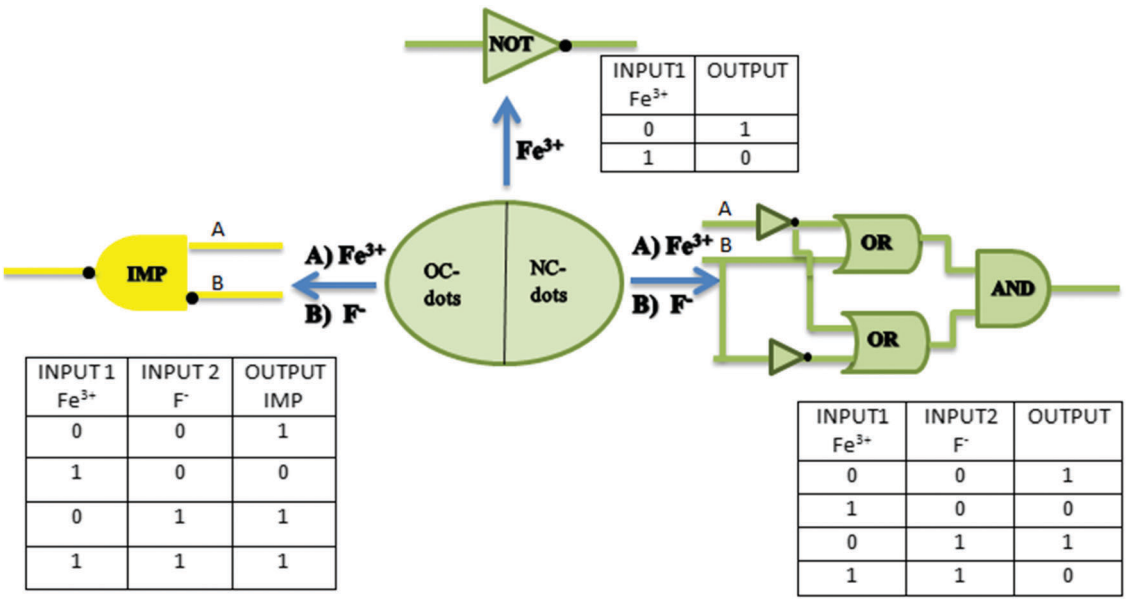

Fig. 8 Schematic representation of logic gates obtained for OC-dots/Fe^{3+}/F^- and NC-dots/Fe^{3+}/F^-.

Table 4 Detection of fluoride ions using the OC-dots probe and ICP-AES

Sample	Concentration of F^- ions (μM)	ICP-AES (μM)	OC-dots	Recovery (%)
Tap water	2	1.89	1.988 ± 0.023	99
	4	3.89	4.052 ± 0.012	96
	6	5.99	5.781 ± 0.035	96
	8	8.0	7.832 ± 0.038	98
Lake water	2	1.79	1.978 ± 0.013	90.4
	4	3.58	3.998 ± 0.012	89.7
	6	5.53	6.011 ± 0.025	91
	8	7.99	8.232 ± 0.038	97

4. Conclusion

In this paper, we have synthesized C-dot based chemosensors with different surface passivation using cheap precursors (citric acid, urea, and mosambi peel) under mild reaction conditions. Both the OC-dots and NC-dots were found to be partially monodispersed and spherical with an average diameter of 2–4 nm and showed good photostability. These fluorescent probes were used for the selective and sensitive determination of cations and anions, which was confirmed by determining the variation in their PL properties and zeta potentials. The sensing procedure involved two steps, first, the quenching of the PL intensities of the C-dots with Fe^{3+}, followed by PL intensity recovery by the addition of F^- ions. The results revealed that both types of C-dots showed good interaction with Fe^{3+} ions. However, the mixture of OC-dots and Fe^{3+} was found to be more sensitive than that of the NC-dots towards F^- ions, with a LOD of 0.01 μM. In view of these impressive results, we also developed different molecular logic gates, such as NOT, IMP, AND and OR, by using metal ions and anions as the chemical inputs for the practical application. Moreover, the sensing efficiency of one of the probes was investigated in real samples (lake and tap water) and compared with the ICP-AES results. Overall, these newly developed low-cost, ecological fluorescent nanoprobes have a good future in molecular electronic and nano-devices and are also beneficial for use in the real-time detection of fluoride ions.

Conflicts of interest

The authors declare that there is no conflict of interests regarding the publication of this manuscript.

Acknowledgements

The authors are thankful to DST (Grant No: SB/FT/CS-178/2013), New Delhi and BRNS (Grant No: 34/14/63/2014) for financial and instrumental (microwave and BET) support. We are also thankful to Dr Banibrata Maity, SCBC, TIET for suggestions and discussions.

References

1 J.-M. Liu, L.-P. Lin, X.-X. Wang, L. Jiao, M.-L. Cui, S.-L. Jiang, W.-L. Cai, L.-H. Zhang and Z.-Y. Zheng, *Analyst*, 2013, **138**, 278–283.
2 S. Mohapatra, S. Sahu, S. Nayak and S. K. Ghosh, *Langmuir*, 2015, **31**, 8111–8120.
3 R. Chavali, N. S. K. Gunda, S. Naicker and S. K. Mitra, *Anal. Chem. Res.*, 2015, **6**, 26–31.
4 X. Zheng, W. Zhu, D. Liu, H. Ai, Y. Huang and Z. Lu, *ACS Appl. Mater. Interfaces*, 2014, **6**, 7996–8000.
5 A. Basu, A. Suryawanshi, B. Kumawat, A. Dandia, D. Guin and S. B. Ogale, *Analyst*, 2015, **140**, 1837–1841.
6 M. Cametti and K. Rissanen, *Chem. Soc. Rev.*, 2013, **42**, 2016–2038.
7 A. Roy, A. Datar, D. Kand, T. Saha and P. Talukdar, *Org. Biomol. Chem.*, 2014, **12**, 2143–2149.
8 H. Yahyavi, M. Kaykhaii and M. Mirmoghaddam, *Crit. Rev. Anal. Chem.*, 2016, **46**, 106–121.
9 S. Yamaguchi, S. Akiyama and K. Tamao, *J. Am. Chem. Soc.*, 2001, **123**, 11372–11375.
10 M. O. Dekaliuk, O. Viagin, Y. V. Malyukin and A. P. Demchenko, *Phys. Chem. Chem. Phys.*, 2014, **16**, 16075–16084.
11 A. P. Demchenko and M. O. Dekaliuk, *Nanoscale*, 2016, **8**, 14057–14069.
12 Y. Lou, Y. Zhao and J.-J. Zhu, *Nanoscale Horiz.*, 2016, **1**, 125–134.
13 P. Singh, A. A. Prabhune, C. S. P. Tripathi and D. Guin, *ACS Sustainable Chem. Eng.*, 2017, **5**, 982–987.
14 N. Dhenadhayalan, K. C. Lin, R. Suresh and P. Ramamurthy, *J. Phys. Chem. C*, 2016, **120**, 1252–1261.
15 Y. Wang and A. Hu, *J. Mater. Chem. C*, 2014, **2**, 6921–6939.
16 Y. P. Sun, B. Zhou, Y. Lin, W. Wang, K. A. S. Fernando, P. Pathak, M. J. Meziani, B. A. Harruff, X. Wang, H. Wang, P. G. Luo, H. Yang, M. E. Kose, B. Chen, L. M. Veca and S. Y. Xie, *J. Am. Chem. Soc.*, 2006, **128**, 7756–7757.
17 D. Garg, A. Mehta, A. Mishra and S. Basu, *Spectrochim. Acta, Part A*, 2018, **192**, 411–419.
18 A. Mehta, P. D. A. Thakur and S. Basu, *New J. Chem.*, 2017, **41**, 4573–4581.
19 Y. Dong, R. Wang, G. Li, C. Chen, Y. Chi and G. Chen, *Anal. Chem.*, 2012, **84**, 6220–6224.
20 H. Xu, X. Yang, G. Li, C. Zhao and X. Liao, *J. Agric. Food Chem.*, 2015, **63**, 6707–6714.
21 F. P. Schmidtchen and M. Berger, *Chem. Rev.*, 1997, **97**, 1609–1646.
22 R. Martínez-Máñez and F. Sancenón, *Chem. Rev.*, 2003, **103**, 4419–4476.
23 S. O. Kang, J. M. Llinares, D. Powell, D. VanderVelde and K. Bowman-James, *J. Am. Chem. Soc.*, 2003, **125**, 10152–10153.
24 B. Sui, B. Kim, Y. Zhang, A. Frazer and K. D. Belfield, *ACS Appl. Mater. Interfaces*, 2013, **5**, 2920–2923.
25 T. W. Hudnall, Y. M. Kim, M. W. P. Bebbington, D. Bourissou and F. P. Gabbaï, *J. Am. Chem. Soc.*, 2008, **130**, 10890–10891.
26 X. Y. Liu, D. R. Bai and S. Wang, *Angew. Chem.*, 2006, **118**, 5601–5604.
27 H. Huang, Y. Xu, C.-J. Tang, J.-R. Chen, A.-J. Wang and J.-J. Feng, *New J. Chem.*, 2014, **38**, 784–789.
28 F. Yan, Y. Zou, M. Wang, X. Mu, N. Yang and L. Chen, *Sens. Actuators, B*, 2014, **192**, 488–495.

29 B. H. Irving and R. J. P. Williams, *J. Chem. Soc.*, 1953, 3192–3210.
30 L. Fang, Q. Xu, X. Zheng, W. Zhang, J. Zheng, M. Wu and W. Wu, *J. Nanopart. Res.*, 2016, **18**, 224.
31 P. Singhal, B. G. Vats, S. K. Jha and S. Neogy, *ACS Appl. Mater. Interfaces*, 2017, **9**, 20536–20544.
32 Z. Barghouthi and S. Amereih, *Int. J. Environ. Anal. Chem.*, 2013, **93**, 565–577.
33 J. Musijowski, B. Szostek, M. Koc and M. Trojanowicz, *J. Sep. Sci.*, 2010, **33**, 2636–2644.
34 M. Bayón Montes, A. Garcia Rodríguez, J. I. García Alonso and A. Sanz-Medel, *Analyst*, 1999, **124**, 27–31.
35 T. Takayanagi, H. Yamashita, S. Motomizu, J. Musijowski and M. Trojanowicz, *Talanta*, 2008, **74**, 1224–1230.
36 J. A. Gu, Y. J. Lin, Y. M. Chia, H. Y. Lin and S. T. Huang, *Microchim. Acta*, 2013, **180**, 801–806.
37 U. N. Yadav, P. Pant, D. Sharma, S. K. Sahoo and G. S. Shankarling, *Sens. Actuators, B*, 2014, **197**, 73–80.
38 Z. R. Yang, M. M. Wang, X. S. Wang and X. B. Yin, *Anal. Chem.*, 2017, **89**, 1930–1936.
39 J. H. Guo, D. M. Kong and H. X. Shen, *Biosens. Bioelectron.*, 2010, **26**, 327–332.
40 J. Zhu, L. Zhang, T. Li, S. Dong and E. Wang, *Adv. Mater.*, 2013, **25**, 2440–2444.

Plasmonics (2018) 13:1785–1793
https://doi.org/10.1007/s11468-018-0692-8

Quantitative Detection of Thiopurines by Inter-particle Distance-Dependent Properties of Gold Nanoparticles

Shagun Kainth[1] · Soumen Basu[1]

Received: 1 August 2017 / Accepted: 3 January 2018 / Published online: 21 January 2018

Abstract

As thiopurines are the source of chemotherapeutic drug which is helpful in treating acute lymphoblastic leukaemia, so the proper quantification of different purines is essential. As plasmonic nanoparticles (NPs) reported as colorimetric sensor due to their inter-particle variation in the presence of biomolecules. Here we have synthesised four different sizes (8–30 nm) gold nanoparticles (AuNPs) and chose as the analytical tool for the quantification of different purines. The characterisation of synthesised AuNPs was done by using FT-IR, TEM, DLS, EDS and UV-Vis spectroscopy. They showed remarkable stability for 10–15 days in the presence of long-range pH (3–12) and high concentration of the salt solution (100 μl, 0.1 M NaCl). Study of SPR variation was done for the quantification of purines. It has been seen that as the particle size, the concentration of purine and pH of the solution varies then SPR peak ~ 521 nm of AuNPs undergoes red shift and intensity of existing peak get reduced with time. The appearance of this new peak at ~ 700 nm justified the sensitivity of AuNPs towards purines. It was observed that the larger size AuNPs (30 nm) is more sensitive for detecting different purines at very low concentration (10^{-7} M for 6-thioguanine and 6-mercaptopurine).

Keywords Surface plasmon resonance · Gold nanoparticles · Aggregation · Thiopurines · Quantitative detection

Introduction

Purine is a heterocyclic aromatic compound found in high concentration in meat and meat products, especially internal organs such as liver and kidney. They are well-known in the body and perceived for primary two functions: (1) as building blocks for DNA (the primary genetic material in our cells) and (2) as substances that could be broken down to form a uric acid (which can potentially increase the risk of gout). The minimum intake of purine per day is in the range of 1430–1800 mg. Even in the field of pharmacy and biochemistry, thiopurines exclusively show diverse applications. Some purines such as 6-thioguanine (6-TG), 6-mercaptopurine (6-MP) and azathioprine are used as a prodrug for the treatment of acute leukaemias and chronic myeloid leukaemia [1]. 6-TG is widely used as a chemotherapeutic drug for treatment of advanced stages of leukaemia [2, 3]. 6–TG easily gets incorporated into the nucleic acid during synthesis and blocks further progression of the disease [4]. 6-TG is highly toxic and causes Thrombocytopenia, anaemia, anorexia, nausea and vomiting, hepato-toxicity, etc. [5, 6]. Therefore, it is very critical to maintain (2–3 mg/kg/day for both paediatric and adults) [7] of the drug in plasma level to avoid high toxicity maintaining efficiency. To reduce unwanted side effects of cancer chemotherapeutic drug and to improve life quality of the patients and keeping adequate effectiveness, maintenance of steady drug concentration in the system is important. For this reason, periodic estimation of drugs/drug metabolites concentrations in body fluid(s) like serum, plasma, urine, etc. is of immense importance. So, the proper and exact quantification of thiopurines in vegetables, pulses and drugs is required on urgent basis.

Several reported techniques have been accounted for the quantification of purines including voltammetry [8], fluorimetry [9], luminescence analysis [10], HPLC [11–14] and electrochemical strategy [15]. However, there are still a few points of confinement in these strategies. One critical point of confinement of HPLC and spectrometric techniques is that it lacks sufficient UV absorption and also

Electronic supplementary material The online version of this article (https://doi.org/10.1007/s11468-018-0692-8) contains supplementary material, which is available to authorized users.

✉ Soumen Basu
soumen.basu@thapar.edu

[1] School of Chemistry and Biochemistry, Thapar Institute of Engineering and Technology (Deemed University), Patiala 147004, India

Table 1 Details of different ratio of [$HAuCl_4$]/[citrate] and their colour variation

Sample name	Volume of $HAuCl_4$ 10^{-2} M (μl)	Volume of citrate (1%) (μl)	Colour	λ_{max} (nm)	Size of AuNPs from TEM images (± 3 nm)
A	1250	2000	Dark red	521	8
B	1250	875	Red	525	13
C	1250	625	Pink	530	20
D	1250	400	Light pink	535	30

need a suitable mobile phase and a reactant which obviously increased the cost and analytical complexity. Therefore, with the advancement of nanotechnology, other techniques have been developed such as surface plasmon resonance and electroanalytical methods to estimate the drug from the body fluid. But due to the requirement of sophisticated instrumentation, expensive reagents and cumbersome sample preparation, other available methodologies despite their good sensitivities have not become very popular. Thus, the development of a new technique with high sensitivity, fast, high throughput and simple practical method for the determination of purine is still in a great demand.

Plasmonic nanoparticles (NPs) such as Au, Ag and Cu etc. have optical properties which depend on their inter-particle distance and their SPR occur in the visible region and due to this reason, they have gained incredible attention as colorimetric/optical sensors [16]. AuNPs is attaining intense attention scientifically and technically as a source of optical nanoprobe, because of its stability in meteorological conditions which allow them to show excellent biocompatibility with biomolecules and distance-dependence optical absorbance [17–21]. They also exhibit different colours range from red to purple, to blue and almost black due to the variation in the inter-particle distance of AuNPs [22–24]. This unusual phenomenon gives rise to a new analytical and sensing technique which leads to the development of surface-enhanced Raman scattering and enhancement in surface plasmon resonance immune sensing effect [25, 26] because Au colloid monolayer can adsorb molecules in their closed space [27, 28]. The presence of negative surface charge helps them in improving their binding efficiency with several biomolecules such as selective detection of DNA templates [29], polynucleotides [30, 31], aminothiols and amino acid [17, 32]. Unfortunately, there is still some complications in surface charge adjustment via, e.g., change of pH and salt concentration which may lead to loss of charge-based repulsive forces and that may bring variation in the quantitative determination of important biological moieties. Till now, different shapes of AuNPs were already used for sensing of 6-TG, but still, some study is yet to make on sensitivity and the interaction of different size AuNPs towards purines. This method will be better or comparable in the case of sensitivity and will involve less sample preparation and high output than the available methods. This research may open up a new avenue introducing nanomaterials into practical applications.

Here we have synthesised four different sizes AuNPs ranging from 8 to 30 nm to investigate the impact of purines on the surface chemistry of AuNPs together with pH through colour change and SPR variation. The experimental result demonstrated the ability of this method and found to be quick, easy, effective and safe for quantitative detection of purines.

Experimental Section

Materials

AR-grade reagents were used for performing the experiment. Chloroauric acid ($HAuCl_4.3H_2O$) and trisodium citrate were purchased from Aldrich. 6-MP and 6-TG were received from the Tokyo Chemical Industry (TCI). Distilled water is used for the preparation of a stock solution of purines and different size AuNPs.

Preparation of Gold Nanoparticles

Size-controlled synthesis of AuNPs was done by modifying the Fren's method. One thousand two hundred and fifty microliters of 10^{-2} M $HAuCl_4$ was added in 50 ml distilled water and the solution was heated at 97 °C. Trisodium citrate (1%)

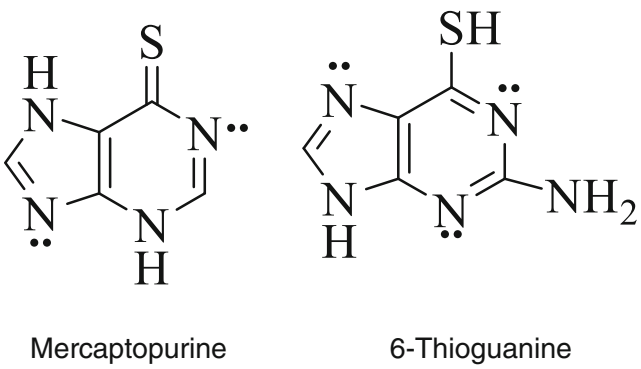

Fig. 1 Molecular structure of 6-thioguanine and 6-mercaptopurine

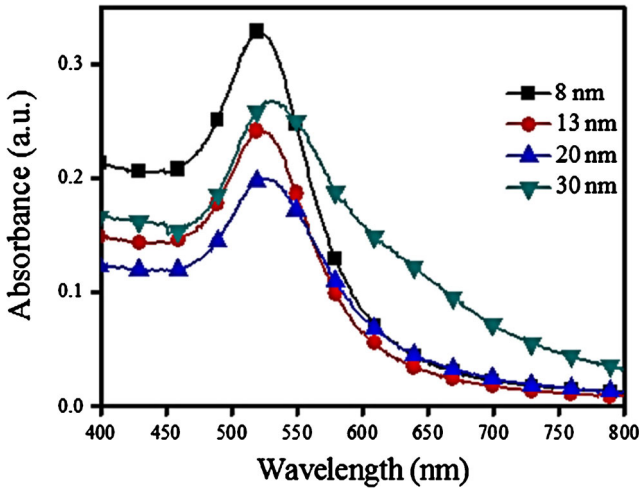

Fig. 2 UV-Vis spectra for different size gold nanoparticles

was used as reducing and stabilising agent for the conversion of Au^{+3} to Au^{0}. On addition of citrate to the boiling mixture of gold salt solution, the colour starts changing from yellow to blue to purple to red [16]. Once the red colour obtained, the solution kept at room temperature to cool down. Then, few drops of the $NaBH_4$ solution was added to it for the completion of the reaction (Au^{+3} to Au^{0}). Summarised information on the synthetic procedure, as well as verification of different sizes, is incorporated in Table 1.

Synthesis of Thiopurines/AuNPs Assemblies

The firstly different concentration of purine solutions was prepared from their stock solution (10^{-2} M). To sustain the stability of AuNPs and molecular structure of biomolecules pH of the gold solution was adjusted using HCl (10^{-2} M, 100 μl) to pH ~ 4. Thiopurine/AuNP assemblies were prepared, with the addition of 30 μl of purine into 3000 μl AuNPs solution. Then, the prepared mixture was analysed through UV-Vis spectroscopy to study their interaction with AuNPs [16]. The molecular structure of 6-MP and 6-TG are given in Fig. 1.

Instrumentations

The SPR of AuNPs was done using Champion UV-500 (AQ1205017) spectrophotometer and data analysed using software; Origin Pro 8. X-ray spectroscopy (EDS) images were obtained with the FEI Technai G2 F20, operating at 200 kV. Attenuated total reflectance infrared spectroscopy (ATR-IR) was recorded to know the purity of nano-material and their interactions with purines by using Agilent Resolution Pro-carry 660. Particle size and charge distribution were determined by Microtrac's dynamic light scattering (DLS), Nanotrac. For morphology and size determination, transmission electron microscopy (TEM) was done by drop casting of 10 μl purified AuNPs dispersions on the carbon-coated copper grid and allowing them to dry in air for size determination using TEM operating at 200 kV.

Result and Discussion

Characterisation Studies of AuNPs

Four different sizes gold NPs (8–30 nm) have been synthesised to investigate the variation in the inter-particle distance of AuNPs during ligand exchange reaction by different purines. As NPs stability and particle size depending upon the surface charge, size-controlled AuNPs were achieved by varying the citrate ion concentration (Table 1). To analyse the size variation in AuNPs, UV-Vis extinction spectra were recorded for each sample. It was observed that as the volume of citrate solution decreases (2000 to 400 μl), SPR shifts from 521 to 535 nm which is shown in Fig. 2. The red shifting of SPR was due to increment in the dipole-dipole interaction among AuNPs and dielectric constant of the medium, i.e. described in Mie scattering theory [33] and Maxwell-Garnett effective medium theory [16]. But on the addition of purines, the citrate layer gets disrupted that causes rapid particle aggregation and due to a decrease in the inter-particle distance the SPR peak of AuNPs undergoes a red shift. According to Mie theory, this bathochromic shift occurred along the long axis of the AuNP chains due to longitudinal electronic plasma oscillation [34]. Also upon the addition of purine to the citrate-stabilised gold particles, the colour of all the AuNPs solutions becomes red to pink to blue indicating the formation of aggregates of AuNPs.

Surface zeta potential and average particle size were also recorded before and after the addition of purines in AuNPs which are listed in Table 2. High negative zeta potential (− 32.1 mV) was observed for more citrate ion capped AuNPs which decreases the final size of the NPs. When purines were

Table 2 Average diameter and zeta potential of AuNPs before and after the addition of purines

Sample	Before addition of purines		After addition of purines	
	Diameter (nm)	Zeta potential (mV)	Diameter (nm)	Zeta potential (mV)
A	10	− 32.1	70	− 24.4
B	15	− 24.7	115	− 21.2
C	25	− 20.4	150	− 19.2
D	40	− 17.5	200	− 14.5

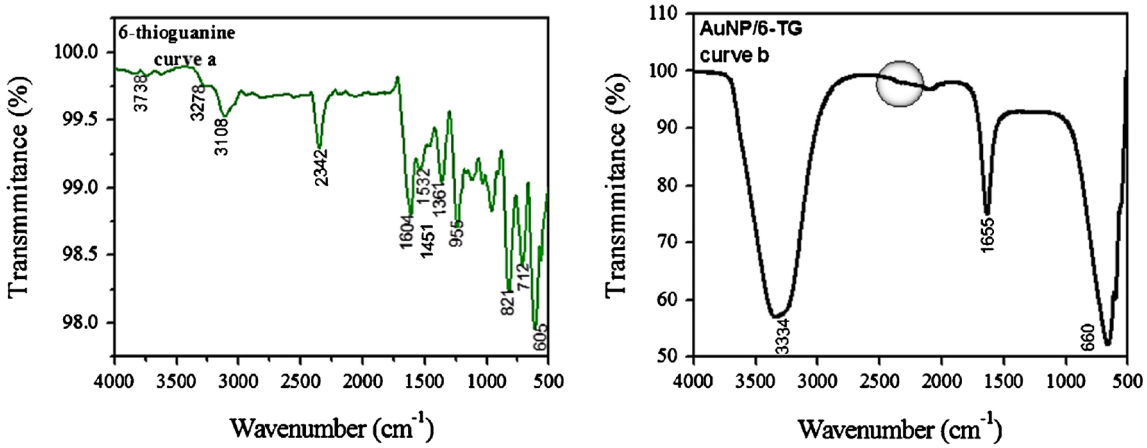

Fig. 3 FT-IR spectra of (a) pure 6-TG and (b) 6-TG-induced gold nanoparticle aggregates at pH ~ 4

added to the colloidal AuNPs solution, their surface charge decreases due to placing exchange reaction [35] between purines and citrate ions. It is clear from the result that replacement of citrate ions with 6-TG molecules destabilised the NPs and leads to aggregation which was confirmed by the huge increase in average particle size (Table 2). It was found that average particle diameter increased on the addition of purines and more pronounced for larger particles. This rapid aggregation of AuNPs for larger size AuNPs is due to less negative surface charge and facile cross-linkage through sulphur and nitrogen between AuNPs and purines [34].

FT-IR Studies

To confirm the citrate capping and interaction of AuNPs with purines, FT-IR spectra was recorded in the spectral frame 400–4000 cm^{-1}. AuNPs show pronounced peak around 1500–1630 and 1305–1415 cm^{-1} due to the symmetric and asymmetric stretching vibration of COO^- [36] (Fig. S1, in supporting information). The presence of surface-bound purines is justified when N–H stretch for free purines at 3100 cm^{-1} shifted to 3344 cm^{-1} for Au aggregates and S-H stretch/bending at 2338/600 cm^{-1} is disappeared (Fig. 3). The

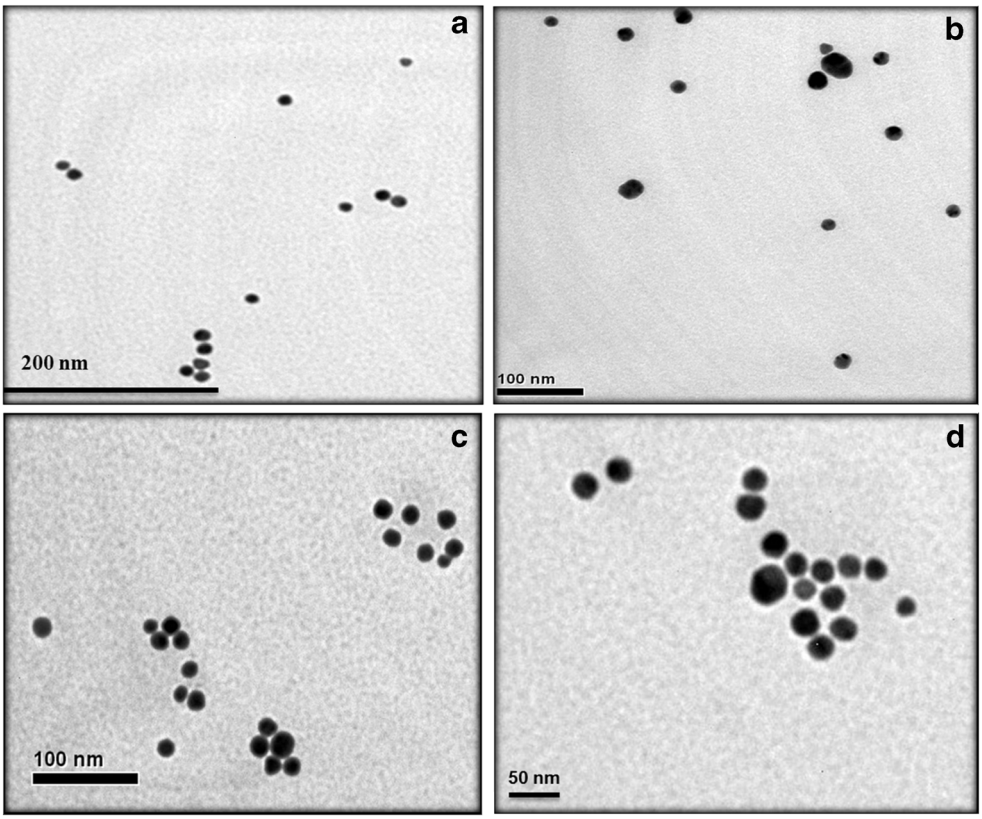

Fig. 4 TEM images of non-aggregated AuNPs **a** 8, **b** 13, **c** 20 and **d** 30 nm

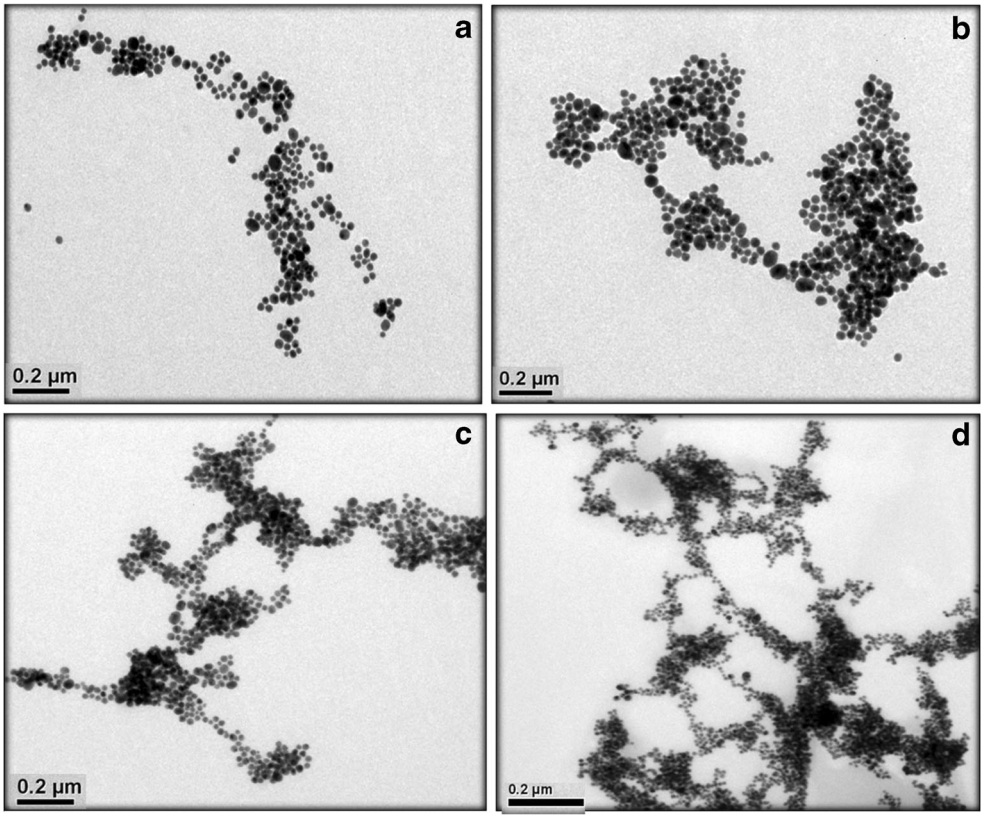

Fig. 5 TEM images for AuNPs aggregates **a** 8, **b** 13, **c** 20 and **d** 30 nm

perceived observation showed that AuNPs have a stronger affinity for nitrogen and sulphur moieties. Even some pronounced peak of citrate moiety also disappears (Fig. S1). This confirms the interaction of purines with AuNPs and replacement of citrate moiety from the surface of AuNPs.

TEM Studies

The synthesis process followed to obtain a broad range of AuNPs sizes that was clearly observed from TEM images. The TEM images of citrate-capped AuNPs of four different sizes (8, 13, 20 and 30 nm) showed in Fig. 4, which confirms their monodispersity and non-aggregating nature. But upon addition of purines, AuNPs were aggregated which is shown in Fig. 5. From the TEM images, it is evident that there is no particular geometry of the aggregated particles is formed.

Stability and Optimisation Studies for Sensing Activity of AuNPs

The steadiness of colloidal nanoparticle systems is the key for proper applications in physical and biological disciplines which were based on Derjaguin-Laudua-Verwey-Overbeck (DLVO) theory. It was found that citrate ions clouds around the AuNPs lead to $F_{\text{ree}} >> F_{\text{ast}\ \mathit{T}\text{rac}}$ due to negative surface charge that prevents their aggregation [16]. So, to study the effect of pH and salt on their surface charge and its stability, UV-Visible spectra were recorded at different pH and salt concentrations. When different volume (10–100 μl) of 0.1 M NaCl was added to AuNPs, the peak at 521 nm sustained (Fig. S2A. in supporting information) but after 10–15 days, AuNPs aggregation starts in the presence of NaCl salt. Whereas in huge pH (4–12) range, the AuNPs are highly stable but at high acidic condition (pH < 3); it leads to aggregation and the colour change from red to purple to blue which was occurred due to surface charge neutralisation of AuNPs

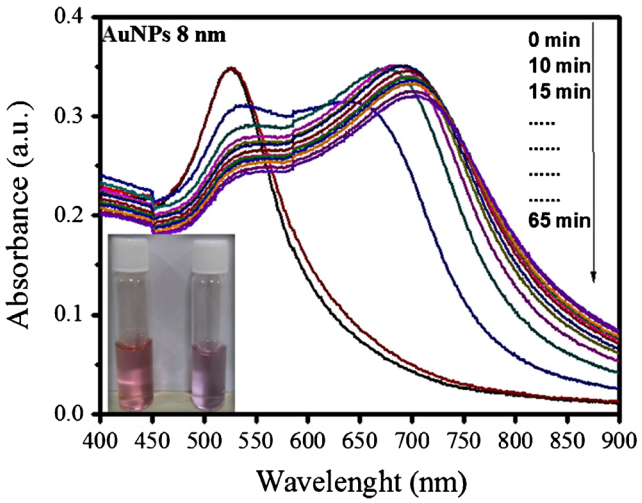

Fig. 6 Time-dependent UV-Vis spectra recorded at various times after addition of purine (10 mM, 30 μl) in AuNPs (0.25 mM, 3 ml)

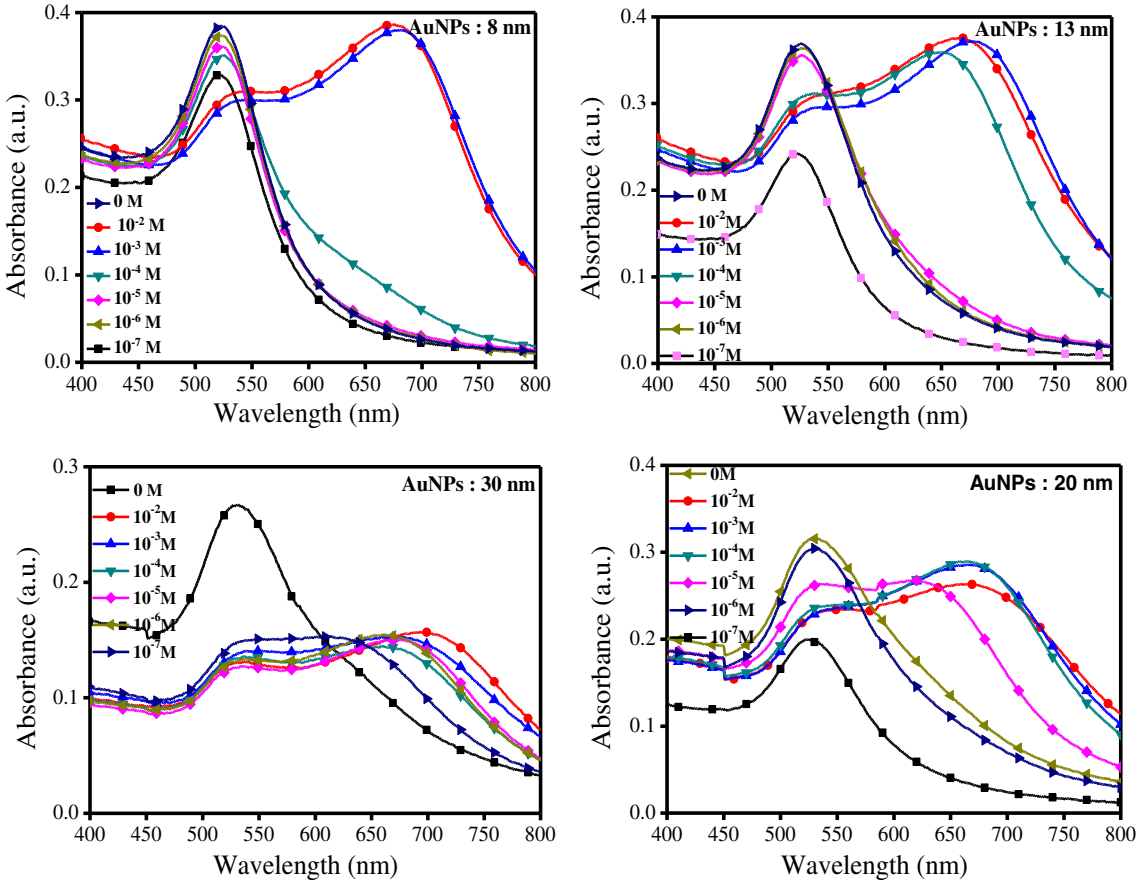

Fig. 7 UV-Vis spectra of Au aggregates at various concentration of 6-TG at pH ~ 4 using **a** 8, **b** 13, **c** 20 and **d** 30 nm AuNPs

(Fig. S2B) [16]. After obtaining these outcomes, to sustain the stability of AuNPs fresh preparation is to be done and only pH ~ 4 were advised to use for the detection of purines as at low pH, the binding efficiency of negatively charged AuNPs with protonated purines are enhanced.

Kinetic Study

Effect of Reaction Time

Kinetic studies were done to see the effect of purines on the inter-particle distance of AuNPs by measuring SPR. The absorption spectra for AuNPs and its mixture with purine were recorded at different time intervals. It was stated in Mie theory [33] that single peak is attained due to the dipole plasma oscillation for AuNPs induced by an external field. When purines are added to the colloidal solution of AuNPs, the inter-particle spacing between the particles decreases. With the increase of time period, the first peak at 521 nm becomes weaker and second peak at a longer wavelength (~ 700 nm) intensifies and red shifted. But after 30 min, peak variation gets almost constant and blue colour was obtained which confirms the completion of the place exchange reaction (Fig. 6).

Quantitative Detection of Thiopurines

Morphology of AuNPs and optical properties vary with the concentration of biological moieties. To study the interaction and quantification of purines, the different molar ratio of [purines]/[AuNPs] from 10^{-2}–10^{-7} M were used. It was

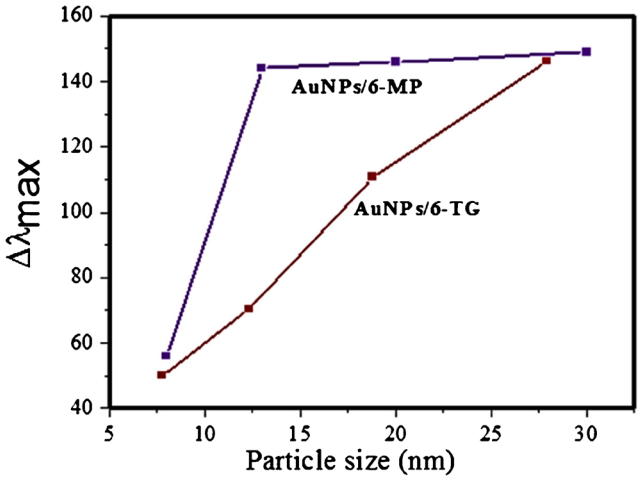

Fig. 8 Plot of $\Delta\lambda_{max}$ vs. particle size

Table 3 A comparative account for the detection of 6-TG

Methods	Detection system	Limit of detection (mM/L)	Reference
HPLC	Fluorescence	0.0027	[37]
DPSV	$[Fe(CN_6)]^{3-}$	0.2	[38]
Spectrofluorometery	–	0.05	[39]
SWV	$Co(bpy)^{2+}$/p-aminophenol	0.12/0.08	[40, 41]
DPV	FDCCNTE	0.009	[42]
SPR	Different size AuNPs	10^{-4}	This work

pragmatic that dipole plasmon of AuNPs shifted to higher λ_{max}, i.e. the intensity of the ~ 521 nm progressively weakens and the shoulder crest nearly at ~ 700 nm overwhelms and showed a broad peak. Whereas with the decrease in a number of purines (10^{-2}–10^{-7} M) SPR peak position perceived at identical λ_{max}, i.e. 521 nm. This variation in the absorption spectrum of AuNPs and purines mixture was due to the change of inter-particle distance of AuNPs due to Au-S/Au-N interactions which get reduced for a dilute solution of purines [16, 34]. When different size of AuNPs was analysed with different concentrations of purine (10^{-2}–10^{-7} M), it was found that larger size AuNPs (30 nm) was more sensitive towards purines even at their lower concentration (10^{-7} M), because large size AuNPs have small surface charge energy which triggers the aggregation process (Fig. 7 and Fig S3 in supporting information). To analyse the sensitivity of AuNPs towards two different purines having similar functional groups, SPR peak displacement, $\Delta\lambda_{max}$ (between two dipole plasmon peaks) against particle size was plotted (Fig. 8). An almost linear increase in peak displacement against particle size is observed for 6-TG, but little bit deviating for 6-MP. These investigations concluded that larger size AuNPs is more sensitive for purine molecule detection and the lower limit of detection is 10^{-7} M.

Comparison of Different Methods for Sensing of Purines

A comparative study was done for detection of 6-TG with different known techniques by colorimetric/optical sensors (Table 3). It was found that our, as synthesised AuNPs are a highly efficient sensor for detection of purines and this system, may be used for several other biomolecules.

Conclusion

Here, we demonstrated the simple but effective method for quick determination of purines based on the SPR of different size AuNPs. Facile synthesis of different size AuNPs was performed by varying the citrate concentration that helps in managing inter-particle distance and stability of AuNPs. UV-Vis spectra were used to study the effect of purines on the inter-particle distance of AuNPs. It reveals that place exchange reaction is responsible for the interaction of purines and AuNPs which leads to their aggregation. These variations were observed by the naked eyes through the colour change from red to blue and recorded spectra in which bathochromic shift was observed in SPR signal of AuNPs. Various other studies related to time, pH of colloidal sol, the concentration of purines and peak displacement vs. particle size, and was also done for purine detection. This excellent selectivity and high limit of detection (10^{-7} M) make different size AuNPs an efficient analytical tool that has huge potential for practical application in clinical chemistry and medicinal diagnosis.

Funding Information The authors are thankful to BRNS-DAE (Grant No: 34/14/63/2014) and SERB-DST (Grant No: SB/FT/CS-178/2013) for financial assistance. We are also thankful to DST-FIST, Sprint Testing solutions-Mumbai and Thapar University for providing instrumental facilities.

Compliance with Ethical Standards

Conflict of Interest The authors declare that they have no conflict of interest.

References

1. Lennard L, Lilleyman JS, Van Loon J, Weinshilboum RM (1990) Genetic variation in response to 6-mercaptopurine for childhood acute lymphoblastic leukaemia. Lancet 336(8709):225–229. https://doi.org/10.1016/0140-6736(90)91745-V
2. Al-Ghobashy MA, Hassan SA, Abdelaziz DH, Elhosseiny NM, Sabry NA, Attia AS, el-Sayed MH (2016) Development and validation of LC-MS/MS assay for the simultaneous determination of methotrexate, 6-mercaptopurine and its active metabolite 6-thioguanine in plasma of children with acute lymphoblastic leukemia: correlation with genetic polymorphism. J Chromatogr B Anal Technol Biomed Life Sci 1038:88–94. https://doi.org/10.1016/j.jchromb.2016.10.035
3. Munshi P, Lubin M, Bertino J (2014) 6-thioguanine: a drug with unrealized potential for cancer therapy. Oncologist 19(7):760–765. https://doi.org/10.1634/theoncologist.2014-0178
4. Sean CS (2009) Martindale: the complete drug reference, 34th edn. Pharmaceutical Press, London, 884–886
5. Oancea I, Png CW, Das I, Lourie R, Winkler IG, Eri R, Subramaniam N, Jinnah HA, McWhinney BC, Levesque JP, McGuckin MA, Duley JA, Florin THJ (2013) A novel mouse model of veno-occlusive disease provides strategies to prevent thioguanine-induced hepatic toxicity. Gut 62(4):594–605. https://doi.org/10.1136/gutjnl-2012-302274

6. Tack GJ, Asseldonk DP, Wanrooij RLJ, Bodegraven AA, Mulder CJ (2012) Tioguanine in the treatment of refractory coeliac disease - a single centre experience. Aliment Pharmacol Ther 36(3):274–281. https://doi.org/10.1111/j.1365-2036.2012.05154.x
7. Fishman M, Mrozek-Orlowski M (1999) Cancer Chemotherapy Guidelines and Recommendations for Practice, 2nd edn. Oncology Nursing Press Inc, Pittsburgh PA, pp 25
8. Madueño R, Pineda T, Sevilla JM, Blázquez M (2004) An electrochemical study of 6-thioguanine monolayers on a mercury electrode in acid and neutral solutions. J Electroanal Chem 565(2): 301–310. https://doi.org/10.1016/j.jelechem.2003.10.024
9. Rowland K, Lennard L, Lilleyman JS (1998) High-performance liquid chromatographic assay of methylthioguanine nucleotide. J Chromatogr B Biomed Sci Appl 705(1):29–37. https://doi.org/10.1016/S0378-4347(97)00495-7
10. Mawatari H, Kato Y, Nishimura SI et al (1998) Reversed-phase high-performance liquid chromatographic assay method for quantitating 6-mercaptopurine and its methylated and non-methylated metabolites in a single sample. J Chromatogr B Biomed Appl 716(1-2):392–396. https://doi.org/10.1016/S0378-4347(98)00329-6
11. Keuzenkamp-Jansen CW, De Abreu RA, Bökkerink JPM, Trijbels JMF (1995) Determination of extracellular and intracellular thiopurines and methylthiopurines by high-performance liquid chromatography. J Chromatogr B Biomed Sci Appl 672(1):53–61. https://doi.org/10.1016/0378-4347(95)00206-X
12. Lennard L, Singleton HJ (1992) High-performance liquid chromatographic assay of the methyl and nucleotide metabolites of 6-mercaptopurine: quantitation of red blood cell 6-thioguanine nucleotide, 6-thioinosinic acid and 6-methylmercaptopurine metabolites in a single sample. J Chromatogr B Biomed Sci Appl 583(1):83–90. https://doi.org/10.1016/0378-4347(92)80347-S
13. Lennard L (1987) Assay of 6-thioinosinic acid and 6-thioguanine nucleotides, active metabolites of 6_mercaptopurine, in human red blood cells. J Chromatogr Biomed Appl Elsevier Sci Publ BV 423: 169–178. https://doi.org/10.1016/0378-4347(87)80340-7
14. Lennard L (1985) Assay of 6-mercaptopurine in human plasma. J Chromatogr B Biomed Sci Appl 345:441–446. https://doi.org/10.1016/0378-4347(85)80186-9
15. Lavi LE, Holcenberg JS (1985) A rapid and sensitive high-performance liquid chromatographic assay for 6-mercaptopurine metabolites in red blood cells. Anal Biochem 144(2):514–521. https://doi.org/10.1016/0003-2697(85)90148-4
16. Basu S, Ghosh SK, Kundu S, Panigrahi S, Praharaj S, Pande S, Jana S, Pal T (2007) Biomolecule induced nanoparticle aggregation: effect of particle size on interparticle coupling. J Colloid Interface Sci 313(2):724–734. https://doi.org/10.1016/j.jcis.2007.04.069
17. Zhong Z, Patskovskyy S, Bouvrette P, Luong JHT, Gedanken A (2004) The surface chemistry of Au colloids and their interactions with functional amino acids. J Phys Chem B 108(13):4046–4052. https://doi.org/10.1021/jp037056a
18. Lubomirsky I, Wang TY, Gartsman K et al (2000) Biologically programmed nanoparticle assembly. Adv Mater 12(2):147–150. https://doi.org/10.1002/(SICI)1521-4095(200001)12:2<147::AID-ADMA147>3.0.CO;2-U
19. Mrksich M (2000) A surface chemistry approach to studying cell adhesion. Chem Soc Rev 29(4):267–273. https://doi.org/10.1039/a705397e
20. Bright RM, Walter DG, Musick MD, Jackson MA, Allison KJ, Natan MJ (1996) Chemical and electrochemical Ag deposition onto preformed Au colloid monolayers: approaches to uniformly-sized surface features with Ag-like optical properties. Langmuir 12(3): 810–817. https://doi.org/10.1021/la950429h
21. Alvarez MM, Khoury JT, Schaaff TG, Shafigullin MN, Vezmar I, Whetten RL (1997) Optical absorption spectra of nanocrystal gold molecules. J Phys Chem B 101(19):3706–3712. https://doi.org/10.1021/jp962922n
22. Takeuchi Y, Ida T, Kimura K (1996) Temperature effect on gold nanodispersion in organic liquids. Surf Rev Lett 3(01):1205–1208. https://doi.org/10.1142/S0218625X96002175
23. Kreibig U, Genzel L (1985) Optical absorption of small metallic particles. Surf Sci 156:678–700. https://doi.org/10.1016/0039-6028(85)90239-0
24. Thanh NTK, Rosenzweig Z (2002) Development of an aggregation-based immunoassay for anti-protein A using gold nanoparticles. Abstr Pap Am Chem Soc 223:U74–U74
25. Andrew Lyon L, Musick MD, Natan MJ (1998) Colloidal Au-enhanced surface plasmon resonance immunosensing. Anal Chem 70(24):5177–5183. https://doi.org/10.1021/ac9809940
26. Musick MD, Keating CD, Lyon LA, Botsko SL, Peña DJ, Holliway WD, McEvoy TM, Richardson JN, Natan MJ (2000) Metal films prepared by stepwise assembly. 2. Construction and characterization of colloidal Au and Ag multilayers. Chem Mater 12(10):2869–2881. https://doi.org/10.1021/cm990714c
27. Storhoff JJ, Mucic RC, Mirkin CA (1997) Strategies for Organizing Nanoparticles into Aggregate Structures and Functional Materials. J Clust Sci 8:179–216. https://doi.org/10.1023/A:1022632007869
28. Freeman RG, Grabar KC, Allison KJ et al (1995) Self-assembled metal colloid monolayers: an approach to SERS substrates. Science 267(80):1629–1632. https://doi.org/10.1126/science.267.5204.1629
29. Taton T, Mirkin C, Letsinger R (2000) Scanometric DNA array detection with nanoparticle probes. Science 289(5485):1757–1760. https://doi.org/10.1126/science.289.5485.1757
30. Storhoff JJ, Elghanian R, Mucic RC, Mirkin CA, Letsinger RL (1998) One-pot colorimetric differentiation of polynucleotides with single base imperfections using gold nanoparticle probes. J Am Chem Soc 7863(9):1959–1964. https://doi.org/10.1021/ja972332i
31. Elghanian R, Storhoff JJ, Mucic RC et al (2010) Selective colorimetric detection of polynucleotides based on the distance-dependent optical properties of gold nanoparticles. Science 1078(80):1078–1081. https://doi.org/10.1126/science.277.5329.1078
32. Templeton AC, Chen S, Gross SM, Murray RW (1999) Water-soluble, isolable gold clusters protected by tiopronin and coenzyme A monolayers. Langmuir 15(1):66–76. https://doi.org/10.1021/la9808420
33. Physik ADER, Vol N (1908) Beiträge zur Optik trüber Medien, speziell kolloidaller Metallösungen; von Gustav Mie. Ann Phys 25:1–52
34. Basu S, Pande S, Jana S, et al (2008) Controlled Interparticle Spacing for Surface-Modified Gold Nanoparticle Aggregates Controlled Interparticle Spacing for Surface-Modified Gold Nanoparticle Aggregates. Langmuir 8276–8282. https://doi.org/10.1021/la8000784
35. Park J, Shumaker-parry JS (2005) Structural study of citrate layers on gold nanoparticles: role of intermolecular interactions in stabilizing nanoparticles. Langmuir 21(21):1–33. https://doi.org/10.1021/la0504560
36. Park JW, Shumaker-Parry JS (2014) Structural study of citrate layers on gold nanoparticles: role of intermolecular interactions in stabilizing nanoparticles. J Am Chem Soc 136(5):1907–1921. https://doi.org/10.1021/ja4097384
37. Olesen KM, Hansen SH, Sidenius U, Schmiegelow K (2008) Determination of leukocyte DNA 6-thioguanine nucleotide levels by high-performance liquid chromatography with fluorescence detection. J Chromatogr B Anal Technol Biomed Life Sci 864(1-2): 149–155. https://doi.org/10.1016/j.jchromb.2008.02.007
38. Warren DJ, Slørdal L (1993) A high-performance liquid chromatographic method for the determination of 6-thioguanine residues in DNA using precolumn derivatization and fluorescence detection. Anal Biochem 215(2):278–283. https://doi.org/10.1006/abio.1993.1587

39. Thomas A (1976) Spectrofluorometric determination of thiopurines—I: 6-Thioguanine. Talanta 23(5):383–386. https://doi.org/10.1016/0039-9140(76)80051-3
40. Wang W, Wang SF, Xie F (2006) An electrochemical sensor of non-electroactive drug 6-thioguanine based on the dsDNA/AET/Au. Sensors Actuators B Chem 120(1):238–244. https://doi.org/10.1016/j.snb.2006.02.012
41. Mirmomtaz E, Ensafi AA, Karimi-Maleh H (2008) Electrocatalytic determination of 6-tioguanine at a p-aminophenol modified carbon paste electrode. Electroanalysis 20(18):1973–1979. https://doi.org/10.1002/elan.200804273
42. Ensafi AA, Karimi-Maleh H (2010) Modified multiwall carbon nanotubes paste electrode as a sensor for simultaneous determination of 6-thioguanine and folic acid using ferrocenedicarboxylic acid as a mediator. J Electroanal Chem 640(1-2):75–83. https://doi.org/10.1016/j.jelechem.2010.01.010